ISBN 978-82-326-1932-0 (printed version)
ISBN 978-82-326-1933-7 (electronic version)
ISSN 1503-8181

Doctoral theses at NTNU, 2016:297

Krzysztof Jan Zięba

Towards understanding the glacial impact on sedimentary basins using numerical methods

NTNU
Norwegian University of
Science and Technology

NTNU
Norwegian University of
Science and Technology

NTNU
Norwegian University of
Science and Technology
Faculty of Engineering
Science and Technology
Department of Geology and Mineral Resources
Engineering

Doctoral theses at NTNU, 2016:297

NTNU

Krzysztof Jan Zięba

Towards understanding the glacial impact on sedimentary basins using numerical methods

Thesis for the degree of Philosophiae Doctor

Trondheim, October 2016

Norwegian University of Science and Technology
Faculty of Engineering
Science and Technology
Department of Geology and Mineral Resources Engineering

NTNU
Norwegian University of
Science and Technology

NTNU
Norwegian University of Science and Technology

Thesis for the degree of Philosophiae Doctor

Faculty of Engineering
Science and Technology
Department of Geology and Mineral Resources Engineering

ISBN 978-82-326-1932-0 (printed version)
ISBN 978-82-326-1933-7 (electronic version)
ISSN 1503-8181

Doctoral theses at NTNU, 2016:297

Printed by Skipnes Kommunikasjon as

Preface

The work forming the basis for this Ph.D. thesis was carried out at the Department of Geology and Mineral Resources Engineering, Faculty of Engineering Science and Technology, NTNU - Norwegian University of Science and Technology from February 2013 until May 2016. The Ph.D. work was supervised by Prof. Stephen John Lippard and co-supervised by Arnt Grøver (Sintef Petroleum AS). It was a part of SINTEF Petroleum project "Impact of Cenozoic structural development and glacial erosion on gas expansion, hydraulic fracturing and leakage in the Western Barents Sea" founded by ENI Norge.

This thesis consists of an introduction and three scientific papers, providing new insights about the Pleistocene impact on the sedimentary basins and petroleum systems in the southern Barents Sea. The research papers are:

Paper 1: Zieba, K.J., Felix, M., Knies, J., (2016). The Pleistocene contribution to the net erosion and sedimentary conditions in the outer Bear Island Trough, western Barents Sea. Arktos, Springer.

Paper 2: Zieba, K.J., Omosanya, K.O., Knies, J., (submitted). The Pleistocene evolution of the Barents Sea bathymetry: a flexural isostasy modelling approach. Norwegian Journal of Geology, Geological Society of Norway.

Paper 3: Zieba, K.J., Grøver, A., (2016). Isostatic response to glacial erosion, deposition and ice loading. Impact on geometry of the southwestern Barents Sea hydrocarbon traps. Marine and Petroleum Geology, Elsevier.

During the last three years I was actively involved in the Sintef Petroleum project work. The project focused on the petroleum-related subjects. I was responsible for basin modelling, analysis of the results, reporting and attending the project meetings. The outcome of the project has been described in a separate report that is not included in this thesis. In the course of my Ph.D. I attended six courses at NTNU and at the University Centre in Svalbard (UNIS) that provided me a relevant background knowledge. I also gave eight talks and presented posters at national and international conferences including AGU, EAGE, ICAM and NGF meetings. As a first author, I wrote a journal paper addressing the problem of the uplift and erosion in the southwestern Barents Sea. I also contributed as a co-author in a journal paper concerning palaeo-water depth reconstruction.

Acknowledgements

First I would like to thank my supervisors. Stephen Lippard (NTNU), for having an eye for details and helpful advice. Arnt Grøver (Sintef), for overall support and always positive attitude. I would like to extend my gratitude to my former supervisor Matthias Daszinnies for his long time support and advice.

Special thanks to Benjamin Udo Emmel for stimulating discussions, valuable feedback, critical questions and limitless patience during the last three years. I am grateful to the staff at Sintef Petroleum, Basin Modelling Group who helped me in one or other way at different stages of my Ph.D. and for providing an inspiring and supportive working environment. I am very grateful to ENI, especially to Filippos Tsikalas for valuable discussions and sharing his extensive knowledge.

I would like to acknowledge Maarten Felix for providing a long training of the writing skills. Thanks to Jochen Knies for giving me valuable hints and ideas at the very beginning of the Ph.D. work. I thank my colleagues at NTNU for discussions and social activities. I am grateful to my friends and family for keeping my spirit up. Finally I would like to thank Karolina for her support and patience during three years of intensive work.

Abstract

The Cenozoic tectonism and the Pleistocene glaciations had a strong impact on the sedimentary basins and petroleum systems of the Barents Sea. The impact of these processes are often considered together resulting in an unclear understanding of the consequences of each process alone. This thesis focuses on the glacial impact on the sedimentary basins but it also provides an insight about the relative contribution of the glacial and pre-glacial processes to the net erosion, uplift, topography development and depletion of the hydrocarbon traps. Various numerical methods were used in this study. These include a novel approach used for determination of the glacial ages, a new Monte-Carlo-based method for estimating the erosion rates, flexural isostatic and hydrocarbon secondary migration modelling.

The main results show that the western Barents Sea was glaciated during four marine isotope stages: MIS 16, MIS 12, MIS 6, and MIS 2, for a total duration of 29 kyr. During the first glacial event the study area was subjected to an erosion of 24.2 ± 8.5 mm/yr. After the first event the rates have significantly changed varying from -12.6 ± 1.6 mm/yr (net deposition) to 1.6 ± 1.8 mm/yr. The results show that in the proximal part of the Bear Island Trough Mouth Fan, the Pleistocene glacial contribution to the total net erosion was small. The most likely glacial contribution in this area reaches 100 ± 90 m, which is about 9% of the total net erosion. In the more distal part of the wedge, the glaciations did not contribute to the net erosion.

The pre-glacial relief was modelled close to the sea level with the deepest parts at about 100 - 150 m bsl (below sea level) and the shallowest at about 300 m asl (above sea level). Between the Early and Middle Pleistocene the relief was deepened by 0 - 200 m. During the Middle-Late Pleistocene the shelf was deepened by up to 300 m in the troughs and up to 100 m on the banks. The Middle Pleistocene shelf represented shallow marine water depths with some elevated parts above the sea level. The model suggests that the inflow of the North Atlantic Current to the Barents Sea was barred by the topography up to ~0.7 Ma. Overall it was found that the contrasting bathymetry of deep troughs and shallow banks was affected by regional isostatic adjustments. The results show that the glacial erosion together with the sea level change caused an isostatic uplift in the range of 250 - 400 m in the troughs and below 200 m on the banks. According to the literature the total uplift magnitude is estimated at about 1 - 2 km so the isostatic component of the uplift is considered to be relatively small.

The hydrocarbon trap capacities could have been changed by ± 5 - 14% between the onset of glaciations and the present. The magnitude of capacity change was found to be dependent on

tilt values and pre-glacial trap geometry. The western Barents Sea traps with spill points to the west and south at present might have experienced trap capacity increase and were not susceptible to spillage during the Pleistocene, while those with spill points to the east and north might have experienced either volume increase or reduction. Changes of the trap geometry caused by the Pleistocene tilting alone could not have been responsible for any major loss of oil and gas. The tilting together with gas volume expansion might however explain some part of the hydrocarbon loss during the ice ages. It was found that the Pleistocene burial history and tilting cannot be responsible for thick palaeo-oil columns observed in the well cores in the Bjørnøyrenna Fault Complex at the present.

Table of contents

1 Introduction

The Cenozoic structural development driven by tectonic and glacial processes had a major impact on the burial, thermal and hydrocarbon migration history of the Barents Sea basins (Nyland et al., 1992; Doré and Jensen, 1996). Literature often refers to the problem of the complex Cenozoic development on the sedimentary basins and petroleum systems with special focus on uplift and erosion (e.g. Doré and Jensen, 1996; Faleide et al., 1996). The consequences of the tectonic and glacial processes are, however, often considered together leading to limited understanding of contribution of each process alone. The topic of glacial impact on sedimentary basins has received attention (Kjemperud and Fjeldskaar, 1992; Riis and Fjeldskaar, 1992; Lerche et al., 1997; Butt et al., 2002), but many issues remain underexplored. Consequently the relation between basin development and the most recent geological history is still ambiguous. In turn, a detailed understanding of physical and chemical processes occurring in the sedimentary basins is challenged by an incomplete knowledge of the burial and uplift histories influenced by the interlinked processes of ice sheet loading, sedimentation-erosion, palaeoceanography and paleoclimate change.

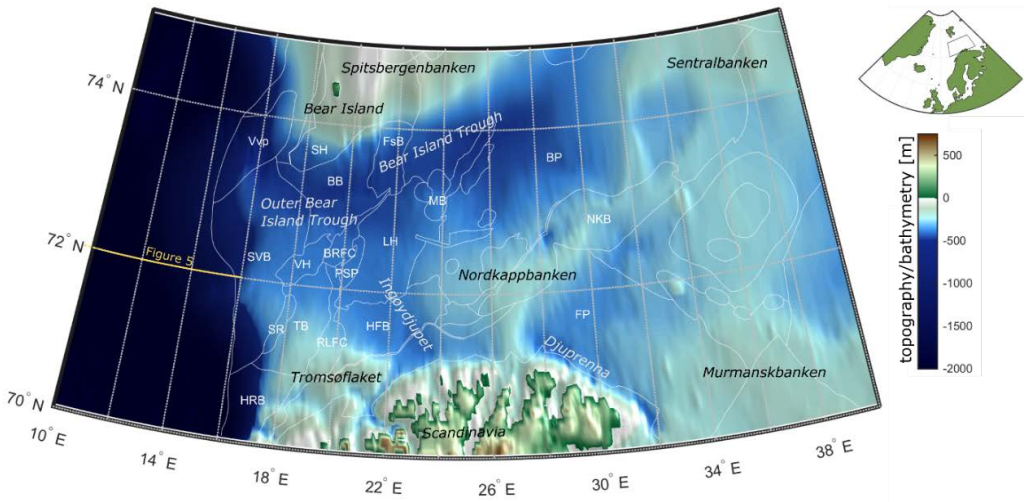

Figure 1 Present-day bathymetry of the study area including names of the most important geomorphological features and discussed structural elements (Etopo5 model, http://www.ngdc.noaa.gov/mgg/global/etopo5.html). BB: Bjørnøya Basin, BP: Bjarmeland Platform, BRFC: Bjørnøyrenna Fault Complex, HFB: Hammerfest Basin, FsB: Fingerdjupet sub-basin, FP: Finnmark Platform, HRB: Harstad Basin, LH: Loppa High, MB: Maud Basin, NKB: Nordkapp Basin, PSP: Polheim Subplatform, RLFC: Ringvassøy-Loppa Fault Complex, SH: Stappen High, SR: Senja Ridge, SVB: Sørvestsnaget Basin, VH: Veslemøy High, Vvp: Vestbakken volcanic province. Orange line shows location of seismic profile across the Bear Island Trough Mouth Fan shown in Figure 5.

The Barents Sea and Svalbard region has attracted the attention of the geological community since the 19th Century. A substantial growth of the present-day knowledge of the Svalbard-Barents Sea ice sheet has been stimulated by newly acquired terrestrial data and marine geological evidence since the 1980's (Ingólfsson and Landvik, 2013; Patton et al., 2015). During approximately the same time a significant development in understanding of the Cenozoic tectonic and sedimentary processes has taken place, supported by new well and seismic data often delivered by the oil industry (Doré, 1995). The literature has addressed various aspects of the Pleistocene geological history. Due to a lack of preserved geological evidence the research has been mostly focused on the youngest part of the Pleistocene. The addressed aspects include: late Pleistocene geomorphology and ice sheet behaviour (Vorren et al., 1990; Andreassen et al., 2004; Laberg et al., 2010; Rüther et al., 2011; Winsborrow et al., 2012; Bjarnadóttir et al., 2014; Rebesco et al., 2014), late Pleistocene ice extent and ages of glaciations (Sættem et al., 1992; Landvik et al., 1998; Mangerud et al., 1998; Svendsen et al., 2004; Larsen et al., 2006; Lambeck et al., 2010; Winsborrow et al., 2010), Pleistocene sedimentary conditions (Vorren et al., 1991; Faleide et al., 1996; Fiedler and Faleide, 1996; Hjelstuen et al., 1996; Laberg and Vorren, 1996; Elverhøi et al., 1998; Laberg et al., 2012), topographic development (Rasmussen and Fjeldskaar, 1996; Dimakis et al., 1998; Butt et al., 2002), isostasy (Riis and Fjeldskaar, 1992; Siegert and Dowdeswell, 2002) and consequences for petroleum systems (Kjemperud and Fjeldskaar, 1992; Lerche et al., 1997; Cavanagh et al., 2006; Duran et al., 2013).

This study intends to provide new insights on the Pleistocene impact on the sedimentary basins in the Barents Sea by using numerical methods. These include the interlinked subjects of glaciation ages, ice-sheet extent, sedimentary conditions, glacial and sediment impact on the lithospheric movements as well as topographic relief development. Some of the outcomes were further used for evaluating the consequences of the Pleistocene basin development on petroleum systems. The assessment of the glacial impact on the sedimentary basins and petroleum systems also provides new arguments to discussions about relative contribution of the glacial and pre-glacial processes on net erosion, uplift and depletion of the hydrocarbon traps (Doré and Jensen, 1996; Henriksen et al., 2011a).

The study area (Figure 1) is located in the southern Barents Sea. It corresponds with the drainage area of the Bear Island Trough Mouth Fan (Vorren et al., 1991) that lies in the Norwegian and Russian sectors of the Barents Sea. Some of the work was carried out in a smaller area which represents the outer Bear Island Trough (the westernmost part of the shelf). The area is in the focus of an extensive hydrocarbon exploration campaign at the present. In addition, the study

area represents a transition between the mostly erosive inner shelf and the mostly depositional outer Barents Sea shelf during the Late Pleistocene (Faleide et al., 1996). As a result, analysis of the geological processes within the study area might help in understanding the shelf development during extreme climatic changes during the glacial and interglacial periods.

2 Geological background

2.1 Prior to the Pleistocene

The evolution of the western Barents Sea was mostly controlled by Devonian to Cenozoic tectonic events mainly related to rifting and break-up in the northern Atlantic. Those events generated a complex geological setting with deep basins, platforms and highs and the associated deposition and erosion history (Gabrielsen et al., 1990; Faleide et al., 2008; Gernigon et al., 2014) (Figure 2, Figure 3). The sedimentary successions of the eastern Barents Sea basin have more continuous character showing less evidence of major extensional movements (Gac et al., 2012). The eastern Barents Sea basins have been located on a stable continental platform since the Late Paleozoic (Ebbing et al., 2007).

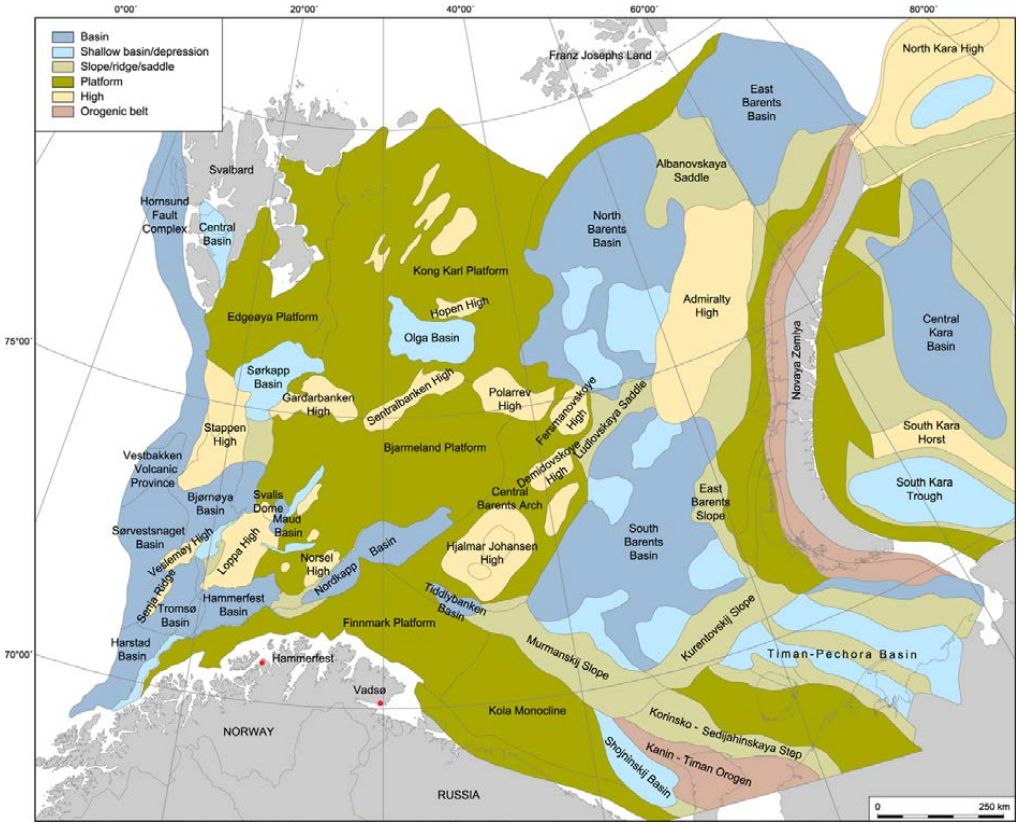

Figure 2 Main structural elements of the Barents Sea (Henriksen et al., 2011b).

The crystalline crust in the southwestern Barents Sea is believed to represent a northward continuation of the Caledonian orogenic belt (developed between Late Cambrian to Silurian) observed in the northern Scandinavia (Breivik et al., 1998; Roberts, 2003; Gee et al., 2008).

The structural configuration of the basement formed by the orogeny follows a general NE-SW trend (Roberts, 2003; Faleide et al., 2008; Gernigon et al., 2014) (Figure 2). The oldest sediments found in the southern-central Barents Sea are attributed to deposition in post-Caledonian times. The sediment delivery might have initiated formation of the Paleozoic basins including for example the Nordkapp Basin (Gudlaugsson et al., 1998; Larssen et al., 2002). After a first major rifting event (Late Devonian–Carboniferous) the Barents Sea became a regional shallow-marine basin where carbonate and evaporate deposition dominated and formed the Bjarmeland and Gipsdalen groups, and later more shale and sandstone-dominated Tempelfjorden Group (Larssen et al., 2002). This late Paleozoic rifting event probably initiated development of sedimentary basins in the western and central Barents Sea, including the Tromsø, Bjørnøya, Fingerdjupet, Maud and Hammerfest basins (Gudlaugsson et al., 1998). During the Late Devonian–Late Permian the Uralian Orogeny affected large parts of the eastern Barents and Kara sea region (Gudlaugsson et al., 1998). The far-field effects of this event caused uplift of the Ural Mountains and Novaya Zemlya separating the Barents and Kara seas. The rapid subsidence in the eastern Barents Sea basins during the Permian–Triassic times was caused by fast sedimentation of clastic material sourced by the Uralian orogenic belt (Johansen et al., 1992). The effect of the increased sediment delivery is now observed as thick sequence of the Middle Permian–Middle Jurassic sediments (Dalland et al., 1988; Glørstad-Clark et al., 2011).

The Uralian Orogeny is also thought to source the Early–Middle Triassic progradational sequences of the Sassendalen Group in the central-western Barents Sea (Glørstad-Clark et al., 2011) (Figure 3). The sediments are dominated by shales with some of them showing high source rock potential (Dalland et al., 1988). The Late Triassic–Middle Jurassic Kapp Toscana Group was deposited in shallow marine and deltaic conditions in the western Barents Sea. The group comprises of shales, siltstones and sandstones (Stø, Tubåen formations) partly with very good reservoir quality (Dalland et al., 1988).

The Late Jurassic–Early Cretaceous rifting events shaped the present day structural configuration of the western Barents Sea shelf (Gabrielsen et al., 1990; Faleide et al., 1993; Henriksen et al., 2011b). The intense tectonic activity resulted in the formation of fault blocks and led to different subsidence rates along the Bjørnøya, Hammerfest and Tromsø basins and inversion of some of the structural highs (Gabrielsen et al., 1990; Faleide et al., 1993). The Late Jurassic was dominated by the deposition of fine-grained organic-rich shales, including black shales of the Hekkingen Formation that is one of the most important hydrocarbon source rocks in the western Barents Sea (Figure 3). During

the Jurassic–Cretaceous transition open marine environments were established in the entire Barents Sea (Worsley, 2008; Setoyama et al., 2011). The subsidence rates increased in the southwestern Barents Sea resulting in deposition of thick Cretaceous strata of the Adventdalen Group in the Harstad, Tromsø, Bjørnøya and Sørvestsnaget basins (Faleide et al., 1993; Breivik et al., 1998). Very high sedimentation rates in the west contrast with lower deposition rates in central and eastern Barents Sea (Johansen et al., 1992; Klitzke et al., 2015). During the Late Cretaceous the Barents Shelf was uplifted resulting is erosion of the older sedimentary units (Richardsen et al., 1993). The Late Cretaceous strata are only preserved in the western marginal basins, such as in the Tromsø and Sørvestsnaget basins (Ryseth et al., 2003).

The Cenozoic structural development of the Barents Sea is mostly related to Early Cenozoic rifting, continental breakup and subsequent opening of the Norwegian-Greenland Sea. The breakup might have resulted in an uplift and erosion of the central-eastern Barents Sea, at about 65 - 45 Ma. The uplift was a consequence of the seafloor spreading and thermal activity in Norwegian-Greenland Sea (Faleide et al., 1993; Green and Duddy, 2010). During the Late Paleocene marine conditions were established in the western Barents Sea and persisted throughout the Eocene (Wood et al., 1989; Gabrielsen et al., 1990; Vorren et al., 1991; Riis, 1996; Ryseth et al., 2003; Faleide et al., 2008; Japsen et al., 2014). This resulted in substantial amount of deposition in the entire western Barents Sea including most of the structural highs, except for the Veslemøy and Stappen highs (Ryseth et al., 2003). The latter was uplifted and eroded during the Early Eocene rifting and volcanism, providing sediments for the Vestbakken Volcanic Province (Faleide et al., 1993).

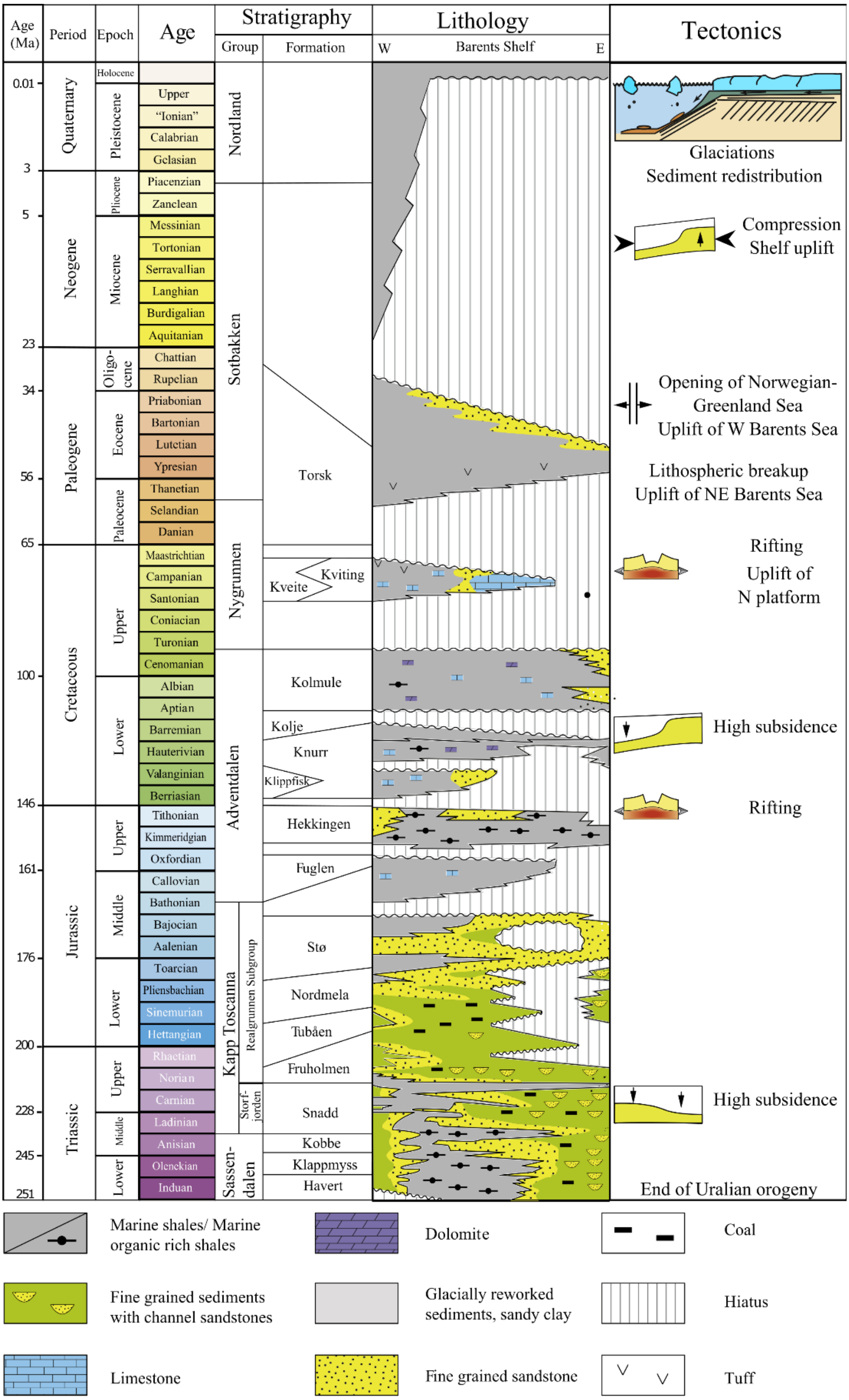

Figure 3 Lithostratigraphic chart of the Norwegian Barents Sea including key tectonic and sedimentary events during the Mesozoic and Cenozoic. Modified from Ostanin et al. (2012).

Plate tectonic movements caused several phases of compression and basin inversion in the northeastern Atlantic realm during the Oligocene and Miocene. The relative phase of uplift and erosion affected wide areas of the Arctic region including Greenland, Alaska, Svalbard and Barents Sea occurred during the Eocene–Oligocene transition, at about 40 - 30 Ma (Faleide et al., 1993; Green and Duddy, 2010; Japsen et al., 2014). This widespread uplift might have been caused by changes in plate motion at ~33 Ma and a resulting mechanical flexure (Rasmussen and Fjeldskaar, 1996; Japsen et al., 2014) and/or by magmatic activity in Eastern Greenland and related flexure of the lithosphere (Dimakis et al., 1998; Japsen et al., 2014). From the Oligocene onwards the Barents shelf became tectonically stable (Faleide et al., 1993; Clark et al., 2014). Oligocene–Middle Miocene sedimentary conditions are however uncertain due to a regional hiatus (Figure 3). Isostatic models suggest that marine conditions existed in a major part of the Barents Sea during this time interval (Rasmussen and Fjeldskaar, 1996).

Late Miocene-Pliocene uplift and erosion affected large areas in the Arctic including the Barents Sea, Svalbard and both margins of Greenland (Faleide et al., 2008; Green and Duddy, 2010; Japsen et al., 2014; Zattin et al., 2016). In the Barents Sea this event began between 10 and 5 Ma (Anell et al., 2009; Green and Duddy, 2010; Zattin et al., 2016) and was possibly related to a change in stress field in the northeastern Atlantic from extension to compression and related basin inversion (Doré et al., 1999; Zattin et al., 2016). Another possible explanation is thermal and lithospheric-scale anomalies and resulting elevation of the lithosphere-asthenosphere boundary (Zattin et al., 2016). The elevated subaerial Barents shelf prevailed until ~1.6 - 1.0 Ma and developed further into a submarine-subglacial relief (Dimakis et al., 1998; Butt et al., 2002).

2.2 The Pleistocene

2.2.1 Glaciation ages and ice extent

The southern Barents Sea has been covered by ice sheets since about 1.5 - 1.0 Ma (Knies et al., 2009; Laberg et al., 2010). The youngest glacial history is relatively well constrained, but little is known about the glaciations prior to the Saalian (Ingólfsson and Landvik, 2013; Patton et al., 2015). During the Saalian glaciation (>140 ka), Marine Isotope Stage 6 (MIS 6), the entire Barents Sea was covered by the ice sheet, reaching the shelf break of the western and northern Barents Sea. The evidence of this glaciation is represented by a regional till unit (Sættem et al., 1992; Svendsen et al., 2004). During the Early Weichselian (100 - 90 ka, MIS 5d) the northern and eastern parts of the Barents Sea were glaciated while the south-southwestern parts remained ice-free (Svendsen et al., 2004) The Barents Sea ice sheet also reached the western and northern

shelf breaks during the Middle Weichselian (70 - 65 ka, MIS 4). During the Late Weichselian, Last Glacial Maximum (25 - 15 ka, MIS 2) the entire Barents Sea was advanced by the ice sheet leaving a regional till unit over large areas on the Barents Sea shelf (Landvik et al., 1998; Patton et al., 2015)

2.2.2 Geomorphology and sediment redistribution

At present the Barents shelf shows a contrasting bathymetry of subglacial troughs and shallow banks, various erosional features and glacial deposits sub-cropped by an erosional unconformity (Figure 1). The water depths in the southern Barents Sea range from approximately 500 m in the deepest parts of the troughs to less than 100 m in the banks. The present-day relief is a result of selective glacial erosion and significant sediment redistribution over the shelf-continental slope area (Vorren et al., 1989; Laberg et al., 2010) (Figure 4).

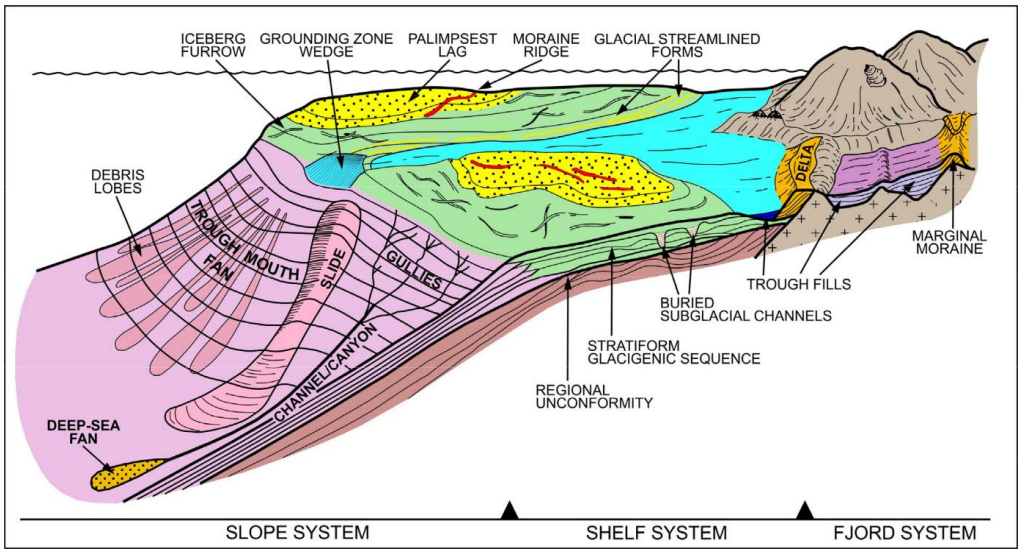

Figure 4 Main geomorphological elements and lithofacies of the passive glaciated continental margin of northern Norway (Rydningen, 2014).

Glacial advances occurring during the Early-Middle Pleistocene (between ca. 1.5 and 0.7 Ma) covered large areas of the entire Barents Sea shelf (Laberg et al., 2012). Large-scale glacial erosion resulted in seabed sculpturing, development of the Upper Regional Unconformity (URU) and massive sediment redistribution (Solheim and Kristoffersen, 1984; Laberg et al., 2012). According to mass balance calculations, 330 - 420 m of sediments (an average) were eroded from the shelf during this time span (Laberg et al., 2012). Between ca. 0.7 and 0.0 Ma, the glaciations were dominated by episodes of ice streaming. The ice streams occupied areas

of the present-day troughs and resulted in between 440 and 530 m of erosion in the major troughs. Little erosion took place outside the troughs (Laberg et al., 2012).

The products of glacial and pro-glacial erosion form the upper part of the Bear Island Trough Mouth Fan (Vorren and Laberg, 1997; Laberg et al., 2012) (Figure 5). The lower part of the fan consists of sediments deposited from the Paleocene–Eocene (Vorren et al., 1991; Fiedler and Faleide, 1996; Laberg et al., 2012) On the shelf, the fan is separated from the underlying rocks by the URU that represents a major seismic reflector. The deposits above the URU are bounded by several unconformities associated with seismic reflectors. The most important recent reflectors are R7, R5, and R1, which, together with the seafloor, separate sediment packages GI, GII and GIII (Faleide et al., 1996) (Figure 5). The age of reflector R7 is dated at ~2.7 - 2.3 Ma, R5 at ~1.5 Ma (Knies et al., 2009) and R1 at ~700 - 440 ka (Sættem et al., 1992; Elverhøi et al., 1998; Laberg et al., 2010). The oldest package GI represents fluvial and glaciofluvial deposits, while overlying packages GII and GIII consist of the products of glacial erosion (Laberg and Vorren, 1996; Laberg et al., 2012). In large parts of the shelf only the Last Glacial Maximum and Holocene deposits overlay the URU. In contrast, in the western part of the shelf sediments represent a glacigenic succession deposited during several glacial and interglacial events (Sættem et al., 1992). Flexural isostatic modelling shows the Pliocene-Pleistocene sediment redistribution resulted in 900 - 1400 m of isostatic uplift in the western Barents Sea and 700 - 1800 m of subsidence below the Bear Island Trough Mouth Fan (Riis and Fjeldskaar, 1992).

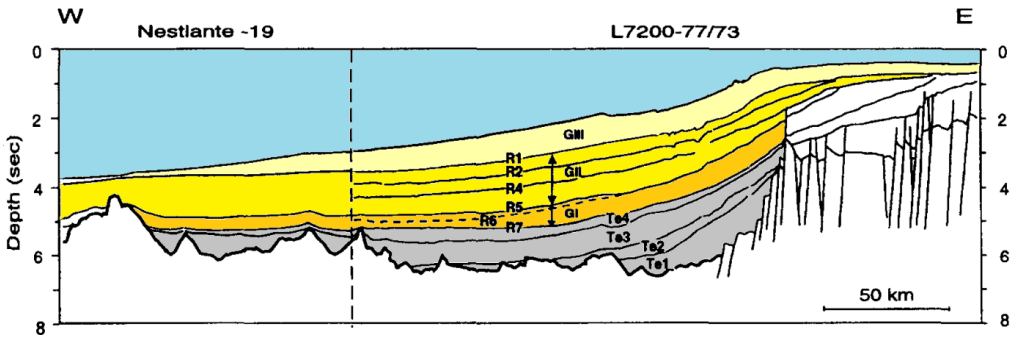

Figure 5 Seismic profile across the Bear Island Trough Mouth Fan including key seismic horizons and the sediment packages. Sediment packages Te1 - Te4 (grey) represents Paleogene to early Neogene sequences. Packages GIII - GI (orange-yellow) represents Plio-Pleistocene sediments. See text for details. For location of the profile see Figure 1. Modified from Fiedler and Faleide (1996).

The thickness of the Barents Sea ice sheet during the Weichselian was estimated by using various numerical methods showing significant discrepancies in results (Kjemperud and Fjeldskaar, 1992; Siegert and Dowdeswell, 2004; Peltier et al., 2015). The estimation of ice thickness is significantly challenged by several assumptions which need to be made based on available observations that often are poorly constrained (Gowan et al., 2016). Late Weichselian Barents Sea ice sheet models usually show thicknesses ranging from 0 at the western shelf break up to about 3 km in the eastern part of the Barents Sea (Kjemperud and Fjeldskaar, 1992; Siegert et al., 2001; Lambeck et al., 2006; Peltier et al., 2015). Such ice-sheet loading could be responsible for isostatic downwarping of the seabed and the underlying sedimentary sequences by up to 800 m during the ice advance and the same magnitude of isostatic rebound during the ice sheet retreat (Kjemperud and Fjeldskaar, 1992).

2.3 Uplift and erosion

The Pleistocene and pre-Pleistocene basin development of the Barents Sea was significantly affected by regional-scale events of uplift and erosion (for definitions see 3.1.1). The main recognized uplift and erosion events were caused by tectonic and isostatic forces during the Cenozoic (Nyland et al., 1992; Richardsen et al., 1993; Doré and Jensen, 1996; Henriksen et al., 2011b).

The precise ages of the uplift and erosion events are difficult to constrain due to missing stratigraphic sections from pre-Cenozoic to Pliocene below the Upper Regional Unconformity. The sub-crop map (Figure 6) shows that large parts of the Barents Sea lacks most of the Cenozoic sequence, and in some parts (e.g. Loppa and Stappen highs) the hiatus covers even longer periods. In the westernmost areas including the Sørvestsnaget Basin almost the entire Cenozoic succession is complete (Ryseth et al., 2003). In spite of lack of direct evidence, the literature suggests ages of uplift and erosion events that are mostly based on the regional and thermal data. The main episodes include: the Late Paleocene–Eocene, the Eocene–Oligocene transition, the Late Miocene–Pleistocene and the Pleistocene (see 2.1 and 2.2.2).

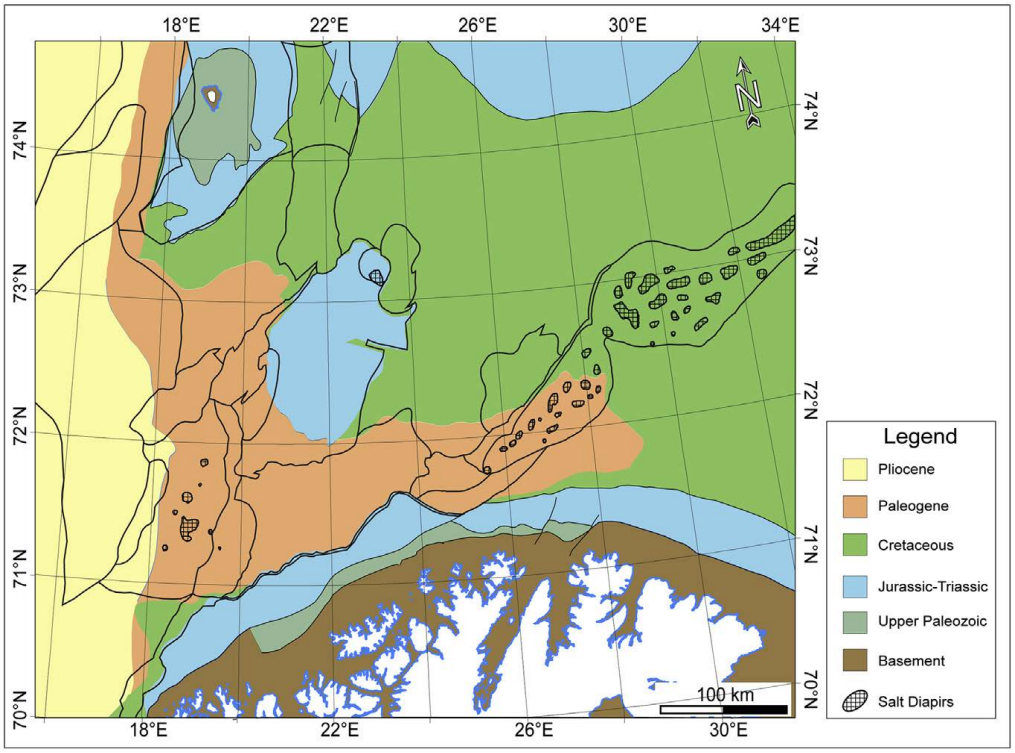

Figure 6 Sub-crop map below the Pleistocene–Holocene deposits (below Upper Regional Unconformity) (Baig et al., 2016).

Several different methods, including mass balance, seismostratigraphy, seismic velocities, vitrinite reflectance, fission track analysis, compaction, diagenesis, fluid inclusions and basin modelling, have been applied to assess the total Cenozoic net erosion thickness (Berglund et al., 1986; Bjørlykke et al., 1989; Wood et al., 1989; Vorren et al., 1991; Linjordet and Grung-Olsen, 1992; Liu et al., 1992; Løseth et al., 1992; Nyland et al., 1992; Riis and Fjeldskaar, 1992; Tsikalas, 1992; Eidvin et al., 1993; Richardsen et al., 1993; Reemst et al., 1994; Sættem et al., 1994; Fiedler and Faleide, 1996; Rasmussen and Fjeldskaar, 1996; Lerche et al., 1997; Dimakis et al., 1998; Elverhøi et al., 1998; Butt et al., 2002; Cavanagh et al., 2006; Ohm et al., 2008; Green and Duddy, 2010; Henriksen et al., 2011a; Laberg et al., 2012; Duran et al., 2013; Zieba et al., 2015; Zattin et al., 2016). It is concluded that the Barents Sea was subjected to between 0 and 3 km of net erosion (Figure 7). The lowest values are associated with areas close to the western shelf break, and the highest in the Stappen High and Svalbard areas (Cavanagh et al., 2006; Henriksen et al., 2011a; Baig et al., 2016 and references therein).

An important information source about the erosion magnitude in the southern Barents Sea is a stack of sediments deposited as the Bear Island Trough Mouth Fan. The fan consists of

sediments delivered from the Barents Sea shelf by erosional processes from the Paleocene-Eocene to the Pleistocene (Vorren et al., 1991; Fiedler and Faleide, 1996; Laberg et al., 2012) (see 2.2.2). The literature suggests that the fan consists of 70% of glacial and 30% of pre-glacial sediments (Vorren et al., 1991; Fiedler and Faleide, 1996; Laberg et al., 2012). Some researchers (Fiedler and Faleide, 1996; Laberg et al., 2012) used this ratio for direct estimation of the glacial to pre-glacial (tectonic) contributions to the total Cenozoic net erosion, while some used other methods such as thermal methods (Dimakis et al., 1998; Green and Duddy, 2010; Duran et al., 2013). The average ratio usually varies from 1:2 to 2:1 (Nyland et al., 1992; Dimakis et al., 1998; Cavanagh et al., 2006; Ohm et al., 2008; Duran et al., 2013). Based on the mass balance method applied for the Bear Island Trough Mouth Fan and its drainage area, the glacially-driven erosion thickness alone was estimated suggesting between 500 and 1000 m of glacial erosion in the southern and eastern Barents Sea since 1.5 - 1.0 Ma (Fiedler and Faleide, 1996; Hjelstuen et al., 1996; Laberg et al., 2012) (see also 2.2.2).

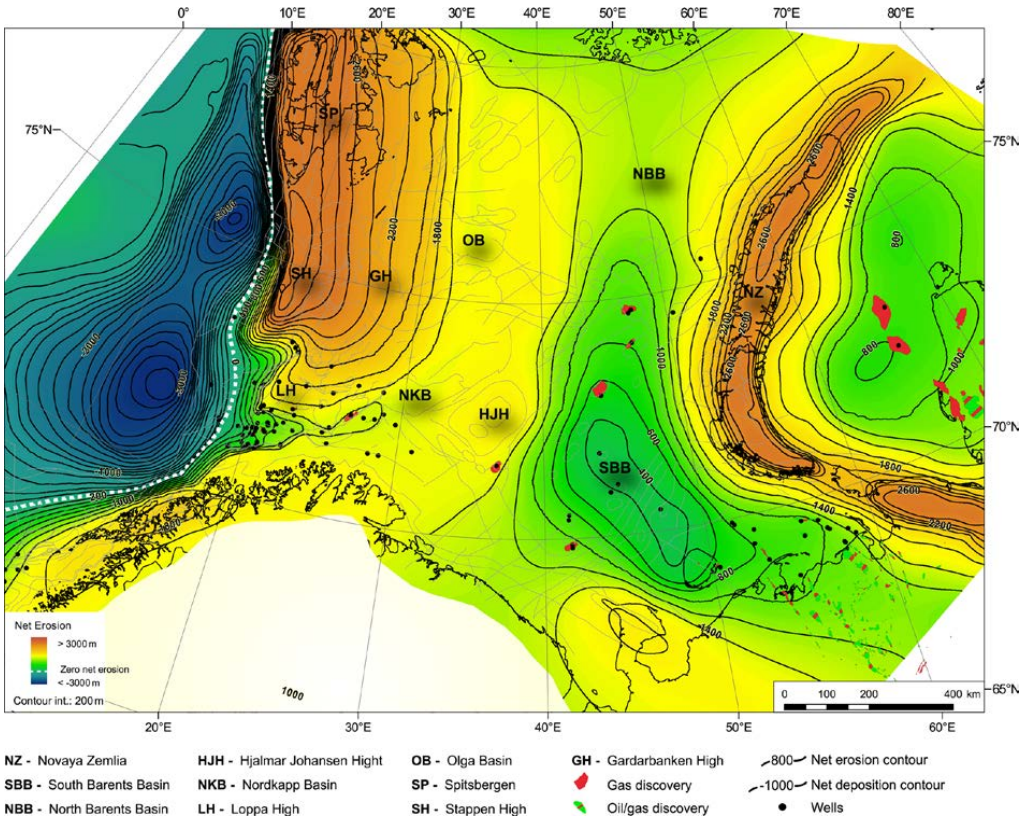

Figure 7 Net erosion map of the Barents and Kara seas (Henriksen et al., 2011a).

3 Theory and definitions

3.1 Uplift, erosion and topography changes

3.1.1 Definitions

The vertical depth of a sedimentary unit can be measured as *total* or *burial depth*. The total depth is measured from the sea level, while the burial depth is from the sediment-water or sediment-air interface. Sedimentation always leads to an increase in the burial depth, but does not necessarily result in an increase of the total depth. The total depth increases if deposition leads to the isostatically-driven process of *subsidence* or *downwarping*. Lack of subsidence, together with lack of compaction of the underlying rocks, results in a gradual infilling of the accommodation space and an increase of topography. Normally the deposition rate is higher than the isostatic subsidence rate so that deposition usually results in increase of topography.

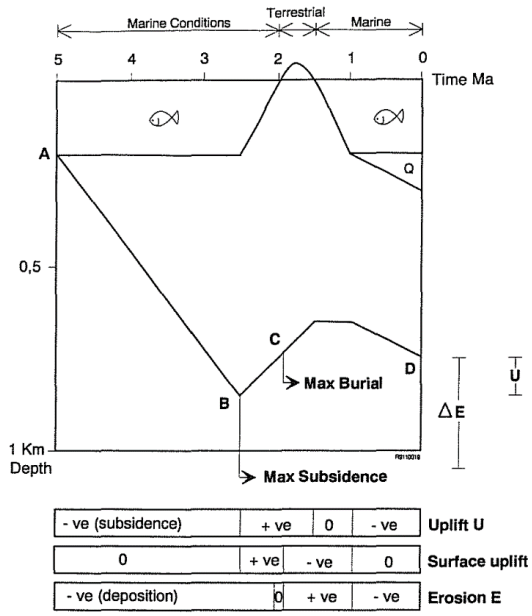

Figure 8 A hypothetical burial history curve of a marker horizon. The plot shows the relationship between rock uplift (U), surface uplift and erosion (E) changes. The changes can be either positive, negative or zero (ve). Point A marks deposition onset of a marker horizon at 5 Ma. Points B and C show maximum subsidence and maximum burial respectively. D represents the present-day depth of the marker horizon. Q is Quaternary sediments (Riis and Jensen, 1992).

The term *erosion* refers to removal of the surface material by different agents such as wind, rivers or glaciers. Erosion reduces the topography because the isostatic compensating rock uplift rate is normally lower than the erosion rate. In some cases a local erosion (e.g. deeply incised river valley) might result in no associated uplift due to a regional character of the

isostatic response (for details see 3.2). The *rock uplift* (or simply uplift) is defined as displacement of the rocks in respect to the geoid. Upward movement (i.e. *uplift*) is positive, downward movement (i.e. *subsidence, downwarping*) is negative (Riis and Jensen, 1992). Tectonic and magmatic processes (e.g. magmatic intrusions) might lead to a *surface uplift* that is defined as displacement of the surface with respect to the geoid (England and Molnar, 1990). The surface is meant as the interface between rock and air (or water). In some cases surface uplift leads to a major erosion due to elevation increase. Significant erosion rate increase occurs or the erosion begins when the surface is brought from submarine to subaerial conditions. However, the erosion on the elevated surface might lead in turn to isostatic rock uplift. The processes of erosion and uplift are therefore closely interrelated, and are often considered as a typical chicken and egg problem (England and Molnar, 1990). Due to this close interrelation the uplift and erosion are often described in the literature as a single effect (Doré and Jensen, 1996; Corcoran and Doré, 2005). *Exhumation* is defined as an upward displacement of the rocks with respect to the surface. The exhumation rate is therefore equal to the erosion rate (England and Molnar, 1990). Also the exhumation might be defined as the difference between rock and surface uplifts. The relation between rock uplift, surface uplift and erosion is shown in Figure 8. *Net erosion* (or *net exhumation*) is defined as the difference between maximal burial and the present-day burial depth as a reference unit (Corcoran and Doré, 2005; Henriksen et al., 2011a). The net erosion represents therefore a balance between total erosion and total deposition measured from the time point when the maximum burial depth was reached. The term is often used in connection to hydrocarbon exploration where net changes in the burial depth are important for assessing the potential of a petroleum system.

3.1.2 Measurements

Measurements of the uplift involve considering the elevation changes (England and Molnar, 1990). This is rarely feasible because it requires the preservation of a sequence of rocks that were deposited during that uplift, containing evidence of surface elevation at the times of their deposition. If an uplift event occurred above the sea level this condition is not often fulfilled because erosion commonly takes place in subaerial settings. In contrast, if the uplift occurred in marine environments, the sedimentary record might be present making the uplift measurement possible (England and Molnar, 1990).

The net erosion thickness (i.e. change in a burial depth for a marker horizon) can be measured by using various methods (Table 1). Generally the methods might be divided into tectonic-, thermal-, compaction- and stratigraphic-based methods (Corcoran and Doré, 2005).

Table 1 Methods used for determining (net) erosion magnitude. The references refer to applications of the methods to the Barents Sea.

Methods	Application examples to the Barents Sea
Tectonic-based	Clark et al. (2014)
Thermal-based	Linjordet and Grung-Olsen (1992); Nyland et al. (1992); Green and Duddy (2010)
Compaction-based	Tsikalas (1992); Richardsen et al. (1993)
Stratigraphic-based	Faleide et al. (1996); Laberg et al. (2012)

Tectonic-based methods use lithospheric stretching models that predict subsidence rate versus time for a given stretching factor β (McKenzie, 1978). The theoretical subsidence curves are compared with observed tectonic subsidence curves derived by backstripping calculations (Allen and Allen, 2004; Clark et al., 2014). Deviation of the curves might indicate erosion events. By using several assumptions the magnitude and ages of erosion can be estimated. The methods are not applicable in areas where the McKenzie model cannot be used, i.e. where no crustal stretching was involved (Corcoran and Doré, 2005).

Thermal methods are based on peak palaeotemperatures interpreted from vitrinite reflectance (VR), apatite fission-track analysis (AFTA), fluid inclusions and other palaeo-thermal indicators in sedimentary sequences (Green et al., 1986; Sweeney and Burnham, 1990; Walderhaug, 1992). The maximum palaeo-temperatures are then used for constructing the thermal gradient profiles and compared with theoretical profiles based on the present-day temperatures. The comparison provides an insight about the sequences that were subjected to higher heating than expected from the present-day burial depth. This might be interpreted as former deeper burial and based on assumptions the erosion thickness can be estimated. In addition, AFTA provides direct estimates of erosion timing (Green et al., 1986). Application of the thermal methods is mostly limited in areas where advective heating has occurred (Corcoran and Doré, 2005).

Compaction-based methods use the principle that sediments reduce their porosity during burial as a result of mechanical and thermochemical processes (Corcoran and Doré, 2005). The measured compaction profiles can be compared with set of standard compaction curves (e.g. Sclater and Christie, 1980). Based on the discrepancy between theoretical and measured curves greater burial depths can be indicated and the erosion thickness might be estimated. Often the porosity profiles are estimated by using seismic techniques, e.g. sonic transit time (Richardsen et al., 1993).

Stratigraphic correlation-based techniques use present-day outcrop distributions as indicators for the time-integrated erosion history of an area. These techniques cover a wide family of methods that include geomorphological analysis, seismic stratigraphic interpretation, stratigraphic and palaeo-geographic reconstructions (Riis and Jensen, 1992; Corcoran and Doré, 2005). The mass-balance method should specially be pointed out because the method has often been used for estimating the total glacial erosion amount in the Barents Sea (Fiedler and Faleide, 1996; Hjelstuen et al., 1996; Dimakis et al., 1998; Elverhøi et al., 1998; Laberg et al., 2012). The method uses a volume of the clastic sediments from a given time period in a depocenter which is compared with the size of drainage area.

3.1.3 Consequences of the isostatic movements

Overall the processes of uplift, erosion and ice loading might have a strong impact on sedimentary basins and petroleum systems (Nyland et al., 1992; Doré and Jensen, 1996; Lerche et al., 1997; Doré et al., 2002; Cavanagh et al., 2006) (Table 2 and Figure 9).

Differential uplift (a part of a basin is uplifted by a different magnitude than the other part) leads to significant changes in the basin architecture causing either movements along faults or tilting of the entire basin (Nyland et al., 1992; Doré and Jensen, 1996). The differential movements and pressure gradient changes are important factors leading to hydrocarbon trap capacity changes (see Paper 3 for details) as well as changes in drainage and hydrocarbon migration directions (Doré and Jensen, 1996; Ohm et al., 2008). Uplift and erosion are key factors controlling the cap-rock (seal) properties potentially resulting in cap-rock fracturing and/or cap-rock capacity decrease due to reduction of confining pressure and temperature (Doré et al., 2002).

Table 2 Impact on uplift, erosion and ice loading with related isostatic response on sedimentary basins and petroleum systems.

Uplift	**Erosion**	**Ice loading**	**Impact on**
x		x	Structural changes in a sedimentary basin
x		x	Hydrocarbon trap capacity change
x	x	x	Fault reactivation
x	x	x	Change of drainage and migration patterns
x	x	x	Fracturing of cap-rock
	x	x	Change in reservoir quality
	x	x	PVT changes in the reservoirs
	x	x	Change in cap-rock capacity
	x	x	Changes in thermal regime

Basins subjected to erosion show higher degrees of compaction level at the same depth compared to basins which did not experience erosion due to different maximum burial depths (Henriksen et al., 2011a). Erosion leads to change in the temperature and pressure in reservoirs, and in result, fluid density changes. This in turn might cause hydrocarbon spillage due to volumetric changes of the reservoir fluids (Ohm et al., 2008). The removal of overburden impacts the thermal gradients of a sedimentary basin leading to a decrease in the temperatures at the same depth leading to reduction of the hydrocarbon generation rates (Duran et al., 2013)

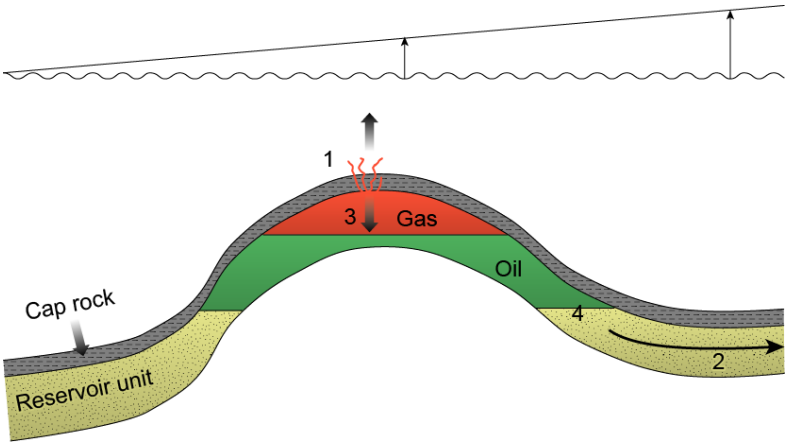

Figure 9 A hypothetical hydrocarbon trap (not to scale) affected by uplift and erosion. Major potential consequences of uplift and erosion for petroleum systems (1-4). 1: Fracturing of cap rock due to depressurisation (reduction of the pore pressure, driven by erosion), 2: Changed migration paths due to tilting, 3: Gas exsolution from oil due to depressurisation, 4: Reduced generation and expulsion due to reduced burial depth. Sintef Petroleum (unpublished).

Potential consequences of ice sheet loading are similar to these described for uplift and erosion and incorporate the structural, thermal and pressure changes in sedimentary basins (Kjemperud and Fjeldskaar, 1992; Riis and Fjeldskaar, 1992; Lerche et al., 1997) (Table 2). The main driving mechanism of these processes is weight of the ice sheet and temperature change at the surface. Glaciations can cause structural changes, including tilting, fault reactivation, fracturing, and as a result hydrocarbon spillage, drainage and secondary migration patterns change. Pressure and temperature gradient alterations can also impact the migration directions, fluid and cap-rock property changes. Due to shift of the surface temperature the temperature gradient of a sedimentary basin can also be altered (Lerche et al., 1997; Cavanagh et al., 2006).

3.2 Isostasy

The principle of *isostasy* explains the state of gravitational equilibrium between the crust and mantle of the Earth in the absence of disturbing forces (Watts, 2001). Isostasy describes why different

topographic features can exist at the surface such as high mountains. It also explains at what magnitude different geological processes disturbing the equilibrium state, such as sediment redistribution, ice loading and volcanism, are compensated by the isostatic forces. Different hypotheses have been suggested based on this principle. The traditional Pratt-Hayford hypothesis assumes that the isostatic depth is constant and different topographic heights are compensated by lateral changes in rock density. According to the Airy-Heiskanen hypothesis the crust of the Earth floats on the mantle so that topographic highs are compensated by changes in the crustal thickness. The main differences in the hypotheses are presented in Figure 10.

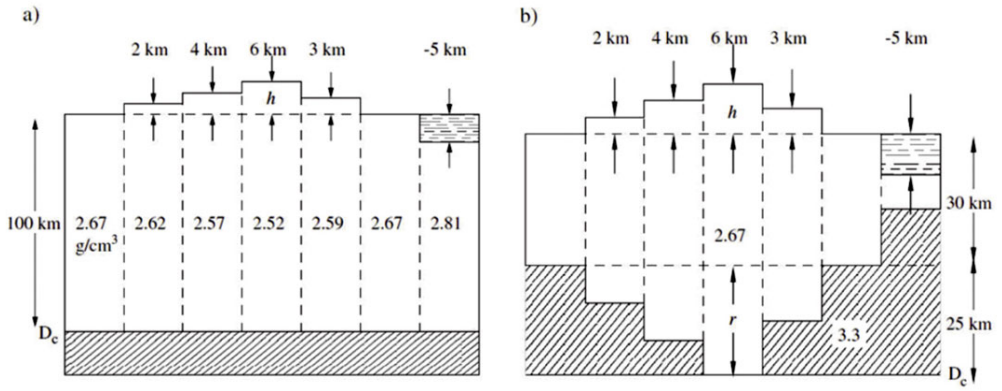

Figure 10 a) Isostatic compensation model of Pratt-Hayford. Topography, h, is supported by columns of different density, above a compensation depth, Dc, relative to normal density crust. b) Airy-Heiskanen's model of isostasy. Topography, h, is supported by a crustal root, r, of lower density relative to mantle density (Close, 2010).

Airy-Heiskanen and Pratt-Hayford models assume the load is compensated by local changes of the crustal thickness or crustal density in which each column exerts an equal pressure at the compensation level (Lowrie, 2007). Based on present-day knowledge state small irregularities in the Earth's crust are however not supported by either variable crustal thickness nor density changes. Also the isostatic response was found to cover larger areas than the area of actual loading. It might be said that the isostatic response has not a local (as suggested by Airy-Heiskanen and Pratt-Hayford's models) but a regional character. A modified Airy-Heiskanen model, where the regional compensation aspect is considered, was formulated by Vening-Meinesz (1941). It is often called a flexural isostasy model because the applied load results in development of a flexure (Figure 11).

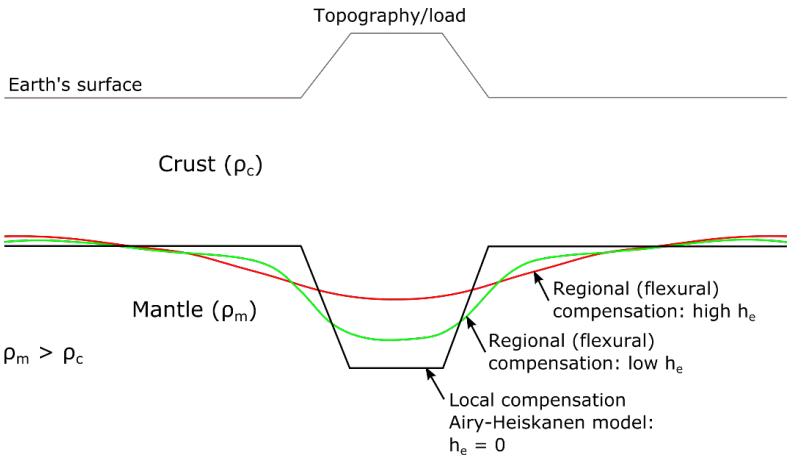

Figure 11 Expected deflection in local (Airy-Heiskanen) and regional/flexural (Vening-Meinesz) compensation models. ρ_c = crustal density, ρ_m = mantle density, h_e = elastic thickness of the lithosphere. Modified after Close (2010).

An applied load (positive or negative) causes bending (flexure) of the lithospheric plate. The applied load is partly supported by the shear stress of the lithosphere and partly by the buoyant forces of the asthenosphere (Turcotte and Schubert, 2002). The flexure depends on the elastic properties of the lithosphere. The property that controls the resistance to bending of an elastic plate overlying the asthenosphere is defined as flexural rigidity (D):

$$D = \frac{E{h_e}^3}{12(1-\upsilon^2)}$$

where E is Young's modulus, υ is Poisson's ratio and h_e is elastic plate thickness. Figure 11 shows that deflection size depends on thickness of the elastic lithosphere. The thicker the elastic plate is, the more the regional character of the deflection. For thinner plates the deflection tends to local deflection. A perfectly local isostatic response ($h_e = 0$) is defined by Airy-Heiskanen model. For the Scandinavia and Barents Sea region the thickness of the elastic plate is normally estimated as 10 - 50 km (Fjeldskaar et al., 2000; Gac et al., in press).

The deflection caused by a loading is dependent on the distance from the load center (Figure 11). It might be observed that in peripheral parts a load does not cause a depression, but instead shows a peripheral bulge (upwarp) adjacent to the deflection (Figure 11). In flexural isostasy relation between applied force per unit length q, flexural rigidity D, horizontal force P and resulting deflection w as a function of distance x is given by:

$$q(x) = D\frac{d^4w}{dx^4} + P\frac{d^2w}{dx^2}$$

Bending of the elastic plate is also dependent on a load size. For long-wavelength loads the lithosphere has no rigidity. In that case the applied load causes flexure and full compensation by the buoyant forces of the asthenosphere. On the other hand, for short-wavelength loads the lithosphere becomes infinitely rigid. It occurs if a load wavelength λ, is sufficiently shorter than $2\pi(D/\rho_c g)^{1/4}$ (also in length dimension) where ρ_c is crust density and g is gravitational acceleration. As a result, loads of this scale cause almost no flexural response. In this context the lithosphere is called a low-pass filter. It filters out low-wavelength loads that do not cause any deflection and passes only high-wavelength loads. For this reason a short topographic anomalies such as narrow valleys may not cause bending of the lithosphere (Turcotte and Schubert, 2002).

The lithosphere floats on the asthenosphere which is of low viscosity. The isostatic response is therefore not immediate but time-dependent and represented by relaxation time which is the time required for a function to decrease to 1/e (36.8%) of the equilibrium value. The relaxation time of the Scandinavia region is usually estimated as a few thousand years (Fjeldskaar, 1997; van den Berg et al., 2008), so on a geological-time scale the response is almost instantaneous. The relaxation time is independent on a load composition and whether the load is positive or negative (for example erosion).

4 Methods

Different numerical methods have been used in this thesis for evaluating the glacial impact on sedimentary basins of the Barents Sea (Table 3). Some of them are novel methods, developed for this thesis, while some are well-established methods. Description of the methods is provided in the attached papers. Background information and detailed worflow regarding flexural isostasy modelling in 3D is not provided in the papers but it is summarized in 3.2 and further in this chapter.

Most of the data used in this thesis comprise published literature and publically available datasets. The literature data are listed in the papers. The main datasets include well data (Norwegian Petroleum Directorate, http://factpages.npd.no/factpages) and present-day topographic relief model Etopo5 (NOAA American National Oceanic and Atmospheric Administration, http://www.ngdc.noaa.gov/mgg/global/etopo5.html). The seismic data used in Paper 3 was kindly provided by ENI Norge.

Table 3 List of the methods used in this study.

Method	**New/ established**	**Used in paper**	**Provided description**
Estimation of the local glacial ages	New	Paper 1	Full explanation in the paper
Assessment of the glacial contribution to net erosion	New	Paper 1	Full explanation in the paper
3D Flexural isostasy modelling and topography reconstruction	Established	Papers 2 and 3	Background information and detailed workflow in the thesis
Secondary migration modelling	Established, partly modified	Paper 3	Full explanation in the paper

4.1 Flexural isostasy modelling and topography reconstruction

In Papers 2 and 3 the magnitude of the isostatic response due the Pleistocene redistribution and ice loading was calculated by using flexural isostasy modeling. The isostatic response calculations were also used for restoring palaeo-topography of the Barents Sea region (Paper 2). A general modelling scheme of the isostatic response to the sediment redistribution and topographic reconstruction is shown in Figure 12. The isostasy and palaeo-relief was calculated backward in time. It practically means that the present-day topography is used as the initial one (Figure 12A). The past loads are restored to their original position at intended age of reconstruction (Figure 12B). Next, the isostatic response effect of the restored loads is modelled

and the topography is adjusted to the isostatic movements (Figure 12C). Modelling of the isostatic response and topography at older ages involves the reconstructed topography from the younger age as the initial one and the same procedure as described before.

Modelling of the lithosphere downwarp due to ice sheet loading (Paper 3) involves a simple forward-time exercise. The effective weight of the ice sheet is applied on a lithosphere and the flexural isostatic deflection is calculated. The effective weight refers to the ice weight reduced by the buoyancy of the sea water the ice sheet is immersed in. Therefore the effective weight is dependent on the bathymetry.

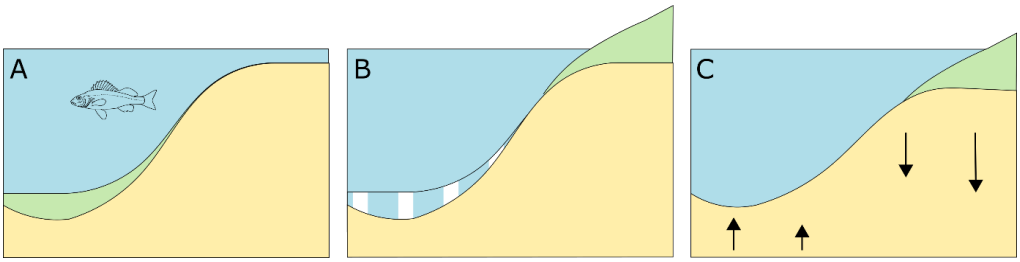

Figure 12 A simplified view of restoration of the palaeo-relief and calculations of the isostatic response to the sediment redistribution. A) Present-day bathymetry. Green unit represents redistributed sediments. B) Sediment restoration. The sediments that were deposited in the deep parts (left) are moved back to their original position at the shallow parts (right). C) Calculation of the isostatic response to the sediment restoration (arrows). Adjustment of the relief to the isostasy.

The topography and isostasy reconstructions were performed by using 3D flexural isostasy Matlab script (Cardozo, 2009). For input variables see Papers 2 and 3. The modelling generally follows the description provided above. Technically, created modelling workflow involves several interlinked calculation steps where the script is executed for multiple times. For workflow see Figure 13.

The eustatic sea level varied between 0 and 100 m during the Pleistocene (de Boer et al., 2014). Eustasy can affect the results to some degree and therefore its effect is considered in the reconstructions. In step 1 the isostatic response to the sea level change is calculated. The final outcome represents a topographic relief adjusted for the sea level change and isostasy. In step 2 this relief is used as a basis for calculations of the isostatic response to the sediment redistribution. Here, it is calculated the isostatic response to the sea water that is either replaced by the sediments or added due to sediment removal. Thanks to this calculation step the problem of the inhomogeneous sea water depth (that counteracts sediment weight due to the buoyancy) and variable sediment thickness is eliminated in the subsequent calculations (step 3). The isostatic response calculated in step 2 causes changes in of the sea water depths that in turn

disturb the isostatic equilibrium. Therefore the weight of created/removed water needs to be stored and the isostatic response to the sea water thickness needs to be calculated later (step 4). In step 3 the response to actual sediment redistribution is calculated. The calculations are performed without correcting for the sea water buoyancy (this is eliminated in step 2). In step 3 the isostatic response again causes changes in the sea water depths. The weight of the created/removed water is stored and the isostatic response to sea water thickness is calculated in step 4. In step 4 response to the created/removed water due to the isostatic adjustments (from step 2 and 3) is calculated. The aim of step 5 is to model a final palaeo-topography. The reconstructed bathymetry for the eustatic sea level change is taken as a basis for the calculations. The sediments are then restored in the same way as in Figure 12B resulting in a temporary topography. As a final stage, all of the isostatic corrections (from step 2, 3 and 4) are applied to the temporary relief. The relief with restored sediments and corrected for the isostasy represents the final outcome of the modelling workflow.

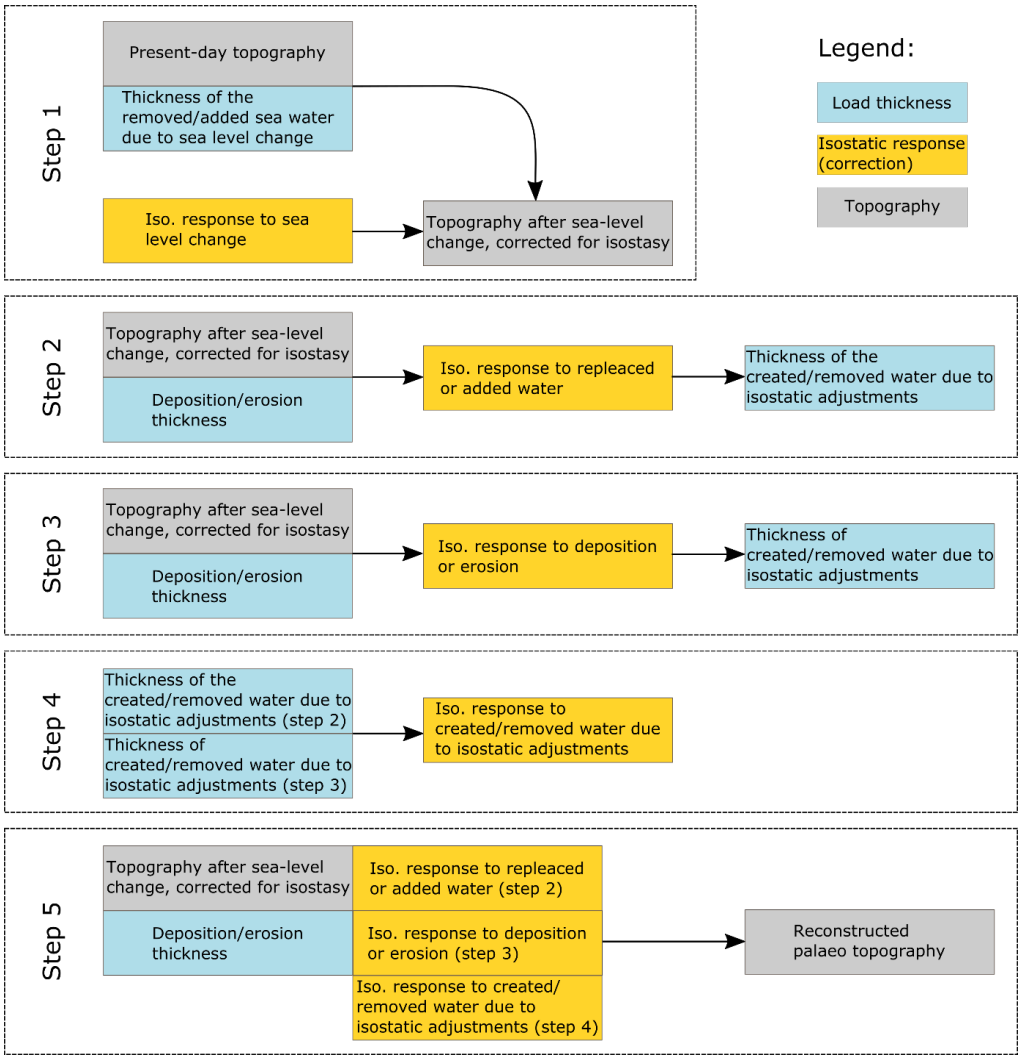

Figure 13 The workflow used for reconstruction of the palaeo topography and isostatic response to the sediment redistribution. Iso. = isostatic. See text in this chapter for details.

5 Work synthesis

The three interlinked papers provide a new insight on several aspects about the Pleistocene impact on the sedimentary basins and petroleum systems in the Barents Sea. Overall the thesis results apply to the southern Barents Sea, while some of the work was focused in the outer Bear Island Trough (Figure 1). Paper 1 presents a first attempt to estimate the glaciation ages in the westernmost Barents Sea for most of the Pleistocene (1.5 - 0.0 Ma). This outcome combined with available literature data resulted in a first approximation of the Pleistocene glacial history of the Barents Sea. Thanks to estimates of the glacial durations and available sedimentary record, a new assessment of the Pleistocene sedimentary conditions on a glacial-time scale (1 - 10 kyr) was made. The average net glacial and interglacial deposition rates were constrained in the outer Bear Island Trough which represents the transition between mostly erosional and depositional areas of the Barents Sea shelf during the Pliocene-Pleistocene (Faleide et al., 1996; Laberg et al., 2012). Rates of net deposition were further used for estimating the total thickness of eroded and deposited sediments, and as a result, a balance between them considered as glacial contribution to the net erosion. The net erosion is thought to develop due to both glacial activity and pre-glacial, tectonically-driven mechanisms during the Cenozoic (Riis and Fjeldskaar, 1992; Doré and Jensen, 1996; Dimakis et al., 1998; Cavanagh et al., 2006; Henriksen et al., 2011a; Japsen et al., 2014; Baig et al., 2016). The work is concluded by providing a quantitative ratio of the glacial vs. tectonic contribution to the net erosion in the outer Bear Island Trough.

The problem of the glacial sediment redistribution was followed up in the Paper 2. In the paper a link between the sediment redistribution, isostatic movements and topography changes was addressed. The resulting uplift magnitude was used to assess the importance of the isostatic vs. tectonic components of the total Barents Sea uplift providing new arguments for discussion about the uplift mechanisms (Nyland et al., 1992; Doré, 1995; Doré and Jensen, 1996; Rasmussen and Fjeldskaar, 1996; Cavanagh et al., 2006; Henriksen et al., 2011a). The topography reconstructions presented in Paper 2 include pre-glacial and Middle Pleistocene relief. The early Pleistocene relief was correlated with Miocene–Pliocene shelf break development inferred from seismic data. At present, the bathymetry of the Barents Sea consists of deep troughs and adjacent shallow banks developed in response to selective glacial erosion and deposition (Vorren et al., 1989; Sættem et al., 1994; Andreassen et al., 2008; Laberg et al., 2012). A hypothesis of regional isostatic uplift affecting the topographic relief was also tested. The Barents Sea bathymetry controls the northern Atlantic thermohaline circulation and climate at high northern latitudes (Hurdle, 1986). In Paper 2 this issue was addressed providing

estimates for how long the topography restricted bifurcation of the North Atlantic Current during the Pleistocene. The reconstructed shelf relief was also used for providing first approximations of the maximum Barents Sea ice sheet extent prior to the Weichselian.

The main conclusions of Paper 2 regarding the Pleistocene isostatic adjustments were used in the Paper 3. In addition, in Paper 3 the isostatic response to the ice sheet loading was quantified. The consequences of the isostatic movements on tilting of sedimentary basins, geometrical changes of hydrocarbon traps and fluid migration were addressed. The main objective of Paper 3 was to study if the Pleistocene burial history could have been responsible for major hydrocarbon loss in the Bjørnøyrenna Fault Complex, western Barents Sea, demonstrated by the palaeo-oil shows at present. It was quantified at what magnitude the hydrocarbon trap capacities could have been changed and how much of the hydrocarbons could have been spilled out during the Pleistocene. It was shown which factors control the trap capacity change and amount of spillage. Also, issues of the hydrocarbon spill direction and potential secondary migration pattern changes were addressed. The paper is concluded by giving estimates of how much of the hydrocarbon loss is attributed to glacial spillage and how much to other processes including leakage and pre-glacial spillage (Doré and Jensen, 1996; Ohm et al., 2008; Fanavoll et al., 2012; Duran et al., 2013; Hermanrud et al., 2014).

6 Papers

6.1 Paper 1

Zieba, K.J., Felix, M., Knies, J., (2016). The Pleistocene contribution to the net erosion and sedimentary conditions in the outer Bear Island Trough, western Barents Sea. Arktos, Springer.

The main aim of Paper 1 was to estimate glacial contribution to the net erosion that is measured by using different methods in the Barents Sea shelf. The study area focuses on a transitional zone between mostly erosional and depositional areas during the Pliocene-Pleistocene (Faleide et al., 1996; Laberg et al., 2012). The problem was approached by a new Monte Carlo-type method by testing wide ranges of erosion and deposition rates. The calibration was performed by comparing the modelled glacigenic cover thickness with measured thickness at well locations. This approach requires definite ages when the ice sheet was present in the study area. Ages for the modelling time period were not available, therefore the ages were assessed by using a new method based on a regional ice-sheet-volume curve.

The main modelling results suggest that the western Barents Sea was glaciated during 4 marine isotope stages: MIS 16 (635.6 - 624.7 ka), MIS 12 (438.7 - 428.0 ka), MIS 6 (138.6 - 134.6 ka) and MIS 2 (19.3 - 16.0 ka) for a total duration of 29 kyr. During the first event the study area was subjected to relatively homogenous erosion of 24.2 ± 8.5 mm/yr. Between the first and the second glacial events a shift in sedimentary conditions was modelled resulting in inhomogeneous erosion rates over the study area and substantial change of the erosion rates. In the most eastern part, at the proximal part of the Bear Island Trough Mouth Fan, the possible rates reached their maximum values (1.6 ± 1.8 mm/yr). Further west, in the more distal part of the fan, the possible rates were modelled as -12.6 ± 1.6 mm/yr (net deposition). Average deposition rates during warm periods were found to be relatively homogeneous in the Bear Island Trough during the Middle–Late Pleistocene. The most likely values were modelled at about 0.12 ± 0.1 mm/yr. In contrast to the inner shelf area, in the outer Bear Island Trough the net erosion was found to be mainly the effect of tectonic uplift and subsequent erosion prior to the glacial ages. The results show that in the proximal part of the Bear Island Trough Mouth Fan, the Pleistocene glacial contribution to the total net erosion was small. The most likely glacial contribution in this area reaches 100 m, which is about 9% of the total net erosion. In the more distal part of the fan, the glaciations did not contribute to the net erosion.

Paper 1

Is not included due to copyright

6.2 Paper 2

Zieba, K.J., Omosanya, K.O., Knies, J., (submitted). The Pleistocene evolution of the southern Barents Sea bathymetry: a flexural isostasy modelling approach. Norwegian Journal of Geology, Geological Society of Norway.

The problem of the bathymetric development of the Barents Sea shelf during the Pleistocene was a main focus of Paper 2. In the paper an issue of the regional lithospheric compensation to the glacial erosion and deposition was addressed. Another aim of the paper was to provide an insight about tectonic versus isostatic cause of the Cenozoic uplift in the Barents Sea. Also the impact of the topographic relief on potential ice sheet extent and on the thermohaline circulation in the northeastern Atlantic was studied. The addressed issues were approached in the paper by using the flexural isostasy modelling method. Seismic interpretation was also used for correlation of the Miocene-Pliocene shelf development with the Pleistocene topography.

The results show the pre-glacial relief was close to the sea level with the deepest parts at about 100 - 150 m bsl (below sea level) and the shallowest at about 300 m asl (above sea level). The most prominent present-day bathymetric features were initiated before the glaciations possibly formed as a response to tectonic uplift and related structural development. Between the Early and Middle Pleistocene the relief was deepened by 0 - 200 m with the highest values in the Bear Island and Ingøydjupet troughs and the lowest on the banks. During the Middle Pleistocene the Barents Sea shelf was modelled at shallow marine conditions with some elevated parts above the sea level. During the Middle–Late Pleistocene the shelf was deepened by up to 250 m in the troughs and up to 100 m on the banks. The model suggests that the inflow of the North Atlantic Current to the Barents Sea was barred by the topography up to ~0.7 Ma, about 0.3 Ma later than proposed in the literature before. Conceptual maximum ice extent lines suggest the maximum extent can be expected to occur during the most recent glaciations. The maximum ice extent lines during the Early and Middle Pleistocene were located up to 90 km east of the present-day shelf edge. The results show the glacial erosion together with the sea level change caused the isostatic uplift in the range of 250 - 400 m in the troughs and below 200 m in the banks. Given that the total uplift magnitude is estimated at about 1 - 2 km (Nyland et al., 1992; Green and Duddy, 2010), the isostatic component of the uplift is deemed to be relatively small. The literature suggests that the glacial erosion and deposition controlled by initial topography were the main factors that shaped the Barents Sea relief during the Pleistocene (Vorren et al., 1989; Sættem et al., 1994; Andreassen et al., 2008; Laberg et al., 2012). The topographic relief was

however also affected by the regional isostatic adjustments that were found to be partly responsible for shaping the present-day bathymetry.

Paper 2

The Pleistocene evolution of the southern Barents Sea bathymetry: a flexural isostasy modelling approach

Krzysztof Jan Zieba[a], Kamaldeen Olakunle Omosanya[b], Jochen Knies[c,d]

[a] *Department of Geology and Mineral Resources Engineering, Norwegian University of Science and Technology (NTNU), NO-7491 Trondheim, Norway*

[b] *Department of Petroleum Engineering and Applied Geophysics, Norwegian University of Science and Technology (NTNU), NO-7491 Trondheim, Norway*

[c] *Geological Survey of Norway, Leiv Eirikssons vei 39, NO-7040 Trondheim, Norway*

[d] *CAGE - Centre for Arctic Gas Hydrate, Environment and Climate; Department of Geology, University of Tromsø, NO-9037 Tromsø, Norway*

Submitted to Norwegian Journal of Geology, Geological Society of Norway.

Abstract

The topographic relief of the southern Barents Sea shelf was subjected to major changes during the past 1.5 million years (Ma) mostly due to sediment redistribution driven by glacial activity. This paper addresses the problem of the Pleistocene bathymetry evolution by using a numerical modelling approach that considers an aspect of regional isostasy influence on the relief development. The results show that most of the prominent bathymetrical features were initiated prior to the first documented shelf edge glaciations at around 1.5 Ma. During the Early Pleistocene the Barents Sea shelf was close to sea level with some areas elevated to about 300 m. Most of the shelf experienced up to 200 m topography reduction during the Early to Middle Pleistocene (1.5 - 0.7 Ma). Later during the Middle Pleistocene–Present (0.7 – 0.0 Ma) the relief deepened by approximately 0 to 250 m. The results suggest that the present-day topography of the southern Barents Sea is the result of glacial activity affected by the regional isostatic component developed in response to selective trough erosion and significant deposition at the Barents Sea margins.

Keywords

Barents Sea; shelf; Pleistocene; glaciations; bathymetry; topography; numerical modelling; flexural isostasy

1 Introduction

The Barents Sea has experienced a gradual change in topography since the intensification of the Northern Hemisphere glaciation (INHG), 2.7 million years ago. A subaerial to shallow marine shelf was transformed to the contrasting submarine relief of deep troughs and relatively shallow banks observed at the present (Andreassen et al., 2008; Laberg et al., 2010; Vorren et al., 1991). The topography development is often attributed to glacial carving and sediment transport driven by glacial activity (Andreassen et al., 2004; Andreassen et al., 2007; Patton et al., 2015; Vorren et al., 1989). Sediment redistribution might have also caused regional isostatic adjustments exceeding the area of actual erosion or deposition due to the lithosphere rigidity (Medvedev et al., 2013). This in turn might have also affected the development of the relief, but the actual contribution of the process is unknown.

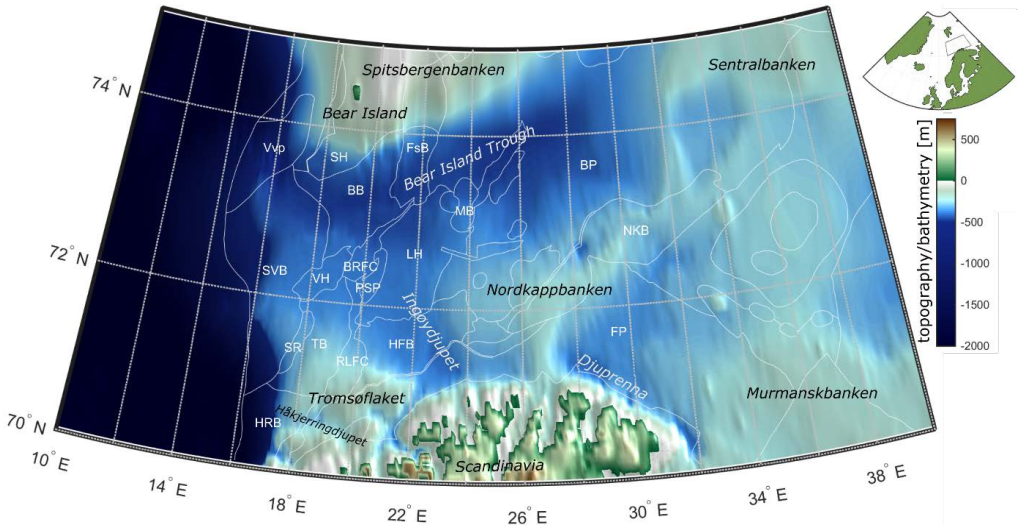

Fig. 1 Present-day bathymetry of the study area including names of discussed geomorphological features and structural elements (Etopo5 model, http://www.ngdc.noaa.gov/mgg/global/etopo5.html). BB: Bjørnøya Basin, BP: Bjarmeland Platform, BRFC: Bjørnøyrenna Fault Complex, HFB: Hammerfest Basin, FsB: Fingerdjupet sub-basin, FP: Finnmark Platform, HRB: Harstad Basin, LH: Loppa High, MB: Maud Basin, NKB: Nordkapp Basin, PSP: Polheim Subplatform, RLFC: Ringvassøy-Loppa Fault Complex, SH: Stappen High, SR: Senja Ridge, SVB: Sørvestsnaget Basin, VH: Veslemøy High, Vvp: Vestbakken volcanic province.

The first efforts that tackled the problem of the Pleistocene bathymetry date back to the work of Nansen (1904). He, mostly based on the present-day bathymetry and onshore observations, suggested a subaerially exposed shelf prior to the glaciations. The problem was revisited later in the 1990s and early 2000s mostly thanks to new geophysical data containing information about the sediment volumes eroded from the shelf and deposited as the Bear Island and

Storfjorden trough mouth fans during the Cenozoic (Butt et al., 2002; Dimakis et al., 1998; Elverhøi et al., 1998; Knutsen et al., 1992; Rasmussen and Fjeldskaar, 1996; Vorren et al., 1991). Rasmussen and Fjeldskaar (1996) proposed a first numerical approach based on a combination of the volume of pre-glacial deposits and tentative post-rift topography outlines. Further developments resulted in topography reconstruction of both prior and after the INHG (Butt et al., 2002; Dimakis et al., 1998). The bathymetrical reconstructions conducted by using local isostatic response to the sediment unloading (Airy model) were based on generalized (but the only available at that time) estimates of glacial sediment volume and homogeneous erosion distribution on the shelf.

This paper presents a numerical approach towards development of the Pleistocene relief of the southern Barents Sea region (Fig. 1). The reconstruction uses of the revisited Pleistocene erosion and deposition maps (Laberg et al., 2012) and incorporates the effects of the global sea level change (de Boer et al., 2014). The reconstructions are made for two time slices: (1) The early Pleistocene (~1.5 Ma), and (2) the middle Pleistocene (~0.7 Ma). The results also provide a first approximation of the geometry and water depth evolution along the western continental margin that potentially affected the maximum ice sheet extent (Stokes et al., 2015) as well as northward heat and salt transport through advection of warm North Atlantic waters (Hurdle, 1986). Regional isostatic response on the massive sediment deposition and selective erosion, as well as topographic development, will be addressed in this paper. In addition, modelled isostatic response to the sediment redistribution will also provide new arguments in the discussion of tectonic vs. isostatic contributions to the Barents Sea uplift (Cavanagh et al., 2006; Doré, 1995; Doré and Jensen, 1996; Henriksen et al., 2011; Nyland et al., 1992; Rasmussen and Fjeldskaar, 1996).

2 Cenozoic evolution of the southern Barents Sea

The evolution of the southwestern Barents Sea was mostly controlled by Devonian to Cenozoic tectonic events mainly related to rifting in the northern Atlantic. Those events generated the complex geological setting with deep basins, platforms and highs and the associated deposition and erosion history (Faleide et al., 2008). The sedimentary succession of the southeastern Barents Sea basin does not show evidence of any large extensional movements and is thought to have remained relatively stable since the Late Paleozoic (Faleide et al., 1993; Klitzke et al., 2015).

The Cenozoic structural development of the Barents Sea is mostly related to early Cenozoic rifting and development of a sheared margin in the west, continental breakup and subsequent opening of the Norwegian-Greenland Sea (Faleide et al., 2008). The breakup and related thermal activity might have resulted in an uplift and erosion of the central-eastern Barents Sea (Faleide et al., 1993; Green and Duddy, 2010). During the Late Paleocene marine conditions were established in the western Barents Sea and persisted throughout the Eocene resulting in substantial amount of deposition in the entire Barents Sea shelf (Faleide et al., 2008; Gabrielsen et al., 1990; Japsen et al., 2014; Riis, 1996; Ryseth et al., 2003; Vorren et al., 1991; Wood et al., 1989). A major reorganization in the plate motion took place at the Eocene–Oligocene boundary (Faleide et al., 2008; Japsen et al., 2014; Lundin and Doré, 2002). During the Oligocene and Miocene several phases of compression and basin inversion occurred as a result of plate tectonic movements in the northeastern Atlantic realm. A main phase of uplift and erosion affecting wide areas of the Arctic regions occurred during the Eocene–Oligocene transition, with onset between 40 and 30 Ma (Faleide et al., 1993; Green and Duddy, 2010; Japsen et al., 2014). The widespread uplift might have been caused by changes in plate motion or a thermal process and resulting flexure (Dimakis et al., 1998; Japsen et al., 2014; Rasmussen and Fjeldskaar, 1996). From the Oligocene the Barents shelf become tectonically stable (Clark et al., 2014; Faleide et al., 1993). The sedimentary conditions during the Oligocene–Middle Miocene are questionable due to a regional hiatus developed by the Cenozoic erosion events. Isostatic modelling suggests largely marine conditions in the Barents Sea at this time (Rasmussen and Fjeldskaar, 1996).

Late Miocene–Pliocene (10-5 Ma, Green and Duddy (2010)) uplift and erosion affected large areas in the Arctic including the Barents Sea (Anell et al., 2009; Faleide et al., 2008; Green and Duddy, 2010; Japsen et al., 2014; Zattin et al., 2016). Possible causes of this uplift event are a change of the stress field in the northeastern Atlantic and related basin inversion and/or thermal, lithospheric-scale anomalies and resulting elevation of the lithosphere-asthenosphere boundary (Dore et al., 1999; Zattin et al., 2016). The elevated subaerial Barents shelf is thought to prevail until ~1.6-1.0 Ma and developed further into a submarine-subglacial relief (Butt et al., 2002; Dimakis et al., 1998).

The Barents Sea represented a passive glaciated continental margin during the Pleistocene (Vorren et al., 1989) with the first shelf-edge glaciation occurring ca. 1.5 million years ago (Knies et al., 2009; Laberg et al., 2010). The youngest glacial history (post-Saalian, < 0.14 Ma) is relatively well constrained but little is known about the glacial extent prior to the Saalian

(Ingólfsson and Landvik, 2013; Knies et al., 2009; Patton et al., 2015; Svendsen et al., 2004). The glaciations led to sediment redistribution over the shelf-continental slope area and left a significant imprint on the Barents Sea shelf geomorphology characterized by deep troughs and relatively shallow banks. Most of the sediments eroded from the southern Barents Sea shelf by glacial and earlier pro-glacial processes were deposited on the outer shelf and on the continental slope as Bear Island Trough Mouth Fan developed at the mouth of the Bear Island Trough (Laberg et al., 2012; Vorren and Laberg, 1997).

3 Theory/calculation

3.1 Flexural isostasy modelling

Sediment redistribution will result in isostatic response of the effectively elastic lithosphere considered as a flat structure fixed at its sides. Erosion will be compensated for the loss of sediment weight by isostatic uplift while deposition by downwarping of the elastic plate (Turcotte and Schubert, 2002). The importance of this effect is numerically examined in the case of the southern Barents Sea by moving back the sediments to the original area and calculating the flexure of the lithosphere.

The palaeo-relief was modelled backward in time by adjusting the initial relief to the magnitude of the elastic response. The reconstruction of the elevation is provided for two time slices: (1) the early Pleistocene (1.5 Ma) and (2) the middle Pleistocene (0.7 Ma). The initial relief for the reconstruction at 0.7 Ma is the present-day relief, while for the reconstruction at 1.50 Ma the modelled relief at 0.7 Ma is used as the initial one. The relaxation time for the isostatic response in the Scandinavian region is usually estimated as a few thousand years (Fjeldskaar, 1997; van den Berg et al., 2008). Therefore it is reasonable to assume that the isostatic equilibrium was achieved during sediment redistribution events lasting for 0.1 – 1 Ma. Flexure calculations were performed by using the Matlab script of Cardozo (2009). The elastic calculations were performed on a 10 km grid resolution. The initial present-day elevation model ETOPO5 of 5-minute latitude/longitude grid was used.

The effective elastic thickness of the lithosphere (EET) is assumed to be 20 km uniformly distributed in the study area (Fjeldskaar, 1997; van den Berg et al., 2008). In order to quantify the influence of different EETs, a sensitivity test was performed where values of 10 km and 50 km were tested. The value of 10 km resulted in relief differences (comparing to 20 km EET) up to 50 m in confined areas, while 50 km gave topography differences up to 100 m, mostly in a

restricted area between 18 and 22°E. In this paper the results are provided only for EET = 20 km since different EET values do not alter first-order conclusions.

For simplicity, the density of the eroded sediments is considered to be equal to that of the deposited sediments (2200 kg/m^3) following Riis and Fjeldskaar (1992). A lower sediment density (1800 kg/m^3) was also tested, as suggested by Butt et al. (2002) and Rasmussen and Fjeldskaar (1996). This value results in higher topography compared to the used sediment density (2200 kg/m^3). The maximum difference was modelled as 50-100 m. In the model the density of the mantle is 3300 kg/m^3 and sea water 1025 kg/m^3.

3.2 Input loads

The main input to the elastic response and further to topography reconstruction includes Pleistocene erosion/deposition thickness estimates of Laberg et al. (2012). The erosion and deposition values were interpolated to maps as shown in Fig. 2. The erosion/deposition estimates are provided for two timespans constrained by ages of seismic reflectors R5 and R1. The age of reflector R5, that often marks onset of glaciations in the southern Barents Sea is dated at ~1.5 Ma (Knies et al., 2009; Mattingsdal et al., 2014). Reflector R1 is usually dated at ~700-440 ka (Elverhøi et al., 1998; Laberg et al., 2010; Sættem et al., 1992). Here, the oldest age of R1 is used so that the erosion/deposition estimates are considered to represent the time intervals of 1.5-0.7 Ma (Early–Middle Pleistocene) and 0.7-0.0 Ma (Middle Pleistocene–Present).

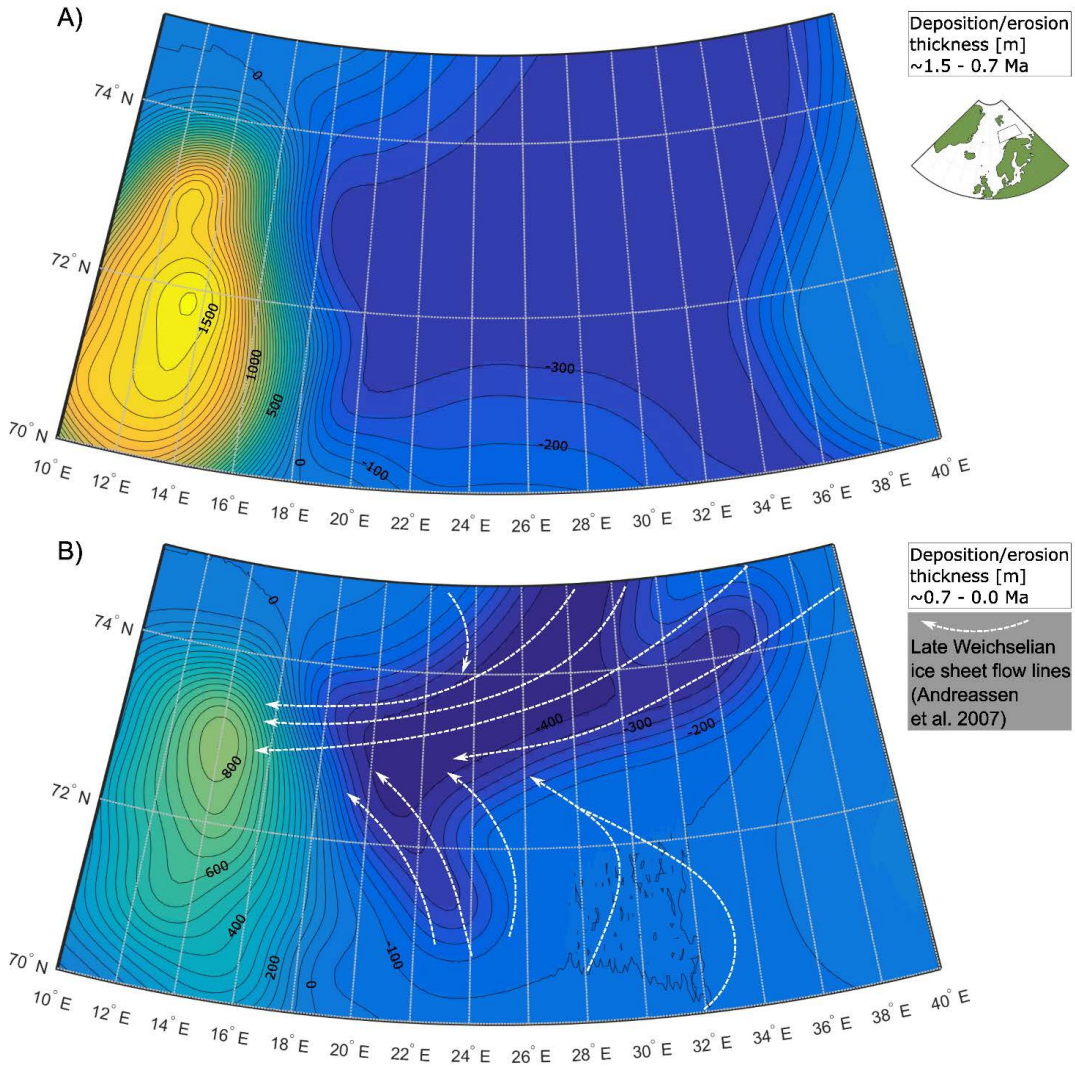

Fig. 2 Erosion/deposition thickness input data used in isostatic modelling. The data was interpolated from Laberg et al. (2012). A) Early Pleistocene – Middle Pleistocene sediment redistribution. B) Middle Pleistocene – Present sediment redistribution.

During the first time interval (1.5-0.7 Ma) glacial erosion resulted in the removal of an average of 330-420 m of sediments from the Barents Sea shelf (Laberg et al., 2012). The erosion is thought to have affected both troughs and banks by approximately the same magnitude. The erosion decreased to the south towards Scandinavia and to the north towards Spitsbergenbanken (Laberg et al., 2012). As modelling input it is assumed that the central Barents Sea experienced 330 m of erosion decreasing to 100-200 m in all directions (Fig. 2A). The outer shelf and continental slope experienced high deposition of the material transported by the glacial erosion

from the inner parts of the shelf. The deposition thickness reached ~1500 at its maximum value (Laberg et al., 2012).

The second time interval of sediment redistribution (0.7-0.0 Ma) resulted in high erosion of the troughs (440-530 m) and low erosion of the banks (Laberg et al., 2012). The maximum erosion thickness (here set as 440 m) is considered to occur in the Bear Island and Ingøydjupet troughs (Fig. 2B). The erosion of banks is conceptually set as 100 m increasing towards the troughs. The outer shelf and the continental slope deposition reached about 800 m at its maximum (Laberg et al., 2012).

The erosion estimates cover the drainage area of the Bear Island Trough Mouth Fan. Some parts of the study area (central-eastern part, Fig. 5) lie outside the drainage area where no erosion estimates are available. The erosion values outside the drainage area were however interpolated in order to avoid sharp input contrasts that can disturb the isostatic response. On topography/bathymetry reconstructions the area is masked as shown in Fig. 5. A model of topographic relief of the northernmost Scandinavia is provided along with the reconstructions of the southern Barents Sea. The used data and grid resolution is however too sparse for a detailed and reliable reconstruction. The topographic model of onshore Scandinavia, which is not a main focus of this paper, should therefore be treated only as a first approximation.

The modelling approach presented here takes into consideration the weight of removed or added water due to variations of the eustatic sea level changes. The values of the sea level relative to the present (de Boer et al., 2014) are as follows: The Early Pleistocene (1.50 Ma) sea level is considered as -50.2 m while the Middle Pleistocene (0.7 Ma) sea level was set as -22.2 m.

3.3 Seismic data

The seismic data used to complement this research is a post-stack time migrated 3D seismic cube acquired in 1998. The cube has a bin spacing of 12.5 m. With a P-wave velocity of ca. 2100 m/s and a dominant frequency of 40 Hz, the vertical seismic resolution for seismic cube is 13 m. Horizontal resolution of the data is equivalent to the bin size. The seismic data is displayed in Society for Exploration Geophysicists (SEG) normal polarity convention. An increase in acoustic impedance with depth is a positive reflection or peak. Peaks are black reflections on seismic sections. The red reflections are troughs or negative reflections while the white reflections represent the zero-crossings. Furthermore, check shot information from wellbore 7216/11-1S was used to do the seismic to well ties and define the ages of the horizons. There seems to be disparity in the age assigned to the horizons above the Miocene. Hence, this

study relied on the most common ages used for the Pliocene to Pleistocene reflectors. Furthermore, the shelf-edge position defined by Omosanya et al. (2016) was used to compare some of the results from the present study to see how the model fits with their seismic interpretation.

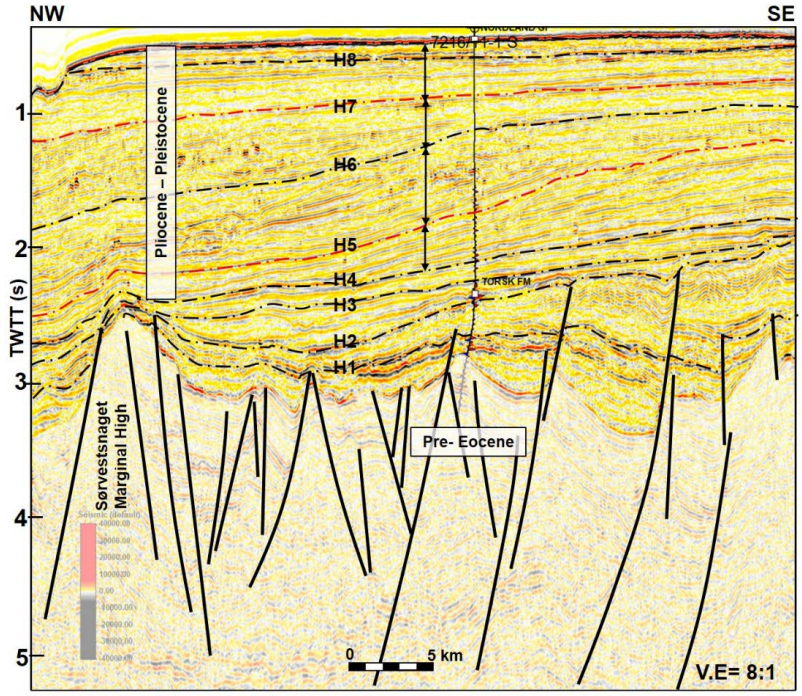

Fig. 3 NW to SE seismic section through the Sørvestsnaget Basin. The horizons of interest to this study are H4 to H8. Three Pliocene packages are defined and the trace of their shelf/edge position was identified by mapping the trajectory of shelf-edge clinoforms within them. H1 to H4 represent sediments of Eocene to Miocene ages while the underlying sediments are older and are severely faulted.

The seismic character of the main horizons used in this study is shown in Table 1. Horizon H4 corresponds to the base of the Pliocene and Pliocene 1 of Omosanya et al. (2016). Seismic reflector H5 represents Pliocene 2 (Omosanya et al., 2016). H7 corresponds to top Pliocene 3 of Omosanya et al. (2016) and base of the Pleistocene of Ryseth et al. (2003). On seismic sections, the packages underlying all these three horizons are characterized by shelf-margin clinoforms that are more than 1 km in height and about 40 km in length (Fig. 3). Omosanya et al. (2016) considered the packages to have flat to descending clinoforms from H4 to H5, which changes to high-angle ascending clinoforms from H5 to H6 and to low-angle ascending clinoforms at the top i.e., H6 to H7. The outline of the shelf-edge positions defined for these three packages is shown in Fig. 5A. All the previous authors agree that the package above H7

is Pleistocene in age (Butt et al., 2000; Geissler and Jokat, 2004; Hjelstuen et al., 2007; Knies et al., 2009; Mattingsdal et al., 2014; Myhre et al., 1995; Omosanya et al., 2016; Ryseth et al., 2003).

Table 1 The seismic character and ages of some of the interpreted seismic section.

Reflector	**Omosanya et al. (2016) /Ryseth et al. (2003)**
H4 **(High amplitude and continuous trough)**	Pliocene 1 (5.3 Ma) Flat to descending clinoforms
H5 **(High amplitude and continuous peak)**	Pliocene 2 High-angle ascending clinoforms
H7 **(High amplitude and continuous trough)**	Pliocene 3 (2.6 Ma) low-angle ascending clinoforms

4 Results

4.1 Isostatic readjustments of the lithosphere

The Early Pleistocene to Middle Pleistocene sediment redistribution (Fig. 2A) and sea level change (see 3.2) resulted in major isostatic readjustments of the Barents Sea region (Fig. 4A). The shelf area was largely uplifted between the Early Pleistocene (1.5 Ma), representing the onset of glaciations in the southern Barents Sea sensu Laberg et al. (2010) and Mattingsdal et al. (2014), and the Middle Pleistocene (0.7 Ma). The magnitude of uplift in the shelf area was modelled as being relatively uniform (150-200 m). The maximum values reaching 200 m were modelled in the Bear Island and Ingøydjupet troughs where most of the erosion took place (Fig. 2A). The uplift values were modelled to decrease towards peripheral parts of the shelf. This is mostly related to lower erosion rates on Spitsbergenbanken and the eastern part of the study area. On the outer shelf and continental slope high deposition rates resulted in a significant downwarping reaching up to 540 m at the deposition center (Fig. 2A).

The Middle Pleistocene–Present sediment redistribution (Fig. 2B) and sea level change resulted in isostatic uplift up to 200 m in the shelf area (Fig. 4B). The maximum values follow the erosion trend along the Bear Island Trough (Fig. 2B). Outside the Bear Island Trough the uplift values decrease in all directions. Almost no uplift or downwarping was modelled in the areas close to the present-day shelf edge and in the easternmost part of the study area. Further west the stratigraphic units of the present-day outer shelf and continental slope were subjected to downwarping (Fig. 4B). The maximum value is about 280 m within the deposition center (Fig. 2B).

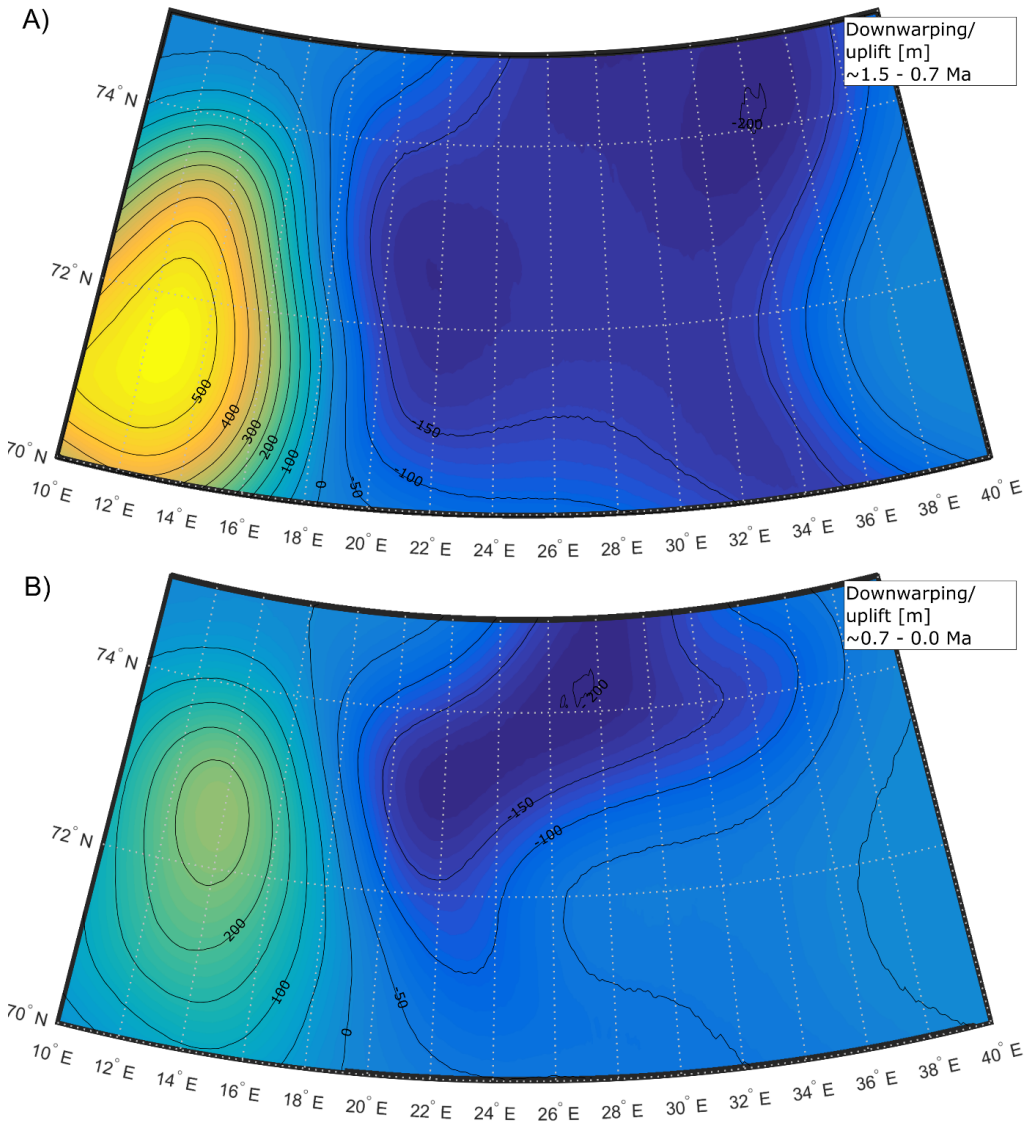

Fig. 4 A) Isostatic response to the Early Pleistocene – Middle Pleistocene sediment redistribution. B) Isostatic response to the Middle Pleistocene – Present sediment redistribution.

4.2 Topographic relief evolution

4.2.1 Early Pleistocene (1.5 Ma)

During the Early Pleistocene the Barents Sea shelf was modelled generally close to the sea level (of about 50 m lower than at present). The deepest parts of the shelf were modelled at about 100-150 m bsl (meters below sea level) and the most elevated parts at about 300 m asl (meters above sea level, Fig. 5A). The shelf gently slopes down towards the west to water depths of about 100-150 m. Below that depth the gradient significantly increases reaching maximum value at

about 1850 m bsl. Between 100 and 1850 m bsl the gradient is modelled as about 0.8°. Below that depth the gradient gradually decreases.

The deepest parts of the shelf were modelled in the present-day area of Djuprenna, Håkjerringdjupet and western part of present-day Bear Island Trough (Fig. 5A). The Bear Island Trough was modelled as a clear depression between today's Spitsbergenbanken and a continuous area at the southern side of the trough. The areas elevated above 50 m asl represent the present-day Spitsbergenbanken including Bear Island, the southwestern part of Sentralbanken, the northern part of Murmanskbanken, Tromsøflaket, Nordkappbanken, an area on the southern side of the Bear Island Trough, as well as the northern part of Scandinavia.

4.2.2 Middle Pleistocene (0.7 Ma)

Most of the shelf bathymetry was modelled from about 100 to 200 bsl. The deepest parts were at 200-300 m bsl and the shallowest to about 200 m asl (Fig. 5B). Except for the areas west of the Spitsbergenbanken and Tromsøflaket the seabed gently slopes to water depths of about 700-900 m. Below 700-900 m bsl the gradient steepens to about 1° and remains the same for an additional depth of 1000 m. Below 1700-1900 m bsl the slope becomes gentler again. The deepest parts of the shelf comprise today's Djuprenna, Bear Island Trough, Håkjerringdjupet and an area southwest of Ingøydjupet. The bathymetric highs include Nordkappbanken, Tromsøflaket, Murmanskbanken and an area on the southern side of Bear Island Trough. The subaerial highs include Spitsbergenbanken, part of western Sentralbanken and northern Scandinavia (Fig. 5B).

Compared to the Early Pleistocene relief (Fig. 5A), the central Barents Sea shelf relief was deepened by about 150 m. This value decreases towards Scandinavia (70-80 m), Spitsbergenbanken (between 100 and 0 m), and to the eastern part of the study area. The highest deepening (150-210 m) was modelled at the mouth of Bear Island Trough and to the south of the trough (including Tromsøflaket and the elevated area to the south of the Bear Island Trough). The outer shelf and continental slope relief was shallowed by up to about 1000 m in the thickest parts of the Bear Island Trough Mouth Fan (Fig. 2).

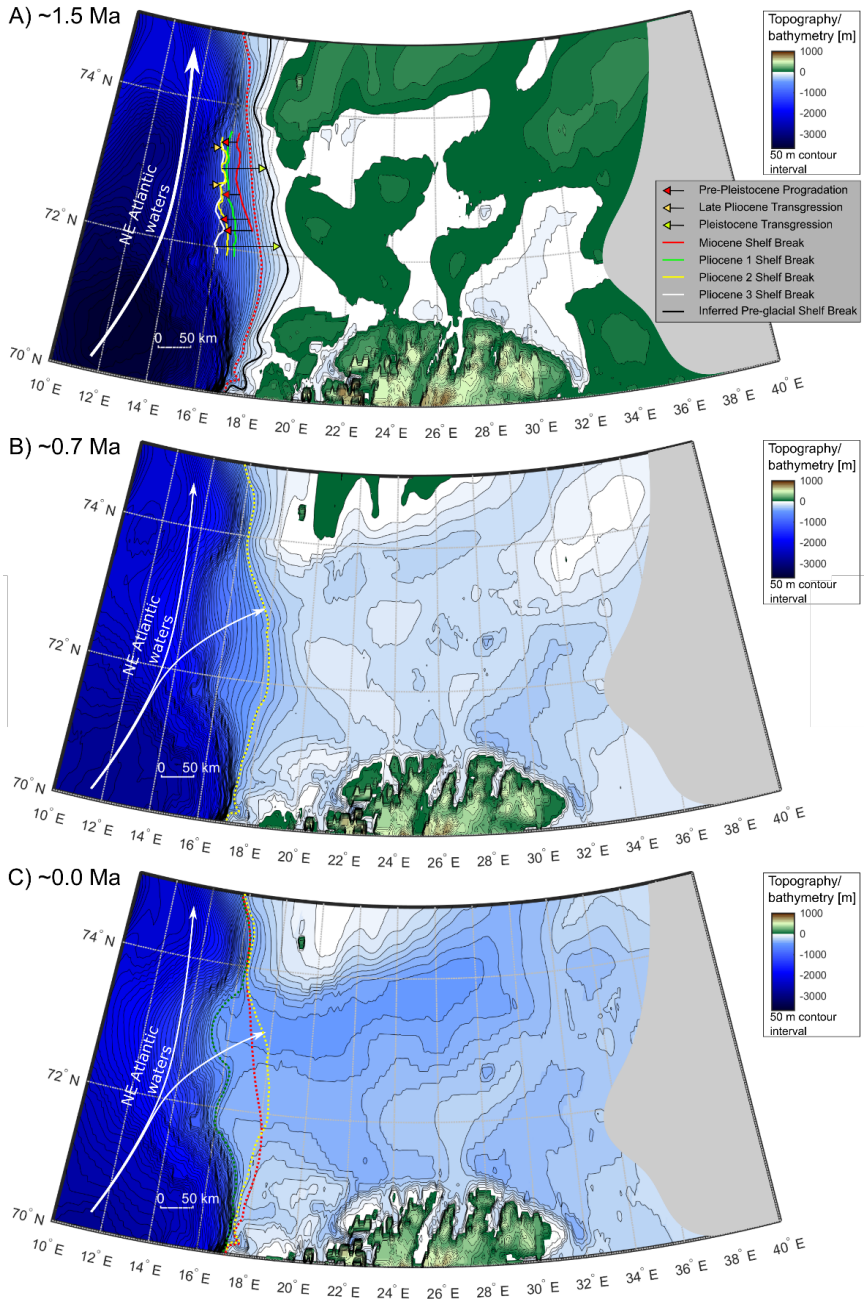

Fig. 5 A) Reconstructed topography during Early Pleistocene representing onset of glaciations (~1.5 Ma). Solid lines represent palaeo-shelf breaks. The Miocene-Pliocene shelf breaks were constrained by Omosanya et al. (2016). Red dotted line shows the 400 m bsl isoline that can mark the maximum ice extent (for details see 5.3) B) Reconstructed topography during the Middle Pleistocene (~0.7 Ma). Yellow dotted line shows the 400 m bsl isoline. C) Present-day topography (etopo5 model). Green dotted line marks the present day shelf edge that lies at about 500 m bsl (Vorren et al., 1991), yellow and red dotted lines show 400 m isoline at ~0.7 and 1.5 Ma respectively. Grey patches in A-C mask areas where erosion estimates were not available (for details see 3.2).

4.2.3 Present

The present-day bathymetry comprises the troughs of Bear Island Trough (up to 500 m bsl), Ingøydjupet, Djuprenna and Håkjerringdjupet (all up to 400 m bsl) and banks of Spitsbergenbanken with elevated areas above the sea level such as Bear Island, Sentralbanken, Nordkappbanken, Murmanskbanken and Tromsøflaket (all elevated to about 150-200 m bsl). The present-day shelf edge lies at about 500 m bsl (Vorren et al., 1991). The edge clearly separates the relatively flat shelf and the steep continental slope. Below 500 m bsl the slope gradient suddenly increases and remains approximately constant (about 1.1°) to about 1200 m bsl and below that depth the gradient becomes gentler again.

The area of Bear Island Trough and Ingøydjupet was deepened up to 260 m between the Middle Pleistocene and present. The highest values are associated with the mouth of Bear Island Trough. The elevation difference diminishes from the trough centers towards their margins. Outside the troughs the deepening of the relief was modelled as 40-60 m in Nordkappbanken, Murmanskbanken and Djuprenna, 0-100 m in Spitsbergenbanken, 60-100 m in southwestern Sentralbanken. The present-day outer shelf and continental slope relief is modelled up to 580 m shallower than during the Middle Pleistocene.

5 Discussion

The model results support previous inferences that the pre-glacial Barents Sea shelf (prior to 1.5 Ma) represented an elevated area generally close to sea level with some parts raised up to about 300 m asl (Butt et al., 2002; Dimakis et al., 1998; Rasmussen and Fjeldskaar, 1996). The reconstruction at 1.5 Ma indicates a shallow-marine to subaerial southern Barents Sea shelf (Fig. 5A) and suggests strongly elevated (up to about 300 m) areas of the Spitsbergenbanken and Sentralbanken separated by an elongated depression represented by the present-day Bear Island Trough (Fig. 5A). In contrast to Butt et al. (2002), the present study models a submerged Djuprenna area prior to 1.5 Ma. According to Butt et al. (2002), the shallow marine (0 - 100 m bsl) shelf is thought to persist until ~1.0 Ma, however, our model suggests that shallow marine relief could have remained for longer times, at least until about 0.7 Ma, with a deepening of the Bear Island Trough after 0.7 Ma and formation of the Ingøydjupet during most recent glacial events. The reconstruction proposed here fits the sediment geometry of the Bear Island Trough Mouth Fan (Fiedler and Faleide, 1996; Laberg et al., 2012). It shows that prior to 0.7 Ma, sediments forming the fan were deposited over large areas across the western Barents Sea shelf break while after 0.7 Ma sediments were more constrained to the Bear Island Trough mouth

fan. It suggests that most of the erosion beneath the trough could not have occurred before 0.7 Ma (Fiedler and Faleide, 1996; Laberg et al., 2012).

Direct comparison of the modelled pre-glacial topography to the water depth and basin geometry indicators (e.g. seismo-stratigaphy, microfossils) is feasible only at the outer shelf area (Sørvestsnaget Basin, Vestbakken Volcanic Province, Fig. 1) due to removal of sedimentary evidence from the inner shelf (Nyland et al., 1992). The available information was found to support the proposed reconstruction (Fig. 5A). Thickening of the Late Pliocene sedimentary wedge from the western part of the Veslemøy High to the western part of the Sørvestsnaget Basin suggests increasing accommodation space and increasing water depths to the west (Omosanya et al., 2016; Ryseth et al., 2003). A similar setting was proposed for the Vestbakken Volcanic Province where the Late Pliocene sedimentary wedge filled the available accommodation space in a slope-inner shelf environment (Sættem et al., 1994).

The modelled result fits with the seismic interpretation of Omosanya et al. (2016). By analysing the trajectories of several shelf-margin clinoforms, these authors show that prior to the Pleistocene the shelf edge position has shifted westwards and that the beginning of the Pleistocene was dominated by marine processes and deep-water sediments. Their trajectory analyses revealed flat to descending clinoforms during the earliest Pliocene, which changes to high-angle clinoforms in mid-Pliocene and later to low angle clinoforms at the end of Pliocene. This is evidence that the area has witnessed fluctuating sea level conditions and has alternated between continental to marine processes from early to late Pliocene. In addition, the authors also show that there is evidence for transgression of the shoreline in late Pliocene especially towards the northern part of Sørvestsnaget Basin. Hence, the prediction of a marine setting prior pre-glaciation is in support of a deep marine environment for the area. The inferred shelf edge for the pre-glacial relief is thus east of the Pliocene positions as a result of transgression and dominant marine processes (Fig. 5A).

5.1 Driving forces for the bathymetry evolution

5.1.1 Prior to 1.5 Ma

The glacial erosion is thought to represent 65% of the total Cenozoic erosion in the Bear Island Trough (Baig et al., 2016). Based on the same erosion model as used by Baig et al. (2016), the glacial erosion was modelled to induce 250-400 m of isostatic uplift in the Bear Island and Ingøydjupet troughs. This value decreases to about 200 m outside the troughs and to negative values in the westernmost parts of the shelf (Fig. 4). The total uplift amount is suggested to vary

between 1 km and more than 2 km (Green and Duddy, 2010; Nyland et al., 1992; Zattin et al., 2016). The Pleistocene isostatic component of uplift is therefore deemed to be relatively small varying from 10 to 20% in the banks and from 10 to 40% in the troughs. It is therefore suggested that most of the Barents Sea uplift is related to tectonic uplift events at the Eocene-Oligocene transition and/or during the Miocene-early Pliocene as documented by Green and Duddy (2010); Japsen et al. (2014); Knies et al. (2014); Sættem et al. (1994).

The volumes of sediments deposited in the Bear Island Trough Mouth Fan as a result of the Cenozoic erosion comprise of approximately 70% glacial and 30% pre-glacial sediments (Baig et al., 2016; Fiedler and Faleide, 1996; Laberg et al., 2012; Vorren et al., 1991). High glacial erosion resulted therefore in low amounts of uplift, while high tectonic uplift induced relatively low erosion. It can therefore be suggested that the tectonically uplifted shelf prior to 1.5 Ma was subjected to low-efficient sediment removal compared to large-scale glacial episodes after 1.5 Ma. This seems reasonable since the glacial erosion is one of the most efficient erosion mechanisms (Hallet et al., 1996). Another explanation for low sediment delivery to the Bear Island Trough Mouth Fan during the pre-1.5 Ma times is the short duration of erosion events. This is also a possible explanation since the literature suggests deep marine environments during the Late Paleocene-Eocene and marine conditions in most of the western Barents Sea during the Oligocene-Middle Miocene (Gabrielsen et al., 1990; Japsen et al., 2014; Rasmussen and Fjeldskaar, 1996; Riis, 1996; Ryseth et al., 2003; Vorren et al., 1991; Wood et al., 1989) suggesting depositional conditions.

Our reconstruction (Fig. 5A) suggests a mostly subaerially elevated shelf before the glaciation onset being probably a remnant of the uplift during the Late Miocene - Early Pliocene (Green and Duddy, 2010; Japsen et al., 2014). The results show that some of the present-day troughs (Bear Island Trough, Djuprenna, and Håkjerringdjupet) represented submerged areas (up to 100-150 m) before the glacial ages. The initial depressions might have been formed by fluvial erosion earlier in the Cenozoic further acting as conduits for ice movement during the Middle to Late Pleistocene (Laberg et al., 2010; Vorren et al., 1989). Also most of the banks, including Spitsbergenbanken, Murmanskbanken, Sentralbanken, Nordkappbanken, and Tromsøflaket, were modelled to exist >1.5 Ma, as documented for example by Lebesbye and Vorren (1996) for Spitsbergenbanken. To some degree the modelled pre-glacial highs and depressions coincide with post-rift topography that could have been preserved through a tectonically stable Late Cenozoic (Clark et al., 2014). It is thought that wide Barents Sea platform has been uplifted in relation to the Sørvestsnaget, Tromsø and Bjørnøya basins (Clark et al., 2014; Faleide et al.,

1993; Worsley, 2008) which are related to the modelled depressions (west of Tromsøflaket and in western part of the Bear Island Trough respectively, Fig. 5C) surrounded by elevated areas.

5.1.2 After 1.5 Ma

Selective glacial erosion and deposition occurring after 1.5 Ma and controlled by initial topography were the main processes that shaped the present-day bathymetry of the Barents Sea (Andreassen et al., 2008; Laberg et al., 2012; Sættem et al., 1994; Vorren et al., 1989). Regional isostatic adjustments to these processes might have affected a larger area than the area of actual erosion/deposition due to the lithosphere's rigidity (Medvedev et al., 2013). As a result, local isostatic response can be disturbed by a regional isostatic component caused by significant loading/unloading leading to unanticipated changes in topography evolution as explained by Fig. 6.

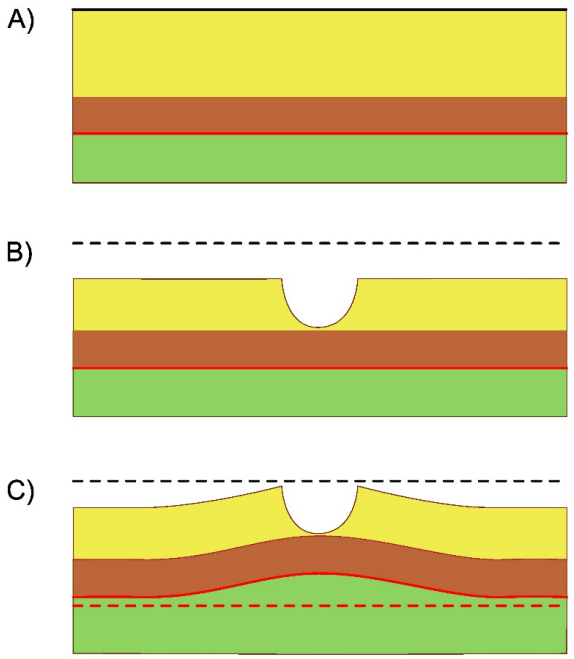

Fig. 6 Influence of the regional isostatic response on erosion with extra high erosion in the center. Such a setting might represent the Barents Sea shelf with moderate erosion outside the troughs and high erosion in the troughs. The highest uplift is expected at the central part being driven by extra high erosion. The margins to the trough areas also experience elevated uplift values resulting in high erosion thickness to uplift magnitude ratio. A) Original relief, B) Erosion, C) Isostatically adjusted relief. The model uses a three layer lithosphere consisting of upper sedimentary part (yellow), a rigid part of the lithosphere (brown), and an inviscid mantle (green). Modified from Medvedev et al. (2013).

In the erosional realm (like most of the Barents Sea shelf during the Pleistocene) high compensating uplift results in low elevation loss while low compensating uplift leads to high

elevation loss and substantial deepening of the topography. The Middle-Late Pleistocene erosion of the Barents Sea was focused in the Bear Island and Ingøydjupet trough areas (Fig. 2) causing higher elevation loss in trough centers (300-400 m) than in the areas outside the troughs (0-300 m). A map of compensating uplift to erosion ratio (Fig. 7) shows higher values (55-65%) along the margins of the troughs (mostly associated with present-day banks) than within and outside the troughs (below 50%). High compensating uplift together with low erosion thickness led to low topography reduction in the banks. In contrast, low compensation of the high erosion thickness resulted in very efficient drainage of the troughs (Fig. 6C). Therefore, the compensation level difference is thought to enhance the relief contrast between the troughs and banks caused by selective erosion.

High compensation ratios in the bank areas and mainland northern Scandinavia are however also influenced by initial topography as previously suggested (Andreassen et al., 2008; Hall et al., 2013; Laberg et al., 2012; Sættem et al., 1994; Vorren et al., 1989). For most of the Pleistocene northern Scandinavia, Spitsbergenbanken and southwestern Sentralbanken were modelled as subaerial areas. The same amount of erosion is more compensated by the uplift in onshore than in offshore environments due to water weight counteracting the uplift. In conclusion, the model suggests that present-day banks, often reflecting the bedrock morphology (Vorren et al., 1989), are not only an effect of the selective erosion and deposition controlled by initial topography. The contrasting bathymetry of the deep troughs and adjacent shallow banks is considered here to be a result of glacial activity affected by regional isostatic adjustments to these processes.

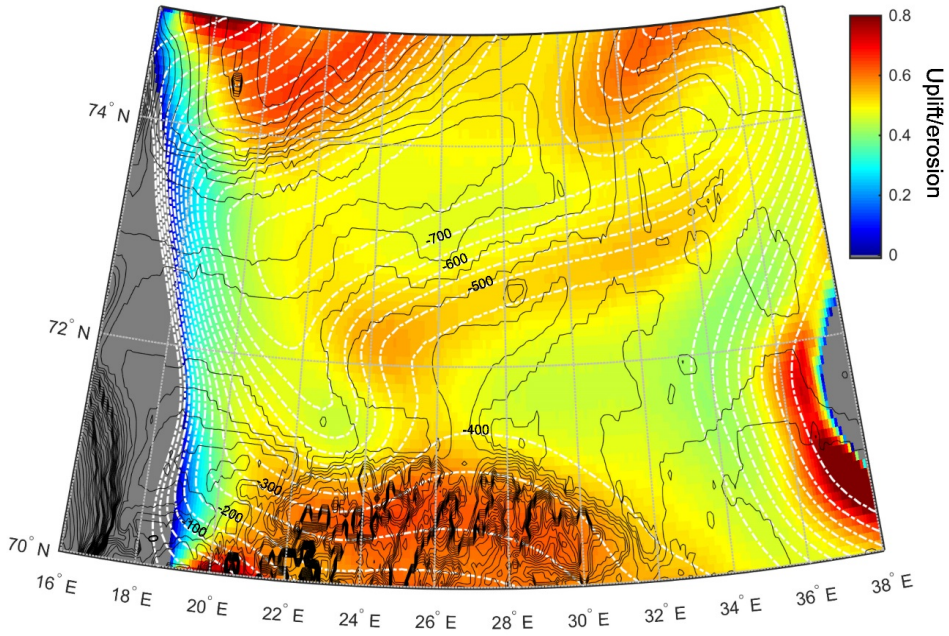

Fig. 7 Total isostatic uplift to total erosion ratio. The contrasting values might indicate an additional regional component to the local isostasy. Differences might also be attributed to different initial topography. Black lines show contours of present-day topography with 50 m intervals. White dashed lines with numbers show total erosion thickness. For details and interpretation see section 5.1.

The westernmost part of the shelf shows uplift to erosion ratios declining to the west (Fig. 7). The lowest ratios are modelled as negative values suggesting the erosion is not compensated by any uplift, but the lithosphere down-warped those areas. Reduced compensation ratio in the westernmost shelf area is attributed to pulldown of the lithospheric plate in the western part of the study area (continental slope and outer shelf, Fig. 4). The pulldown is linked to significant deposition on the outer shelf and continental slope (Fig. 2) causing sinking of the plate in the area larger than the area of the actual deposition. High influence of the sinking plate in the west together with erosion could have been a very effective topography reduction mechanism. As a result the same erosion amount leads to a very different amount of the bathymetry reduction dependent on location in the study area. For example 500 m of erosion at the mouth of Bear Island Trough with 25% of compensating uplift results in 375 m of topography reduction. In Nordkappbanken, the same amount of erosion with 60% of compensating uplift results in only 200 m of deepening. High erosion thickness together with the lithosphere pulldown explains also why the highest topography reduction was modelled at the mouth of the Bear Island Trough (representing the westernmost part of the trough, see 4.2).

5.2 Impact on northern Atlantic thermohaline circulation

Recent climate in the Arctic is controlled by the advection of the warm and saline Atlantic waters into the Nordic Seas (Hurdle, 1986). At present about 40% of northward flowing waters are directed to the Barents Sea while the remaining part flows towards the Fram Strait (Simonsen and Haugan, 1996). In the past, the elevated palaeo-relief of the Barents Sea (Fig. 5) has prevented bifurcation of the North Atlantic Current (the northernmost extension of the Atlantic thermohaline circulation) and, as a result, warm and salty waters could be directed towards the Fram Strait resulting in heat transport further north and potential sea ice feedbacks. Indeed, Hill (2015) showed that uplifted landmasses in the Barents Sea can produce a significant temperature response at high latitudes and may have played an important role for the observed low meridional temperature gradient in the Pliocene North Atlantic-Arctic gateway region. Butt et al. (2002) argued that this non-analogue ocean circulation pattern with a subaerial Barents Sea shelf existed until ca. 1 million years ago. This timing is roughly in agreement with the present study suggesting that the Barents Sea shelf was close to or somehow elevated (~300 m) above the sea level at around 1.5 Ma. However, in contrast to Butt et al. (2002), we show that inflow of warm Atlantic-derived water masses to the inner Barents Sea shelf did first occur at ca. 0.7 Ma. Regardless the ultimate timing of subsidence, bifurcation of northward flowing Atlantic-derived water masses into the Barents Sea between 1.0 and 0.7 Ma is supported by numerous observations of large-scale, shelf edge glaciations in the Barents Sea (Flower, 1997; Kristoffersen et al., 2004) and potentially northern Eurasia (Astakhov, 2004) and are manifested by distinct freshwater pulses in the Atlantic-Arctic gateway (Knies et al., 2007). Thus, the increase of global ice volume during the Mid Pleistocene transition (~1.25 Ma – 0.7 Ma) (Hays et al., 1976) may be supported by the gradual subsidence of the Barents Sea relief. Less northward flowing volumes of warm and salty waters might have caused positive feedbacks for Arctic sea ice dynamics in the Fram Strait (Stein and Fahl, 2013). More eastward penetration of Atlantic waters towards the inner Barents Sea shelf could have acted as an additional moisture source for build-up of massive Eurasian ice sheets as documented by Flower (1997); Kristoffersen et al. (2004).

5.3 Influence on extent of ice sheets

Grounded ice sheets in the Barents Sea are thought to have reached the shelf edge multiple times during the Pleistocene (Laberg and Vorren, 1996). The model shows the well-defined shelf edge developed during the Late Pleistocene being the result of high sediment delivery to the outer shelf (Fig. 5). Due to the unclear position of the modelled shelf edge the maximum ice

extent during the Early and Middle Pleistocene is ambiguous. Moreover, modelling of the extent of grounded marine ice sheets is a complex process that requires reliable ice thickness data in the simplest approximations (Blatter et al., 2011; Kirchner et al., 2011; Stokes et al., 2015). The data are not available for such long time periods in the study area and the modelling of the ice extent is not the main focus of this study.

It might, however, be speculated about the Barents Sea ice sheet extent at the western shelf margin based on the grounding line position from the Last Glacial Maximum (LGM). In a marine environment the grounding line represents a transition between flowing and floating ice (Stokes et al., 2015). The LGM grounding line bathymetry lies at approximately 500 m of the present water depths (Landvik et al., 1998). Given that sea level was approximately 100 m lower than at the present (de Boer et al., 2014) the past grounding lines can be expected at about 400 m below past sea levels.

Based on these simplistic assumptions the maximum extent of grounded ice can be approximated for the southwestern Barents Sea margin (Fig. 5). It must be stressed that the proposed Pleistocene ice extent boundaries are only conceptual lines and should be considered only as a first approximation. The results suggest that between the onset of shelf edge glaciations at ~1.5 Ma and the Middle Pleistocene (0.7 Ma) the area experienced sediment accumulation and shallowing only in the deep parts of the outer shelf/shallow continental slope and erosion east of that area. This resulted in almost no change in position of the 400 m bsl isoline in the southern and northern parts. Some regression of the isoline to the east (up to about 30 km) might have occurred only in the central part of the study area (Fig. 5). Major shelf progradation modelled between the Middle Pleistocene and the present might have resulted in advance of the 400 m bsl isoline to the west. The maximum ice sheet extent can therefore be expected to occur during the most recent glaciations. A significant advance of the maximum grounding line between the Middle and Late Pleistocene occurred in the area occupied by the Bear Island Trough Ice Stream, at the mouth of the Bear Island Trough (up to 90 km). Such high ice sheet extent become possible from the Late Pleistocene thanks to shelf progradation driven by significant glacial deposition at the mouth of the Bear Island Trough (Laberg et al., 2012). West of Tromsøflaket and Spitsbergenbanken the maximum ice extent has not been changed much since the Early Pleistocene due to similarly steep slopes in these areas, which are modelled to have occurred prior to the glaciations.

6 Conclusions

The issues of the Pleistocene bathymetry development in the southern Barents Sea are addressed in this work by using the isostatic modelling approach. The aspect of the regional isostatic response to the redistributed sediments was also considered in relation to evolution of the contrasting submarine relief at present. The main findings are as follows:

1. The pre-glacial (>1.5 Ma) relief of the southern Barents Sea was modelled generally close to the sea level. The deepest parts of the shelf were modelled at about 100-150 m bsl and the most elevated parts at about 300 m asl.
2. The results show that most of the prominent present day troughs and banks were initiated prior to large scale glaciations around 1.5 Ma, possibly as a response to tectonic uplift and related structural development.
3. Between the Early and Middle Pleistocene (1.5 - 0.7 Ma) the relief was deepened by 0-200 m (considering the same sea level) with the highest topography reduction in the major trough areas and the lowest on the banks. The Middle Pleistocene shelf is modelled as a shallow marine relief with Spitsbergenbanken elevated above the sea level.
4. Between the Middle Pleistocene and the present (0.7 – 0.0 Ma) the shelf was deepened by up to 250 m in the trough areas. On the banks the topography reduction rarely exceed 100 m.
5. Glacial erosion is modelled to induce isostatic uplift in the range of 250-400 m in the troughs and below 200 in the remaining areas in the southern Barents Sea. Isostatic component of the total shelf uplift (1-2 km) is deemed to be relatively small favoring the tectonic component of the Barents Sea uplift.
6. The topography throughout the Pleistocene was mostly shaped by glacial erosion and deposition controlled by initial topography as suggested by previous literature. The present-day relief was found to be also affected by regional isostatic adjustments exceeding actual areas of the focused trough erosion and significant deposition on the shelf margins.
7. The model suggest the inflow of the North Atlantic Current to the Barents Sea was barred by the topography up to ~0.7 Ma, about 0.3 Ma later than proposed in literature before. The age of restricted bifurcation coincides with glacial expansions in the Barents Sea and potentially northern Eurasia.

Acknowledgements

This study is a part of the project "Impact of Cenozoic structural development and glacial erosion on gas expansion, hydraulic fracturing and leakage in the Western Barents Sea" sponsored by ENI Norge. KJZ is thankful to ENI Norge for financial support of his Ph.D. and Sintef Petroleum AS for providing infrastructure and overall support. We also thank Stephen Lippard for proof reading the manuscript.

References

Andreassen, K., Laberg, J.S., Vorren, T.O., 2008. Seafloor geomorphology of the SW Barents Sea and its glaci-dynamic implications. Geomorphology 97, 157-177.

Andreassen, K., Nilssen, L.C., Rafaelsen, B., Kuilman, L., 2004. Three-dimensional seismic data from the Barents Sea margin reveal evidence of past ice streams and their dynamics. Geology 32, 729.

Andreassen, K., Ødegaard, C.M., Rafaelsen, B., 2007. Imprints of former ice streams, imaged and interpreted using industry three-dimensional seismic data from the south-western Barents Sea, in: Davies, R.L., et al. (Ed.), Seismic Geomorphology: Applications to Hydrocarbon Exploration and Production. Geological Society of London Special Publication, pp. 151-169.

Anell, I., Thybo, H., Artemieva, I.M., 2009. Cenozoic uplift and subsidence in the North Atlantic region: Geological evidence revisited. Tectonophysics 474, 78-105.

Astakhov, V., 2004. Middle Pleistocene glaciations of the Russian North. Quaternary Science Reviews 23, 1285-1311.

Baig, I., Faleide, J.I., Jahren, J., Mondol, N.H., 2016. Cenozoic exhumation on the southwestern Barents Shelf: Estimates and uncertainties constrained from compaction and thermal maturity analyses. Marine and Petroleum Geology 73, 105-130.

Blatter, H., Greve, R., Abe-Ouchi, A., 2011. Present State and Prospects of Ice Sheet and Glacier Modelling. Surveys in Geophysics 32, 555-583.

Butt, F.A., Drange, H., Elverhoi, A., Ottera, O.H., Solheim, A., 2002. Modelling Late Cenozoic isostatic elevation changes in the Barents Sea and their implications for oceanic and climatic regimes: preliminary results. Quaternary Science Reviews 21, 1643-1660.

Butt, F.A., Elverhoi, A., Solheim, A., Forsberg, C.F., 2000. Deciphering Late Cenozoic development of the western Svalbard Margin from ODP Site 986 results. Marine Geology 169, 373-390.

Cardozo, N., 2009. 3D flexural modeling. Continuous plate of variable elastic thickness (finite difference solution). Matlab script.

Cavanagh, A.J., Di Primio, R., Scheck-Wenderoth, M., Horsfield, B., 2006. Severity and timing of Cenozoic exhumation in the southwestern Barents Sea. Journal of the Geological Society 163, 761-774.

Clark, S.A., Glorstad-Clark, E., Faleide, J.I., Schmid, D., Hartz, E.H., Fjeldskaar, W., 2014. Southwest Barents Sea rift basin evolution: Comparing results from backstripping and time-forward modelling. Basin Research 26, 550-566.

de Boer, B., Lourens, L.J., van de Wal, R.S., 2014. Persistent 400,000-year variability of Antarctic ice volume and the carbon cycle is revealed throughout the Plio-Pleistocene. Nature Communications 5, 2999.

Dimakis, P., Braathen, B.I., Faleide, J.I., Elverhøi, A., Gudlaugsson, S.T., 1998. Cenozoic erosion and the preglacial uplift of the Svalbard–Barents Sea region. Tectonophysics 300, 311-327.

Doré, A.G., 1995. Barents Sea Geology, Petroleum Resources and Commercial Potential. Arctic 48, 207-221.

Doré, A.G., Jensen, L.N., 1996. The impact of late Cenozoic uplift and erosion on hydrocarbon exploration: offshore Norway and some other uplifted basins. Global and Planetary Change 12, 415-436.

Dore, A.G., Lundin, E.R., Jensen, L.N., Birkeland, O., Eliassen, P.E., Fichler, C., 1999. Principal tectonic events in the evolution of the northwest European Atlantic margin, Petroleum Geology Conference Proceedings, pp. 41-61.

Elverhøi, A., Hooke, R.L., Solheim, A., 1998. Late Cenozoic erosion and sediment yield from the Svalbard–Barents Sea region: implications for understanding erosion of glacierized basins. Quaternary Science Reviews 17, 209-241.

Faleide, J.I., Tsikalas, F., Breivik, A.J., Mjelde, R., Ritzmann, O., Engen, O., Wilson, J., Eldholm, O., 2008. Structure and evolution of the continental margin off Norway and Barents Sea. Episodes 31, 82-91.

Faleide, J.I., Vagnes, E., Gudlaugsson, S.T., 1993. Late Mesozoic-Cenozoic Evolution of the South-Western Barents Sea in a Regional Rift Shear Tectonic Setting. Marine and Petroleum Geology 10, 186-214.

Fiedler, A., Faleide, J.I., 1996. Cenozoic sedimentation along the southwestern Barents Sea margin in relation to uplift and erosion of the shelf. Global and Planetary Change 12, 75-93.

Fjeldskaar, W., 1997. Flexural rigidity of Fennoscandia inferred from the postglacial uplift. Tectonics 16, 596-608.

Flower, B.P., 1997. Overconsolidated section on the Yermak Plateau, Arctic Ocean: Ice sheet grounding prior to ca. 660 ka? Geology 25, 147-150.

Gabrielsen, R.H., Færseth, R.B., Jensen, L.N., Kalheim, J.E., Riis, F., 1990. Structural elements of the continental shelf. Part I: The Barents Sea Region. Norwegian Petroleum Directoriate bulletin 6, p. 33.

Geissler, W.H., Jokat, W., 2004. A geophysical study of the northern Svalbard continental margin. Geophysical Journal International 158, 50-66.

Green, P.F., Duddy, I.R., 2010. Synchronous exhumation events around the Arctic including examples from Barens Sea and Alaska Slope. Petroleum Geology Conference series 7, 633-644.

Hall, A.M., Ebert, K., Kleman, J., Nesje, A., Ottesen, D., 2013. Selective glacial erosion on the Norwegian passive margin. Geology.

Hallet, B., Hunter, L., Bogen, J., 1996. Rates of erosion and sediment evacuation by glaciers: A review of field data and their implications. Global and Planetary Change 12, 213-235.

Hays, J.D., Imbrie, J., Shackleton, N.J., 1976. Variations in the earth's orbit: Pacemaker of the ice ages. Science 194, 1121-1132.

Henriksen, E., Bjornseth, H.M., Hals, T.K., Heide, T., Kiryukhina, T., Klovjan, O.S., Larssen, G.B., Ryseth, A.E., Ronning, K., Sollid, K., Stoupakova, A., 2011. Chapter 17 Uplift and erosion of the greater Barents Sea: impact on prospectivity and petroleum systems. Geological Society, London, Memoirs 35, 271-281.

Hill, D.J., 2015. The non-analogue nature of Pliocene temperature gradients. Earth and Planetary Science Letters 425, 232-241.

Hjelstuen, B.O., Eldholm, O., Faleide, J.I., 2007. Recurrent Pleistocene mega-failures on the SW Barents Sea margin. Earth and Planetary Science Letters 258, 605-618.

Hurdle, B.G., 1986. The Nordic Seas. Springer Verlag.

Ingólfsson, Ó., Landvik, J.Y., 2013. The Svalbard–Barents Sea ice-sheet – Historical, current and future perspectives. Quaternary Science Reviews 64, 33-60.

Japsen, P., Green, P.F., Bonow, J.M., Nielsen, T.F.D., Chalmers, J.A., 2014. From volcanic plains to glaciated peaks: Burial, uplift and exhumation history of southern East Greenland after opening of the NE Atlantic. Global and Planetary Change 116, 91-114.

Kirchner, N., Hutter, K., Jakobsson, M., Gyllencreutz, R., 2011. Capabilities and limitations of numerical ice sheet models: a discussion for Earth-scientists and modelers. Quaternary Science Reviews 30, 3691-3704.

Klitzke, P., Faleide, J.I., Scheck-Wenderoth, M., Sippel, J., 2015. A lithosphere-scale structural model of the Barents Sea and Kara Sea region. Solid Earth 6, 153-172.

Knies, J., Matthiessen, J., Mackensen, A., Stein, R., Vogt, C., Frederichs, T., Nam, S.I., 2007. Effects of Arctic freshwater forcing on thermohaline circulation during the Pleistocene. Geology 35, 1075-1078.

Knies, J., Matthiessen, J., Vogt, C., Laberg, J.S., Hjelstuen, B.O., Smelror, M., Larsen, E., Andreassen, K., Eidvin, T., Vorren, T.O., 2009. The Plio-Pleistocene glaciation of the Barents Sea–Svalbard region: a new model based on revised chronostratigraphy. Quaternary Science Reviews 28, 812-829.

Knies, J., Mattingsdal, R., Fabian, K., Grøsfjeld, K., Baranwal, S., Husum, K., De Schepper, S., Vogt, C., Andersen, N., Matthiessen, J., Andreassen, K., Jokat, W., Nam, S.-I., Gaina, C., 2014. Effect of early Pliocene uplift on late Pliocene cooling in the Arctic–Atlantic gateway. Earth and Planetary Science Letters 387, 132-144.

Knutsen, S.M., Richardsen, G., Vorren, T.O., 1992. Late Miocene-Pleistocene sequence stratigraphy and mass movements on the western Barents Sea margin, in: Vorren, T.O., et al. (Ed.), Arctic Geology and Petroleum Potential. Norwegian Petroleum Society Special Publication, pp. 573-606.

Kristoffersen, Y., Coakley, B., Jokat, W., Edwards, M., Brekke, H., Gjengedal, J., 2004. Seabed erosion on the Lomonosov Ridge, central Arctic Ocean: A tale of deep draft icebergs in the Eurasia Basin and the influence of Atlantic water inflow on iceberg motion? Paleoceanography 19.

Laberg, J.S., Andreassen, K., Knies, J., Vorren, T.O., Winsborrow, M., 2010. Late Pliocene-Pleistocene development of the Barents Sea Ice Sheet. Geology 38, 107-110.

Laberg, J.S., Andreassen, K., Vorren, T.O., 2012. Late Cenozoic erosion of the high-latitude southwestern Barents Sea shelf revisited. Geological Society of America Bulletin 124, 77-88.

Laberg, J.S., Vorren, T.O., 1996. The Middle and Late Pleistocene evolution of the Bear Island Trough Mouth Fan. Global and Planetary Change 12, 309-330.

Landvik, J.Y., Bondevik, S., Elverhøi, A., Fjeldskaar, W., Mangerud, J., Salvigsen, O., Siegert, M.J., Svendsen, J.I., Vorren, T.O., 1998. The last glacial maximum of Svalbard and the Barents sea area: Ice sheet extent and configuration. Quaternary Science Reviews 17, 43-75.

Lebesbye, E., Vorren, T.O., 1996. Submerged terraces in the southwestern Barents Sea: origin and implications for the late Cenozoic geological history. Marine Geology 130, 265-280.

Lundin, E., Doré, A.G., 2002. Mid-Cenozoic post-breakup deformation in the 'passive' margins bordering the Norwegian - Greenland Sea. Marine and Petroleum Geology 19, 79-93.

Mattingsdal, R., Knies, J., Andreassen, K., Fabian, K., Husum, K., Grøsfjeld, K., De Schepper, S., 2014. A new 6 Myr stratigraphic framework for the Atlantic–Arctic Gateway. Quaternary Science Reviews 92, 170-178.

Medvedev, S., Souche, A., Hartz, E.H., 2013. Influence of ice sheet and glacial erosion on passive margins of Greenland. Geomorphology 193, 36-46.

Myhre, A., Thiede, J., Firth, J.A., 1995. Proceedings of the Ocean Drilling Program. Initial Reports, Leg 151, Ocean Drilling Program, College Station, Texas, USA, p. 951.

Nansen, F., 1904. The Bathymetric Features of the North Polar Seas, with a Discussion of the Continental Shelves and Previous Oscillations of the Shore-Line: Norwegian Polar Expeditions 1893–1896 Scientific Results Volume 4. Jacob Dybwad, Christiania.

Nyland, B., Jensen, L.N., Skagen, J., Skarpnes, O., Vorren, T., 1992. Tertiary uplift and erosion in the Barents Sea: magnitude, timing and consequences. Structural and tectonic modelling and its application to petroleum geology, 153-162.

Omosanya, K.O., Harishidayat, D., Marheni, L., Johansen, S.E., Felix, M., Abrahamson, P., 2016. Recurrent mass-wasting in the Sørvestsnaget Basin Southwestern Barents Sea: A test of multiple hypotheses. Marine Geology 376, 175-193.

Patton, H., Andreassen, K., Bjarnadóttir, L.R., Dowdeswell, J.A., Winsborrow, M.C.M., Noormets, R., Polyak, L., Auriac, A., Hubbard, A., 2015. Geophysical constraints on the dynamics and retreat of the Barents Sea ice sheet as a paleobenchmark for models of marine ice sheet deglaciation. Reviews of Geophysics 53, 1051–1098.

Rasmussen, E., Fjeldskaar, W., 1996. Quantification of the Pliocene-Pleistocene erosion of the Barents Sea from present-day bathymetry. Global and Planetary Change 12, 119-133.

Riis, F., 1996. Quantification of Cenozoic vertical movements of Scandinavia by correlation of morphological surfaces with offshore data. Global and Planetary Change 12, 331-357.

Riis, F., Fjeldskaar, W., 1992. On the magnitude of the Late Tertiary and Quaternary erosion and its significance for the uplift of Scandinavia and the Barents Sea, in: Larsen, R.M., Brekke, H., Larsen, B.T., Talleraas, E. (Eds.), Structural and Tectonic Modelling and its Application to Petroleum Geology. NPF Special Publication, pp. 163-185.

Ryseth, A., Augustson, J.H., Charnock, M., Haugerud, O., Knutsen, S.-M., Midbøe, P.S., Opsal, J.G., Sundsbø, G., 2003. Cenozoic stratigraphy and evolution of the Sørvestsnaget Basin, southwestern Barents Sea. Norsk Geologisk Tidskrift, 107-130.

Simonsen, K., Haugan, P.M., 1996. Heat budgets of the Arctic Mediterranean and sea surface heat flux parameterizations for the Nordic Seas. Journal of Geophysical Research: Oceans 101, 6553-6576.

Stein, R., Fahl, K., 2013. Biomarker proxy shows potential for studying the entire Quaternary Arctic sea ice history. Organic Geochemistry 55, 98-102.

Stokes, C.R., Tarasov, L., Blomdin, R., Cronin, T.M., Fisher, T.G., Gyllencreutz, R., Hättestrand, C., Heyman, J., Hindmarsh, R.C.A., Hughes, A.L.C., Jakobsson, M., Kirchner, N., Livingstone, S.J., Margold, M., Murton, J.B., Noormets, R., Peltier, W.R., Peteet, D.M., Piper, D.J.W., Preusser, F., Renssen, H., Roberts, D.H., Roche, D.M., Saint-Ange, F., Stroeven, A.P., Teller, J.T., 2015. On the reconstruction of palaeo-ice sheets: Recent advances and future challenges. Quaternary Science Reviews 125, 15-49.

Svendsen, J.I., Alexanderson, H., Astakhov, V.I., Demidov, I., Dowdeswell, J.A., Funder, S., Gataullin, V., Henriksen, M., Hjort, C., Houmark-Nielsen, M., Hubberten, H.W., Ingólfsson, Ó., Jakobsson, M., Kjær, K.H., Larsen, E., Lokrantz, H., Lunkka, J.P., Lyså, A., Mangerud, J., Matiouchkov, A., Murray, A., Möller, P., Niessen, F., Nikolskaya, O., Polyak, L., Saarnisto, M., Siegert, C., Siegert, M.J., Spielhagen, R.F., Stein, R., 2004. Late Quaternary ice sheet history of northern Eurasia. Quaternary Science Reviews 23, 1229-1271.

Sættem, J., Bugge, T., Fanavoll, S., Goll, R.M., Mørk, A., Mørk, M.B.E., Smelror, M., Verdenius, J.G., 1994. Cenozoic margin development and erosion of the Barents Sea: Core evidence from southwest of Bjørnøya. Marine Geology 118, 257-281.

Sættem, J., Poole, D.A.R., Ellingsen, L., Sejrup, H.P., 1992. Glacial geology of outer Bjørnøyrenna, southhwestern Barents Sea. Marine Geology 103, 15-51.

Turcotte, D.L., Schubert, G., 2002. Geodynamics second edition. Cambridge University Press.
van den Berg, J., van de Wal, R.S.W., Milne, G.A., Oerlemans, J., 2008. Effect of isostasy on dynamical ice sheet modeling: A case study for Eurasia. Journal of Geophysical Research: Solid Earth 113.
Vorren, T.O., Laberg, J.S., 1997. Trough mouth fans - palaeoclimate and ice-sheet monitors. Quaternary Science Reviews 16, 865-881.
Vorren, T.O., Lebesbye, E., Andreassen, K., Larsen, K.B., 1989. Glacigenic sediments on a passive continental margin as exemplified by the Barents Sea. Marine Geology 85, 251-272.
Vorren, T.O., Richardsen, G., Knutsen, S.M., 1991. Cenozoic erosion and sedimentationn in the western Barents Sea. Marine and Petroleum Geology 8, 317-340.
Wood, R.J., Edrich, S.P., Hutchinson, I., 1989. Influence of North Atlantic tectonics on the large-scale uplift of the Stappen High and Loppa High, western Barents Shelf. Extensional tectonics and stratigraphy of the North Atlantic margins, 559-566.
Worsley, D., 2008. The post-Caledonian development of Svalbard and the western Barents Sea. Polar Research 27, 298-317.
Zattin, M., Andreucci, B., de Toffoli, B., Grigo, D., Tsikalas, F., 2016. Thermochronological constraints to late Cenozoic exhumation of the Barents Sea Shelf. Marine and Petroleum Geology 73, 97-104.

6.3 Paper 3

Zieba, K.J., Grøver, A., (2016). Isostatic response to glacial erosion, deposition and ice loading. Impact on geometry of the southwestern Barents Sea hydrocarbon traps. Marine and Petroleum Geology, Elsevier.

Literature often indicates that loss of the hydrocarbons in the Barents Sea is attributed to processes of spillage and remigration as well as leakage through the cap rock (seal) and faults. The magnitude of these mechanisms remains however uncertain. In addition, all of the processes could have occurred before and during the Pleistocene glaciations, but the exact timing is unknown. Another uncertainty related to hydrocarbon exploration in the Barents Sea is related to ambiguous spill directions prior and during the glaciations. This leads to problems in prediction of the secondary migration paths, and as a result, in the locations of the present-day accumulations. These issues were addressed in Paper 3 by using a combination of flexural isostasy with hydrocarbon secondary migration modelling. The method was applied in one of the most active hydrocarbon exploration areas (Bjørnøyrenna Fault Complex) by using examples of three real hydrocarbon trap structures.

The results indicate that hydrocarbon trap capacities could have been changed by 5 - 14% between the onset of glaciations and the Present. The change could have been either positive or negative (potentially causing hydrocarbon loss). The change in magnitude was found to be dependent on tilt values, pre-glacial trap geometry including spill point orientation, and the relationship between the orientation of the maximum tilt and the longest trap axis. The western Barents Sea traps with present spill points to the west and south might have experienced trap capacity increase and were not susceptible to spillage during the Pleistocene, while those with spill points to the east and north might have experienced either volume increase or reduction depending on the pre-glacial location of their spill points. The Pleistocene sediment redistribution caused a switch of the spill directions in two (of total three) of the analysed traps. Also events of glacial loading were responsible for short-term spill point shifts in the same traps. Changes of the trap geometry caused by the Pleistocene tilting alone could not have been responsible for any major loss of oil and gas. The tilting, together with gas volume expansion driven by fluctuations in the burial history, might however explain some part of the hydrocarbon loss during the ice ages. It was found that the Pleistocene burial history and tilting cannot explain large palaeo-oil shows observed in the wells cores in the Bjørnøyrenna Fault Complex at the present.

Paper 3

Marine and Petroleum Geology 78 (2016) 168–183

Contents lists available at ScienceDirect

Marine and Petroleum Geology

journal homepage: www.elsevier.com/locate/marpetgeo

Research paper

Isostatic response to glacial erosion, deposition and ice loading. Impact on hydrocarbon traps of the southwestern Barents Sea

Krzysztof Jan Zieba [a, *], Arnt Grøver [b]

[a] Department of Geology and Mineral Resources Engineering, Norwegian University of Science and Technology (NTNU), NO-7491, Trondheim, Norway
[b] Sintef Petroleum, S. P. Andersens veg 15B, NO-7031, Trondheim, Norway

ARTICLE INFO

Article history:
Received 27 April 2016
Received in revised form
25 July 2016
Accepted 13 September 2016
Available online 14 September 2016

Keywords:
Barents sea
Pleistocene
Glaciations
Hydrocarbon traps
Migration
Spillage
Isostasy
Numerical modelling

ABSTRACT

Previous work indicates that a part of hydrocarbon loss from traps in the Barents Sea is attributed to the Pleistocene (glacially-related) spillage due to isostatically-driven depth changes and tilting. It is, however, unknown how severe the Pleistocene spillage was and how much hydrocarbons were depleted due to other mechanisms including leakage and pre-glacial spillage. In addition, it remains uncertain how much the orientation of the hydrocarbon traps and thus trap capacities and spill directions was affected by glacial sediment redistribution and ice loading.

The effect of the Pleistocene burial history on trap capacity and spillage is addressed by using a combination of the flexural isostasy and secondary migration modelling. The impact is modelled in three trap structures in the Bjørnøyrenna Fault Complex.

The results show that the Pleistocene burial history led to either increase or decrease the trap capacities in the range of 5–14%. The geometrical changes also affected the spill directions of some of the traps. Apart from the tilt magnitude the most important factor controlling the trap capacity change and spill directions in the analyzed traps was the initial geometric setting of the traps. The traps in the western Barents Sea with present spill points to the west and south experienced trap capacity increase and were not susceptible to spillage during the Pleistocene. Location of the pre-glacial spill points determines whether the traps with the present spill points to the east and north experienced capacity increase or reduction. Structural changes of the traps caused only by the tilting could not have resulted in major loss of oil and gas. The tilting together with gas volume expansion might however have been responsible for some part of the hydrocarbon loss during the Cenozoic.

1. Introduction

Spillage and remigration of hydrocarbons in the Barents Sea is often attributed to isostatic adjustments and related tilting of hydrocarbon traps during the Cenozoic. It is suggested that these processes might explain previously larger degrees of trap filling demonstrated by palaeo-oil shows (Cavanagh et al., 2006; Doré, 1995; Doré and Jensen, 1996; Duran et al., 2013; Henriksen et al., 2011; Nyland et al., 1992). Some of the hydrocarbon spillage is linked to isostatic movements due to cycles of Pliocene-Pleistocene ice-sheet loading/unloading and glacial sediment redistribution (Cavanagh et al., 2006; Doré and Jensen, 1996; Duran et al., 2013; Kjemperud and Fjeldskaar, 1992; Lerche et al., 1997). It is however uncertain what was the magnitude of isostatic response caused by these processes and how, as a result, the processes affected the orientation of hydrocarbon traps. Reconstructed trap orientation together with a complete Pleistocene burial history can provide an insight into how much of the hydrocarbons were spilled out of the traps due to the glaciations, and how much of the loss is attributed to other processes including leakage and pre-glacial spillage.

Literature considered problem of the isostatic response to the ice sheet loading in the Barents Sea (Amantov and Fjeldskaar, 2016; Fjeldskaar et al., 2000; Kjemperud and Fjeldskaar, 1992; Landvik et al., 1998; Lerche et al., 1997) and isostatic response to glacial sediment redistribution (Amantov et al., 2011; Butt et al., 2002; Dimakis et al., 1998; Rasmussen and Fjeldskaar, 1995; Riis and Fjeldskaar, 1992). Existing literature lacks however a coherent Pleistocene burial history model that demonstrates vertical movements of the stratigraphic units over long time scales (1–2

* Corresponding author.
E-mail address: krzysztof.j.zieba@ntnu.no (K.J. Zieba).

http://dx.doi.org/10.1016/j.marpetgeo.2016.09.009
0264-8172/

Ma) incorporating recent ice sheet models (e.g. Peltier et al., 2015) and the newest findings regarding regional erosion-deposition trends (Laberg et al., 2012).

In a synthetic case it was shown that the glacially induced tilting could have had a pronounced impact on the Barents Sea trap capacities leading to up to 30% of hydrocarbon loss (Kjemperud and Fjeldskaar, 1992). In addition the study points out the importance of the initial trap geometry on hydrocarbon loss. Different trap geometries make some traps more sensitive to tilt-driven spillage than the others. This issue was however not addressed before in connection to the trap structures in the Barents Sea, and as a result the actual glacial impact on the hydrocarbon loss is uncertain. Moreover, it has been proposed that the Cenozoic spillage might have resulted in a major hydrocarbon remigration from central to peripheral parts of the Barents Sea basins (Lerche et al., 1997; Ohm et al., 2008). Detailed understanding of the pre-glacial migration patterns and locations of oil and gas accumulations are however challenged by uncertain hydrocarbon trap orientation and basin geometry prior to the ice ages.

Hydrocarbon trap orientation at the onset of glaciations (at ~1.50 Ma) and the impact of subsequent burial history on the traps will be addressed here by using a combination of flexural isostasy and secondary migration modelling. The study has been undertaken with data from the Bjørnøyrenna Fault Complex (western Barents Sea), one of the most active hydrocarbon exploration areas on the Norwegian Continental Shelf (Fig. 1). Besides major discoveries including for example 7220/4-1 and 7220/8-1, many of the traps are dry showing thick palaeo-oil columns (e.g. 7219/9-1) suggesting hydrocarbon depletion due to spillage and/or leakage. By using these trap structures it will be shown how much of the hydrocarbons might have been lost due to the Pleistocene spillage alone challenged by non-uniform vertical movements of the lithosphere and changes of the hydrocarbon densities.

2. Methods and data

2.1. Isostatic response to ice loading and sediment redistribution

2.1.1. Flexural isostasy modelling

The elastic lithosphere is thought to float on a denser viscous substratum – the asthenosphere (Vening-Meinesz, 1941). An applied load (positive or negative) causes bending (flexure) of the lithospheric plate. The applied load is partly supported by the shear stress of the lithosphere and partly by the buoyant forces of the asthenosphere. In this paper, the elastic plate is considered as 2500 × 2500 km flat structure with fixed sides (no displacement at the sides is modelled). Horizontal forces acting on the plate are not considered. The isostatic deflection is not an immediate process since the mantle is of low viscosity (e.g. Turcotte and Schubert, 2002). The time-dependent deflection is related to mantle relaxation time before which a state of the isostatic equilibrium is not reached. The relaxation time of the Scandinavia region is usually estimated as a few thousand years (Fjeldskaar, 1997; van den Berg et al., 2008). In this paper the time-dependent deflection is not considered. Time-dependency might be neglected for modelling of erosional/depositional processes lasting for 10^{-1} - 10^{0} Ma because flexural equilibrium is rather achieved during such long timespans. For short-time glaciations (lasting for thousands of years) the equilibrium might not been fully achieved. For longer periods including the Last Glacial Maximum (LGM) shelf-edge glaciation, lasting for 7 ka (Peltier et al., 2015) the equilibrium can be achieved.

Flexure calculations were performed by using the Matlab script of Cardozo (2009). The calculations were performed on a 10 km grid resolution. The elastic thickness is assumed to be 20 km, uniformly distributed in the study area following Fjeldskaar (1997) and van den Berg et al. (2008). Values of 5 km and 50 km were also tested. For the sake of simplicity, the density of the eroded sediments is considered to be the same as that of the deposited sediments (2200 kg/m^3). Density of the mantle is assumed as 3300 kg/m^3, water 1025 kg/m^3 and ice 917 kg/m^3.

2.1.2. Erosion/deposition and ice thickness models

Modelling of the isostatic response due to sediment redistribution was conducted by using erosion/deposition model of Laberg et al. (2012). The model was created by using a mass-balance method where volumes of glacial deposits are compared with their drainage area and the thickness of removed sediments is calculated accordingly. The drainage area used for calculation of the erosion thickness was estimated based on structure-contour map of the upper regional unconformity and the present-day

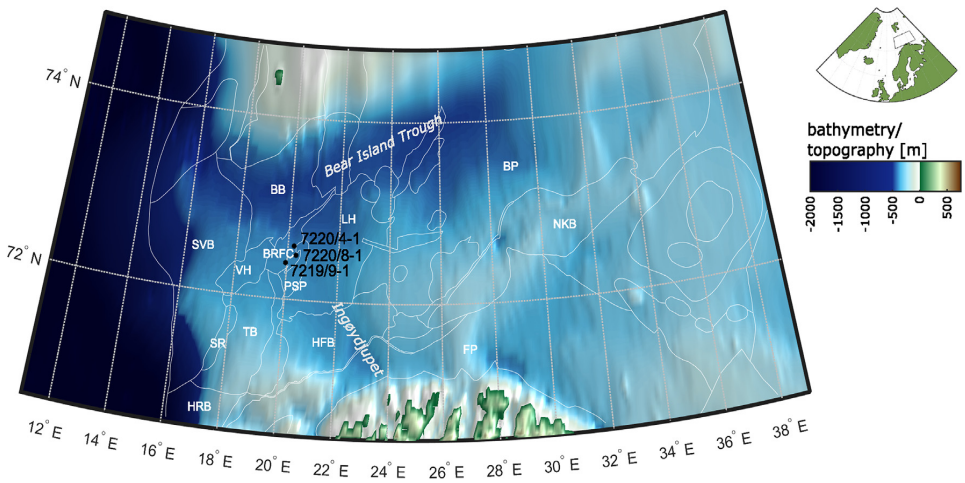

Fig. 1. The location of the study area overlaid by bathymetry/topography (ETOPO5, http://www.ngdc.noaa.gov/mgg/global/etopo5.html). The figure shows main structural elements, and well names of the hydrocarbon trap structures analyzed in this paper. BB: Bjørnøya Basin, BP: Bjarmeland Platform, BRFC: Bjørnøyrenna Fault Complex, HFB: Hammerfest Basin, FP: Finnmark Platform, HRB: Harstad Basin, LH: Loppa High, NKB: Nordkapp Basin, PSP: Polheim Subplatform, SR: Senja Ridge, SVB: Sørvestsnaget Basin, VH: Veslemøy High.

bathymetry (Vorren et al., 1991). The sediment redistribution model provides general erosion trends with averaged values over the shelf area. Volumes of glacial deposits in the western outer shelf and continental slope were estimated based on the seismic interpretation. The model does not account for on-shelf glacial deposition and does not consider sediment inflow from outside the drainage area. Compaction level of the accumulated erosional products is assumed the same as the compaction level of the source rocks.

The erosion values were interpolated to maps shown in Fig. 2A and Fig. 2B by using a nearest-neighbor interpolation, smoothed by a 30 km-width filter applied 3 times. No estimates of erosion thickness are provided for the central-eastern part of the study area (east of 35°E). The estimates are provided for time spans of 1.50–0.70 Ma and 0.70–0.00 Ma constrained by ages of seismic reflectors R5 and R1 respectively. The age of reflector R5 is normally dated at ~1.50 Ma (Knies et al., 2009; Mattingsdal et al., 2014) and R1 at ~700-440 ka (Elverhøi et al., 1998; Laberg et al., 2010; Sættem et al., 1992). In this paper the youngest age of R1 is used, therefore the erosion/deposition values are considered to represent time-spans of 1.50–0.44 Ma and 0.44–0.00 Ma.

Between 1.50 and 0.44 Ma the glacial erosion resulted in sediment removal of up to 330–420 m from the central Barents Sea shelf. The erosion is thought to decrease to the south, towards the Scandinavia and to the north towards the present-day banks north of the Bear Island Trough (Laberg et al., 2012). Here the maximum value of 330 m is used (Fig. 2A). The erosion thickness values in the southernmost and northernmost areas are here assumed to decrease to 100–200 m. The outer shelf and continental slope area experienced high deposition of the eroded material brought from the inner parts of the shelf. The deposition thickness slightly exceeded 1500 m at its maximum value (Laberg et al., 2012).

The sediment redistribution between 0.44 and 0.00 Ma resulted in up to 440–530 m of erosion in trough areas including the Bear Island and Ingøydjupet troughs. Erosion of banks is thought to be much lower than in the troughs (Laberg et al., 2012). The maximum value for the trough areas is set as 440 m decreasing in all directions to 100 - 0 m (Fig. 2B). Deposition thickness on the outer shelf and on the continental slope reached about 800 m at its maximum (Laberg et al., 2012).

The isostatic impact of the ice loading on the lithosphere was assessed by using the Last Glacial Maximum (~0.02 Ma) ice thickness model of Peltier et al. (2015) that has been smoothed to the 10 km grid resolution (Fig 2C) by using gridfit Matlab script (https://www.mathworks.com/matlabcentral/fileexchange/8998-surface-fitting-using-gridfit). The model represents ice thickness at 24 ka, the thickest and the largest in extent during the LGM in this region (Peltier et al., 2015). No high-resolution-ice model is available for older glaciations. Clay mineral and IRD data acquired from boreholes along the Barents Sea margin suggest similar ice extent (reaching shelf break) of repeatable glacial events in the western Barents Sea shelf between ~1.0 Ma and the LGM (Knies et al., 2009). In addition, the western shelf break that limits the ice sheet extent prograded only by about 20–30 km towards the west between the Middle Pleistocene and present (Vorren et al., 1989, 1991). Considering these similarities the LGM ice model is used as an approximation for a potential shelf-edge glaciation at ~0.44 Ma. The LGM ice thickness model is thought to be a rather unreliable approximation for glaciations prior to the Middle Pleistocene thus the glacial events before the Middle Pleistocene were not modelled. The middle-late Pleistocene ice sheet might have had different size and extent than the ice sheet during the Middle-Early Pleistocene due less polar conditions prior to ~0.7–1.0 Ma (Laberg et al., 2010; Knies et al., 2009). In addition, the ice sheet configuration and extent might have been significantly different during these two periods due to change from subaerial to submarine environments and more eastern position of the shelf break (Butt et al., 2002; Vorren et al., 1989, 1991).

The modelling of the isostatic response takes into consideration variations of the eustatic sea level changes. The values of the sea level (de Boer et al., 2014) for the modelling ages are presented in Table 1. Technically the isostatic response was modelled backwards in time at fixed ages associated with the erosion/deposition time-spans. In addition deflection of the lithosphere at the same ages during the ice loading were evaluated. The results are thus further presented at following ages: ~1.50 Ma, ~0.44 Ma (ice-free conditions), ~0.44 Ma (during glaciation, 'ICE'), ~0.44 Ma (after ice retreat, 'AR'), ~0.00 Ma (ice-free conditions), ~0.00 Ma (during glaciation, 'ICE'), ~0.00 Ma (after ice retreat, 'AR').

2.2. Impact of the isostatic movements on trap capacity changes and hydrocarbon spillage

2.2.1. Background information

The hydrocarbon spillage within a trap might be caused by 1) hydrocarbon volume increase and/or by 2) trap capacity decrease. The hydrocarbon volume increase within a trap is a result of two processes: i) continuous infill of migrating hydrocarbons, and ii) hydrocarbon volume expansion related to reservoir pressure and temperature alterations that are linked to burial depth changes. During exhumation and related burial depth reduction a trap experiences pressure reduction which may cause an under-saturation of the hydrocarbon fluid. Gas dissolved in the oil will then be released resulting into a two-phase system. The gas expansion may result in exceeding overall hydrocarbon volume beyond the trap capacity, forcing part of the hydrocarbon volume below the spill point (e.g. Silverman, 1965; Doré and Jensen, 1996; Ohm et al., 2008).

The second reason for the hydrocarbon spillage is related to trap capacity change controlled by its geometry and pore volume. The geometry of a trap is defined by top reservoir, reservoir thickness, and in some cases by discontinuities such as faults. The lowest point in a trap below which no accumulation is present is defined by a spill point (Allen and Allen, 2004). Trap capacity can be altered during changing geological conditions including sedimentation, erosion and tectonism (Verweij, 1993). Burial leads to changes of the pore space and trap capacity through mechanical and chemical compaction processes (Sclater and Christie, 1980; Walderhaug 1994). Tectonic movements might cause changes of trap geometry and orientation by fracturing, faulting, folding and also tilting of the entire trap structures leading to development of palaeo-hydrocarbon columns (Verweij, 1993). Tilting can be induced by differential loading/unloading due to for example non-uniform ice thickness or erosion and deposition. It can cause either trap capacity reduction or increase due to change of the trap volume above the spill point level. The magnitude of capacity change is dependent on deformation gradient, number of isostatic events, orientation of the trap axes and spill points (Kjemperud and Fjeldskaar, 1992).

Fig. 3 explains a theoretical impact of westerly directed tilting on the structural trap capacity. Due to the tilting the western part of the trap is downwarped in relation to the spill point causing capacity reduction visible on cross sections and as trap outlines. The capacity reduction might force hydrocarbons to be spilled out through the spill point and develop palaeo-hydrocarbon columns that can be detected at present in the well cores. In contrary, if the trap was tilted in the opposite direction that would result in the trap capacity increase due to deepening of the spill point.

2.2.2. Secondary migration modelling: model setup

The Pleistocene burial history impact on hydrocarbon trap

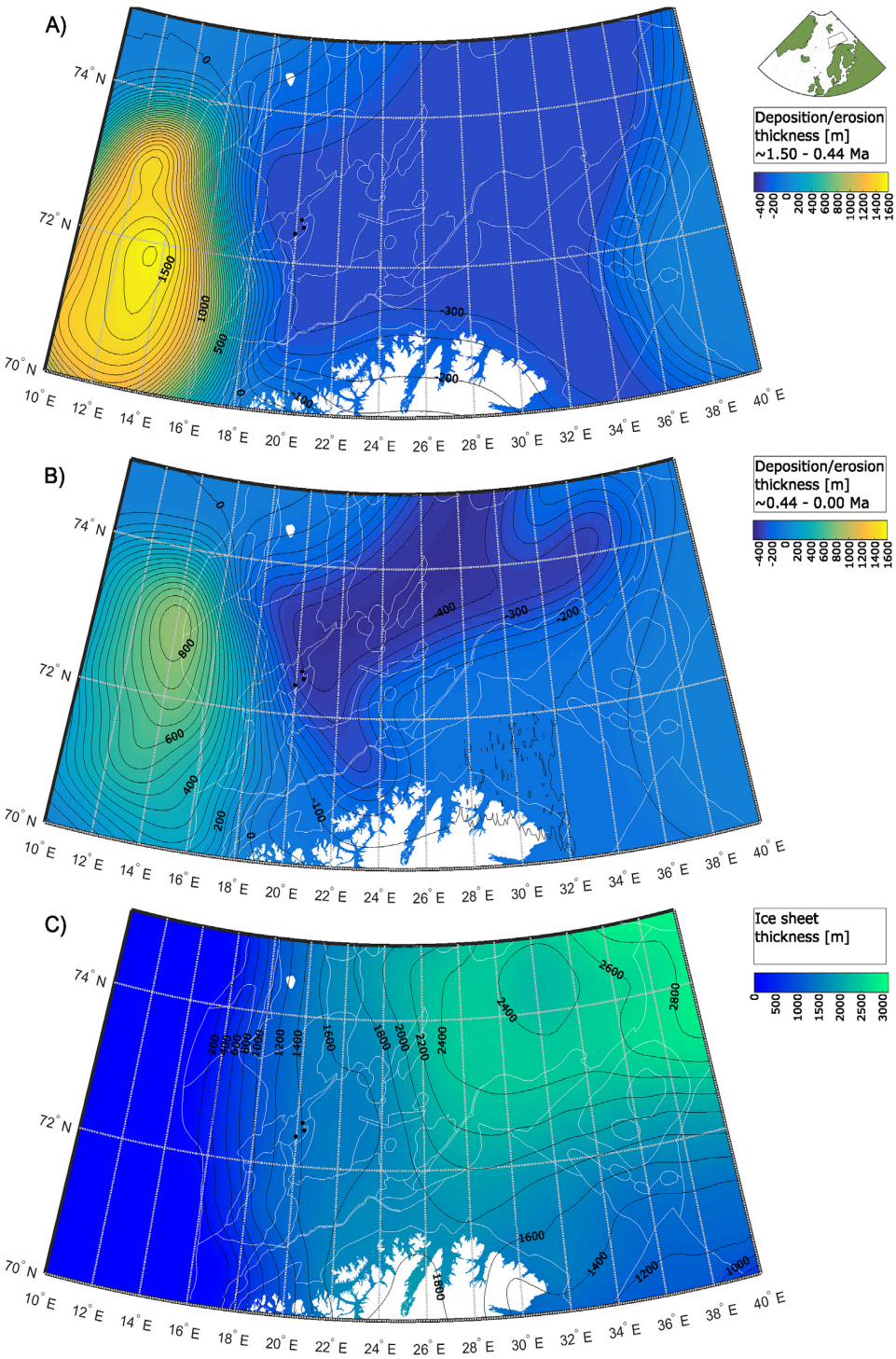

Fig. 2. Modelling input data. A) Deposition (positive values) and erosion (negative values) thicknesses between 1.50 and 0.44 Ma. B) Deposition (positive values) and erosion (negative values) thicknesses between 0.44 and 0.00 Ma. C) Ice thickness used for glacial events at ~0.44 and ~0.00 Ma. Well locations shown as black dots.

Table 1
Isostatic responses at the modelling ages (upper row) were calculated by applying/removing the load to/from the lithosphere in equilibrium state. The eustatic sea level changes (de Boer et al., 2014) are also considered in the load budget (middle row). The lower row shows used sediment/water or sediment/ice temperatures (Cavanagh et al., 2006) for hydrocarbon density calculations. ICE: at ice conditions, AR: after retreat.

Modelling age	~1.50 Ma	~0.44 Ma	~0.44 Ma ICE	~0.44 Ma AR	~0.00 Ma	~0.00 Ma ICE	~0.00 Ma AR
Applied/removed load	Fig. 2A and B	Fig. 2B	Figs. 2B and 3C	Fig. 2B	none	Fig. 2C	none
Eustatic sea level change [m]	−50.2	−101.7	−101.7	−101.7	−91.7	−91.7	0
Sediment/water or sediment/ice temperature [°C]	3	3	0	3	3	0	6

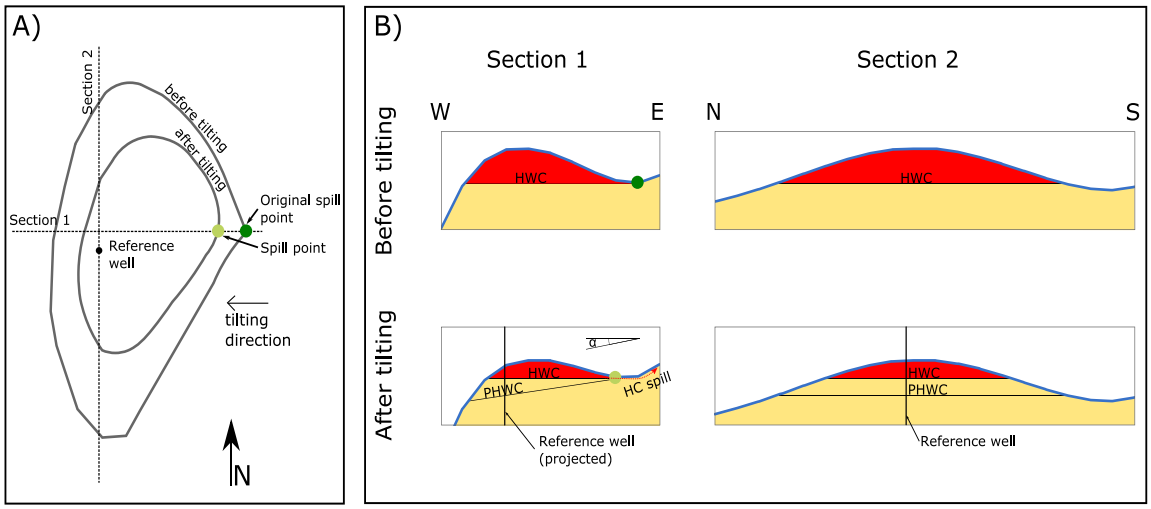

Fig. 3. Changes of the trap orientation and hydrocarbon contacts due to tilting in western direction (tilt magnitude represented by α). The trap structure imitates a typical Bjørnøyrenna Fault Complex trap geometry. The structure is bounded by a steep fault to the west. A) Trap outline changes. B) Changes in cross sections. HWC: hydrocarbon-water contact, PHWC: palaeo-hydrocarbon-water contact, HC spill: spillage of hydrocarbons. The area between HWC and PHWC represents the palaeo-oil zone.

capacity and related spillage was evaluated for three trap structures in the Bjørnøyrenna Fault Complex (Fig. 1) where the following wells were drilled: 7220/4-1 (gas discovery), 7220/8-1 (oil and gas discovery) and 7219/9-1 (dry with oil shows). The main reservoirs include the Jurassic Stø, Nordmela and Tubåen formations (Løseth et al., 2014). Present-day trap geometry was obtained from seismic interpretation of top Stø Formation with grid resolution of 200 × 200 m. Based on the well data (Norwegian Petroleum Directorate) a uniform thickness of 350 m of the reservoir was used.

The amount of the hydrocarbon loss due to the spillage is here modelled as a result of 1) change of trap capacity, and 2) volume changes of the hydrocarbons occupying the pore space within the trap. The cap rock is considered as totally impermeable seal and faults are also assumed not to leak. No hydrocarbon charge is modelled between 1.50 Ma and the present.

The model assumes the change of trap capacity is related only to regional tilting caused by isostatic adjustments to sediment redistribution and ice loading. Past trap orientation was reconstructed by applying deflection values obtained from the flexural isostasy modelling (section 2.1). No porosity changes is modelled throughout the entire modelling time-span. The reservoir pore space is considered here as a function of the maximum burial depth (Sclater and Christie, 1980). The Bjørnøyrenna Fault Complex reached its maximum burial depth before the glacial ages (Zattin et al., 2016) therefore no ice- or sediment-weight-driven compaction is modelled. Trap orientation change through geological time might lead to alteration of the spill point (section 2.2.1 and Fig. 3). The spill point location is modelled as the lowest point in a trap structure that can retain hydrocarbons. The major factors controlling the modelling of the spill point according the model are: 1) the seismic interpretation of present-day geometry, 2) erosion/deposition maps, 3) ice thickness maps, and 4) the elastic thickness model used for flexural isostasy modelling.

For simplicity sake effects of pressure and temperature changes on the fluid state are further studied for single oil-phase and single gas-phase. The corresponding effect on hydrocarbon volume expansion/contraction were analyzed versus trap capacities, in order to evaluate the spillage related to density changes.

The oil and gas spillage was assessed by filling the reconstructed traps either by oil or gas to their spill points at the onset of glaciations (1.50 Ma). Due to trap capacity and hydrocarbon density changes through time some portion of the hydrocarbons were lost. Technically, the hydrocarbon spillage was modelled in two independent hydrocarbon migration modelling runs (one for oil and one for gas phase). An additional exercise with dual phase was also performed in order to evaluate the degree of gas dissolution. In this exercise, the trap at 1.50 Ma was filled with 50% free gas and 50% oil at in-situ (reservoir) conditions. The degree of dissolved gas (gas-oil-ratio, GOR) was then calculated at each time step. Secondary migration (spillage) modelling including PVT-analysis was conducted in the basin modelling software SEMI (Sylta, 2004; Hamborg et al., 2006). The implemented density formulas for oil-gas systems are given by Standing (1977).

As mentioned, hydrocarbon volume per unit mass is related to the reservoir temperature and pressure. Johansen et al. (1996) modelled 3–7 °C temperature change between glacial and interglacial periods in sedimentary units at 1–3 km depth. These reservoir temperature fluctuations are mimicked here by using a

simplistic model that is exclusively dependent on the burial depth (controlled by the geothermal gradient) and temperature at the sediment/water or sediment/ice interface (Table 1). The thermal gradient is considered to be constant during the Pleistocene and equal to the present-day value of 35.1 °C/km, 38.4 °C/km, 35.6 °C/km for 7220/4-1, 7220/8-1 and 7219/9-1 respectively (Norwegian Petroleum Directorate, http://factpages.npd.no/) thus the same shift in the top sediment temperature results in the same shift of the reservoir temperature. No change of the basal heat flow in the Barents Sea during the Pleistocene is expected (Cavanagh et al., 2006; Duran et al., 2013) and therefore not included in the modelling.

The reservoir pressure is assumed to be at hydrostatic conditions during the interglacials. A transition from water (interglacial) to ice conditions is modelled in 10 intermediate time steps. During the transition the water table is reduced from mean-sea level to the base of the ice-sheet, and then the ice builds up gradually reaching the maximum thickness at the last timestep. At each intermediate timestep the hydrostatic pressure level is changed accordingly to the water/ice thickness assuming a tight cap rock. The hydrostatic pressure might be elevated by the ice load (Boulton and Caban, 1995). Here this effect was treated in a simplified manner where warm conditions are assumed, and that the melt water supports the ice load elevating the hydrostatic pressure by half of the ice load (Cavanagh et al., 2006).

3. Results

3.1. Consequences of the isostatic readjustments for the southern Barents Sea

The isostatic response to the Pleistocene sediment redistribution and ice loading events was modelled by using uniform elastic thickness model of 20 km (section 2.1.1). Values of 5 km and 50 km were also tested but the test could not change the first-order conclusions of this paper. The isostatic response results in either uplift or downwarping depending on location (Fig. 4, Fig. 5). This together with the sea level changes led to changes in the total depth (defined as depth below the sea level) of sedimentary units. The depth changes are presented further in relation to palaeo sea levels (total depth) at selected ages during ice-free conditions or sea levels prior to a glacial event during ice conditions.

3.1.1. Sediment redistribution between 1.50 and 0.44 Ma

Glacial erosion and deposition of the erosion products (Fig. 2A) between 1.50 and 0.44 Ma and the sea level change (Table 1) resulted in vertical movements of the stratigraphic units. The Barents Sea shelf was isostatically uplifted by about 150–200 m in the central part of the study area. The uplift magnitude decrease to the south (northern Scandinavia) and to the west towards the outer shelf and continental slope where isostatic downwarping was modelled. The maximum down-warp value (540 m) was modelled at the depocentre located in the southwestern part of the study area (Fig. 2A).

Depth changes resulting from this event are shown in Fig. 4A. The stratigraphic units of westernmost basins including the Harstad and the Sørvestsnaget basins and Vestbakken Volcanic province increased their depth by about 350 m while the depth in central and eastern areas decreased by up to about 270 m. The sediment redistribution resulted in a tilt of up to 5 m/km in the westernmost parts of the study area. In the Bjørnøyrenna Fault Complex (location of the analyzed traps) the tilt values were modelled as about 1 m/km. In the Bjørnøyrenna Fault Complex and in the basins further to the west, the highest depth gradient directions were modelled in W-WSW directions. The central and eastern parts were not much affected by tilting, rarely exceeding values of 1 m/km.

3.1.2. Ice loading at ~0.44 Ma

A potential ice sheet loading event at ~0.44 Ma (Fig. 2C) could have led to isostatic downwarping of the entire shelf area up to about 800 m in the northeastern part, 400-250 m in the Bjørnøyrenna Fault Complex and less than 250 m in the west (of the Bjørnøyrenna Fault Complex).

The ice loading could have affected the depth of the stratigraphic units and the tilting developed due to the sediment redistribution between 1.50 and 0.44 Ma. The depth of the stratigraphic units was deeper during the glaciation at ~0.44 Ma than before the onset of glaciations in the central-eastern parts (up to 600 m deeper, see Fig. 4B). The westernmost parts remained at similar depths as at 0.44 Ma during the ice-free conditions (Fig. 4A). The ice loading event resulted in tilt of the units in approximately opposite direction to the tilt generated by the sediment redistribution between 1.50 and 0.44 Ma. As a result, during the ice conditions the W-WSW directed tilt in the western parts of the study area was reduced by about 1 m/km in relation to ice-free conditions at 0.44 Ma (Fig. 4A). In the central-western parts the tilt azimuth was changed from W-WSW to S and E directions. In the eastern part of the study area the tilt was directed towards the maximum ice thickness location (Fig. 2C).

3.1.3. Sediment redistribution between 0.44 and 0.00 Ma

The sediment redistribution between 0.44 and 0.00 Ma (Fig. 2B) and palaeo-water depth change (Table 1) resulted in further uplift of the central and eastern areas (shelf) and downwarping of the westernmost areas (outer shelf and continental slope). The maximum uplift (up to 190 m) follow the erosion trend along the Bear Island Trough (Fig. 2B). Outside the trough the uplift values were modelled to decrease in all directions. Almost no uplift or downwarping was modelled in the areas close to the present-day shelf edge and in the easternmost part of the study area. Further west the stratigraphic units were subjected to downwarping up to 300 m at the deposition center in the central-western part of the study area (Fig. 2B).

The depth of stratigraphic units in the eastern and central parts (Bear Island Trough) were reduced by up to 350 m between ~1.50 and 0.00 Ma (Fig. 5A). In contrast, the Harstad, Sørvestsnaget basins, the Vestbakken Volcanic province and parts of the Tromsø Basin were modelled up to 750 m deeper than before the glaciations (Fig. 5A). The glacial erosion and deposition resulted in a significant tilting of the stratigraphic units in the central and western parts of the study area. The maximum depth gradient value was modelled west of the Bjørnøyrenna Fault Complex where it reaches approximately 8 m/km (Fig. 5A). In the Bjørnøyrenna Fault Complex the values range from about 1 up to 4 m/km. The central and eastern part experienced lower gradients, locally up to 2 m/km. The tilt direction at ~0.00 Ma is similar to the direction observed at ~0.44 Ma (during ice free conditions) with the main trend in a WSW direction in the central-western part of the study area.

3.1.4. Ice loading at ~0.00 Ma

The model suggests a glacial event at ~0.00 Ma caused a downwarping similar in magnitude to the glacial loading event at ~0.44 Ma. During the ice loading event at ~0.00 Ma (Fig. 2C) the study area was isostatically downwarped by up to 800 m compared to the ice-free conditions at ~0.00 Ma. The deflection caused by the glaciation at ~0.00 Ma is up to 100 m lower than the ice-related deflection at ~0.44 Ma due to different water depths at ~0.00 and ~0.44 Ma (compared to ice-free conditions at the same ages,

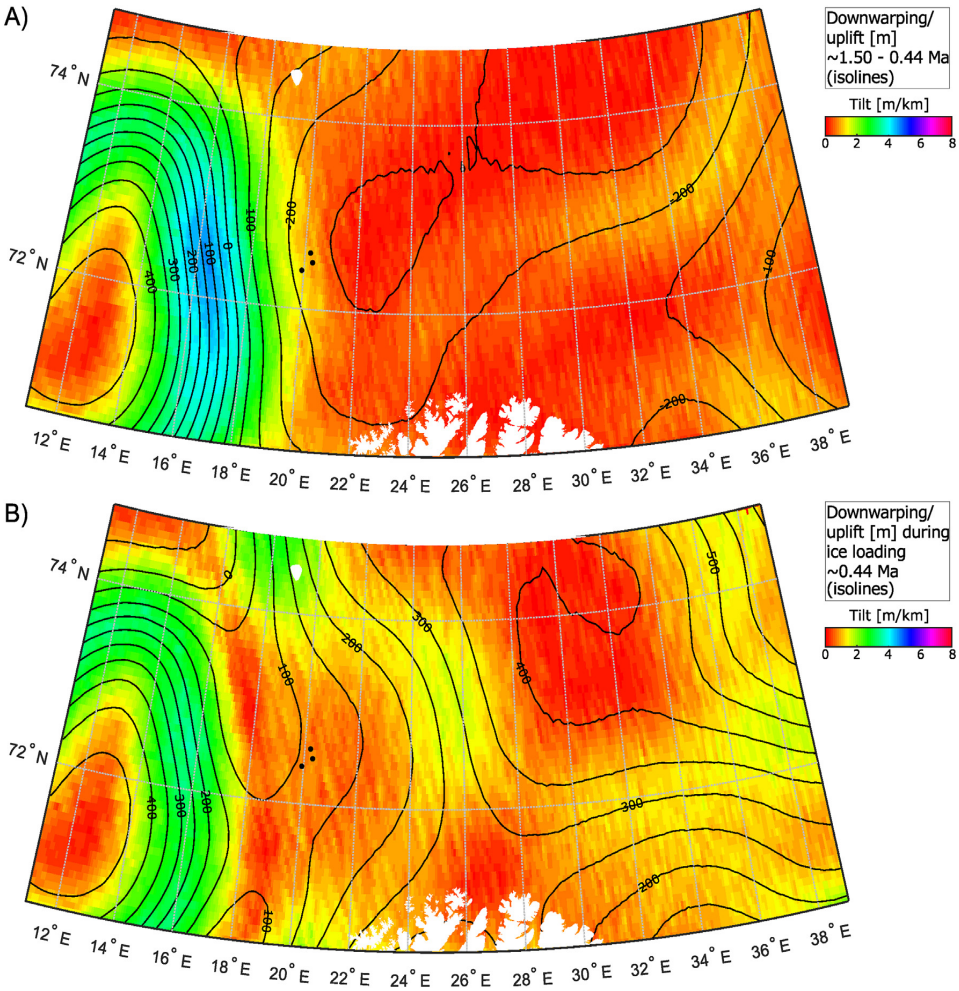

Fig. 4. A) Downwarping (positive values) and uplift (negative values) represented by isolines and induced tilt (solid colors) at ~0.44 Ma relative to onset of glaciations (~1.50 Ma). B) Downwarping (positive values) and uplift (negative values) represented by isolines and induced tilt (solid colors) during an ice loading event at ~0.44 Ma relative to onset of glaciations (~1.50 Ma). Well locations shown as black dots.

Table 1). The same ice thickness caused lower downwarping at ~0.00 Ma due to higher water depths.

As a result, the stratigraphic units during the most recent glaciations were buried deeper than before the glacial ages in most of the study area (Fig. 5B). However, the central (including the Bjørnøyrenna Fault Complex) and northwestern parts were buried shallower than before the glaciations by up to 150 m. During the ice loading the sediment-induced tilt in the Bjørnøyrenna Fault Complex and west of the complex was significantly diminished compared to ice-free conditions at ~0.00 Ma (to about 6 m/km at its maximum, Fig. 5B). Limited areas in the central and eastern parts could have experienced higher depth gradients during glacial than ice-free conditions reaching about 3 m/km.

3.2. Consequences of the isostatic readjustments for the selected traps in the Bjørnøyrenna Fault Complex

3.2.1. Depth and hydrocarbon density fluctuations

Fig. 6 shows depths of the top of the Jurassic reservoir unit together with oil and gas densities in hydrocarbon traps in the Bjørnøyrenna Fault Complex. All of the traps experienced variations in the depth of similar magnitude.

Between 1.50 and 0.44 Ma the depth was reduced by about 200–250 m. A glacial loading event at ~0.44 Ma led to 300–350 m deepening of all of the analyzed traps and the same amount of shallowing after the ice retreat. Between 0.44 and 0.00 Ma the depth of stratigraphic units was decreased by about 100–150 m. The most recent glacial event (at ~0.00 Ma) brought the units 250–300 m deeper than during the ice-free conditions at ~0.00 Ma. The most recent glacial retreat resulted in 150–200 m of depth decrease. The post-glacial depth decrease was lower in magnitude than the depth increase during the glaciation due to the higher sea level at present than before the glaciation (Table 1). Overall, the glacial sediment redistribution (between 1.50 and 0.00 Ma) and sea level change resulted in about 280 m of depth decrease in 7220/4-1 and 7220/8-1 and about 230 m in 7219/9-1.

Hydrocarbon density changes are related to the temperature and pressure fluctuations, here driven by variations of the sediment-water-interface temperature, burial depth and applied ice loading (section 2). All of the analyzed traps were subjected to

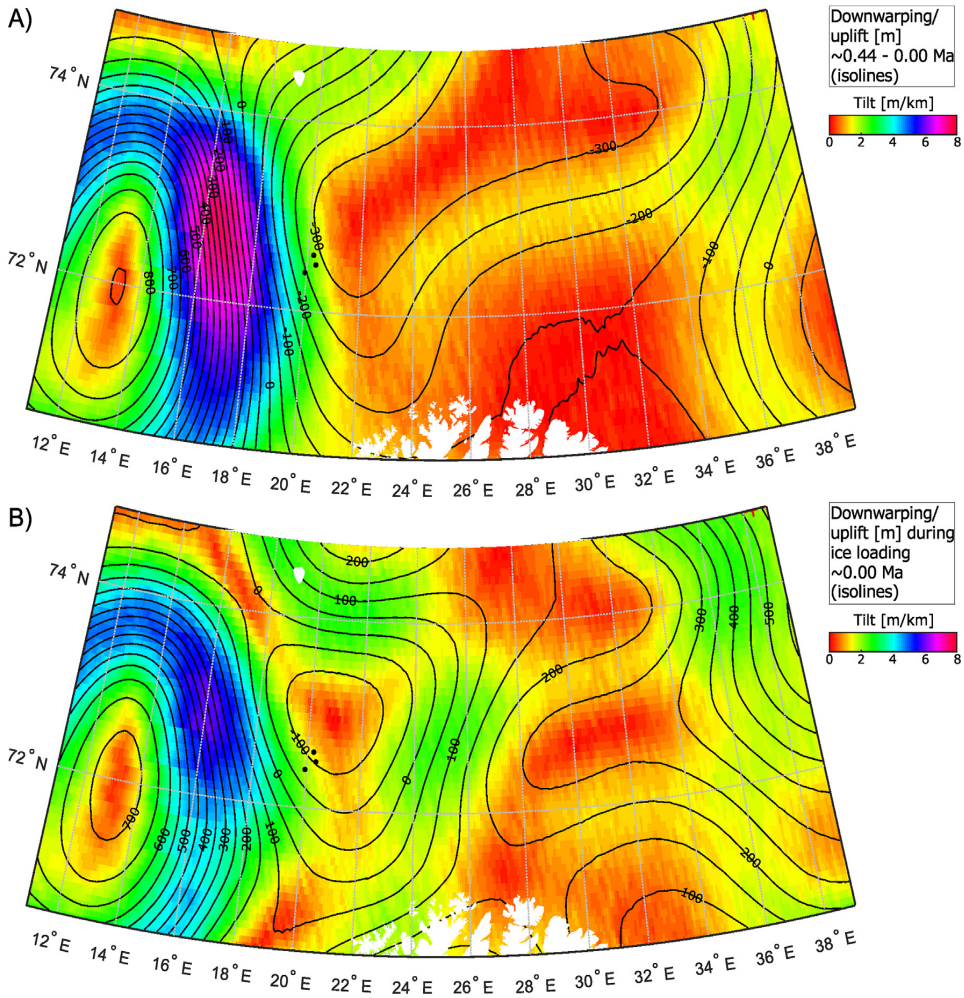

Fig. 5. A) Downwarping (positive values) and uplift (negative values) represented by isolines and induced tilt (solid colors) at ~0.00 Ma (after the most recent ice retreat) relative to onset of glaciations (~1.50 Ma). B) Downwarping (positive values) and uplift (negative values) represented by isolines and induced tilt (solid colors) during an ice loading event at ~0.00 Ma relative to onset of glaciations (~1.50 Ma). Well locations shown as black dots.

depth reduction and corresponding reservoir temperature decrease during the sediment redistribution events. The temperature drop is also linked to the ice loading events and related sediment-water-interface temperature decrease. Between the onset of the glaciations (~1.50 Ma) and the present, the reservoir temperature drop of about 20–25 °C is modelled in the reservoir. During each glaciation the temperature dropped by about 2–3 °C. Removal of the overburden and change of the palaeo-water depths resulted in a pore pressure decrease. Between the onset of glaciations and the present day the drop was modelled as between 2.8 and 3.5 MPa. The ice loading episodes resulted in a significant rises of the pressure due to the load contribution to the total pressure (section 2.2.2). The increase might be as high as 6 MPa during the ice loading at ~0.44 Ma and 3 MPa during the ~0.00 Ma event.

Temperature and pressure fluctuations led to changes of hydrocarbon densities, and as a result, to their volume changes per mass unit. Changes of the hydrocarbon densities were analyzed for two scenarios. The first assumes complete gas filling, and the second complete oil filling (section 2.2.2). During the sediment redistribution event between 1.50 and 0.44 Ma gas density decreased by 4–13% in all the analyzed traps (Fig. 6). Later, during the sediment redistribution event between 0.44 and 0.00 Ma the gas density change is not as high as for the previous event due to lower depth decrease compared to the previous event. A slight decrease (3%) in gas density in 7220/8-1, increase of <1% in 7220/4-1 and increase of 1% in 7219/9-1 were modelled during that period. During both sediment redistribution events the oil density has increased by 1–2% per event. Due to the ice loading episodes the gas density significantly increased (by 13–49%) causing an important volume drop, with maximum increase/decrease modelled in 7220/8-1. Also a slight (up to 1%) oil density rise was modelled during both ice loading episodes. Gas volume decrease between the glaciation onset and the present is about 0% in 7220/4-1, 11% in 7220/8-1 and 3% in 7219/9-1. The relative oil density increase is about 2% in all of the traps.

The density and GOR changes were also modelled for the dual phase mixture (section 2.2.2). In general, the oil density is reduced (Fig. 7) compared to the single oil phase exercise (Fig. 6) what is attributed to the gas dissolution in the oil phase. This effect is the most pronounced during ice loading events. The depth range (i.e.

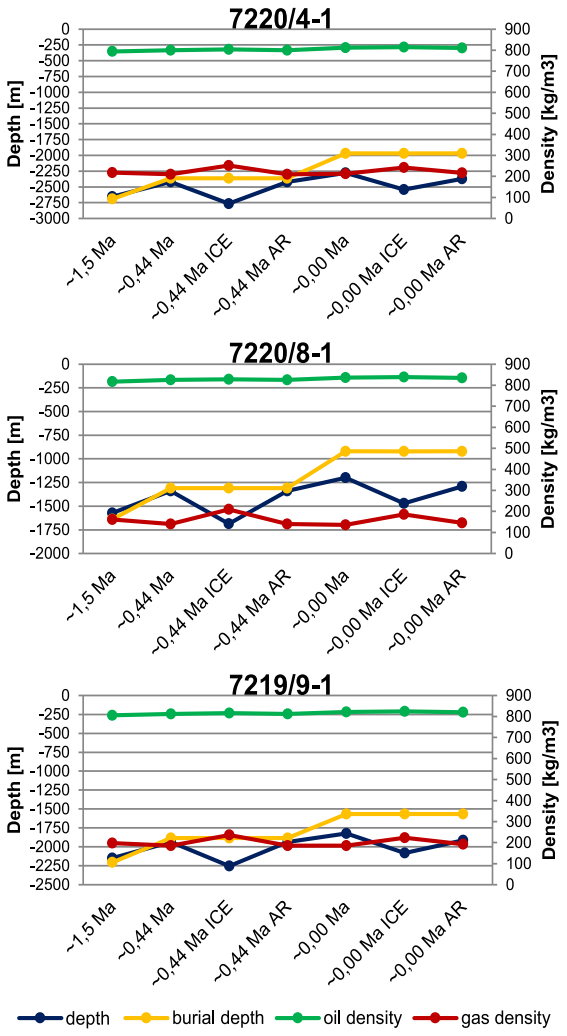

Fig. 6. Depth, burial depth, gas and oil density changes (single-phase scenarios) in the analyzed hydrocarbon traps. ICE: at ice conditions, AR: after retreat.

pressure and temperature regime) of the trap location was also found to be sensitive to this effect. The GOR is lower for 7220/8-1 (ranging between 82 and 142 Sm^3/Sm^3) compared with values in 7220/4-1 (between 158 and 205 Sm^3/Sm^3) and 7219/9-1 (between 130 and 200 Sm^3/Sm^3). Therefore the amount of gas dissolved in the oil is potentially higher in these two locations.

3.2.2. Changes in trap orientation

The trap capacity changes of the analyzed structures in the Bjørnøyrenna Fault Complex during the Pleistocene are shown in Fig. 8. Fig. 9 shows initial (~1.50 Ma) orientation of the studied traps and spill points. The spill point location of traps 7220/4-1 and 7220/8-1 were both modelled at their southernmost tips. In trap structure 7220/4-1 only 7 m of vertical difference between hydrocarbon-water contact and the trap bottom was modelled at its northeast tip (alternative spill point location, see Fig. 9). The spill point location can therefore be easily changed even by slight tilting. Similarly, spill point location of the trap 7220/8-1 is also sensitive to tilting due to 3 m of vertical difference between hydrocarbon-water contact and the trap bottom at its eastern tip (Fig. 9). The spill point location of 7219/9-1 at ~1.5 Ma is modelled at the same location as at the present (Figs. 9 and 10). In contrast to the remaining traps, the spill point location of 7219/9-1 is not very sensitive to tilting (200 m of vertical difference between hydrocarbon-water contact and the trap bottom at southern part).

Fig. 10 depicts changes of the trap outlines due to loading/unloading and changes of the spill point location. The differential uplift between 1.50 and 0.44 Ma caused W-WSW tilt and change of the trap capacities. A slight increase of the trap volume by 2% was modelled in 7220/4-1 and 7220/8-1 while a decrease (7%) of the trap capacity was modelled in 7119/9-1 (Fig. 8). The reason for the relative increase or decrease of the trap volume was found to be related to the orientation of the spill points in relation to the tilt azimuth. The two traps that increased their capacity had their spill points at their southernmost tips at ~1.50 Ma (Fig. 10). Due to W-WSW tilting the traps' spill points were deepened and the trap volume expanded. In 7220/8-1 the deepening of the original spill point resulted in a change of its location to the west which was not the case for 7220/4-1. The reason for that is the location of spill point of 7220/8-1 is more sensitive to tilting than the spill point location of 7220/4-1. Also a more elongated trap shape of 7220/4-1 makes the spill point location switch more difficult to activate than for less elongated trap 7220/8-1. Trap 7119/9-1 decreased its capacity between 1.50 and 0.44 Ma due to shallowing of its spill point located at its northern tip. Ice loading at ~0.44 Ma removed tilting in the W-WSW direction and changed the tilt azimuth to nearly the opposite direction (E-ESE). This resulted in a minor trap volume decrease in 7220/4-1 and volume increase in 7220/8-1 and 7119/9-1. The spill point of 7220/8-1 switched back to its original location (from 1.50 Ma). After the glacial rebound the trap volumes and spill points returned to their values and locations from ~0.44 (ice-free conditions).

The differential uplift between 0.44 and 0.00 Ma led to a deepening of the original spill point in 7220/4-1 and a switch of its location to the northeast. As a result, the trap volume increased by about 4%. The westerly located spill point of 7220/8-1 was significantly shallowed by the WSW directed tilting causing the trap capacity drop of 8% between 0.44 and 0.00 Ma. Similarly the spill point of 7119/9-1 was shallowed causing a 15% drop of the volume. The most recent glaciations (at ~0.00 Ma) led to almost no trap volume change in the 7220/4-1. The spill point was however switched to its original location (at the southern tip). The trap capacity of 7220/8-1 increased during the ice loading event mostly due to the tilt magnitude decrease compared to the ice-free conditions. The same occurred for 7119/9-1. After the ice retreat the trap volumes and spill points returned to their values and locations from ~0.00 Ma (ice-free conditions). At present the trap capacity of 7220/4-1 is 6% larger than before glaciations while 7220/8-1 and 7119/9-1 are 5 and 14% smaller respectively.

3.2.3. Hydrocarbon spillage

The amount of the hydrocarbon spillage is here related to change of trap capacity, and volume changes of the hydrocarbons occupying the pore space within the trap (section 2.2.2). The gas-water and oil-water contacts are shown in Fig. 10. In addition, Fig. 11 shows remaining oil and gas volumes at standard conditions (not affected by the reservoir temperature and pressure) through the Pleistocene.

In the analyzed traps the hydrocarbon spillage occurred during all the sediment redistribution and ice loading events. Between 1.50 and 0.44 Ma gas spillage is modelled in all of the analyzed traps. It occurred regardless of positive or negative changes of the trap capacity (Fig. 8). The main mechanism is therefore related to a substantial volume expansion driven by pressure and temperature

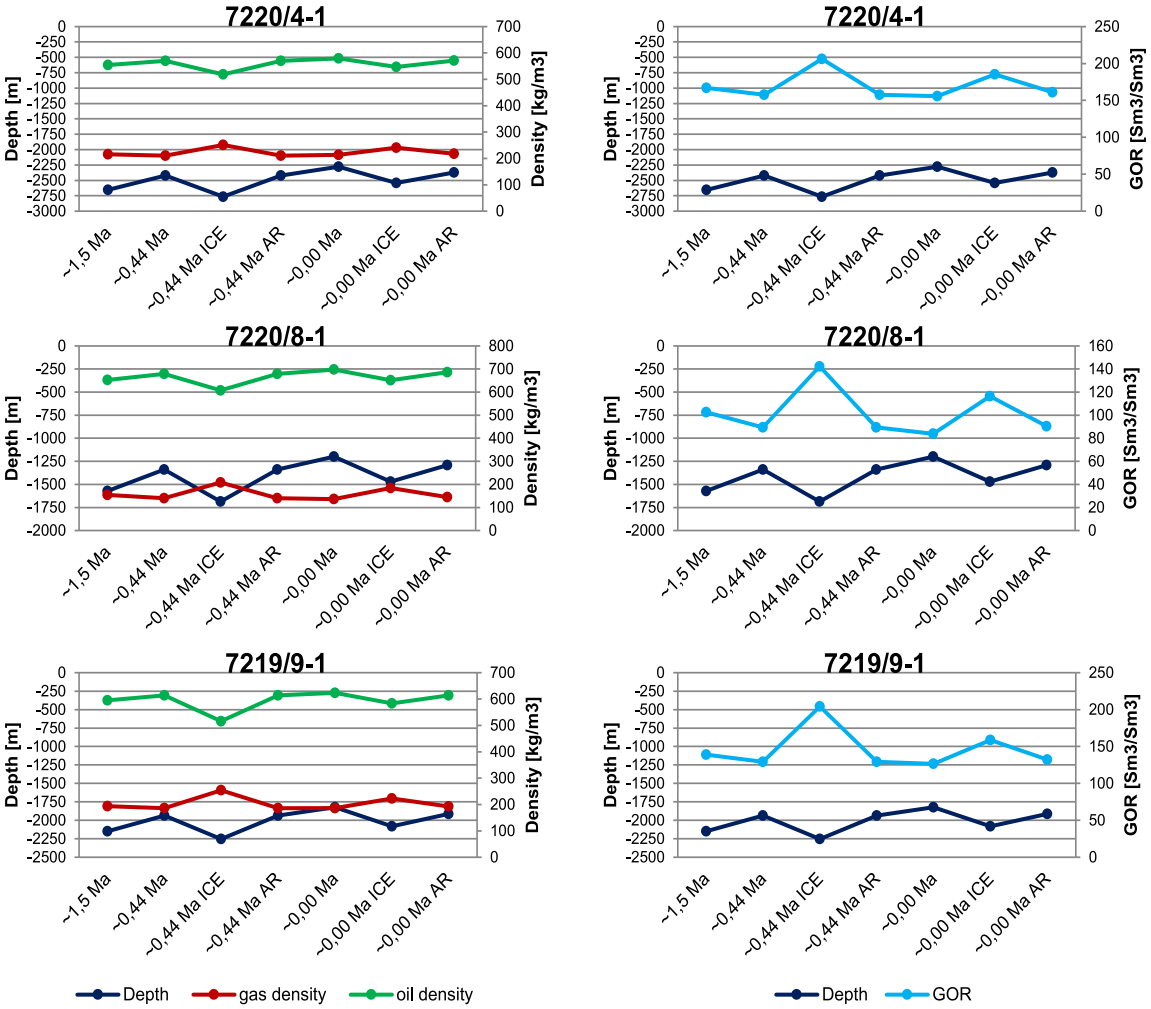

Fig. 7. Hydrocarbon densities and GOR changes for additional dual-hydrocarbon-phase scenario in the analyzed hydrocarbon traps. ICE: at ice conditions, AR: after retreat.

decrease. The gas volumes that exceeded the trap capacity were spilled out through the spill points as shown in Fig. 10. No oil spillage is modelled during the timestep due to oil density increase (Fig. 6) and resulting volume drop (Fig. 10) as well as increase of the trap capacity (7220/4-1, 7220/8-1, see Fig. 8).

The ice loading at ~0.44 Ma caused little gas spillage in 7220/4-1. The gas spillage is modelled due to a gradual build-up of the ice thickness, and resulting short-time pressure drop when the sea water is substituted by a thin ice (section 2.2.2). In all the traps gas volumes visibly decreased at the reservoir conditions (Fig. 10). A slight oil volume drop was also observed. The sediment redistribution and shelf uplift between 0.44 and 0.00 Ma led to gas and oil spillage in 7220/8-1 and 7119/9-1 (Figs. 10 and 11). In both traps the main reason for spillage is the drop of the trap capacity between 0.44 and 0.00 Ma (Fig. 8). The second reason for the gas spillage in 7119/9-1 is the gas expansion (Fig. 6). No spillage occurs in 7220/4-1 due to decrease of the hydrocarbon volumes and increase of the trap capacity. The ice loading and related depth increase at ~0.00 Ma caused a significant gas volume drop and minor spillage in 7220/8-1 and 7119/9-1 (Figs. 10 and 11). The spillage is again related to the gradual build-up of the ice thickness. The entire ice ages resulted in no loss of oil in 7220/4-1 and 4% and 13% of oil loss in 7220/8-1 and 7119/9-1 respectively. The gas loss was found to be higher than the oil loss reaching 3%, 20% and 22% in 7220/4-1, 7220/8-1 and 7119/9-1 respectively.

The hydrocarbon spillage led to minor changes of the hydrocarbon-water-contacts. The calculated difference between the maximum hydrocarbon column height and the present-day height represents the thickness of palaeo-hydrocarbon zone (explained in Fig. 3). The palaeo-hydrocarbon zones were found to be similar regardless of the phase the traps were filled by with. In the well location of 7220/4-1 the zone was modelled as 3 m, in 7220/8-1 1–2 m and in 7119/9-1 as 13–17 m.

4. Discussion

4.1. Modelling limitations and potential impact of different glacial and sediment settings

Previous studies (Doré, 1995; Doré and Jensen, 1996; Duran et al., 2013) point out the problem of the hydrocarbon spillage during the Cenozoic including the ice ages as one of the most

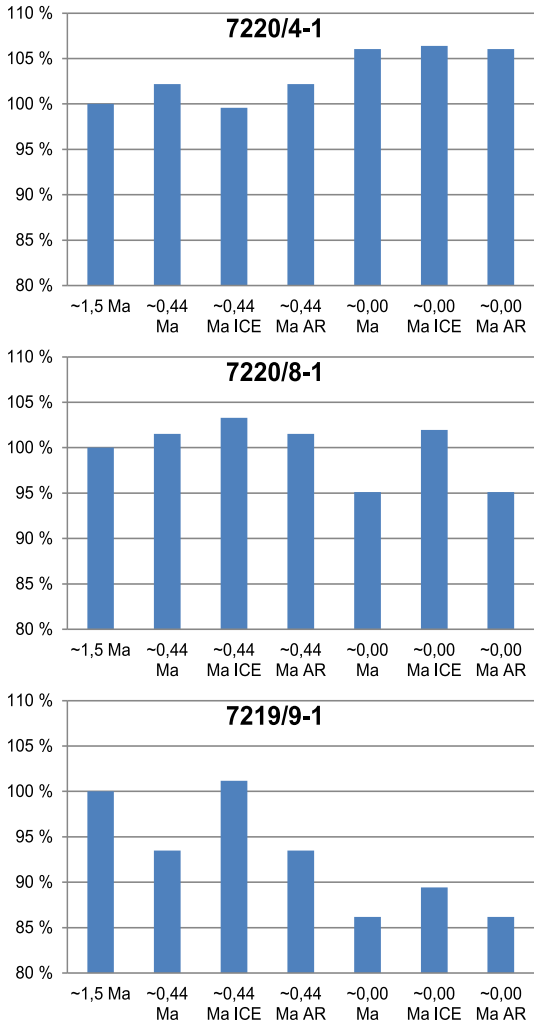

Fig. 8. Trap capacity (total trap volume) change of the analyzed hydrocarbon traps in relation to the onset of glaciations (~1.50 Ma). ICE: at ice conditions, AR: after retreat.

critical for depleting the Barents Sea traps. In this paper that hypothesis was tested for the Bjørnøyrenna Fault Complex by using a combination of flexural isostasy and secondary migration modelling.

The input to the isostatic reconstructions was based on erosion/deposition thickness model of Laberg et al. (2012) where homogenous densities of eroded and deposited sediments were used. By using the homogenous sediment densities one may expect minor underestimation of the uplift amount in the erosional area and minor overestimation of the subsidence in the depositional area. This is due to higher compaction level (and density) of the eroded rocks than redeposited products of the erosion. The thickness values are provided as averages for either the Barents Sea shelf (1.50–0.44 Ma) or the trough areas (0.44–0.00 Ma). In addition to glacial erosion in the study area assumed by the model, some glacial deposition took place during the Pleistocene resulting in deposition of 50–100 m of the Nordland Group in the area of the analyzed traps (Amantov and Fjeldskaar, 2016; Norwegian Petroleum Directorate, http://factpages.npd.no/). The glacial deposits in the outer part of the shelf consist of sediments deposited during different periods during the last 0.44 Ma (Sættem et al., 1992; Vorren et al., 1990). The presence of glacial deposits of different ages suggests that some deposition might have occurred in addition to erosion due to sediment transfer within the drainage area and/or sediment inflow from the outside. This could have occurred both during glacial and interglacial periods. In addition, numerical modelling showed that the study area most likely experienced sedimentary conditions ranging from net erosion (0.68 ± 1.60 mm/a, well 7220/8-1) to net deposition (1.97 ± 1.55 mm/a, well 7219/9-1) during cold periods and deposition during warm periods (0.12 ± 0.1 mm/a) in timespan between 0.44 and 0.00 Ma (Zieba et al., 2016). If glacial erosion is counteracted by the process of glacial deposition then the resulting uplift amount is diminished. Such a situation might have occurred in the area where the hydrocarbon traps were analyzed. The problem of the intermittent glacial deposition is however not addressed here so the uplift values should be considered as the maximum values. Tilting might also be expected to deviate somehow from provided directions and values. Used erosion/deposition model provides generalized and averaged erosion trends based on main erosion indicators i.e. mega-scale glacial lineations (Laberg et al., 2012). The model differs from Weichselian erosion/deposition model (the last 0.12 Ma) showing more local character of sediment redistribution (Amantov et al., 2011). The local erosion/deposition model might in turn lead to more pronounced tilting than by using averaged erosion models. In addition, tilt directions could be altered leading to a shift of the spill point locations and directions of the secondary migration. This is especially important for traps 7220/4-1 and 7220/8-1 which are susceptible for change of the spill point locations due to a low depth difference between hydrocarbon-water contact and alternative spill points (section 3.2.2). Moreover, locations of the modelled spill points of these traps can be challenged due to uncertainties related to input data (section 2.2.2). The effect of local sediment redistribution on the flexural isostasy model is the most pronounced in areas where the elastic part of the lithosphere is sufficiently thin since the thin lithosphere has low rigidity for short-wavelength loads (Turcotte and Schubert, 2002).

This paper gives an overview of the impact of shelf-edge glaciations on the hydrocarbon traps after ~0.44 Ma. The LGM ice sheet model at the age of its maximum thickness was used (Peltier et al., 2015) giving the highest isostatic response values. A complete influence of the Pleistocene glaciations on hydrocarbon loss is not addressed here. A full overview of potential impact of the Pleistocene glaciations on the hydrocarbon traps should in addition attempt to consider available pre ~0.44 Ma and Weichselian ice sheet models. Knies et al. (2009) provided ice sheet extent models for a timespan of ~3.5–1.0 Ma. The minimum models imply only the northern Barents Sea (including Svalbard and Frans Josef Land) were glaciated. The maximum model of glaciations between ~2.4 and ~1.0 Ma implies the Barents Sea Ice Sheet extended from the northern shelf break to the central-southern Barents Sea. This potentially can lead to tilting of the study area to the north, differently than the dominant tilt direction presented in this paper (east). Potential tilting to the north could have shallowed the modelled spill points of 7220/4-1 and 7220/8-1 located at the southern parts of the traps at ~1.50 Ma and decrease the traps' capacities. The tilting to the north could have resulted in the opposite effect in 7219/9-1, i.e. deepening of the spill point located at the northern tip and increase of the trap capacity. Switch of the spill point is not considered likely in 7219/9-1 because the spill point of this trap is not very sensitive to tilting (section 3.2.2). In the light of uncertain location of the spill points of 7220/4-1 and 7220/8-1 at the early stages of the glacial ages (section 3.2.2) it seems likely that the hydrocarbon traps had indeed the spill points to the

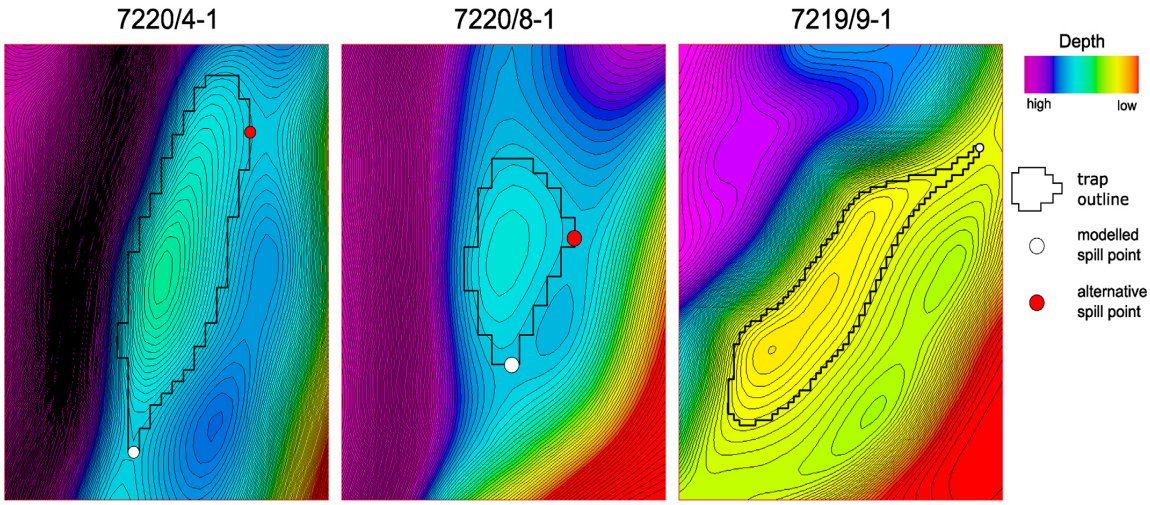

Fig. 9. Pre-glacial (~1.50 Ma) trap outlines and modelled spill points over top reservoir depth map. Black isolines show top reservoir depth. 7220/4-1 and 7220/8-1 isoline interval = 10 m, 7219/9-1 isoline interval = 50 m. For explanation of alternative locations of the spill points see text in section 3.2.2.

south for at least short time intervals. Siegert et al. (2001); Svendsen et al. (2004) proposed Barents Sea ice models for the most recent glaciations (~0.14–0.02 Ma). The ice models show generally lower thicknesses than the model used in this study (Peltier et al., 2015) what could result in lower isostatic downwarping and tilt magnitudes than modelled in this study. During the Early Weichselian (0.09–0.08 Ma) the Bear Island Trough and southwestern Barents Sea is thought to remain ice-free while surrounding areas are considered to be glaciated. Ice loading of such extent might have alternated tilt directions in the study area to the north, favorable for setting the spill points of 7220/4-1 and 7220/8-1 at the southern part of the traps. During the Early Weichselian glaciation the spill points of 7220/4-1 and 7219/9-1 could have been located at the same position as at modelled ice conditions at ~0.00 Ma (Fig. 10). In contrast, the Early Weichselian loading could have led to switch of the 7220/8-1's spill point from the east to the south to approximately the same position as during modelled ice loading event at ~0.44 Ma (Fig. 10). The early Weichselian glacial event might have resulted in either minor trap capacity reduction or minor increase in 7220/4-1 and 7220/8-1 compared to the ice free conditions at ~0.00 Ma. The magnitude of capacity change is dependent on the ice thickness which is somehow uncertain at this age (Siegert et al., 2001). The early Weichselian glaciation would result in trap capacity increase in regard to the ice-free conditions in 7219/9-1 due to deepening of the northerly located spill point.

The LGM shelf-edge glaciation lasted for about 7 ka (Peltier et al., 2015). For this duration the isostatic equilibrium can be fully achieved (Fjeldskaar, 1997; van den Berg et al., 2008). The western Barents Sea deglaciated within about 1–2 ka, first retreating from the deep Bear Island Trough and southwestern Barents Sea (Amantov and Fjeldskaar, 2013; Winsborrow et al., 2010). This event might temporarily tilt the sedimentary units to the north leading to similar changes of the trap orientation and capacities as for the early Weichselian glaciation. The impact of this event was not assessed in this paper due to short duration that might resulted in minor isostatic readjustment and thus small influence on the tilting directions.

Another factor that potentially can alter modelled tilt values is a movement of fault blocks due to applied or removed loads, for example an ice sheet load. Instead of the flexure the crust can responded to the applied/removed load by a displacement of fault blocks which does not lead to tilting (Hetzel and Hampel, 2005). The magnitude of such displacements in the Barents Sea is however unknown and this factor is not addressed here in this paper.

4.2. Trap capacity changes

Kjemperud and Fjeldskaar (1992) suggested a synthetic trap located in the Barents Sea can loss 30% of trap capacity due to only glacial loading events. Both model of Kjemperud and Fjeldskaar (1992) and the model presented in this paper assume that traps were completely filled by hydrocarbons prior to isostatic events. Model of Kjemperud and Fjeldskaar (1992) differs however in respect to trap geometry, number of isostatic events and hydrocarbon density fluctuations through burial history. Their model assumes a synthetic bar triangular in section trap structure, orientated along E-W axis. They considered 3 isostatic events of different magnitudes. In contrast to this study, the model of Kjemperud and Fjeldskaar (1992) aims only for calculation of the closure volume change where fluid density changes are not considered. According to the results presented in this paper such high volume reduction cannot be expected for the analyzed traps in the Bjørnøyrenna Fault Complex. Here it was shown that structural changes due to ice loading and differential uplift can lead to either increase or decrease of the total trap capacity in a range of 5–14%.

The trap capacity change is dependent on tilt magnitude, orientation of the longest trap axis to the maximum tilt direction as well as spill point orientation (Kjemperud and Fjeldskaar, 1992). Here it is shown that the initial geometrical setting controls the magnitude of capacity change of the trap structures in the Bjørnøyrenna Fault Complex. Trap 7219/9-1 experienced maximum tilting in the same direction as the direction of its longest axis and the highest tilt values from all of the analyzed traps. As a result, trap 7219/9-1 recorded the highest volume reduction of all of the traps.

The spill point orientation versus tilt direction was shown to be a critical factor for the capacity changes of traps 7219/9-1 and 7220/4-1. The traps show similar direction of the longest trap axis, similar tilt azimuth and a small difference of the tilt magnitude. The initial spill point of 7219/9-1 was located at its northern tip, while the spill point of 7220/4-1 was situated at its southern tip. The WSW

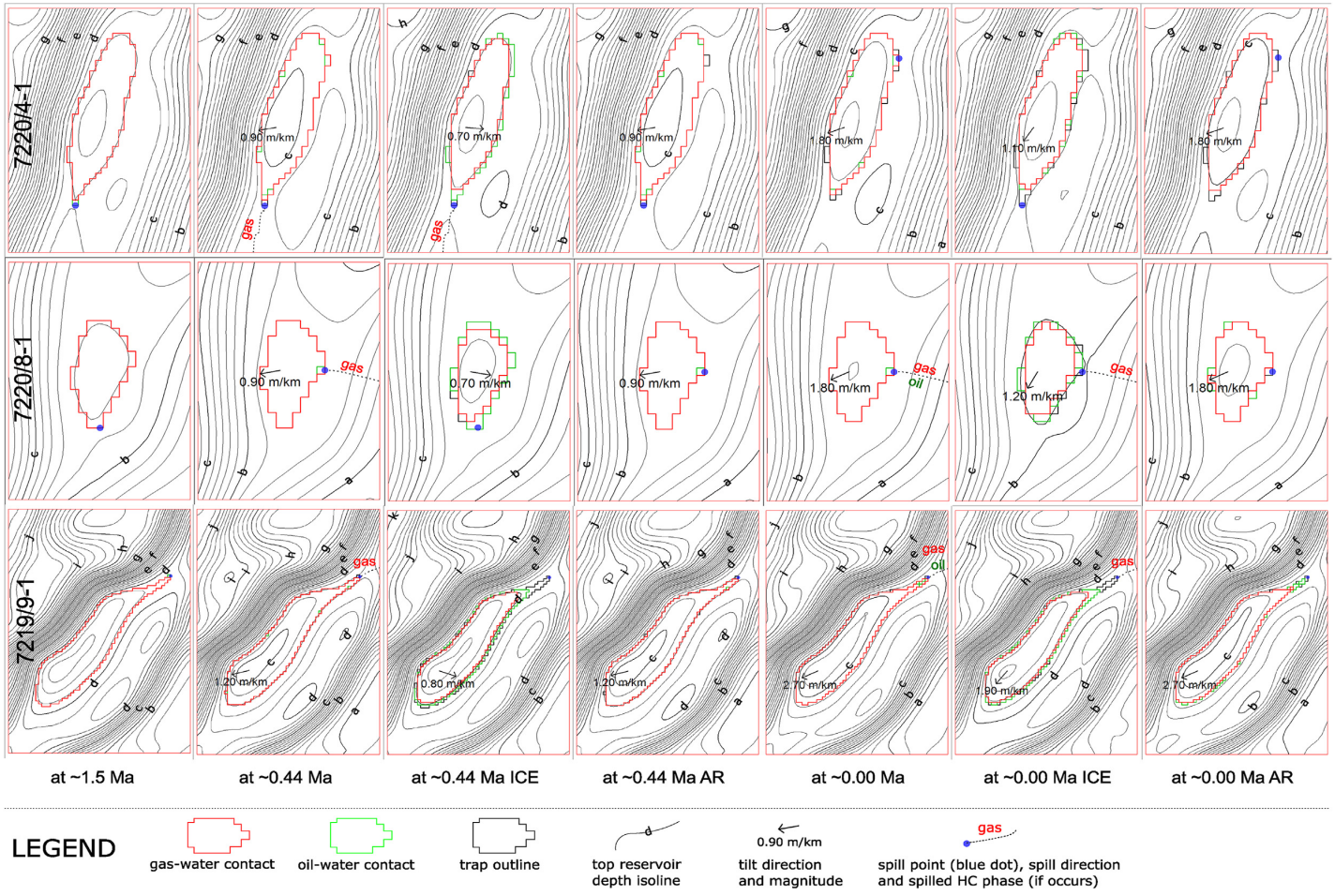

Fig. 10. Changes in the trap orientation and hydrocarbon contacts during the Pleistocene. The maps show changes in trap outlines (black lines), gas-water contacts (if the trap is filled by gas, red line), oil-water contacts (if the trap is filled by oil, green line) and spill-point (blue dot), spill-directions (black irregular lines). Some of the contacts might overlap. The gas-water contacts are on top of the oil-water contacts and trap outlines. The maps show also tilt direction and its magnitude induced by sediment redistribution or ice loading. Thin black isolines show top reservoir depth. Depths are labelled by letters where 'a' represents the lowest value and 'k' the highest. Isoline interval = 500 m. The same labels in different traps do not represent the same values. ICE: at ice conditions, AR: after retreat.

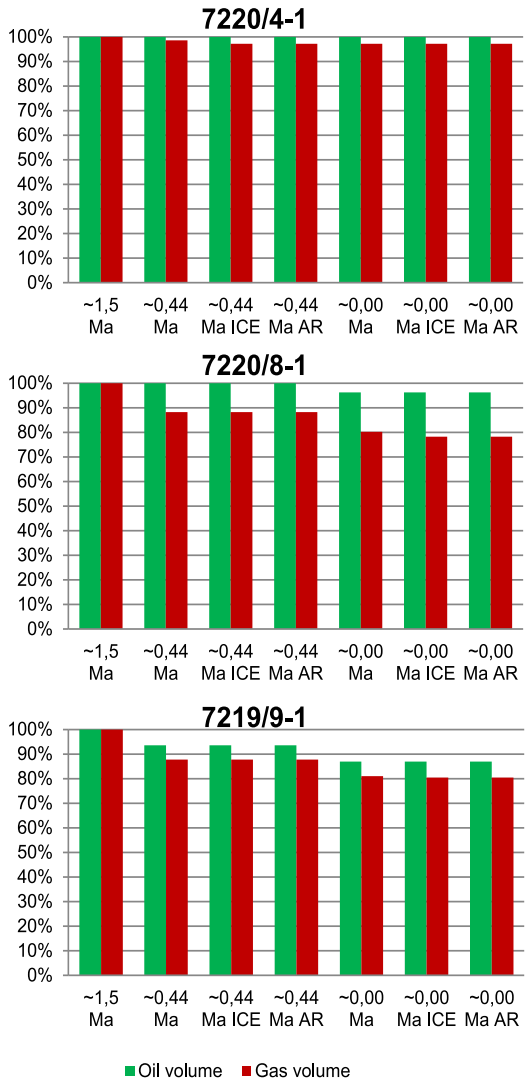

Fig. 11. Oil and gas volume changes in the analyzed hydrocarbon traps in relation to the onset of glaciations (~1.50 Ma). ICE: at ice conditions, AR: after retreat.

directed maximum tilt resulted in shallowing of the spill point in 7219/9-1 and 14% of trap volume reduction. In contrast, the original spill point of 7220/4-1was deepened resulting in 6% increase of trap volume and switch of the spill point location.

Since the deformation gradient plays also a major role in the trap volume change (Kjemperud and Fjeldskaar, 1992), it is expected that the high tilt of the stratigraphic units in the areas west of the Bjørnøyrenna Fault Complex might have led to much higher variations in the trap capacity, potentially causing a higher amount of spillage. In order to roughly estimate the isostatic impact on trap capacity change in the westernmost basins (the highest tilt values, Figs. 4 and 5), the analyzed traps from the Bjørnøyrenna Fault Complex were simply moved to the central part of the Sørvestsnaget Basin (Fig. 5A). The present-day trap depths and geometry remained unchanged. The results showed a 15% trap capacity increase in 7220/4-1, a 3% capacity reduction in 7220/8-1 and a 31% capacity reduction in 7219/9-1. Compared to the volume changes from the Bjørnøyrenna Fault Complex, 7220/4-1 and 7219/9-1 experienced 2–3 times larger trap capacity changes when the traps were moved to the Sørvestsnaget Basin. In contrast, the capacity change of 7220/8-1 was 2 times lower if the trap is moved to the west. The trap volume change estimates provided by this simplistic exercise cannot be treated as realistic numbers for the traps located in the Sørvestsnaget Basin simply due to different trap geometry. The exercise gives however an insight of the trap capacity change magnitudes due to higher deformation gradient (7220/4-1 and 7219/9-1), but it again demonstrates that the resulting trap volume change is very dependent on the orientation of the trap axis and spill point (7220/8-1). In the latter case 4–5 m/km higher depth gradient caused a lower trap volume loss than the original one (in the Bjørnøyrenna Fault Complex). This is due to a shift of the maximum tilting direction to more perpendicular to the trap axis and spill point direction than it was where the trap was originally located. It might also be expected that lower tilt values that were modelled in the areas east of the Bjørnøyrenna Fault Complex could potentially have lower impact on trap capacity than on those in the Bjørnøyrenna Fault Complex. In some parts of the Bjarmeland or Finnmark platforms the glacially-induced tilt is close to zero (Figs. 4 and 5), potentially not causing any spillage. The realistic trap capacity loss/increase in the eastern parts of the study area has to be however evaluated considering the initial geometry of the traps.

Generally the western Barents Sea trap structures with present spill points to the west and south experienced Pleistocene trap capacity increase and were not vulnerable to spillage during the glaciations. The traps with the present spill points to the east and north might have experienced either volume reduction or increase. If the pre-glacial spill points were also located in the north or east the traps would have lost their capacities (like 7219/9-1). Traps elongated in the tilting direction can be expected to lose more capacity than non-elongated traps. If the spill points were located to the south or west the traps might have experienced capacity increase at the early stage of the uplift (like 7220/4-1 and 7220/8-1). Further sediment redistribution and isostatic response might have however resulted in capacity reduction if the spill point location was switched to the north or east at the early stage of glaciations (like 7220/8-1).

4.3. Hydrocarbon loss due to spillage

This paper aims to assess the maximum amount of the hydrocarbon spillage due to the ice loading and differential uplift. Therefore the calculations were conducted by filling the traps to their spill points either by gas or oil at the onset of glaciations and conducting reconstruction of trap orientation together with the secondary migration modelling. This approach does not give realistic values of the hydrocarbon spillage amount in the Barents Sea due to possible incomplete filling of the traps prior to glaciations and dual hydrocarbon phases of some traps (Doré and Jensen, 1996; Duran et al., 2013; Henriksen et al., 2011). The approach provides however a considerable insight about the Pleistocene spillage mechanisms.

The general risk of hydrocarbon spillage is increased with reduction in trap capacity and increase in hydrocarbon trap volume. Hydrocarbon filling at time steps where hydrocarbon density is low (Fig. 6), and time steps with decreased trap capacity (Fig. 7) will thus have high risk of hydrocarbon spill. According to the model presented here with no filling between 1.50 Ma and 0.00 Ma most of the hydrocarbon spillage occurred due to the Pleistocene sediment redistribution and an insignificant amount was spilled during the ice loading episodes. The reason for low spillage during the glaciations is related to two factors. The first is linked to trap

volume increase/insignificant reduction due to ice loading in relation to the ice-free conditions at the same time. The second is hydrocarbon (especially gas) volume drop due to deeper burial.

The modelled oil phase loss reflects spillage mostly resulting from the tilting due to very low oil density fluctuations (section 3.2.1). The tilting can result in maximum 0–13% spilled hydrocarbons. In the additional exercise trap 7219/9-1 (the trap that experienced the most spillage) was filled to 86% instead of 100% by oil. This resulted in no spillage at all. Both tilting and the gas volume increase due to uplift can lead to a maximum loss of 3–22% of hydrocarbons (section 3.2.3). Gas expansion might also be a significant mechanism for hydrocarbon trap depletion even if a trap is partly filled by hydrocarbons. 9% of the gas loss was modelled if the trap 7219/9-1 was filled to 88% by gas. In dual hydrocarbon phase situations, gas exsolution is proposed as a mechanism for forcing oil below spill point, especially for traps that do not blead off (leak) gas vertically through the top seal (e.g. Doré, 1995; Ohm et al., 2008). The dissolution/exsolution of gas in oil is sensitive to pressure and temperature regime (Silverman, 1965). The burial depth of trap 7220/8-1 is shallower than other two locations (i.e. lower pressure at hydrostatic conditions), and is potentially dissolving less gas according to the model with dual phase. The overall hydrocarbon volume change between glacial time steps is hence lower for this location compared to the two other locations for dual phase. In other words, the effect of gas exsolution will be more pronounced for 7220/4-1 and 7219/9-1 during ice retreat and the erosion events (Fig. 7). On the contrary, the models indicate that traps in depth regime of 7220/8-1 can be more sensitive to gas expansion/contraction (during ice retreat and erosion events) compared to deeply buried traps like 7220/4-1 and 7219/9-1 (Fig. 6). Overall, The models presented in this paper indicate that gas expansion might have been an important factor for the hydrocarbon depletion from the Bjørnøyrenna Fault Complex traps supporting the literature findings (Doré, 1995; Doré and Jensen, 1996; Henriksen et al., 2011; Ohm et al., 2008), but tilting alone cannot have caused any significant trap depletion during the Pleistocene.

The Cenozoic spillage and leakage are thought to be responsible for previously larger degrees of trap filling demonstrated by palaeo-oil shows (Cavanagh et al., 2006; Doré, 1995; Doré and Jensen, 1996; Duran et al., 2013; Henriksen et al., 2011; Nyland et al., 1992). The maximum thicknesses of palaeo-oil shows induced by the Pleistocene spillage from tilted traps are modelled between 2 and 17 m. The low values fit well core data from the 7220/8-1 that display no oil shows at all. In addition, lack of the palaeo-hydrocarbon column in 7220/8-1 might also be due to the recent filling of the trap. Observed approximately 100 m of residual oil in 7220/4-1 and only residual oil column (without any present accumulation) in 7219/9-1 cannot be explained by the Pleistocene tilting. The reason for the previously larger degree of filling might therefore be related to caprock or fault leakage (Duran et al., 2013; Fanavoll et al., 2012; Hermanrud et al., 2014; Ohm et al., 2008) or pre-glacial spillage (Doré, 1995; Doré and Jensen, 1996). A more detailed explanation of the observed hydrocarbon phases and residual hydrocarbon columns will require an integrated study of expulsion history together with top and fault seal behavior in order to get the timing and magnitude of the complex fill-spill history within the study area of western Barents Sea.

5. Conclusions

The isostatic response on the Pleistocene sediment redistribution and ice loading was evaluated for the Barents Sea. The isostatic impact on hydrocarbon trap capacity changes and hydrocarbon maximum spillage was assessed for the traps in the Bjørnøyrenna Fault Complex. The spillage amount was modelled by filling the traps at Jurassic level by either a gas or an oil phase at the onset of glaciations and calculating the hydrocarbon loss due the structural changes (assuming a tight cap rock). The main findings are as follows.

1. The Pleistocene erosion resulted in up to 350 m of total depth change between onset of glaciations and the present. The highest values were modelled in the Bear Island Trough area.
2. Trap capacity could have been either increased (6% in 7220/4-1) or reduced (5 and 14% in 7220/8-1 and 7219/9-1 respectively) between the onset of glaciations and the present.
3. Apart from the tilt magnitude the most important factor controlling the trap capacity change was the initial geometric setting of the traps. This includes the spill point orientation as well as the relationship between orientation of maximum tilt and the longest trap axis.
4. All of the analyzed hydrocarbon traps have their present spill points at the north-northeastern ends. The preglacial spill points of 7220/4-1 and 7220/8-1 were however located at their southernmost tips. Ice loading events might have caused short-term spill point location switches.
5. The western Barents Sea traps with present spill points to the west and south experienced Pleistocene trap volume increase and were not susceptible to spillage. The traps with the present spill points to the east and north might have experienced either trap volume increase or decrease depending on the pre-glacial location of the spill point.
6. The relative degree of gas expansion/contraction was at maximum between ice and ice-free conditions. During ice retreat this resulted in gas density decrease up to 49% for 7220/8-1, 27% for 7219/9-1 and 20% for 7220/4-1. The degree of gas in solution is higher in 7220/4-1 and 7219/9-1 than in 7220/8-1.
7. The Pleistocene tilting could explain an insignificant part of the palaeo-oil shows that are observed at present in 7220/4-1 and 7219/9-1. The structural changes could not have resulted in any hydrocarbon shows below the oil level in 7220/8-1.
8. Structural changes of the traps caused only by the Pleistocene tilting alone could not have been responsible for any major loss of oil and gas in the Bjørnøyrenna Fault Complex. The tilting accompanied with gas volume expansion might however explain some part of the hydrocarbon loss during the Cenozoic.

Acknowledgements

This study is a part of the project “Impact of Cenozoic structural development and glacial erosion on gas expansion, hydraulic fracturing and leakage in the Western Barents Sea” sponsored by ENI Norge (project number 7020344). KJZ is thankful to ENI Norge for financial support of his Ph.D. and Sintef Petroleum AS for providing infrastructure and overall support. We also thank Filippos Tsikalas for valuable suggestions and Stephen Lippard for correcting the English. We greatly appreciate the constructive comments of Willy Fjeldskaar and one anonymous reviewer which helped us in improving the manuscript.

References

Allen, P.A., Allen, J.R., 2004. Basin Analysis: Principles and Applications, second ed. Wiley-Blackwell.

Amantov, A., Fjeldskaar, W., Cathles, L., 2011. Glacial erosion in the Baltic Sea region: effect on the post-glacial uplift. In: Harff, J., Björck, S., Hoth, P. (Eds.), The Baltic Sea Basin. Springer.

Amantov, A., Fjeldskaar, W., 2013. Geological - geomorphological features of the Baltic region and adjacent areas: imprint on glacial - postglacial development. Regional Geol. Metallog. 53, 90–104.

Amantov, A., Fjeldskaar, W., 2016. Ice age and coastal adaptions. In: Proceedings for EMECS'11 SeaCoasts XXVI. Russia, St. Petersburg.

Boulton, G.S., Caban, P., 1995. Groundwater flow beneath ice sheets: Part II — its impact on glacier tectonic structures and moraine formation. Quat. Sci. Rev. 14, 563–587.
Butt, F.A., Drange, H., Elverhoi, A., Ottera, O.H., Solheim, A., 2002. Modelling Late Cenozoic isostatic elevation changes in the Barents Sea and their implications for oceanic and climatic regimes: preliminary results. Quat. Sci. Rev. 21, 1643–1660.
Cardozo, N., 2009. 3D Flexural Modeling. Continuous Plate of Variable Elastic Thickness (Finite Difference Solution). Matlab script. http://www.ux.uis.no/~nestor/work/matlabScripts.html (accessed 11.07.16).
Cavanagh, A.J., Di Primio, R., Scheck-Wenderoth, M., Horsfield, B., 2006. Severity and timing of cenozoic exhumation in the southwestern Barents sea. J. Geol. Soc. 163, 761–774.
de Boer, B., Lourens, L.J., van de Wal, R.S., 2014. Persistent 400,000-year variability of Antarctic ice volume and the carbon cycle is revealed throughout the Plio-Pleistocene. Nat. Commun. 5, 2999.
Dimakis, P., Braathen, B.I., Faleide, J.I., Elverhøi, A., Gudlaugsson, S.T., 1998. Cenozoic erosion and the preglacial uplift of the Svalbard–Barents Sea region. Tectonophysics 300, 311–327.
Doré, A.G., 1995. Barents sea geology, petroleum resources and commercial potential. Arctic 48, 207–221.
Doré, A.G., Jensen, L.N., 1996. The impact of late Cenozoic uplift and erosion on hydrocarbon exploration: offshore Norway and some other uplifted basins. Glob. Planet. Change 12, 415–436.
Duran, E.R., di Primio, R., Anka, Z., Stoddart, D., Horsfield, B., 2013. 3D-basin modelling of the Hammerfest Basin (southwestern Barents Sea): a quantitative assessment of petroleum generation, migration and leakage. Mar. Pet. Geol. 45, 281–303.
Elverhøi, A., Hooke, R.L., Solheim, A., 1998. Late Cenozoic erosion and sediment yield from the Svalbard–Barents Sea region: implications for understanding erosion of glacierized basins. Quat. Sci. Rev. 17, 209–241.
Fanavoll, S., Ellingsrud, S., Gabrielsen, P.T., Tharimela, R., Ridyard, D., 2012. Exploration with the use of EM data in the Barents Sea: the potential and the challenges. First Break 30, 89–96.
Fjeldskaar, W., 1997. Flexural rigidity of Fennoscandia inferred from the postglacial uplift. Tectonics 16, 596–608.
Fjeldskaar, W., Lindholm, C., Dehls, J., Fjeldskaar, I., 2000. Postglacial uplift, neotectonics and seismicity in Fennoscandia. Quat. Sci. Rev. 19, 1413–1422.
Hamborg, M., Tømmerås, A., Sylta, Ø., Kjennerud, T., Lothe, A.E., Weiss, H.M., Borge, H., 2006. Semi 4.30 User's Manual. SINTEF Petroleum Research, Trondheim.
Henriksen, E., Bjørnseth, H.M., Hals, T.K., Heide, T., Kiryukhina, T., Kløvjan, O.S., Larssen, G.B., Ryseth, A.E., Rønning, K., Sollid, K., 2011. Uplift and erosion of the greater Barents Sea: impact on prospectivity and petroleum systems. Geol. Soc. Lond. Memoirs 35, 271–281.
Hermanrud, C., Halkjelsvik, M.E., Kristiansen, K., Bernal, A., Stromback, A.C., 2014. Petroleum column-height controls in the western Hammerfest Basin, Barents sea. Pet. Geosci. 20, 227–240.
Hetzel, R., Hampel, A., 2005. Slip rate variations on normal faults during glacial-interglacial changes in surface loads. Nature 435, 81–84.
Johansen, H., Fjeldskaar, W., Mykkeltveit, J., 1996. The influence of glaciation on the basin temperature regime: Glob. Planet. Change 12, 437–448.
Kjemperud, A., Fjeldskaar, W., 1992. Pleistocene glacial isostasy - implications for petroleum geology. In: Larsen, R.M., Brekke, H., Larsen, B.T., Talleraas, E. (Eds.), Structural and Tectonic Modelling and its Application to Petroleum Geology. NPF Special Publication, Amsterdam, pp. 187–195.
Knies, J., Matthiessen, J., Vogt, C., Laberg, J.S., Hjelstuen, B.O., Smelror, M., Larsen, E., Andreassen, K., Eidvin, T., Vorren, T.O., 2009. The Plio-Pleistocene glaciation of the Barents Sea–Svalbard region: a new model based on revised chronostratigraphy. Quat. Sci. Rev. 28, 812–829.
Laberg, J.S., Andreassen, K., Knies, J., Vorren, T.O., Winsborrow, M., 2010. Late Pliocene-Pleistocene development of the Barents sea ice sheet. Geology 38, 107–110.
Laberg, J.S., Andreassen, K., Vorren, T.O., 2012. Late Cenozoic erosion of the high-latitude southwestern Barents Sea shelf revisited. Geol. Soc. Am. Bull. 124, 77–88.
Landvik, J.Y., Bondevik, S., Elverhøi, A., Fjeldskaar, W., Mangerud, J., Salvigsen, O., Siegert, M.J., Svendsen, J.I., Vorren, T.O., 1998. The last glacial maximum of Svalbard and the Barents sea area: ice sheet extent and configuration. Quat. Sci. Rev. 17, 43–75.
Lerche, I., Yu, Z., Tørudbakken, B., Thomsen, R.O., 1997. Ice loading effects in sedimentary basins with reference to the Barents Sea. Mar. Pet. Geol. 14, 277–338.
Løseth, L.O., Wiik, T., Olsen, P.A., Hansen, J.O., 2014. Detecting Skrugard by CSEM — Prewell prediction and postwell evaluation. Interpretation 2, SH67–SH78.
Mattingsdal, R., Knies, J., Andreassen, K., Fabian, K., Husum, K., Grøsfjeld, K., De Schepper, S., 2014. A new 6 Myr stratigraphic framework for the Atlantic–Arctic Gateway. Quat. Sci. Rev. 92, 170–178.
Nyland, B., Jensen, L.N., Skagen, J., Skarpnes, O., Vorren, T., 1992. Tertiary uplift and erosion in the Barents Sea: magnitude, timing and consequences. Struct. Tect. Model. Appl. Pet. Geol. 153–162.
Ohm, S.E., Karlsen, D.A., Austin, T.J.F., 2008. Geochemically driven exploration models in uplifted areas: Examples from the Norwegian Barents Sea. AAPG Bull. 92, 1191–1223.
Peltier, W.R., Argus, D.F., Drummond, R., 2015. Space geodesy constrains ice age terminal deglaciation: the global ICE-6G_C (VM5a) model. J. Geophys. Res. Solid Earth 120, 2014JB011176.
Rasmussen, E., Fjeldskaar, W., 1995. Quantification of the Plio-Pleistocene erosion of the Barents sea from present-day bathymetry. Glob. Planet. Change 12, 119–133.
Riis, F., Fjeldskaar, W., 1992. On the magnitude of the late tertiary and quaternary erosion and its significance for the uplift of Scandinavia and the Barents sea. In: Larsen, R.M., Brekke, H., Larsen, B.T., Talleraas, E. (Eds.), Structural and Tectonic Modelling and its Application to Petroleum Geology. NPF Special Publication, pp. 163–185.
Sclater, J.G., Christie, P.A.F., 1980. Continental stretching: an explanation of the post-mid-Cretaceous subsidence of the central north Sea basin. J. Geophys. Res. 85, 3711–3739.
Siegert, M., Dowdeswell, J.A., Hald, M., Svendsen, J., 2001. Modelling the Eurasian ice sheet through a full Weichselian glacial cycle. Glob. Planet. Change 31, 367–385.
Silverman, S.R., 1965. In: Young, A., Galley, J.E. (Eds.), Migration and Segregation of Oil and Gas, Fluids in Subsurface Environments, vol. 4. AAPG Memoir, pp. 53–65.
Standing, M.B., 1977. Volumetric and Phase Behavior of Oil Field Hydrocarbon Systems, SPE. Texas, Richardson.
Svendsen, J.I., Alexanderson, H., Astakhov, V.I., Demidov, I., Dowdeswell, J.A., Funder, S., Gataullin, V., Henriksen, M., Hjort, C., Houmark-Nielsen, M., Hubberten, H.W., Ingólfsson, Ó., Jakobsson, M., Kjær, K.H., Larsen, E., Lokrantz, H., Lunkka, J.P., Lyså, A., Mangerud, J., Matiouchkov, A., Murray, A., Möller, P., Niessen, F., Nikolskaya, O., Polyak, L., Saarnisto, M., Siegert, C., Siegert, M.J., Spielhagen, R.F., Stein, R., 2004. Late Quaternary ice sheet history of northern Eurasia. Quat. Sci. Rev. 23, 1229–1271.
Sylta, Ø., 2004. Hydrocarbon Migration Modelling and Exploration Risk: Dr. Philos. thesis. NTNU Norwegian University of Science and Technology, Trondheim.
Sættem, J., Poole, D.A.R., Ellingsen, L., Sejrup, H.P., 1992. Glacial geology of outer Bjørnøyrenna, southwestern Barents sea. Mar. Geol. 103, 15–51.
Turcotte, D.L., Schubert, G., 2002. Geodynamics Second Edition. Cambridge University Press.
van den Berg, J., van de Wal, R.S.W., Milne, G.A., Oerlemans, J., 2008. Effect of isostasy on dynamical ice sheet modeling: a case study for Eurasia. J. Geophys. Res. Solid Earth 113.
Vening-Meinesz, F.A., 1941. Gravity over hawaiian archipelago and over madeira area. Proc. Koninklijke Nederl. Acad. Wetensia 44, 1–12.
Verweij, J.M., 1993. Hydrocarbon Migration Systems Analysis. Elsevier, Amsterdam.
Vorren, T.O., Lebesbye, E., Andreassen, K., Larsen, K.B., 1989. Glacigenic sediments on a passive continental margin as exemplified by the Barents Sea. Mar. Geol. 85, 251–272.
Vorren, T.O., Lebesbye, E., Larsen, K.B., 1990. Geometry and genesis of the glacigenic sediments in the southern Barents Sea. Geol. Soc. Lond. Spec. Publ. 53, 269–288.
Vorren, T.O., Richardsen, G., Knutsen, S.M., 1991. Cenozoic erosion and sedimentationn in the western Barents Sea. Mar. Pet. Geol. 8, 317–340.
Walderhaug, O., 1994. Precipitation rates for quartz cement in sandstones determined by fluid-inclusion microthermometry and temperature-history modelling. J. Sediment. Res. 64A, 324–333.
Winsborrow, M.C.M., Andreassen, K., Corner, G.D., Laberg, J.S., 2010. Deglaciation of a marine-based ice sheet: late Weichselian palaeo-ice dynamics and retreat in the southern Barents Sea reconstructed from onshore and offshore glacial geomorphology. Quat. Sci. Rev. 29, 424–442.
Zattin, M., Andreucci, B., de Toffoli, B., Grigo, D., Tsikalas, F., 2016. Thermochronological constraints to late cenozoic exhumation of the Barents sea shelf. Mar. Pet. Geol. 73, 97–104.
Zieba, K., Felix, M., Knies, J., 2016. The Pleistocene contribution to the net erosion and sedimentary conditions in the outer Bear Island Trough, western Barents Sea. arktos 2, 1–17.

7 Future research and potential improvements

Future research should aim at testing the hypotheses and results presented in Papers 1-3. In Paper 1 a novel approach used for assessing local glacial ages for long-time scales was proposed. The approach was proven to be valid based on the terrestrial data from the northeastern Poland. However, the method should be tested in more than one area, performing calibration and reliability check in additional regions. The check should preferably be carried out both in marine and non-marine realms.

The main conclusions regarding uplift and burial history (Paper 2 and 3) generally fit conclusions based on thermochronological data (Green and Duddy, 2010; Zattin et al., 2016). The available data coverage is limited and represents only the western Barents Sea. For this reason the results presented in Papers 2 and 3 lack a calibration against data from other than western parts of the Barents Sea. The additional calibration would help in assessing the reliability of the reconstructions provided in Papers 2 and 3.

The flexural isostasy modelling used a uniform elastic thickness model as a main input parameter. The isostatic response and resulting reconstruction of topography might potentially be altered if non-uniform elastic thickness model was used. Such model was recently presented by Gac et al. (in press). In addition, some improvements in the reconstructions could be expected if the modelling script used for calculations of the flexural isostasy could handle different densities of eroded and deposited sediments.

In Paper 3 the impact of the Pleistocene sediment redistribution and glaciations on petroleum systems was addressed. The working area included three trap structures in the Bjørnøyrenna Fault Complex. The paper suggests the impact in the Bjørnøyrenna Fault Complex is rather minor, but it points out that in areas west of the study area the impact could have been more pronounced. It also advocates the impact is very dependent on the initial trap geometry. Therefore, it is suggested to study further the glacial impact in different locations in the Barents Sea shelf, preferably including different trap types than presented in the paper. In Paper 3 the hydrocarbon loss due to only tilting and hydrocarbon volume expansion was studied. It is also suggested that some of the loss during the Pleistocene could be attributed to cap-rock and fault leakage (Doré and Jensen, 1996; Løseth et al., 2014). Future quantitative assessment of the hydrocarbon loss during the Pleistocene should therefore aim at modelling of these leakage processes.

8 Other publications

8.1 Part of reports

Grøver, A., **Zieba, K.J.**, Bakk, A., Frette, O.I., Fjær, E., Beredi, L. (2016). Impact of Cenozoic structural development and glacial erosion on gas expansion, hydraulic fracturing and leakage in the Western Barents Sea. 176 pp. Sintef Petroleum Research (confidential).

This report presents results from the ENI Norge – SINTEF project "Impact of Cenozoic structural development and glacial erosion on gas expansion, hydraulic fracturing and leakage in the Western Barents Sea". Overall the work focussed on interlink between the Cenozoic tectonic history of the Barents Sea and top-seal integrity by using basin modelling methods. The aims of the project were to construct basin models that consider various concepts regarding timing and magnitude of erosion and deposition as well as a new timeframe of glacial and interglacial periods and related ice loading events. The study focus was to develop a new methodology regarding the top-seal integrity. The new methodology was further used to evaluate effects of erosion/deposition and ice loading on the structural evolution of sedimentary basins. Also, the study aimed to evaluate effects of structural evolution on the petroleum system, with special emphasis on spill paths, trap geometries, gas exsolution, gas expansion and top seal integrity.

Krzysztof Jan Zieba (KJZ) was responsible for building basin models further used for secondary migration modelling. The models included two different datasets (different sets of interpreted seismic horizons) and several burial history models. The burial history models include:

- Two scenarios considering Paleogene erosion and sedimentary conditions during the Paleogene–Early Neogene. The scenarios were created based on literature and correlated with seismic data and net erosion estimates from the study area.
- Two scenarios regarding late Neogene erosion/deposition history. The scenarios were developed based on literature data and new ideas regarding the glacial sedimentary conditions in the outer Bear Island Trough, described in Paper 1 "The Pleistocene contribution to the net erosion and sedimentary conditions in the outer Bear Island Trough, western Barents Sea".
- Three scenarios considering the ice-sheet thickness, constructed based on the available models.
- Pleistocene palaeo-water depth maps created based on the outcome from Paper 1.

- Thermal model based on literature data and calibrated to local thermal well data.
- Fault model of the study area constructed based on literature data.

Several migration modelling runs were carried out (in SEMI, Sintef's basin modelling tool) reflecting different basin models, fault assumptions and oil-to-gas-cracking rates. KJZ performed the modelling and analysed results in one of the datasets. The results cover impact of reservoir geometry change (caused by burial history) on trap structures and hydrocarbon migration pathways. In this context, an impact of different fault settings was also addressed. Further, the migration and filling history was studied providing an insight about key structural events controlling the migration history of the study area. In addition, different cap-rock leakage histories were evaluated and compared with corresponding burial history models.

KJZ discussed how different burial history scenarios affected the analysed petroleum system and elaborated the importance of various aspects of the Cenozoic burial history of the western Barents Sea. KJZ showed a relationship between well observations and modelling results providing an expanation of different degree of hydrocarbon fill in selected traps at the present.

8.2 Journal papers

Emmel, B., de Jager, G., **Zieba, K.J.**, Kurtev, K., Grøver, A., Lothe, A.E., Lippard, S.J., Roli, O-A. (2015). A 3D, map based approach to reconstruct and calibrate palaeobathmetries - Testing the Cretaceous water depth of the Hammerfest Basin, southwestern Barents Sea. Continental Shelf Research, v 97, p 21-31.

The paper presents a new method for quantifying and calibrating the palaeo-water depths. The study makes use of shale volume estimated from seismic data and fuzzy logic approach. The method was applied to the Hammerfest Basin, southwestern Barents Sea where the Cretaceous bathymetric development was reconstructed. The study shows that the proposed approach gives reasonable results for simple basin infilling histories and architectures.

Continental Shelf Research 97 (2015) 21–31

Contents lists available at ScienceDirect

Continental Shelf Research

journal homepage: www.elsevier.com/locate/csr

Research papers

A 3D, map based approach to reconstruct and calibrate palaeo-bathymetries – Testing the Cretaceous water depth of the Hammerfest Basin, southwestern Barents Sea

B. Emmel [a,*], G. de Jager [a], K. Zieba [b], K. Kurtev [a], A. Grøver [a], A. Lothe [a], S.J. Lippard [b], O.A. Roli [a]

[a] SINTEF Petroleum, Basin Modelling, S. P. Andersens veg 15 B, Trondheim 7031, Norway
[b] Department of Geology and Mineral Resources Engineering, Norwegian University of Science and Technology (NTNU), NO-7491 Trondheim, Norway

ARTICLE INFO

Article history:
Received 17 June 2014
Received in revised form
17 February 2015
Accepted 18 February 2015
Available online 21 February 2015

Keywords:
Palaeo-bathymetry
Barents Sea
Hammerfest Basin
Cretaceous
Basin modeling

ABSTRACT

A new 3D approach to quantify and calibrate palaeo-water depth (PWD) has been applied to evaluate the Aptian to Maastrichtian/Danian (Cretaceous) bathymetric development in a sub-basin scale within the Hammerfest Basin, southwestern Barents Sea. The results indicate PWD's varying between ca. 200 m and 95 m, recording a local sea-level decrease of ca. 105 m. A calibration against shale volume based on gamma-ray logs from four exploration wells indicates a model sensitivity of ca. +50 m and −150 m. These results are in agreement with empirical PWD estimates obtained from sedimentological and micropalaeontological observations. A comparison with the global eustatic sea level curve indicates that the PWD decrease in the Hammerfest Basin contradicts the general, global trend indicating a primary control by local tectonics such as differential subsidence and uplift along the evolving continental margin offshore north-west Norway.

1. Introduction

The interaction between tectonics, climate and sedimentary processes constantly shapes the Earth's topography resulting in unstable, permanently changing landforms (e.g., Summerfiled et al., 1991; Beaumont et al., 1999). Sedimentary rocks record the changing morphologies and reflect the prevailing palaeo-environmental conditions (e.g., Ganti et al., 2014). Consequently, the dynamics of the sediment transport systems determine the locations of sediment accumulations within a basin. Furthermore, the feedback between seafloor topographies and prevailing currents influence the evolution of aquatic biota (e.g., Nowell and Jumars, 1984). Thus, in aquatic palaeo-environmental (e.g., Mohtadi et al., 2011; Thuy and Meyer, 2013) as well as in basin analysis studies (e.g., Kjennerud and Sylta, 2001; Baur et al., 2010) the depositional depth is one of the most important and challenging parameters of interest. In order to understand routing of sediment transport in complex sediment systems a full three-dimensional (3D) reconstruction of the palaeo-topography, or in a sedimentary basin the palaeo-water depth (PWD), is desirable. However, a full 3D PWD reconstruction requires extensive seismic data coverage and the opportunity to calibrate the restored topographies against external parameters. In a marine setting, micropalaeontological data can help unravel PWD conditions (e.g., Nagy et al., 1997; Speijer et al., 2008; Setoyama et al. 2011) but, in many cases, it is impossible to separate the effect of sediment-transport dynamics and environmental signal preservation (Ganti et al., 2014). For example, a direct extrapolation of modern micropaleontological depth distribution to ancient conditions can be misleading because of sediment re-working (e.g., Emmel et al., 2006) and/or change or shift of an organism's habitat preferences through time (e.g., Thuy and Meyer, 2013). The physical rock record (Immenhauser, 2009) of clastic sediments (Allen, 1967) offers an alternative calibration method. The most obvious PWD indicators are beach deposits, wave ripples or marine erosive surfaces related to very shallow water depths. In commercially explored sedimentary basins usually a good data-coverage of gamma-ray (GR) logs is available and the shale volume (V_{shale}) can be estimated. This parameter can be utilized to calibrate PWD estimates by combining the palaeo-bathymetry reconstruction with litho-facies models derived by applying standard sequence stratigraphical concepts (e.g., Van Wagoner et al. 1988; Catuneanu, 2006).

A suitable region to apply such an approach is the Hammerfest Basin (HB) located offshore northern Norway (Fig. 1a). Since the Devonian final amalgamation of the Caledonian Orogeny this area

* Corresponding author.
E-mail address: BenjaminUdo.Emmel@sintef.no (B. Emmel).

http://dx.doi.org/10.1016/j.csr.2015.02.003
0278-4343/

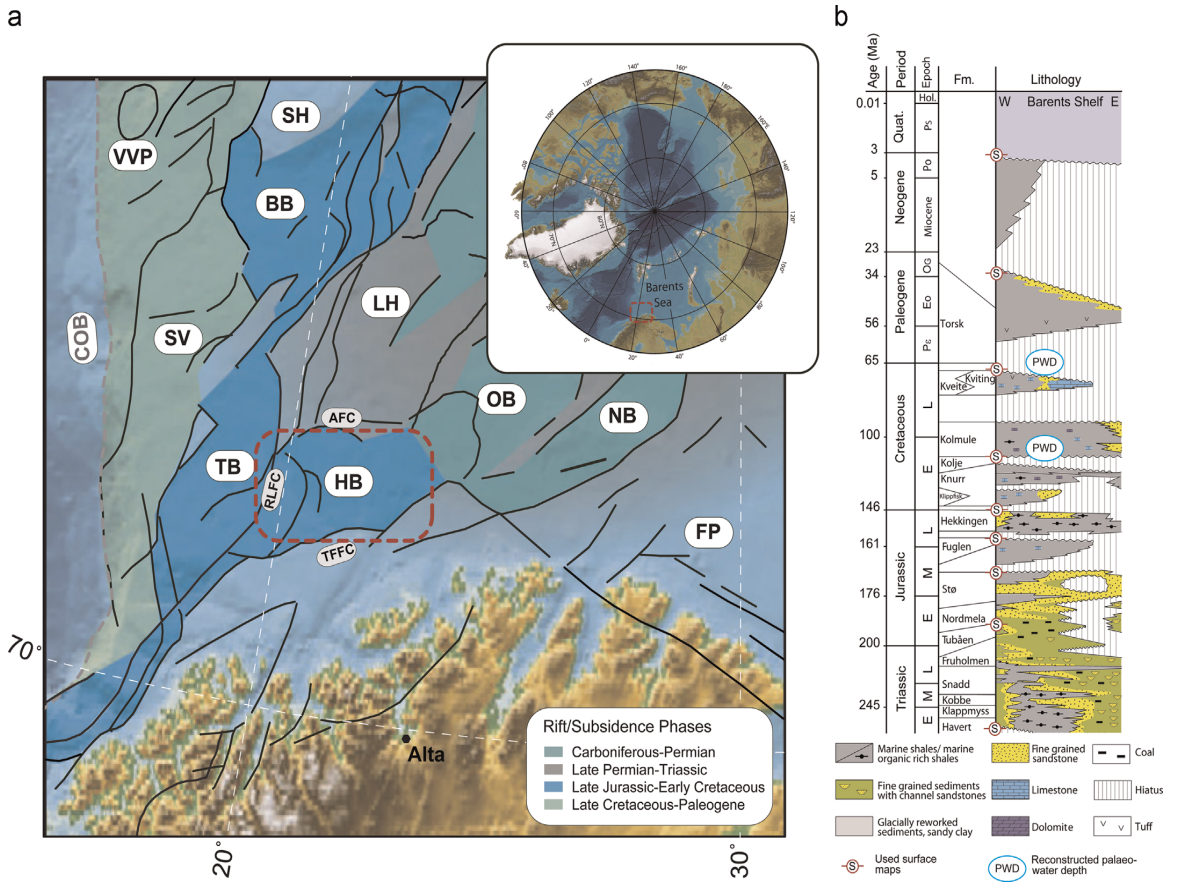

Fig. 1. (a) Location of the working area with main structural elements in the SW Barents Sea, inset shows the location of the Barents Sea within the Arctic region (modified from Clark et al., 2013; based on Jakobsson et al., 2008 and Faleide et al., 2008). (b) Simplified Mesozoic-Cenozoic lithostratigraphy of the southwestern Barents Sea (from Ostanin et al., 2012 based on Dalland et al., 1988). The dashed, red boxes highlight the working area and the reconstructed horizons are indicated by the blue, PWD circle. Abbreviations: AFC: Asterias Fault Complex, BB: Bjørnøya Basin, COB: continent–ocean boundary, FP: Finnmark Platform, HB: Hammerfest Basin, LH: Loppa High, NB: Nordkapp Basin, OB: Ottar Basin, RLFC: Ringvassøy-Loppa Fault Complex, SH: Stappen High, SV: Sørvestsnaget Basin, TB: Tromsø Basin, TFFC: Troms Finnmark Fault Complex, VVP: Vestbakken Volcanic Province. (For interpretation of the references to color in this figure legend, the reader is referred to the web version of this article.)

has been characterized by extensional tectonics (e.g., Gabrielsen et al., 1990; Torsvik et al., 1996). During the progressive break-up of the Pangean supercontinent (Veevers, 2004) the Barents Sea was rifted and late Devonian to Cenozoic sedimentary successions were deposited (e.g., Doré, 1991; Glørstad-Clark et al., 2010). The present bathymetry controls the sediment exchange dynamics with strong currents prevailing along shallow banks and low-energy currents in the deeper parts (Juntilla et al., 2014). This causes the deposition of coarse-grained sediments in shallow depths and of finer material in the deeper areas (Bellec et al., 2008; Juntilla et al., 2014). Similar shelf environment conditions might have controlled the sediment dynamics during the geological past as indicated by benthic foraminifera (Setoyama et al., 2011). Furthermore, since the 1970's the western Barents Sea is a hydrocarbon exploration area and extensive seismic and sedimentological data sets are publically available (www.npd.no).

In this contribution, we focus on the Cretaceous epoch, a time of global atmospheric CO_2 and temperature extremes (e.g., Tarduno et al., 1998) and extraordinary global magmatism (e.g., Storey et al., 1995) which also affected the Arctic region (Tarduno, et al., 1998; Maher, 2000). Here, magmatism relates to the opening of the North Atlantic (e.g., Faleide et al., 2008) which abruptly changed the depositional system in the Barents Sea (e.g., Faleide et al., 1993; Worsley, 2008).

2. Geological and geodynamic setting

The geological record of the Norwegian Barents Sea as a sedimentary sink began after the Early Devonian final phase of the Caledonian Orogeny associated with the consolidation of the Laurasian continent (e.g., Roberts, 2003; Gee et al., 2008). During the late Paleozoic, regional extensional tectonics dominated and favored the initial opening of the Barents Sea along inherited structural basement anisotropies (Gabrielsen et al., 1990; Gernigon et al., 2014). In general, the sedimentary record within the Barents Sea covers late Devonian to Cenozoic successions deposited in the basin provinces and partly on the platforms (e.g., Doré, 1991; Glørstad-Clark et al., 2010). Within the southwestern Barents Sea tectonic realm, the HB belongs to a province of basins south of ca. 74 °N (Fig. 1a). The 150 km long and 70 km wide HB is structurally well defined towards the north, south and west by fault complexes. The basin originated probably during the Late Carboniferous (Gabrielsen et al., 1990) with the main subsidence phases

during the Triassic and Early Cretaceous (Larssen et al., 2002). The oldest sediments penetrated by exploration wells are late Paleozoic, located below Upper Permian successions (Larssen et al., 2002). At least since the late Permian sediments accumulated within the HB reflecting different transgressive and regressive cycles interrupted by periods of tectonics associated with uplift and erosion events.

The major subsidence in the HB occurred during the Late Jurassic- Early Cretaceous associated with the deposition of thick sedimentary strata (Fig. 1a and b). Localized subsidence continued during the Late Cretaceous only in the Sørvestsnaget and Tromsø basins close to the present continent–ocean boundary (Fig. 1a). In contrast, different transgressive/regressive cycles and a regional uplift phase affected the basins located further to the west (including the HB) during the Late Cretaceous (Dalland et al., 1988, Riis, 1996; Worsley 2008). This differential vertical tectonic development is reflected in the decreasing sedimentary thickness of the Cretaceous units from the Tromsø Basin towards the HB (Fig. 1a). For example, the Aptian to mid-Cenomanian shales from the Kolmule Fm. (Fig. 1b) and the condensed calcareous and sandy units of the Kveite and Kviting formations follow this thickness trend. Following, major Cenozoic episodes of sea-floor spreading affected the Barents Sea (Faleide et al., 2008) with plate tectonic reorganizations in the Norwegian–Greenland Sea and the associated development of a predominantly sheared western Barents Sea continental margin (Faleide et al., 1993).

For a more specific and detailed description of the lithologies, facies, tectonic events, we refer to the extensive available published literature (e.g., Berglund et al., 1986; Faleide et al., 2008; Gabrielsen et al., 1990; Larssen et al., 2002; Mørk et al., 1999; Ohm et al., 2008; Ostanin et al., 2012; Worsley, 2008).

3. Database

Eight surface maps of interpreted seismic horizons provided by Statoil ASA and two reconstructed maps (from well data, and mean thickness) define our stratigraphic model to reconstruct the PWD (Table 1). The surfaces represent different interpreted base or top layers from major sequences. We used the following surface maps from the overlying units: seabed, base Pleistocene, base Oligocene, base Torsk; from the underlying units: top Kolje, top Hekkingen, top Fuglen, top Stø, top Tubåen and top Permian (Fig. 1b, Table 1). We assigned for every unit bounded by two surfaces depositional ages and an average typical lithology (Table 1). We simplified the lithology for every unit by defining the proportion of the varying fractions following the suggestions from the webpage of the Norwegian Petroleum Directorate (www.npd.no). V_{shale} values are obtained from digital versions of gamma ray (GR) well log data provided by Statoil ASA.

4. Methodology

We used the SEMI PW software (Sylta, 2004) for a reverse, vertical restoration of palaeo-bathymetries (e.g., Kjennerud, 2001). We modeled palaeo-surfaces using the present-day horizons obtained from interpreted depth converted seismic data. The complete reconstruction procedure is sub-divided into a numerical and calibration part. During the numerical simulations, the water depth at the start of the deposition is determined. The restoration process follows a stepwise manner beginning with the present-day geometries and the seabed as a reference surface. The following calculations are applied (Fig. 2) using the input parameters given in Table 1:

Table 1
Input data for the PWD reconstruction. We used a regular grid with a lateral resolution of 100 × 100 m. RW: reconstructed from well data.

Seismostratigraphic depth maps	Age interval (Ma)	Dual lithology	Content of second fraction
Sea Bed	3–0	Sand/Shale	0.7
Base Pleistocene	34–3	Sand/Shale	0.7
Base Oligocene (RW)	65–34	Sand/Shale	0.7
Base Torsk	120–65	Silt/Limestone	0.15
Top Kolje	140–120	Shale/ Limestone	0.15
Top Hekkingen	156–140	Shale	–
Top Fuglen (RW)	168–156	Shale/ Limestone	0.1
Top Srø	184–168	Sand	–
Top Tubaen	250–184	Silt/Sand	0.3
Top Permian	280–250	Limestone	–

a. The thicknesses of stratigraphic units are determined from depth converted interpreted seismic horizons.
b. The thicknesses at the time of deposition are reconstructed by decompaction (Allen and Allen, 2005) using a porosity-versus-depth relationship (e.g., Sclater and Christie, 1980).
c. The isostatic effect of the load is calculated (assuming Airy isostasy).
d. Accommodation space created by the compaction of the underlying deposits is calculated.

The numerical PWD reconstruction is the sum of the previous adjustments and it gives the accommodation space (or PWD) before the deposition of the investigated sedimentary unit (Figs. 2, 3a). Independent proxies, such as floral, faunal and chemical evidence are useful to calibrate the numerical PWD but are rarely available. Here, we use the physical rock record in the form of grain size variations (Immenhauser, 2009) in a stratigraphic facies model scheme. Nine different PWD scenarios (incremental 50 m) including the initial reference and end member models (Fig. 3a–c) are used to build litho-facies models applying fuzzy logic principles (Fig. 4). For a unified sedimentary layer, located between and defined by two reconstructed PWD surfaces, a shale distribution is modeled using the software OF-Mod 3D (Mann and Zweigel, 2008). A consistent fuzzy logic (e.g., Warren et al., 2007) scheme is used to link palaeo-bathymetries with the supposed sedimentary regime. The applied fuzzy logic sedimentation algorithm that determines the facies at each location is based on the local water depth (Fig. 4a). We defined four rules, which dictate the subdivision into water depth zones and each sedimentary facies (values see Fig. 4):

(1) If PWD on land, then land.
(2) If PWD very shallow, then inner shelf.
(3) If PWD shallow, then continental slope.
(4) If PWD medium deep, then continental slope.

Then, V'_{shale} (modeled shale volume) is defined for each facies (Fig. 4a–c). In zones with overlapping facies V'_{shale} is determined based on the ratios of the two facies (Fig. 4b). This ensures gradual transitions of V'_{shale} values between two facies, instead of discrete, unrealistic jumps.From the resulting litho-facies and associated V'_{shale} distributions (Fig. 5), we extracted the shale fractions for vertical profiles (Fig. 6) and compared them to measured or log interpreted V_{shale} values. There are different methods to gain V_{shale} data from single logs, e.g., from GR, density, neutron, resistivity and self-polarization logs as well as from combinations of those log values. In spite of the number of existing methods, none of them gives a perfect solution. We used a simplified version of the

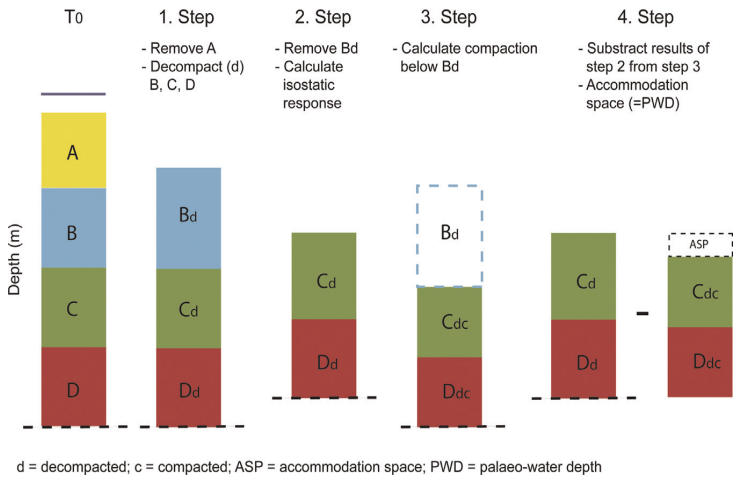

Fig. 2. Palaeo-water depth (PWD) reconstruction workflow used in SEMI PW software. This example shows the reconstruction of layer B. The method is based on a decoupled calculation of isostasy, compaction and decompaction (step one to four). The colored boxes represent different stratigraphic horizons and the black, dashed line is the top of the basement. T_0 is the present day situation.

curved GR method fixing minimum and maximum cut-offs for V_{shale} at 0.02 and 0.98 (Schlumberger, 1972).

$$V_{shale} = \frac{GR - GR_{clean}}{GR_{shale} - GR_{clean}} \quad (1)$$

where GR_{clean} is the GR cut-off for pure sands and GR_{shale} is the GR cut-off for pure shale.

The measured V_{shale} and modeled V'_{shale} for the different water depth models (Fig. 3a–c) were compared at each depth (n_d) where a well data point was available. For each well the Root Mean Square Error ($RMSE_w$) was calculated:

$$RMSE_w = \sqrt{\frac{\sum (V_{shale} - V'_{shale})^2}{n}} \quad (2)$$

As four wells (n_w) were used in the study area, the single $RMSE_w$ values were averaged for each PWD model to obtain the cumulative mean error (E_m):

$$E_m = \frac{\sum RMSE_w}{n_w} \quad (3)$$

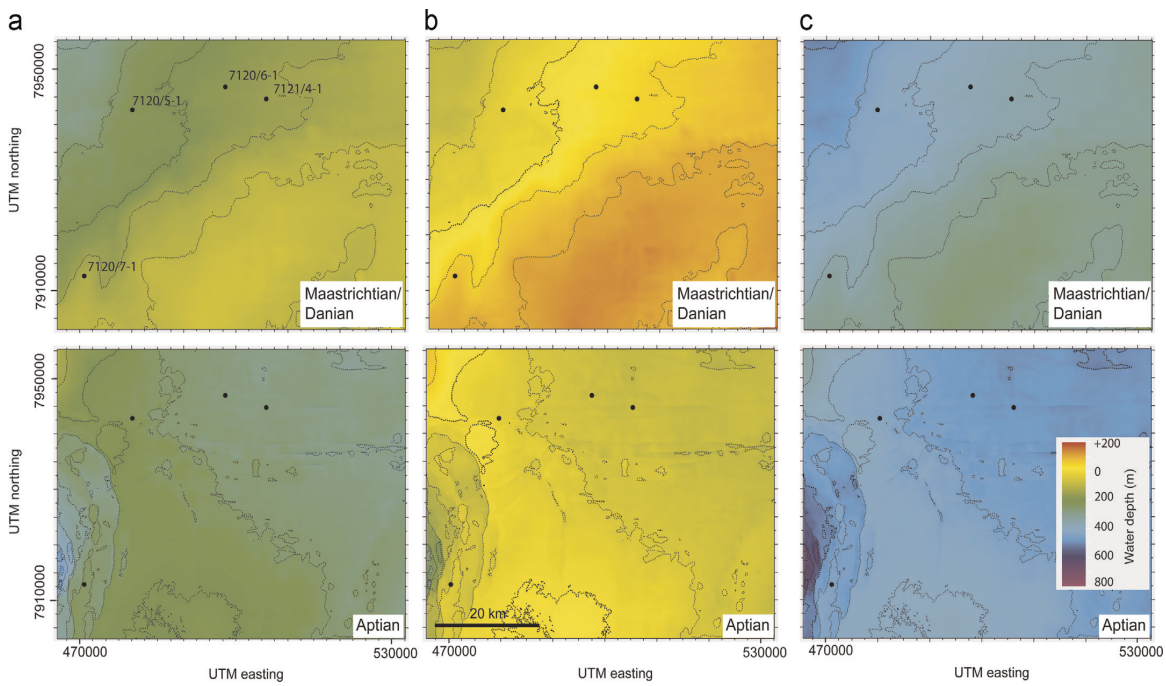

Fig. 3. Results of the numerical reconstructions of PWD's for the Maastrichtian/Danian and Aptian stages. (a) The reference model is the result of the initial PWD reconstruction. (b) The models shallow (+200 m) and (c) deep (−200 m) are extreme values tested for the purpose of calibration. These surfaces are constructed by adding or subtracting the water depth from the reference model.

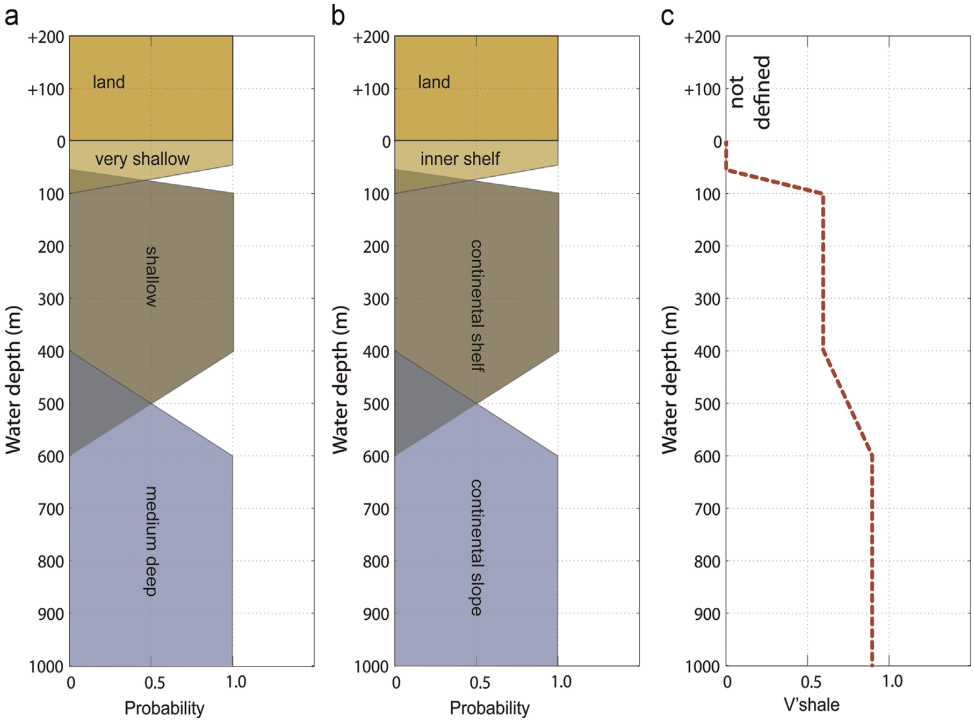

Fig. 4. Illustration of the applied fuzzy logic based on water depth (a) and the associated assignment of facies (b) and shale volume (c).

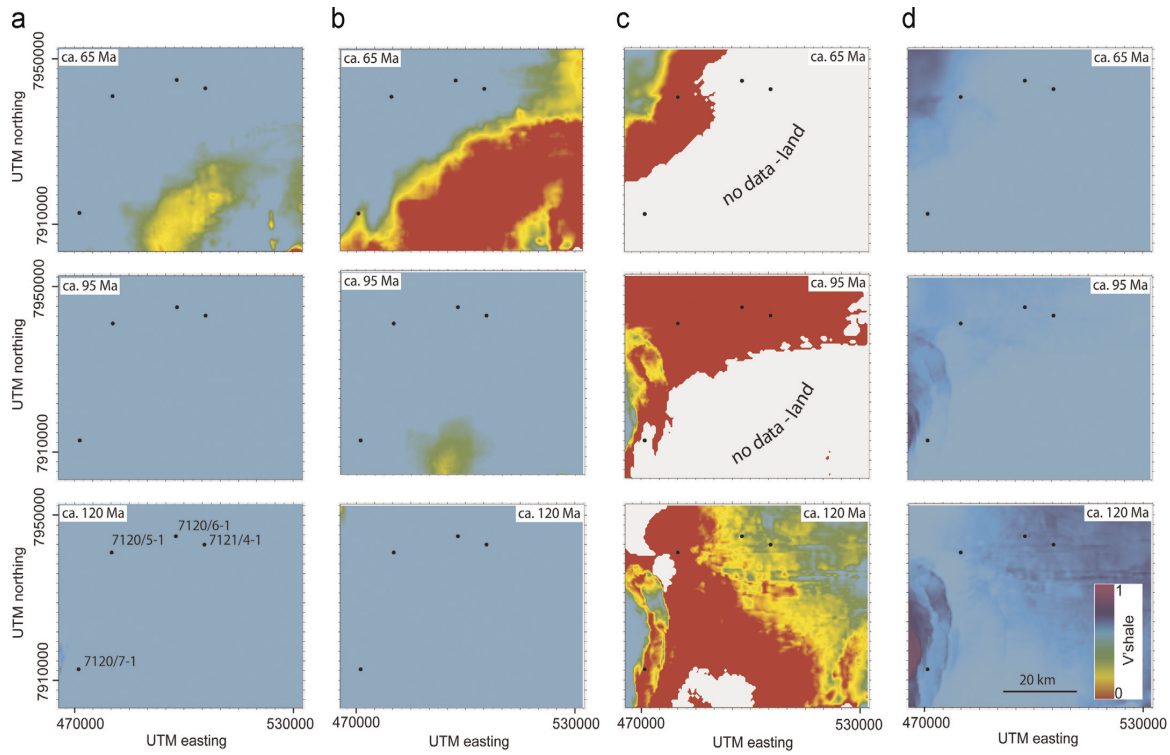

Fig. 5. Modeled shale volume (V'_{shale}) distribution maps at ca. 125 Ma, 95 Ma and 65 Ma for different initial water depth assumptions. The PWD reconstructions (examples given in Fig. 3) served as an input into the facies modelling. We applied a fuzzy logic scheme shown in Fig. 4 using the software OF-Mod 3D to model the facies distribution and the associated V'_{shale}. For 100 layers between the top and bottom layers defined by PWD estimates V'_{shale} values are modeled. (a) Reference model, (b) Model (+50 M), (c) Shallow (+200 m), and (d) Deep (-200 m).

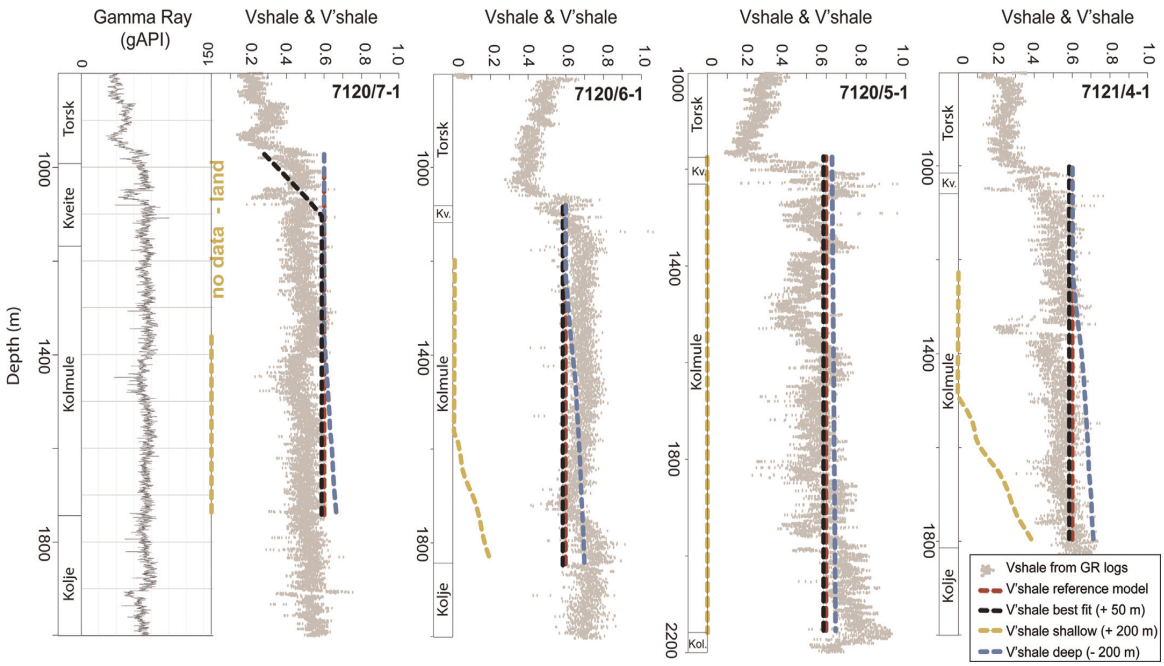

Fig. 6. Comparison of V_{shale} and V'_{shale} (measured and modeled shale volume) values for four locations with well data. The measured V_{shale} values relate to gamma ray logs (shown for well 7120/7-1) and are compared to V'_{shale} values extracted from distribution maps (Fig. 5). By lowering the sea level (model: shallow +200 m) V'_{shale} values show a clear misfit with the observed data. In the extreme case, the modeled surfaces reach land (see Fig. 5c) and V'_{shale} is undefined (e.g., no data-land for well 7120/7-1).

5. Results and interpretation

We restored two PWD's one for the Aptian stage (base Kolmule) and one the Maastrichtian/ Danian stage (top Kviting/ Kveite). In order to test the sensitivity of the models, we varied the *z*-values (water depth) of the initial numerical reconstructions (reference model) in the magnitude of ±200 m incremented by 50 m (examples in Fig. 3). This is in accordance with eustatic sea level changes related to different geological processes such as continental collision, sedimentation and seafloor spreading on a time scale of 1–100 Myr's (Miller et al., 2005). We used PWD pairs (e.g., Aptian shallow +200 m together with Maastrichtian/Danian shallow +200 m etc.) to model the V'_{shale} distribution in the working area (Fig. 5a–d). Following, we extracted V'_{shale} values for four well locations and compared them to GR derived V_{shale} data (Fig. 6). The reference PWD model shows a good correlation with the V_{shale} log data. By varying the PWD's, the V'_{shale} trend lines shift more or less from the GR V_{shale} data (Fig. 6). In the extreme case (shallow +200 m), the local sea level is lowered by 200 m which causes zero values for the V'_{shale} due to proximity to the coast. Moreover, parts of the working area become onshore and V'_{shale} is not modeled (Figs., 5c and 6). An increase of water depths (deep −200 m) has only a limited effect on the simulated V'_{shale} distribution (Figs. 5d and 6). However, the discrepancies between the different models vary depending on the well locations (Fig. 5a–d). The accumulated error estimate for the entire area (Table 2) indicates that larger changes to the reference PWD, cause higher total errors indicating doubtable palaeo-bathymetries (Fig. 7). In contrast, changes in the magnitude of ±50 m to −150 m have only a minor effect and these models are most likely closer to the true PWD (Fig. 6). Model (+50 m) gives the best fit and will be discussed further (Figs. 8 and 9).

5.1. Best-fit PWD reconstruction for the Aptian stage

During the Aptian the reconstruction suggests depths between ca. 464 m and 66 m (all PWD values reported here are relative to modern sea level) with an average depth of ca. 200 m (Figs. 8, 10b). A SE–NW trending basin high, with water depth of ca. 70–200 m separates the area. The high is flanked towards the NE and SW by areas with deeper water depths of ca. 250–200 m and 460–200 m, respectively. An E–W swath profile shown in Fig. 8b demonstrates the separating effect of this area of shallow water depth. In the eastern part, within the HB the PWD gently deceases from ca. 230 m to 160 m before a sharp transition towards deeper water depth occurs (Fig. 8b). The deepest parts are located SW of

Table 2
Error estimates ($RMSE_w$ for each PWD, E_m for all wells E_m) for the mismatch between modeled and measured shale volumes (V'_{shale}, V_{shale}) for all simulated PWD scenarios.

		Models								
		−200	**−150**	**−100**	**−50**	**Reference**	**+50**	**+100**	**+150**	**+200**
Wells	**7120/5–1**	0.131	0.104	0.104	0.104	0.104	0.104	0.104	0.259	0.543
	7120/6-1	0.071	0.094	0.098	0.098	0.098	0.098	0.126	0.409	0.656
	7120/7-1	0.148	0.133	0.133	0.133	0.133	0.120	0.250	0.387	0.504
	7120/4-1	0.148	0.116	0.114	0.114	0.114	0.114	0.137	0.316	0.491
	Average	0.124	0.112	0.112	0.112	0.112	0.109	0.154	0.343	0.549

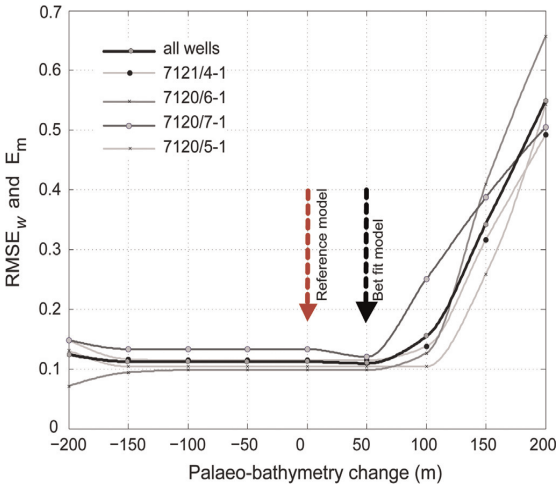

Fig. 7. Combined error estimates from four exploration wells in relation to the changes in the palaeo-bathymetry. Water depth changes from +50 m to −150 m do not significantly influence the fitting of well and modeled data. A major error increase is related to the models where the bathymetry is uplifted (the water depth is lower). The +50 m model indicated by the dashed black arrow revealed the lowest misfit (best fit model). Root Mean Square Error for one well: $RMSE_w$; Mean error for all wells: E_m.

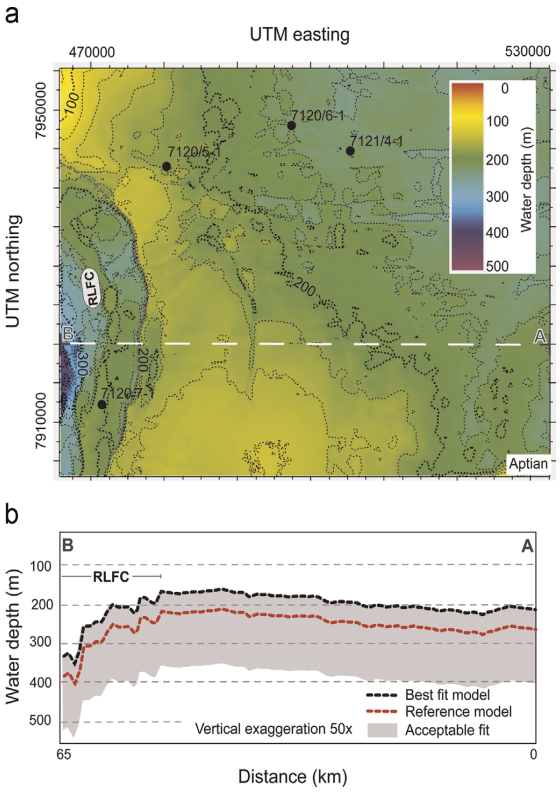

Fig. 8. a) Best fit PWD reconstruction for the Aptian stage. The grey dashed line indicates the border between the HB and the Ringvassøy-Loppa Fault Complex (RLFC). (b) Bathymetric swath profile derived from the best-fit PWD reconstruction.

the Ringvassøy-Loppa Fault Complex separating the HB from the Tromsø Basin (Fig. 1a).

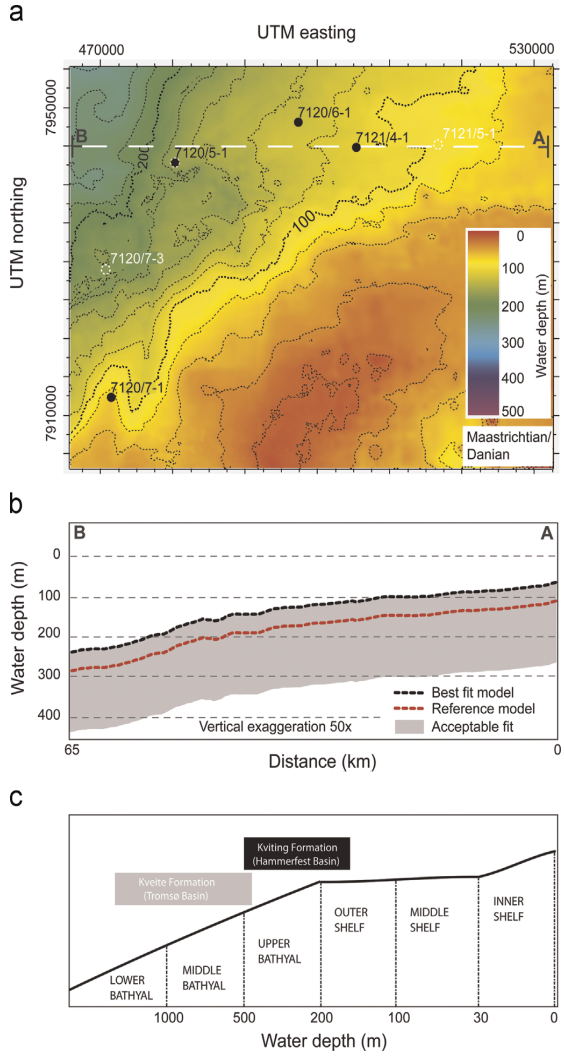

Fig. 9. a) Best fit PWD reconstruction for the Maastrichtian/Danian stage. (b) Bathymetric swath profile derived from the best-fit PWD reconstruction. (c) Upper Cretaceous palaeo-bathymetry estimates based on formaminiferal assemblages (Fig. 12 in Setoyama et al., 2011) observed in five wells. Three wells are located within the working area (dashed white circles) and two wells (7119/9-1 and 7119/12-1) are located in the Tromsø Basin west of the working area.

5.2. Best-fit PWD reconstruction for the Maastrichtian/Danian stage

For the Maastrichtian/Danian stage the best-fit model indicates water depths from ca. 265 m to +30 m (above sea level) with an average depth of ca. 94 m. The area is subdivided into a deeper northern (ca. 60 m to 260 m) and a shallow southern part (ca +30 m to 180 m) superimposed by a general deepening trend towards the NW, i.e. with increasing distance from the present day shoreline (Fig. 9a). The E–W swath profile from the northern part of the study area illustrates the gentle increase of PWD from the east towards the west or from the HB towards the Tromsø Basin (Fig. 9b).

6. Discussion

The PWD is a fundamental parameter of any subaquatic sedimentary environment (Immenhauser, 2009). Types and locations

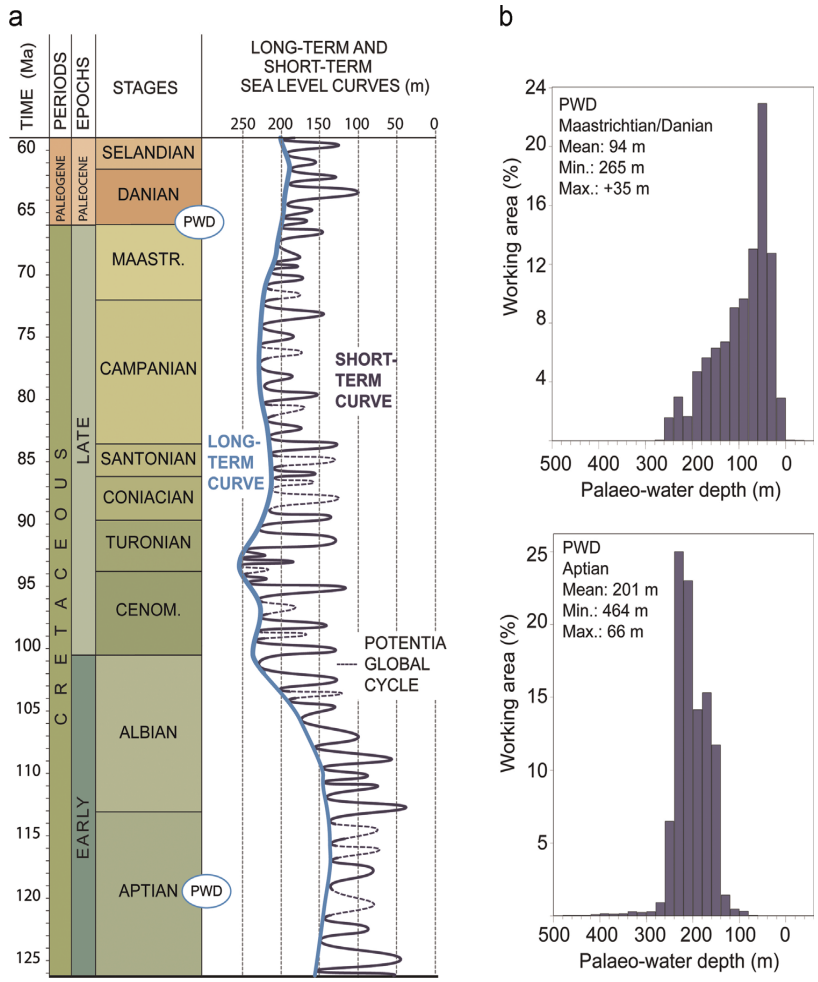

Fig. 10. (a) Cretaceous eustatic sea-level curves (from Haq, 2014), with marked stages for the PWD reconstructions. (b) Histograms of modeled PWD distributions for the Aptian and Maastrichtian/Danian stages. In contrary to the long-term global eustatic sea level trend the PWD results indicate a lower local sea-level during the Maastrichtian/Danian stage.

of present sediment accumulations are pre-determined by the dynamics of sediment transport systems, which are closely associated with the prevailing geometry of the sea floor. Studies on present marine environments in the Barents Sea show the dominating impact of sea-floor topographies on the general ocean current and depositional system (e.g., Gammelsrød et al., 2009; Juntilla et al., 2014). Ancient bathymetries have to be inferred from the preserved sedimentary record (e.g., Flügel, 2004), and reconstructions might be hindered by patchy preservation and ambiguous environmental conditions of fossil communities. Many possible proxies for PWD (Thuy and Meyer, 2013) are used such as sedimentary structures and textures (e.g., Allen, 1967), authigenic minerals (e.g., Porrenga, 1967), stable isotopes (e.g., Schuur Duncan et al., 2000), and fossil assemblages (e.g., Seilacher, 1967; Setoyama et al., 2011). For most of these proxies a water depth reconstruction requires very detailed sampling and precise, laboratory intensive analyses. In general, their spatial and temporal coverage is limited and only empirical, semi-quantitative estimates on PWD are possible. Therefore, 3D restoration methods appear to be more useful to improve the understanding of large-scale palaeo-environments. For example recent publications (Ehlers and Jokat, 2013; Huang et al., 2014) couple global-scaled tectonics, palaeo-bathymetry and palaeoceanography in order to explain complex ancient ocean current systems along critical water exchange connections. As a result of their global tectonic focus, these publications present PWD in a low-resolution, deterministic way and discuss mainly geophysical aspects. In this study, we present a new method to reconstruct and calibrate PWD estimates for a basin or sub-basin scale underlain by continental crust. This method can provide a robust reconstruction of palaeo-sea floor geometries and quantitative estimates of PWD's. Our approach might however show some mismatch between the model and local data (e.g., selected well locations). In the following, we discuss these issues on the examples of the HB.

6.1. Reconstruction and calibration of PWD

The reconstruction of PWD for stratigraphic horizons is a complex problem (Allen and Allen, 2005) because it represents an underdetermined mathematical case. In the demonstrated approach, we applied a simplified, decoupled, steady state numerical model to reconstruct PWD's. Hereby, we assume (i) that the thickness of a stratigraphic layer relates to the accommodation space at the beginning of its deposition; (ii) the accommodation

space represents the PWD; (iii) the thickness of the stratigraphic layer triggers basin subsidence and sediment compaction. This approach neglects different types of uncertainties concerning isostasy, flexural response, compaction, decompaction (due to lithology, thickness and age uncertainty), erosion and brittle deformation, although variations in these parameters alter the final PWD reconstruction results. In order to establish a calibration method that takes some of these uncertainties into account we tested an indirect way using GR data combined with a fuzzy logic litho-facies model (Fig. 5). The accuracy of the calibration depends on the availability and the amount of well data and their spatial distribution. In this study, we used four exploration wells, unequally distributed over the study area probably limited the accuracy of the calibration approach. However, we demonstrated that this calibration method can be utilized for a statistical evaluation of quantitative PWD models (Figs. 6 and 7). The overall reconstruction and calibration approach is applicable to sedimentary basins on the continental shelf and a predominant siliciclastic depositional environment.

6.2. The modeled Aptian to Danian bathymetry compared with published estimates

For the Aptian to mid-Cenomanian Kolmule Fm. no quantitative estimates for palaeo-bathymetries are available. The sedimentary record indicates open marine environments in a shallow sea (Dalland et al., 1988; Ramberg et al., 2008). A reconstruction for the Valanginian stage indicates deep shelf conditions for the area around the HB (Dypvik et al., 2010). However, all empirical estimates give no strict definition for their water depth estimates. Our best-fit model in the HB results in physiography with a gentle slope (Fig. 8b) and a PWD of ca. 200 m indicates a shelf environment (compare with Galloway and Hobday, 1983; Ross, 1982). This general pattern abruptly changes along the Ringvassøy-Loppa Fault Complex where a transition to deeper PWD is modeled (Fig. 8) which could represent a palaeo shelf break. This shelf break most probably developed during the Late Jurassic structural development of the southwestern Barents Sea with intensive faulting along the Ringvassøy - Loppa Fault Complex (e.g., Halland et al., 2014).

Sedimentological evidence from the Turonian to Maastrichtian Kviting and Kveite formations indicate a bimodal sediment distribution with condensed calcareous units (Kviting Fm.) in the HB whilst towards the Tromsø Basin claystones (Kveite Fm.) dominate (Mørk et al., 1999). These lithologies suggest a marine, predominantly bathyal environment, which deepens towards the west (Mørk et al., 1999). A similar bathymetry for the HB is indicated by foraminiferal assemblages (Setoyama et al., 2011) giving water depths in the outer shelf – upper bathyal environment. In their conceptual model, Setoyama et al. (2011) place this environment at a water depth between ca. 150 m and 500 m. Thereby the bathymetry deepens towards the Tromsø Basin in the west (Fig. 9c). A swath profile along the northern part of our best fit model, following the sample transect of Setoyama et al. (2011), suggests very shallow water depths ranging between ca. 100 m and 250 m (Fig. 9b). However the acceptable fitting PWD scenarios match their empirical palaeo-bathymetry estimates (Fig. 9b and c) and the reconstructed PWD reproduce very well the observed trend with deeper water in the western part of the working area (Fig. 9a and b).

6.3. Cretaceous PWD trends in the context of regional tectonic setting

In general, during the Cretaceous the sea level was ca. 50–250 m above the present-day sea-level (e.g., Haq, 2014, Fig. 10 a). The long-term global sea-level curve indicates a ca. 50 m higher sea level during the Maastrichtian/Danian stages compared to the Aptian stage (e.g., Haq, 2014, Fig. 10 a). Thus, we would suggest in a tectonicly stable shelf environment PWD would be deeper during the Maastrichtian/Danian stage. In contrast, our PWD reconstructions indicate a local sea-level drop by ca. 100 m for the HB during this period (Fig. 10 b). If correct, this sea-level drop relates to the regional tectonic and basin development associated with the Late Cretaceous/Paleocene sea-floor spreading in the Norwegian–Greenland Sea and the related evolution of a trans-tensional margin along the western Barents Sea (e.g., Faleide et al., 1993, 2008). These major tectonic events controlled the vertical geodynamic history of the HB. During the Early Cretaceous, the western margin experienced main subsidence phases and thick sedimentary units deposited in the Tromsø Basin leading to increased subsidence in the HB. Whilst subsidence continued in the basins along the westernmost margin of the Barents Sea, the HB was uplifted during the Late Cretaceous (Faleide et al., 1993; Worsley, 2008). The uplift is indicated by seismic observations and interpretations: (i) A prominent regional seismic marker (unconformity) defines the Late Cretaceous/Cenozoic boundary on top of the Kviting and Kveite formations (Faleide et al., 1993; Worsley, 2008; Ostanin et al., 2012). (ii) Prograding clinoforms within the Tromsø Basin (Fig. 1) indicate sediment supply from the emerging Loppa High (Fig. 1) during the Paleogene (Knutsen et al., 1992). Furthermore, this uplift phase might have caused enhanced erosion in the HB (Henriksen et al., 2011). A recent study by Radmacher et al. (2014) of Upper Albian to Lower Maastrichtian dinoflagellate cyst indicates several hiatuses of various ages in the southwestern Barents Sea. The data favors an Upper Cretaceous/Lower Paleogene unconformity, related to regional uplift of the mainland (e.g. Riis, 1996). This uplift together with a low Maastrichtian sea-level might have triggered erosion along the margins shelf (Radmacher et al., 2014). Our reconstructed PWD's indicate mainly very shallow marine conditions (Figs. 9a, 10b). We expect that localized erosion might have had an effect on areas where the water depth was above the palaeo wave base. Bottom water currents might have been another possible cause of erosion below the palaeo wave base (Nagy et al., 1997; Setoyama et al., 2011).

7. Conclusions

We present a new approach to reconstruct and calibrate Cretaceous PWD's within the HB. The results are in general agreement with published PWD estimates based on sedimentology and micropalaeontology. The new PWD estimates support the assumption of a Late Cretaceous uplift phase. The study showed that a simplified approach to model PWD's gives reasonable results for simple basin infilling histories and architectures. Calibration against GR data offers a new possibility for a stochastic analysis of modeled PWD surfaces.

Acknowledgements

We appreciated the introduction into the palaeo-water world by M. Daszinnies. We thank Statoil ASA for providing the interpreted seismic horizons and the digital well log data. Comments of three anonymous reviewers and the associated editor improved the quality of the paper significantly.

References

Allen, J.R.L., 1967. Depth indicators of clastic sequences. Mar. Geol. 5, 429–446.
Allen, P.A., Allen, J.R., 2005. Basin Analysis: Principles and Applications. Blackwell

Science, Malden.
Baur, F., Littke, R., Wielens, H., Lampe, L., Fuchs, T., 2010. Basin modeling meets rift analysis – a numerical modeling study from the Jeanne d'Arc basin, offshore Newfoundland, Canada. Mar. Pet. Geol. 27, 585–599.
Beaumont, C., Kooi, H., Willet, J., 1999. Coupled tectonic-surface process models with applications to rifted margins and collisional orogens In: Summerfield, M. A. (Ed.), Geomorphology and Global Tectonics. John Wiley and Sons Ltd., New York, pp. 29–55.
Bellec, V.K., Wilson, M., Bøe, R., Rise, L., Thorsnes, T., Buhl-Mortensen, L., Buhl-Mortensen, P., 2008. Bottom currents interpreted from iceberg ploughmarks revealed by multibeam data at Tromsøflaket Barents Sea. Mar. Geol. 249, 257–270.
Berglund, L.T., Augustson, J., Faerseth, R., Gjelberg, J.G., Ramberg-Moe, H., 1986. The Evolution of the Hammerfest Basin In: Spencer, A.M. (Ed.), Habitat of Hydrocarbons on the Norwegian Continental Shelf. Norwegian Petroleum Society, Graham & Trotman, London, pp. 319–338.
Catuneanu, O., 2006. Principles of Sequence Stratigraphy. Elsevier, Amsterdam.
Clark, S.A., Faleide, J.I., Hauser, J., Ritzmann, O., Mjelde, R., Ebbing, J., Thybo, H., Flüh, E., 2013. Stochastic velocity inversion of seismic reflection/refraction traveltime data for rift structure of the southwest Barents Sea. Tectonophysics 593, 135–150.
Dalland, A., Worsley, D., Ofstad, K., 1988. A lithostratigraphic scheme for the Mesozoic and Cenozoic succession offshore mid- and northern Norway. Nor. Pet. Dir. Bull., 4.
Doré, A.G., 1991. The structural foundation and evolution of Mesozoic seaways between Europe and the Arctic. Palaeogeogr. Palaeoclimatol. Palaeoecol. 87, 441–492.
Dypvik, H., Tsikalas, F., Mørk, A., 2010. The Mjølnir Impact Event and its Consequences, Impact studies. 320. Springer Verlag, Berlin Heidelberg.
Ehlers, B.-M., Jokat, W., 2013. Paleo-bathymetry of the northern North Atlantic and consequences for the opening of the Fram Strait. Mar. Geophys. Res. 34, 25–43.
Emmel, B., Geiger, M., Jacobs, J., 2006. Detrital apatite fission-track ages in Middle Jurassic strata at the rifted margin of W-Madagascar – indicator for a protracted re-sedimentation history. Sedim. Geol. 186, 27–38.
Faleide, J.I., Vågnes, E., Gudlaugsson, S.T., 1993. Late Mesozoic- Cenozoic evolution of the southwestern Barents Sea in a regional rift shear tectonic setting. Mar. Pet. Geol. 10, 186–214.
Faleide, J.I., Tsikalas, F., Breivik, A.J., Mjelde, R., Ritzmann, O., Engen, O., Wilson, J., Eldholm, O., 2008. Structure and evolution of the continental margin off Norway and Barents Sea. Episodes 31, 82–91.
Flügel, E., 2004. Microfacies of Carbonate Rocks. Springer, Berlin.
Gabrielsen, R.H., Færseth, R.B., Jensen, L.N., Kalheim, J.E., Riis, F., 1990. Structural elements of the Norwegian continental shelf Part I: the Barents Sea region. Nor. Pet. Dir. Bull. 6, 33.
Galloway, W.E., Hobday, D.K., 1983. Terrigenous Clastic Depositional Systems – Application to Petroleum, Coal, and Uranium Exploration. Springer-Verlag, New York, p. 423.
Gammelsrød, T., Leikvin, Ø., Lien, V., Budgell, W.P., Loeng, H., Maslowski, W., 2009. Mass and heat transports in the NE Barents Sea: observations and models. J. Mar. Syst. 75, 56–69.
Ganti, V., Lamb, M.P., McElroy, B.A., 2014. Quantitative bounds on environmental signal preservation in the sedimentary record. Nature . http://dx.doi.org/10.1038/ncomms4298.
Gee, D.G., Fossen, H., Henriksen, N., Higgins, A.K., 2008. From the early Paleozoic platforms of Baltica and Laurentia to the Caledonide orogen of Scandinavia and Greenland. Episodes 31, 44–51.
Gernigon, L., Brönner, M., Roberts, D., Olesen, O., Nasuti, A., Yamasaki, T., 2014. Crustal and basin evolution of the southwestern Barents Sea: from Caledonian orogeny to continental breakup. Tectonics 33, 347–373. http://dx.doi.org/10.1002/2013TC003439.
Glørstad-Clark, E., Faleide, J.I., Lundschien, B.A., Nystuen, J.P., 2010. Triassic seismic sequence stratigraphy and paleogeography of the western Barents Sea area. Mar. Pet. Geol. 27, 1448–1475.
Halland, E.K., Mujezinovic, J., Riis, F., 2014. CO_2 storage atlas. Norwegian continental shelf. Nor. Pet. Dir., 163.
Haq, B.U., 2014. Cretaceous eustasy revisited. Glob. Planet. Change 113, 44–58.
Henriksen, E., Bjørnseth, H.M., Hals, T.K., Heide, T., Kiryukhina, T., Kløvjan, O.S., Larssen, G.B., Ryseth, A.E., Rønning, K., Sollid, K., Stoupakova, A., 2011. Uplift and Erosion of the Greater Barents Sea: Impact on Prospectivity and Petroleum Systems. 35. Geological Society, Memoirs, London, pp. 271–281.
Huang, X., Gohl, K., Jokat, W., 2014. Variability in Cenozoic sedimentation and paleo-water depths of the Weddell Sea basin related to pre-glacial and glacial conditions of Antarctica. Glob. Planet. Change 118, 25–41.
Immenhauser, A., 2009. Estimating palaeo-water depth from the physical rock record. Earth-Sci. Rev. 96, 107–139.
Jakobsson, M., Macnab, R., Mayer, L., Anderson, R., Edwards, M., Hatzky, J., Schenke, H.W., Johnson, P., 2008. An improved bathymetric portrayal of the Arctic Ocean: implications for ocean modeling and geological, geophysical and oceanographic analyses. Geophys. Res. Lett. 35.
Juntilla, J., Carroll, J., Husum, K., Dijkstra, N., 2014. Sediment transport and deposition in the Ingøydjupet trough, SW Barents Sea. Cont. Shelf Res. 76, 53–63.
Kjennerud, T., 2001. Palaeobathymetry and Rift Basin Evolution – With Particular Reference to the Northern North Sea Basin (Ph.D. thesis). NTNU Trondheim, pp. 320.
Kjennerud, T., Sylta, Ø., 2001. Application of quantitative palaeobathymetry in basin modelling, with reference to the northern North Sea. Pet. Geosci. 7, 331–341.
Knutsen, S.-M., Skjold, L.-J., Skott, P.H., 1992. Paleocene and Eocene development of the Tromsø Basin – sedimentary response to rifting and early sea-floor spreading in the Barents Sea. Norsk Geol. Tidskr. 72, 191–207.
Larssen, G.B., Elvebakk, G., Henriksen, L.B., Kristensen, S.-E., Nilsson, I., Samuelsberg, T.A., Stemmerik, L., Worsely, D., 2002. Upper Paleozoic lithostratigraphy of the southern Norwegian Barents Sea. Nor. Pet. Dir., Bull., 9.
Maher, H.D., 2000. Manifestations of the cretaceous high arctic large igneous province in Svalbard. J. Geol. 109, 91–104.
Mann, U., Zweigel, J., 2008. Modelling source rock distribution and quality variations: the OF-Mod approach In: de Boer, P.L., Postma, G., van der Zwan, C.J., Burgess, P.M., Kukla, P. (Eds.), Analogue and Numerical Forward Modelling of Sedimentary Systems; from Understanding to Prediction. Special Publication 40 of the International Association of Sedimentologists, Wiley-Blackwell, Oxford, UK, pp. 239–274.
Miller, K.G., Kominz, M.A., Browning, J.V., Wright, J.D., Mountain, G.S., Katz, M.E., Sugarman, P.J., Cramer, B.S., Christie-Blick, N., Pekar, S.F., 2005. The Phanerozoic record of global sea-level change. Science 310, 1293–1298.
Mohtadi, M., Oppo, D.W., Lückge, A., DePol-Holz, R., Steinke, S., Groeneveld, J., Hemme, N., Hebbeln, D., 2011. Reconstructing the thermal structure of the upper ocean: Insights from planktic foraminifera shell chemistry and alkenones in modern sediments of the tropical eastern Indian Ocean. Paleoceanography 26, PA3219, 10.1029/2011PA002132.
Mørk, A., Dallmann, W.K., Dypvik, H., Johannesen, E.P., Larsen, G.B., Nagy, J., Olaussen, S., Pcelina, T.M., Worsely, D., 1999. Mesozoic lithostratigraphy In: Dallmann, W.K. (Ed.), Lithostratigraphic Lexicon of Svalbard. Review and Recommendations for Nomenclature Use. Upper Paleozoic to Quaternary Bedrock. Norsk Polarinstitutt, Tromsø, pp. 127–214.
Nagy, J., Kaminski, M.A., Johnsen, K., Mitlehner, A.G., 1997. Foraminiferal, palynomorph, and diatom biostratigraphy and paleoenvironments of the Torsk formation: a reference section for the Paleocene–Eocene transition in the western Barents Sea In: Hass, H.C., Kaminski, M.A. (Eds.), Contributions to the Micropaleontology and Paleoceanography of the Northern North Atlantic, 5. Grzybowski Foundation Special Publication, Krakow, Poland, pp. 15–38.
Nowell, A.R.M., Jumars, P.A., 1984. Flow environments of aquatic benthos. Annu. Rev. Ecol. Syst. 15, 303–328.
Ohm, S.E., Karlsen, D.A., Austin, T.J.F., 2008. Geochemically driven exploration models in uplifted areas: examples from the Norwegian Barents Sea. Am. Assoc. Pet. Geol. Bull. 92, 1191–1223.
Ostanin, I., Anka, Z., Di Primio, R., Bernal, A., 2012. Identification of a large upper cretaceous polygonal fault network in the Hammerfest Basin: implications on the reactivation of regional faults and gas leakage dynamics, SW Barents Sea. Mar. Geol. 332–334, 109–125.
Porrenga, D.H., 1967. Glauconite and chamosite as depth indicatorsin the marine environment. Mar. Geol. 5, 495–501.
Radmacher, W., Tyszka, J., Mangerud, G., Pearce, M.A., 2014. Dinoflagellate cyst biostratigraphy of the Upper Albian to Lower Maastrichtian in the southwestern Barents Sea. Mar. Pet. Geol. 57, 109–121.
Ramberg, I.B., Bryhni, I., Nøttvedt, A., Rangnes, K., 2008. The making of a land. Geology of Norway. Norsk Geol. Foren., Trondheim, 624.
Riis, F., 1996. Quantification of Cenozoic vertical movements of Scandinavia by correlation of morphological surfaces with offshore data. Glob. Planet. Change 12, 331–357.
Roberts, D., 2003. The Scandinavian Caledonides: event chronology, palaeogeographic settings and likely, modern analogues. Tectonophysics 365, 283–299.
Ross, D.A., 1982. Introduction to Oceanography. Prentice-Hall, New York.
Schlumberger, 1972. Log Interpretation Principles. vol. I. Schlumberger Ltd., New York.
Schuur Duncan, C., Goff, J.A., Austin, J.A., Fulthorpe, C.S., 2000. Tracking the last sea-level cycle: seafloor morphology and shallow stratigraphy of the latest Quaternary New Jersey middle continental shelf. Mar. Geol. 170, 395–421.
Sclater, J.G., Christie, P.A.F., 1980. Continental stretching: an explanation of the post Mid-Cretaceous subsidence of the central North Sea basin. J. Geophys. Res. 85, 3711–3739.
Seilacher, A., 1967. Bathymetry of trace fossils. Mar. Geol. 5, 413–428.
Setoyama, E., Kaminski, M.A., Tyszka, J., 2011. The Late Cretaceous–Early Paleocene palaeobathymetric trends in the southwestern Barents Sea – Palaeoenvironmental implications of benthic foraminiferal assemblage analysis. Palaeogeogr., Palaeoclimatol., Palaeoecol. 307, 44–58.
Speijer, R.P., Van Loo, D., Masschaele, B., Vlassenbroek, J., Cnudde, V., Jacobs, P., 2008. Quantifying foraminiferal growth with high-resolution X-ray computed tomography: new opportunities in foraminiferal ontogeny, phylogeny, and paleoceanographic applications. Geosphere 4, 760–763.
Storey, M., Mahoney, J.J., Saunders, A.D., Duncan, R.A., Kelley, S.P., Coffin, M.F., 1995. Timing of hot spot-related volcanism and the breakup of Madagascar and India. Science 267, 852–855.
Summerfiled, M.A., 1991. Global Geomorphology. An Introduction to the Study of Landforms. Longman, John Wiley Inc., Harlow, New York, p. 537.
Sylta, Ø., 2004. Hydrocarbon Migration Modelling and Exploration Risk. (Ph.D. thesis). NTNU Trondheim. pp. 200.
Tarduno, J.A., Brinkman, D.B., Renne, P.R., Cottrell, R.D., Scher, H., Castillo, P., 1998. Evidence for extreme climatic warmth from late cretaceous arctic vertebrates. Science 282, 2241.
Thuy, B., Meyer, C.A., 2013. The pitfalls of extrapolating modern depth ranges to fossil assemblages: new insights from Middle Jurassic brittle stars (Echinodermata: Ophiuroidea) from Switzerland. Swiss J. Palaeontol. 132, 5–21.
Torsvik, T.H., Smethurst, M.A., Meert, J.G., Van der Voo, R., McKerrow, W.S., Brasier,

M.D., Sturt, B.A., Walderhaug, H.J., 1996. Continental break-up and collision in the Neoproterozoic and Palaeozoic – a tale of Baltica and Laurentia. Earth-Sci. Rev. 40, 229–258.
Van Wagoner, J.C., Posamentier, H.W., Mitchum, R.M., Vail, P.R., Sarg, J.F., Loutit, T.S., Hardenbol, J., 1998. An overview of the fundamentals of sequence stratigraphy and key definitions In: Wilgus, C.K., Hastings, B.S., Kendall, C.G.S.T.C., Posamentier, H.W., Ross, C.A., Van Wagoner, J.C. (Eds.), In Sea-level Changes: An integrated approach. Society of Economic Paleontologists and Mineralogists, Tulsa, pp. 38–45.
Veevers, J.J., 2004. Gondwanaland from 650–500 Ma assembly through 320 Ma merger in Pangea to 185–100 Ma breakup: supercontinental tectonics via stratigraphy and radiometric dating. Earth-Sci. Rev. 68, 1–132.
Warren, J.D., Robert, V.D., Bartek, L.R., 2007. Fuzzy Predictive Earth Analysis Constrained by Heuristics Applied to Stratigraphic Modeling. Springer, Berlin-Heidelberg.
Worsley, D., 2008. The post-Caledonian development of Svalbard and the western Barents Sea. Polar Res. 27, 298–317.

Zieba, K.J., Daszinnies, M., Emmel, B., Lothe, A.E., Grøver, A., Lippard, S.J. (2015). Assessment of Cenozoic erosion amount using Monte Carlo type-petroleum systems modeling of the Hammerfest Basin, Western Barents Sea. American Journal of Geosciences, v 4(2), p. 40-53.

A novel stochastic basin modelling approach used for quantifying erosion and its uncertainty was proposed. The method uses a combination of Monte Carlo and secondary migration basin modelling techniques. It was applied to the western Hammerfest Basin, southwestern Barents Sea where two erosion events were considered: early and late Cenozoic. The results provide statistical distribution of probable erosion values. The paper gives also an insight about erosion impact on the Jurassic petroleum system of the Hammerfest Basin.

American Journal of Geosciences

Original Research Paper

Assessment of the Cenozoic Erosion Amount using Monte Carlo Type-Petroleum Systems Modeling of the Hammerfest Basin, Western Barents Sea

[1]Krzysztof Jan Zieba, [2]Matthias Daszinnies, [3]Benjamin Emmel, [3]Ane Lothe, [3]Arnt Grøver and [1]Stephen Lippard

[1]Department of Geology and Mineral Resources Engineering, Norwegian University of Science and Technology (NTNU), NO-7491 Trondheim, Norway
[2]Migris AS; PO Box 1208 Pirsenteret, NO-7462 Trondheim, Norway
[3]SINTEF Petroleum; Basin Modelling, S. P. Andersens veg 15 B, NO-7031 Trondheim, Norway

Article history
Received: 01-12-2014
Revised: 20-01-2015
Accepted: 15-02-2015

Corresponding Author:
Krzysztof Jan Zieba
Department of Geology and Mineral Resources Engineering, Norwegian University of Science and Technology (NTNU), NO-7491 Trondheim, Norway
Email: krzysztof.j.zieba@ntnu.no

Abstract: The Cenozoic uplift and erosion is often believed to be a major risk factor in hydrocarbon exploration in the Barents Sea causing petroleum redistribution and leakage from filled traps. Therefore, the estimation of erosion amount is an important but often underrepresented task in the basin modeling procedure. The assessment of erosion magnitudes and spatial distribution by geochemical and thermo chronological methods results in very different estimates and/or does not consider uncertainties of input data. In this study, this problem is approached by using Monte Carlo simulation techniques in secondary migration basin modeling. Thereby, amounts of early and late Cenozoic erosion episodes are described by probability distributions and the modeling results were evaluated considering their uncertainty ranges. In addition, overpressure and related leakage scenarios are considered in the petroleum basin models to study their effect on modeling results. It is shown that the early Cenozoic erosion event had a generally higher erosion magnitude than the late Cenozoic event (1.0-1.3 and 0.4-1.2 km respectively). Modeled erosion estimates are not very sensitive to overpressure modeling which is found to affect only the early Cenozoic erosion amount estimates at low degree.

Keywords: Barents Sea, Hammerfest Basin, Erosion, Basin Modeling, Monte Carlo

1. Introduction

From a hydrocarbon exploration perspective, the southern Norwegian Barents Sea (Fig. 1a) is an immature area in the Arctic region and until now the findings of major gas and oil discoveries are below expectations. One of the reasons for this might be related to the complex Cenozoic thermo-tectonic history of the region (e.g., Dimakis *et al*., 1998; Faleide *et al*., 2008). The Cenozoic Barents Sea (Fig. 1, 2) was affected by several episodes of vertical tectonic movements during the Cenozoic, which influenced the present day seafloor topography (Riis and Fjeldskaar, 1992; Green and Duddy, 2010; Knies *et al*., 2014). Moreover, these episodes were associated with sediment mass re-distribution caused by local erosion and re-deposition influencing the rock and fluid properties of the underlying sedimentary units. For example, dry traps with residual oil shows and paleo-oil water contacts are interpreted to indicate trap drainage during Cenozoic erosion episodes by processes such as cap-rock leakage, reservoir tilting and fault reactivation and associated pressure and temperature changes (Ohm *et al*., 2008). If correct, a better understanding of the dynamic response of the petroleum system to the basin evolution will reduce the risks in hydrocarbon exploration in the region. Accordingly, detailed erosion estimates are crucial in reconstructing the burial histories of the Barents Sea basins. Several approaches have been published to quantify the magnitude, lateral and temporal distribution of erosion via paleo-temperature indications such as Apatite Fission Track Analysis (AFTA), Vitrinite Reflectance (VR), geochemical and geophysical methods or by deterministic basin modeling (Riis and Fjeldskaar, 1992; Richardsen *et al*., 1993; e.g., Cavanagh *et al*., 2006; Ohm *et al*., 2008; Green and Duddy, 2010; Duran *et al*., 2013).

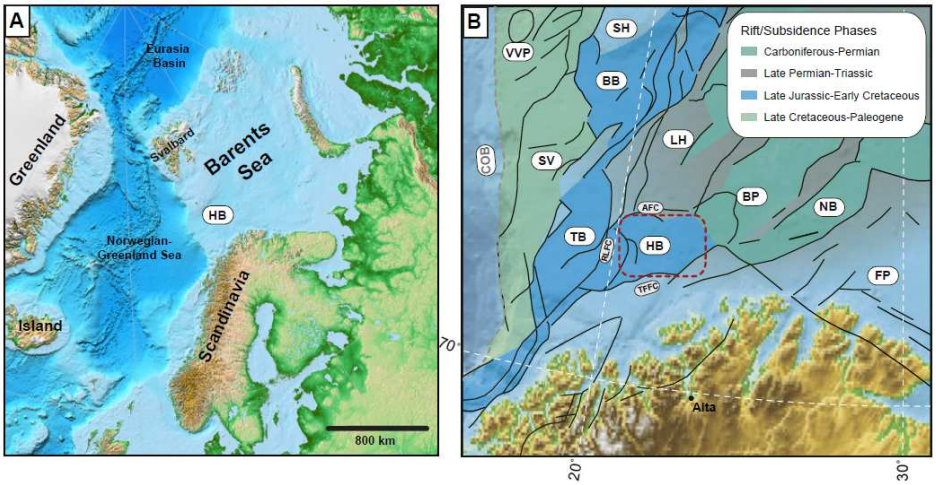

Fig. 1. (A) Location of the working area in the Arctic region based on ETOPO 5 data-set. (B) Main structural elements in the SW Barents Sea. The Hammerfest Basin (highlighted by the red box) is a fault-bounded 150 km long and 70 km wide basin within the SW Barents Sea tectonic realm (modified from Clark *et al*., 2013) and based on Faleide *et al*. (2008); Jakobsson *et al*. (2008). Abbreviations: AFC: Asterias Fault Complex, BB: Bjørnøya Basin, COB: Continent-Ocean Boundary, FP: Finnmark Platform, HB: Hammerfest Basin, LH: Loppa High, NB: Nordkapp Basin, BP: Bjarmeland Platform, RLFC: Ringvassøy-Loppa Fault Complex, SH: Stappen High, SV: Sørvestsnaget Basin, TB: Tromsø Basin, TFFC: Troms Finnmark Fault Complex, VVP: Vestbakken Volcanic Province

However, for the south-western Barents Sea they often lead to very different magnitude estimates ranging from about 0.5 km to more than 2 km.

In this study we focus on the effect of the Cenozoic thermo-tectonic history of part of the Hammerfest Basin (HB), the best investigated basin in the Norwegian Barents Sea. We use a probabilistic secondary migration basin modeling approach (Sylta and Krokstad, 2003; Sylta, 2004) to test different erosion scenarios established using AFT and VR data (Duddy, 1998; Green and Duddy, 2010). The basin modeling results are calibrated against observed oil and gas column heights reported from different exploration wells within the HB.

2. Geological Overview

The sedimentary basins within the Barents Sea comprise late Devonian to recent successions (Dalland *et al*., 1988). In the western Barents Sea, sedimentation patterns are closely linked to extensional tectonic episodes which affected the region since the late Paleozoic. Earliest rift basin formation is documented along structural basement anisotropies (Gabrielsen *et al*., 1990; Gernigon *et al*., 2014), where faulting caused the development of a Devonian graben system in the southern Barents Sea (Faleide *et al*., 2008; Henriksen *et al*., 2011b). During the Late Carboniferous until the Early Permian the entire Barents Sea evolved as a carbonate platform (Worsley, 2008; Henriksen *et al*., 2011b). Subsequently, the sedimentary environment changed to mainly a siliciclastic dominated realm (Fig. 3) and the Late Permian-Triassic basins were filled with eroded material from the hinterland (Glørstad-Clark *et al*., 2010). During the Triassic-Jurassic times several transgressive and regressive cycles prevailed as documented by Glørstad-Clark *et al*. (2010). Widespread deltaic to alluvial systems existed in the Early Jurassic and were submerged by a Middle Jurassic regional transgression (Worsley, 2008). The structural architecture of the present day basin and high configuration was largely determined by the tectonic activity at the end of the Jurassic to Early Cretaceous (Fig. 1b). In particular, the tectonic setting of the Late Jurassic leads to deposition of the major hydrocarbon source rock in the Norwegian Barents Sea i.e., the Hekkingen Formation (Fig. 3).

In the Early Cretaceous, basins along the western margin experienced their main subsidence phase. In this phase depocentres developed in the Tromsø and Bjørnøya basins and an increased subsidence in the HB occurred (Faleide *et al*., 1993; Worsley, 2008). During the Late Cretaceous, rifting and subsidence continued west of the HB, while the areas to the east (including the HB) were subjected to uplift and erosion which continued into the Paleocene (Faleide *et al*., 1993; Worsley, 2008). During the Late Paleocene, the entire western Barents Sea was dominated by subsidence due to a major transgression episode (Vorren *et al*., 1991).

DOI: 10.3844/ajgsp.2014.40.53

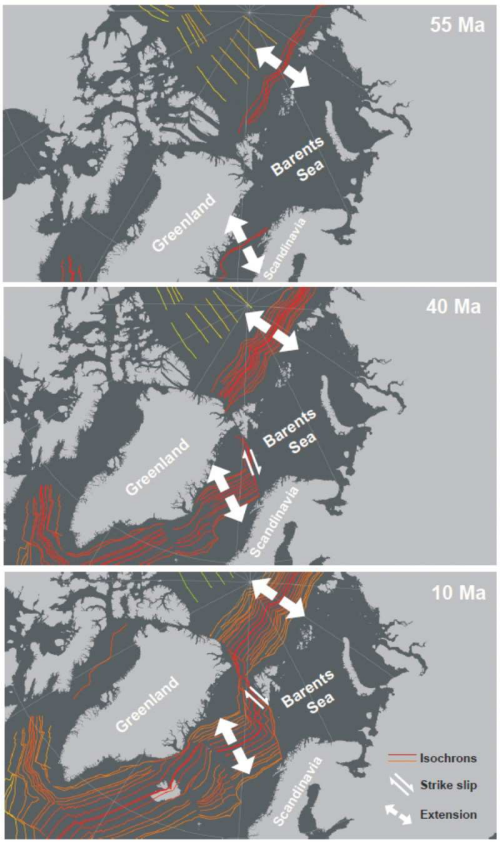

Fig. 2. Plate tectonic reconstruction of the Barents Sea region for 55 Ma, 40 Ma and 10 Ma for the reconstruction we used the GPlates software and data-sets provided by (Seton *et al*., 2012)

Shortly after, major episodes of sea-floor spreading affected the Barents Sea (Faleide *et al*., 2008) and probably caused uplift in the regions close to the main tectonic activity (Fig. 2). In Eocene to Miocene times, the uplifted parts of the Barents Sea shelf were subject to erosion and the eroded material was deposited in the southern and eastern Barents Sea (Rasmussen and Fjeldskaar, 1996; Dimakis *et al*., 1998). In the HB two major cooling phases linked to uplift and erosion, dated between ~40 and 20 Ma and ~20 and 0 Ma, were identified using AFTA (Green and Duddy, 2010). The younger event coincides with latest sediment logical and geochemical evidence from the Atlantic-Arctic gateway, which indicates that the entire northwestern European margin was elevated above sea level and eroded during the late Miocene-early Pliocene (Knies *et al*., 2014).

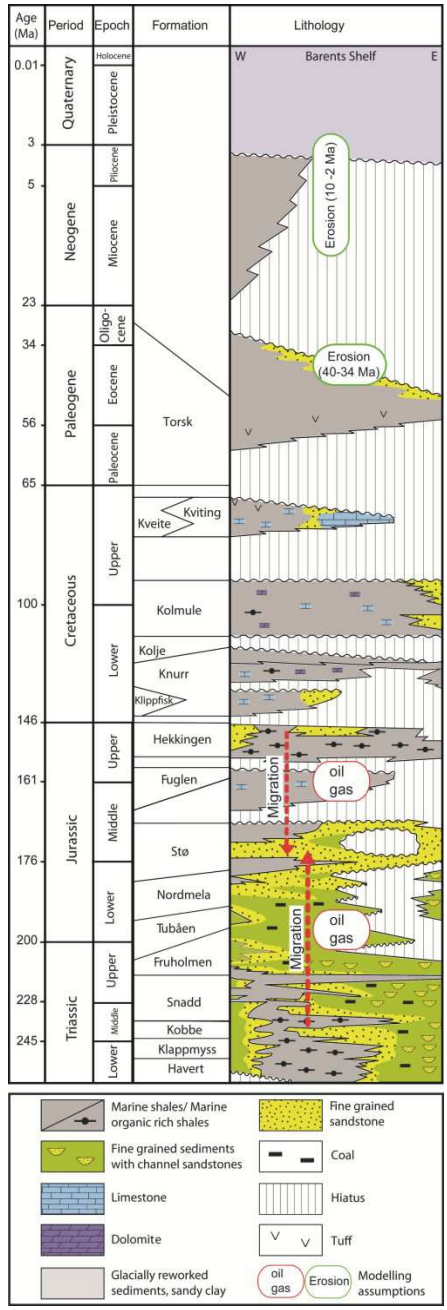

Fig. 3. Simplified lithostratigraphic column of the Barents Sea (from Ostanin *et al*. 2012, based on references given therein) with a schematic overview of the source rock-carrier bed system setup used in the petroleum migration/accumulation modeling

3. Method

The modeling of gas and oil migration in the HB was conducted by using the basin modeling tool SEMI (Sylta, 2004). SEMI was developed to quantify hydrocarbon migration and exploration risk. It includes also functions for simulating the generation and expulsion of hydrocarbons from source rocks. The software uses a ray-tracing technique to migrate fluids from a source rock through a carrier bed into a reservoir. SEMI allows also modeling of hydrocarbon leakage out of the traps. The technique is map-based and pathway directions are mainly determined by the dip of the carrier unit and migration barriers (Sylta, 2004).

The entire basin model of the western part of the HB was set up. The following elements of the basin model were considered: (a) Present day maps of geological layers including properties and type of rocks, (b) deposition ages and stratigraphy of each layer and timing of erosion events, (c) paleo-geometries including water depth maps for each layer and erosion maps, d) temperature boundary conditions (sediment-water-interface temperatures, paleo-thermal model).

The basin modeling involved thickness and paleo-geometry restoration of sedimentary layers by applying the backstripping technique (e.g., Watts and Ryan, 1976). We employed the sedimentary rock porosity-depth relations of Sclater and Christie (1980). The next steps included the simulation of source rock maturation, petroleum expulsion out of the source rock and secondary hydrocarbon migration (Sylta, 2004). Our base model was calibrated against published VR data (NPD data) for maximum paleo-thermal conditions and against BHT and DST thermal data for the present day thermal setting.

The input overpressure maps were simulated using the Pressim software tool which models pressure generation and dissipation over geological time scale (Borge, 2000; Lothe, 2004). The basic assumption behind this technique is that the fluid flow dynamics can be represented and described by pressure compartments defined by faults (Borge and Sylta, 1998). All geological layers are classified as either reservoir or sealing units. A Kozeny-Carman equation is used to relate permeability from the shale porosities. The porosities are provided by the empirical shale compaction models.

Several processes were modelled; compaction, chemical effects like quartz cementation in the reservoir units (Walderhaug, 1996), pressure build up, hydraulic fracturing and leakage (Lothe, 2004). Overpressure maps were used as input into the migration modeling for all the sedimentary layers. SEMI computes the summed total pressures from the water phase (using the overpressure input maps from Pressim) and from the hydrocarbon columns. If the sum of these pressures is larger than the leak-off pressure (set at 0.9 of the overburden), the hydrocarbon columns are reduced until the total pressure no longer exceeds the leak-off pressures. The cap rock reseals itself so that the pressures do not decrease below the leak-off pressures.

All basin modeling steps were subjected to 3000 simulation runs, each using a new and different set of values for selected input parameters (Monte Carlo type simulations; Fig. 4). These parameters were described by deterministic values and an add-on value drawn from probabilistic distributions, characterized by a mean value and a standard deviation.

For each simulation run input values for selected parameters were drawn randomly from their assigned probabilistic distributions. The distribution types were set up based on available geological knowledge. A Gaussian distribution was used if a reasonable (most likely) mean could be estimated, otherwise a uniform distribution was considered. Values for the distribution's standard deviations were chosen in such a way that they account for uncertainties related to different parameter estimations (e.g., published erosion amounts) and different methodologies used for parameter determinations.

3.1. Evaluation of the Monte Carlo Runs

The best fitting results from the Monte Carlo simulation runs were used to determine the most probable value for input parameters initially considered as probabilistic distributions (Fig. 4). This is achieved by selecting those simulation runs which yielded the lowest misfits between modelled and measured hydrocarbon column heights. Measured oil and gas accumulations heights for several wells in the Stø Formation are reported by Norwegian Petroleum Directorate (www.npd.no) and from Statoil ASA (Table 1). Our misfit criterion considers both oil and gas column height fits Equation 1:

$$Misfit = \left[\sum_{i=1}^{N}\left(h_{on}^{obs}\right)^{L}\right]^{\frac{1}{L}} + \left[\sum_{i=1}^{N}\left(h_{gn}^{\mathrm{mod}} - h_{gn}^{obs}\right)^{L}\right]^{\frac{1}{L}} \quad (1)$$

Where:

h_{on}^{mod} = Modelled oil column height for well number n
h_{on}^{obs} = Observed oil column height for well number n
h_{gn}^{mod} = Modelled gas column height for well number n
h_{gn}^{obs} = Observed gas column height for well number n
L = Scaling parameter
N = Number of wells

For every suite of simulations, an individual number of best-fit runs was determined. A threshold is placed at the best 10% or less of the misfit values, determined in a suite of simulations. Therefore, as a 10% misfit value cut off is used, the actual number of best runs is variable between sets of simulations.

DOI: 10.3844/ajgsp.2014.40.53

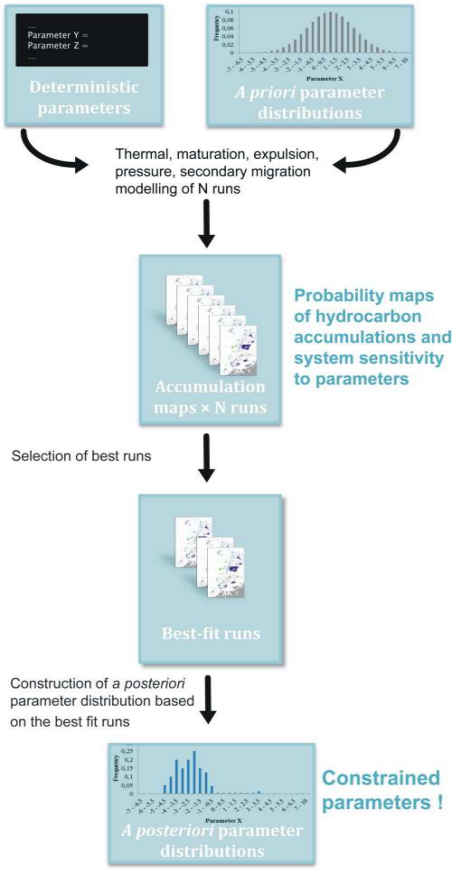

Fig. 4. Workflow for the Monte Carlo-secondary migration approach. This method is employed for constraining distributions of input parameters

Table 1. The Hammerfest Basin wells used for calibration of the modeled hydrocarbon column heights. Stø Fm. refers to Stø Formation - the main reservoir rock unit in the modelled petroleum system

well	longitude	latitude	Stø Fm. content
7120/6-1	497650.92	7946756.85	oil & gas
7120/7-1	7912388.54	471011.63	gas
7120/7-2	7913417.99	476011.92	gas
7120/8-1	7923384.58	479897.51	gas
7120/8-2	7915359.17	480927.89	gas
7120/9-1	498124.67	7932342.99	gas
7121/4-1	505507.86	7944529.35	gas
7121/4-2	7950918.8	502204.76	gas
7121/5-1	514306.93	7944421.61	oil & gas
7121/5-2	7952737.91	523051.48	oil & gas
7121/7-1	503105.18	7930306.01	gas
7121/7-2	7927117.4	501987.36	gas
7120/6-2 S	493948.96	7944559.34	oil & gas
7121/4-F-2 H	501998.86	7945754.16	oil & gas
7121/7-N-3 H	502986.46	7932077.79	oil & gas

The best-fit runs were used to create *a posteriori* input distributions. Differences between the *a priori* (model setup) and *a posteriori* distributions may be interpreted as gain of knowledge about these parameters for the given model and geological setting (Fig. 4).

3.2. Model Setup and Input Data

For the basin model we used interpreted seismic horizon maps provided by Statoil ASA and two constructed horizons (Intra Sotbakken 10 and 34 Ma) (Table 2) as input to the geo-model. The additional horizons enabled the modeling of erosion at the given time steps. Lithological properties of the layers were set up by using available core description data from Norwegian Petroleum Directorate (www.npd.no). SEMI allows for a definition dual-lithology setup, where sedimentary rocks are considered as a proportional mixture of two rock types (Table 2).

This paper is focused on the Middle Jurassic petroleum play in which the Stø Formation is a carrier unit and charged with hydrocarbons from the source rocks of the Kobbe and Hekkingen formations (Fig. 3). For the migration modeling it was assumed that only a certain fraction of the expelled hydrocarbons will migrate to the carrier unit.

3.3. Probabilistic Parameters

Three key model parameters were defined in probabilistic form: (a) Early Cenozoic (40-34 Ma) erosion amount, (b) late Cenozoic (10-2 Ma) erosion amount and (c) temperature gradient. Each of these parameters is composed of the deterministic component value (e.g., a map of the magnitude of erosion) and the probabilistic add-on modifiers. Values of the add-on modifiers are changed for every simulation run, since they represent a draw from assigned probability distributions (see section 3.1). For both, the early and late Cenozoic erosion amounts, the deterministic components were derived from cooling amount assessed by AFTA and VR well data (Duddy, 1998). A conversion into erosion amounts was done by assuming specific geo-thermal gradients during Cenozoic times. A detailed description of the method is given in (Green and Duddy, 2010) and case studies presented in (Japsen *et al*., 2010). The paleothermal gradient maps were constructed by using a combination of maximum paleo-thermal gradients, estimated from VR-depth profiles and present day geothermal gradient from BHT, DST data. These data were gridded up as maps.

In this study, erosion estimates based on input from wells 7120/8-1, 7120/9-2 and 7121/4-1 were employed (Fig. 5). Based on these erosion estimates, maps were created by using standard interpolation methods in Petrel software. We decided to use half of the inferred erosion amounts as the deterministic component of the probabilistic erosion parameter as a base case.

Table 2. Stratigraphic input to the basin model outlining the two dominant lithologies and boundary ages for each stratigraphic unit. For description see text

Base horizon	Top horizon	Age of base [Ma]	Age of top [Ma]	Lithology type 1	Lithology type 2	Rate between lith. 1 and lith. 2
Base Quaternary	Seabed	2	0	Shale	Sand	0.4
Intra Sotbakken	Base Quaternary	10	2	Shale	Sand	0.3
Intra Sotbakken	Intra Sotbakken	34	10	Shale	Sand	0.3
Top Torsk	Intra Sotbakken	40	34	Shale	Sand	0.3
Base Cenozoic	Top Torsk	66	40	Shale	Sand	0.4
Top Kolje	Base Cenozoic	125	66	Shale	Limestone	0.2
Top Hekkingen	Top Kolje	145	125	Shale	Limestone	0.2
Top Fuglen	Top Hekkingen	156	145	Shale	Sand	0.1
Top Stø	Top Fuglen	168	156	Shale	Limestone	0.1
Top Nordmela	Top Stø	183	168	Shale	Sand	0.9
Top Tubåen	Top Nordmela	197	183	Shale	Sand	0.8
Top Fruholmen	Top Tubåen	204	197	Shale	Sand	0.8
Top Kobbe	Top Fruholmen	237	204	Shale	Sand	0.7
Top Permian	Top Kobbe	251	237	Shale	Sand	0.5

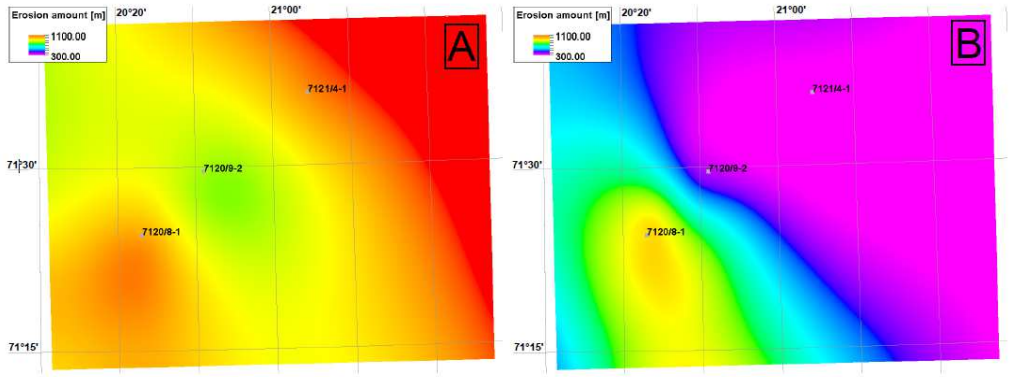

Fig. 5. Early and late Cretaceous base case maps. They are the results of AFTA and VR erosion estimates interpolation. The map values were reduced by 50% in order to add add-on variables which were defined as statistical distributions

We believe, based on the literature and data set review (Bjørlykke *et al*., 1989; Linjordet and Grung-Olsen, 1992; Riis and Fjeldskaar, 1992; Tsikalas, 1992; Walderhaug, 1992; Richardsen *et al*., 1993; Ohm *et al*., 2008), that this base case is a conservative minimum erosion amount estimate for each event in the region. These base case erosion maps yield amounts of 820-1100 and 250-985 m for the early and late Cenozoic events, respectively (Fig. 5). We assumed Gaussian distributions for the add-on modifier of the erosion parameters with a mean value and a standard deviation (1 sigma) of 500 m for the early Cenozoic event and 250 m for the late Cenozoic event. Both distributions were truncated at zero to avoid negative erosion estimates.

For the temperature gradient input parameter a set of gradient maps were constructed as the deterministic component. They are based on present day thermal gradients measured in deep wells. The add-on modifiers are drawn from a Gaussian distribution with mean value of 1°C/km and with standard deviation of 2°C/km (1 sigma).

3.4. Modeling Scenarios

Two scenarios were subjected to Monte Carlo simulation runs. In scenario A, we tested a base case assuming only sedimentary loading as an overpressure generating mechanism (no input overpressure maps used) and capillary leakage from traps was enabled. In scenario B, a pre-calculated overpressure history (see section 3, Appendix 1) of the carrier was incorporated in the model. Overpressure maps were calculated by using Pressim software. Also, hydraulic leakage was enabled as a second trapping failure mechanism. This can be interpreted as an end-member model. Overpressure build up in the carrier is governed by compartments bounded by low permeable faults. It can result in fracturing of the cap rock above traps and trap depletion enclosed in the modelled pressure compartments. The overpressure can

also change the migration paths and possible spill to oil and gas accumulations (Lothe *et al*., 2006). The input maps used from the overpressure modeling are shown in Appendix 1. Except for the overpressure and leakage mechanisms the remaining basin model setup is identical for both models (see section 3.2).

4. Results

4.1. All Modeling Runs

As a result of the 6000 simulation runs for both scenarios, a set of 3000 different input variable combinations were obtained. In general, scenario A simulations show marginally higher misfit values (from 27 to 64 m) then scenario B runs (from 27 to 59 m) (Equation 1). For both scenarios the early Cenozoic erosion amount modifiers vary between 0 and 2225 m with the mean value of 644±394 m. The late Cenozoic modifiers range from 0 to 1124 m with mean value of 320±198 m. Temperature gradient modifier values range from -5.5 to 8.7°C/km with the mean value of 1.1±2°C/km (Table 3).

The hydrocarbon column height fit (defined by misfit parameter) was analyzed against variable input parameters (Fig. 6). The figure shows misfit-input parameters relationships in scenario B, but the trends and values for the scenario A are very alike as summarized in Table 3. It was found that the misfit is not sensitive to temperature gradient modifier (Fig. 6c), but is slightly dependent on the late Cenozoic erosion amount modifier (Fig. 6b) and dependent on the early Cenozoic erosion amount modifier (Fig. 6a). The misfit of the latter parameter is the lowest for the lowest early Cenozoic erosion amount. The parameter shows low misfit for the values below 514 m (in scenario B) and 429 m in scenario A. Above this value misfit increases significantly up to value of 1658 m and for the higher values it decreases again. A certain late Cenozoic erosion amount value may show huge scatter of the misfit values. The minimum possible misfit value may be however achieved if the parameter is around 150 m.

4.2. Best-Fit Runs

For both scenarios the 250 best-fit simulation runs were selected which is 8.3% of all modeling runs. This number relates to rapid increase of the misfit value against the early Cenozoic erosion amount modifier (see section 4.1 and Fig. 6a). The input variables of these 250 runs were analyzed and used to derive *a posteriori* parameter distributions (see section 3).

4.3. Erosion Scenarios

In scenario A the early Cenozoic erosion amount modifiers range from 1 m to 429 m. The mean value is 206±148 m. By adding this mean value to the deterministic base-case erosion map (Fig. 5), the erosion amounts vary between 1026 and 1306 m, (±148 m).

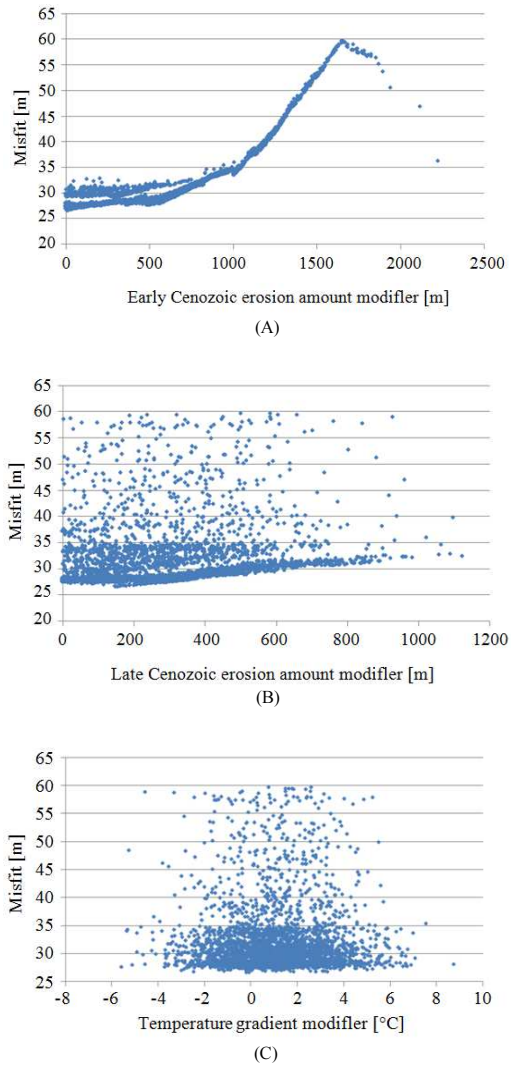

Fig. 6. Model input variables versus misfit for all 3000 runs for scenario B (including overpressure modeling). (A) Early Cenozoic erosion amount modifier, (B) late Cenozoic erosion amount modifier, (C) temperature gradient modifier

In scenario B the minimum and maximum values are quite similar to scenario A spanning a range from 0 m to 514 m, but the mean value and standard deviation is lower (142±122 m). This yields final erosion amounts, achieved by adding this mean value to the deterministic base-case erosion map, of between 962 and 1242 m (±122 m) (Fig. 7a, b, Table 3).

The late Cenozoic erosion amount modifier values of scenario A vary between 1 m and 359 m with mean value of 167±92 m. The total erosion amounts (deterministic base-case map plus the modifier) range from 417 to 1152 m (±92 m). In scenario B the values are very similar to scenario A, ranging from 1 m to 333 m with a mean value of 182±93 m. The total erosion is calculated to range from 432 to 1167 m (±93 m), (Fig. 7c, d and Table 3).

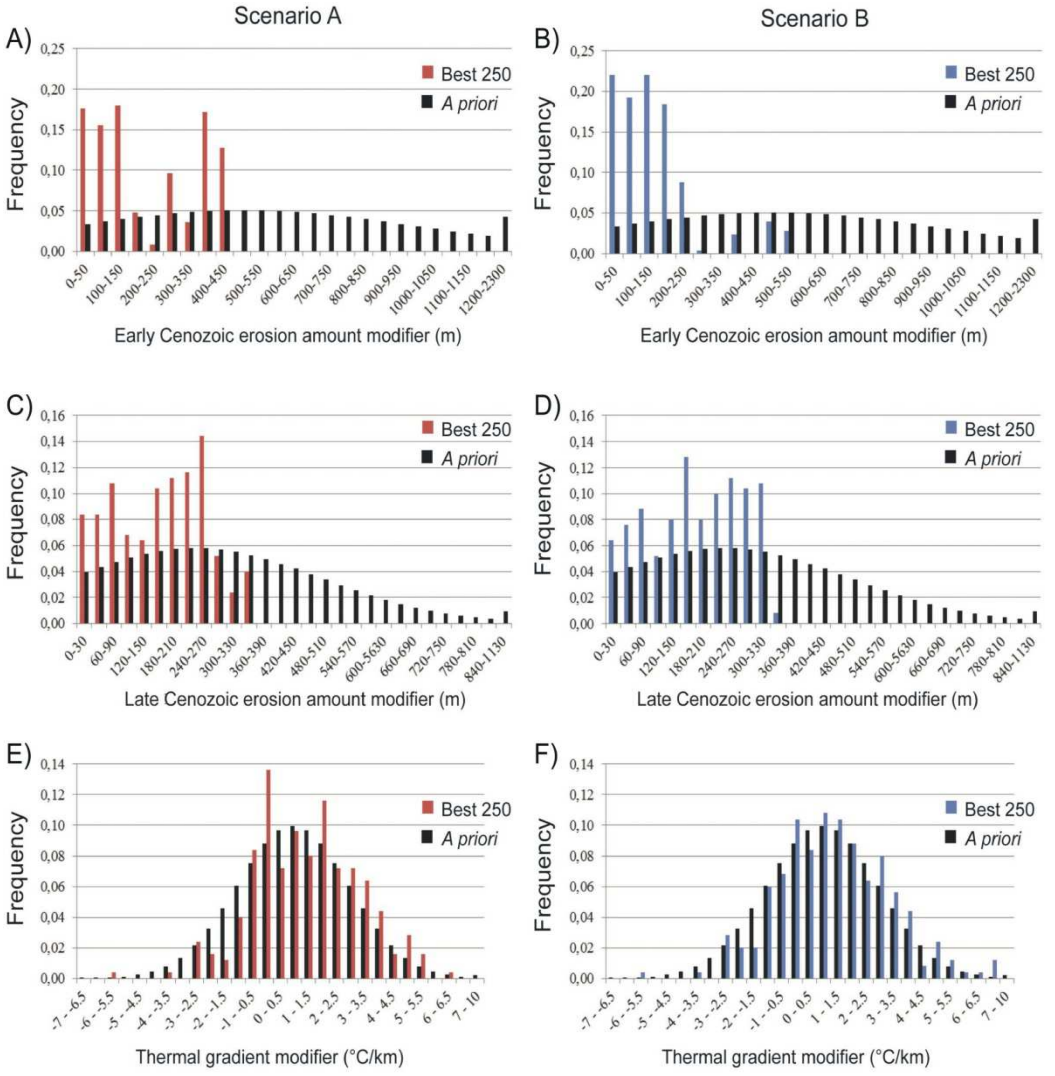

Fig. 7. Probabilistic results for estimates of erosion amount modifiers (A, B, C, D) and thermal gradients (E, F) for modelled scenario A and scenario B (see text for scenario definition). Histograms display both *a priori* (black bars) and *a posteriori* (red and blue bars) probability distributions of the add-on modifiers. The mean early Cenozoic amount of erosion modifier distribution is 500 m with a standard deviation of 500 m (A, B). The mean late Cenozoic amount of erosion modifier distribution is 250 m with a standard deviation of 250 m (C, D). All distributions are normal and truncated at 0. The thermal-gradient model was composed of base-case maps (defined for each time step) and probabilistic add-on modifiers. *A priori* distributions are normal with a mean value of 1°C and a standard deviation of 2°C

Table 3. Outline of statistical parameters for the investigated input of the study results. The table shows a shift in parameter distributions between *a priori* and best 250 simulation runs (*a posteriori*) distributions. *A priori* refers to all 3000 simulation runs performed for two pressure-compaction scenarios. Scenarios A and B refer to different pressure-compaction scenarios. The scenarios are described in the text

		Early Cenozoic ero. am. mod. [m]	Late Cenozoic ero. am. mod. [m]	Temp. gradient modifier [°C/km]
A priori:	min	0	0	-5.5
All runs	max	2225	1124	8.8
	std.	394	198	2.0
	mean	644	320	1.1
Scenario A:	min	1	1	-5.5
The best	max	429	359	6.1
250 runs	std.	148	92	1.9
	mean	206	167	1.1
Scenario B:	min	0	1	-5.5
The best	max	514	333	6.8
250 runs	std.	122	93	2.0
	mean	142	182	1.1

Comparing the results of scenario A (without overpressure) and scenario B (with overpressure history included), we see that the overpressure has a larger influence on the Early Cenozoic erosion amount (Fig. 7a and b) than on the late Cenozoic one (Fig 7c and d). In scenario A, the best 250 runs show the erosion amount modifier value between 0 and 450 m. However, including the overpressure maps through time (Scenario B) most of the best 250 runs have the early Cenozoic erosion amount modifier value between 0 and 250 m (Fig. 7b). For the late Cenozoic erosion amount (Fig. 7c and d), the difference between the 250 best runs (both without and with overpressure history included) is not so large, but slightly higher number of modeling runs which values are higher than 300 m was found.

The total amount of the Cenozoic erosion, which is considered to be a sum of the base-case maps and mean erosion amount values ranges from 1526 to 2411 m for scenario A and from 1477 to 2362 m for scenario B in the study area.

4.4. Net Erosion

Net erosion is defined as a difference between maximum burial depth and present depth for a marker horizon. Therefore it differs from the total erosion amount which does not consider the amount of deposition (England and Molnar, 1990). In fact our erosion amount estimates refer to the total erosion amount which is either equal or higher that the net erosion. Except for (Duddy, 1998; Green and Duddy, 2010; Duran *et al*., 2013) the erosion amount estimates published since the 1980's refer to net erosion amount (Fig. 8b). In order to check how the modeling results fit the literature, calculations of the net erosion were performed by using standard decompaction procedure in the SEMI software.

In both scenarios the maximum burial depth was reached at 40 Ma in the almost entire area. In the neighborhood of the well 7120/8-1 the maximum burial depth was reached a 10 Ma. The resulting net erosion varies between 400 and 784 m in scenario A and between 348 and 733 m in scenario B.

4.5. Thermal Gradient

For the thermal gradient modifier distributions no significant discrepancy was found between *a priori* and *a posteriori* distributions. In both scenarios *a posteriori* mean values are about 1°C/km which is approximately equal to the *a priori* distribution mean value. Similar values were also found in standard deviation which is about 2°C/km in both *a priori* and *a posteriori* distributions (Fig. 7e and f). The best value for the geothermal gradient according to the Monte Carlo simulations is 36.1±2°C/km.

5. Discussion

Our erosion amount estimates distinguish between early and late Cenozoic amounts and the results indicate that overall the early Cenozoic erosion event was dominant with mean erosion amounts of about 1.0-1.3 km depending on basin location and pressure-leakage scenario. Similar amounts are reached locally by the late Cenozoic erosion, but in general the late Cenozoic erosion was lower (0.4-1.2 km). The late Cenozoic erosion is concentrated in southwestern part of the study area due to base case map deviation (Fig. 5). The early Cenozoic erosion is much less localized than the late Cenozoic event showing relatively low erosion amount deviation.

Our early Cenozoic erosion estimates are much lower than the erosion estimate in well 7120/9-2 (Green and Duddy, 2010) but coincide with range of the late Cenozoic erosion amounts reported in the entire HB by Duran *et al*. (2013) (Fig. 8a). The calculated Cenozoic total erosion varies between 1.5 and 2.4 km across the area which is lower than the estimates made by Green and Duddy (2010) (2.8 km) and higher than those made by Duran *et al*. (2013) (0.3-1.5 km). Duran *et al*. (2013) estimates represent a similar petroleum system modeling approach to the one presented here. In their study, three different erosion scenarios (varied spatially) were tested and calibrated against the present day temperature and VR measurements. The best fit was achieved by using the highest possible erosion amount scenario (Fig. 8a) supporting the view that petroleum system modeling of the HB produces matching results if a substantial erosion amount is assigned.

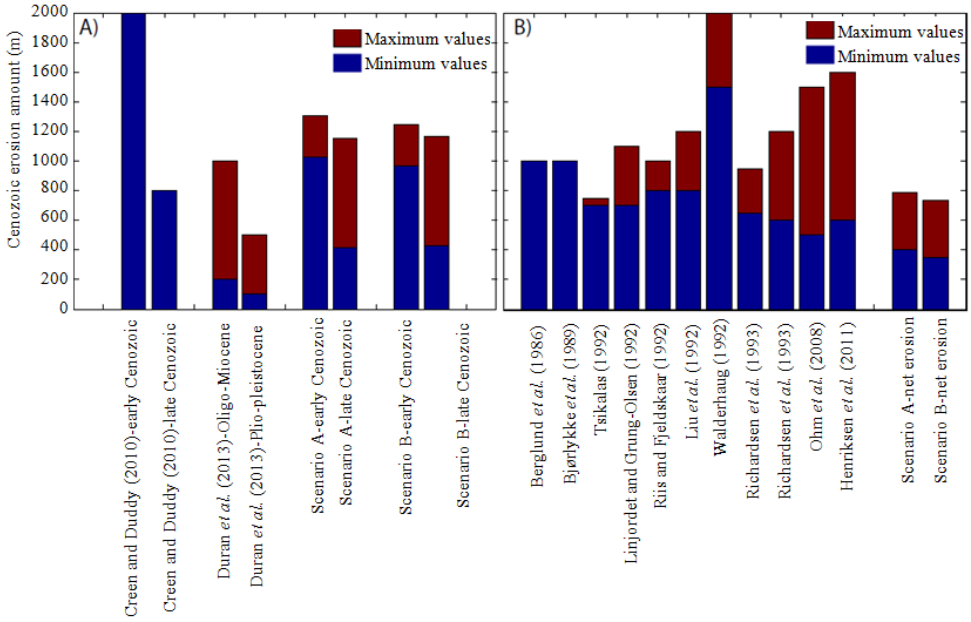

Fig. 8.Compilation of erosion estimates for Cenozoic times from previous publications and the results reported in here. (A) Total erosion amount (B) net erosion amount

We have showed that the net erosion ranges between 0.3-0.8 km. These values correspond with those in the literature but represent rather lower boundary estimates (Fig. 8b). Given that the study area is localized in the western part of the HB, we attribute this difference to a decreasing trend of net erosion amount towards the western margin of the Barents Sea as described by Henriksen *et al*. (2011a).

Literature does not put focus on the effect of water fluid overpressures on hydrocarbon migration modeling combined with erosion and uplift. Cavanagh *et al*. (2006) modelled the reservoir pressure (Stø Formation) in the Snøhvit area in the range of 5-10 MPa, depending on the glacial cycles' character and erosion amount. Their overpressure modeling was carried out for the last 1 Ma similarly to Duran *et al*. (2013) who conducted overpressure modeling for the last 1.2 Ma. In this study, we have modelled hydrocarbon migration including various erosion amounts and different overpressure scenarios for the last 40 Ma. The high overpressure modelled in the Eocene has impact on erosion amount that gives the best fit (Fig. 7a, b and Appendix 1). Moreover the study shows that for the early Cenozoic erosion phase, a low misfit is calculated with erosion map varying from 700 to 1100 m laterally (Fig. 5a) and with a modifier from 0 to about 500 m (Fig. 6a). Higher erosion amounts result in significant misfit increase (Fig. 6a). The same trend cannot however be observed for the late Cenozoic erosion event (Fig. 6b). This result indicates that the effect of the early Cenozoic erosion phase should not be underestimated. Furthermore, the results suggest that tectonic events during the Late Cenozoic might not have had an effect on the migration history as significant as the early Cenozoic uplift event.

Several theories have been proposed about the cause of erosion in the study area. Henriksen *et al*. (2011a) provide a literature review of the erosion amount estimates and driving forces of the Cenozoic uplift. They suggest the following possible uplift and erosion mechanisms: (a) Opening of the Atlantic and Arctic Oceans, (b) compression and/or transpression, (c) isostatic response to sediment unloading and (d) post-glacial rebound. Dating results (Duddy, 1998) mainly support the first two mechanisms. We believe that the two erosion events between 40 and 34 Ma and between 10 and 2 Ma coincide with major plate tectonic reorganizations in sea-floor spreading in the Norwegian-Greenland Sea and the associated development of a trans-tensional regime along the De Geer Zone megashear system (Faleide *et al*., 2008) following the western Barents Sea to Svalbard axis (Fig. 2). The ages of the late Eocene erosion event coincide with timing of the rift flank uplift in the Barents Sea (Dimakis *et al*., 1998) and an increased amount of erosion affecting the southwestern Barents Sea. The late Cenozoic erosion age (10-2 Ma) is supported by sedimentological and

geochemical data from the Atlantic-Arctic gateway showing that the entire northwestern European margin was uplifted during the late Miocene-early Pliocene (Knies *et al*., 2014).

In the Barents Sea the uplifted terrain is believed to be further affected by several glaciations leading to the shelf erosion in a range of 0.8-1.0 km (Laberg *et al*., 2012). Glaciations in the southern Barents Sea are thought to commence about 1.0 Ma (Knies *et al*., 2009) which does not coincide with the ages of erosion detected by AFTA used in this study (Duddy, 1998). According to AFTA dating the most recent Barents Sea cooling episode occurred before glacial events (10-5 Ma). This cooling is thought to be driven by a regional tectonic cause resulting in regional uplift and erosion (Duddy, 1998; Green and Duddy, 2010). As mentioned, we relate this cause to plate tectonic reorganization and seafloor spreading. Moreover, we speculate that another reason why the glaciation events were not detected is the low net erosion amount; below the sensitivity of the AFTA method. This might occur if the glacial erosion coexisted with substantial amount of glacial deposition. However, an estimation of the glacial deposition amounts on the Norwegian shelf has not yet been published and in order to investigate this hypothesis this topic should be studied in detail.

6. Conclusions

Here we presented a novel stochastic basin modelling approach to quantify erosion and associated uncertainties in the western Hammerfest Basin. The modelling results indicate:

- The early Cenozoic erosion amount oscillated between 1.0 and 1.3 km
- The late Cenozoic erosion amount ranges from 0.4 to 1.2 km
- Estimated net erosion varied from 0.3 to 0.8 km
- Overpressure scenarios had a limited effect on modelled erosion amounts
- The early Cenozoic uplift and erosion had a significantly higher impact on the hydrocarbon migration compared to the late Cenozoic event

7. Acknowledgement

We acknowledge Statoil ASA for providing data. We appreciated the profound comments of two anonymous reviewers.

8. Funding Information

This work is a contribution to Strategic Institute Program (SIP 186919) “Top seal integrity and leakage, with relevance for exploration risk in the Barents Sea” (2008-2010) funded by Research Council of Norway.

9. Author’s Contributions

This paper presents the main results from a MSc thesis of KJZ who analyzed, interpreted the results and coordinated the study. The thesis was supervised by SL and MD. MD set up and performed the basin modelling and contributed to sections 3, 4 and 5. BE contributed to all the sections and organized the paper's framework. AL and AG contributed to section 3, 4 and 5.

10. Ethics

This article is original and contains unpublished material. The corresponding author confirms that all of the other authors have read and approved the manuscript and no ethical issues involved.

11. References

Berglund, L.T., J. Augustson, R.B. Færseth, J. Gjelberg and H. Ramberg-Moe, 1986. The evolution of the Hammerfest Basin. In: Habitat of Hydrocarbons on the Norwegian Continental Shelf, Spencer, A.M. (Ed.), Graham and Trotman for the Norwegian Petrolium Society, London, ISBN-10: 0860108333, pp: 319-338.

Bjørlykke, K., M. Ramm and G.C. Saigal, 1989. Sandstone diagenesis and porosity modification during basin evolution. Geologische Rundschau, 78: 243-268. DOI: 10.1007/BF01988363

Borge, H., 2000. Fault controlled pressure modeling in sedimentary basins. Norwegian University of Science and Technology.

Borge, H. and Ø. Sylta, 1998. 3D modelling of fault bounded pressure compartments in the North Viking Graben. Energy Exploration Exploitat., 16: 301-323.

Cavanagh, A.J., R. Di Primio, M. Scheck-Wenderoth and B. Horsfield, 2006. Severity and timing of Cenozoic exhumation in the southwestern Barents Sea. J. Geological Society, 163: 761-774. DOI: 10.1144/0016-76492005-146

Clark, S.A., E. Glorstad-Clark, J.I. Faleide, D. Schmid and E.H. Hartz *et al*., 2013. Southwest Barents Sea rift basin evolution: Comparing results from backstripping and time-forward modelling. Basin Res., 26: 550-566. DOI: 10.1111/bre.12039

Dalland, A., D. Worsley and K. Ofstad, 1988. A Lithostratigraphic Scheme for the Mesozoic and Cenozoic and Succession Offshore Mid- and Northern Norway. 1st Edn., Oljedirektoratet, pp: 130.

Dimakis, P., B.I. Braathen, J.I. Faleide, A. Elverhøi and S.T. Gudlaugsson, 1998. Cenozoic erosion and the preglacial uplift of the Svalbard-Barents Sea region. Tectonophysics, 300: 311-327. DOI: 10.1016/S0040-1951(98)00245-5

Duddy, I.R., 1998. The Barents Sea-thermal, tectonic and hydrocarbon maturation histories assessed using apatite fission track analysis and vitrinite reflectance. Geotrack International Pty Ltd.

Duran, E.R., R. di Primio, Z. Anka, D. Stoddart and B. Horsfield, 2013. 3D-basin modelling of the Hammerfest Basin (South Western Barents Sea): A quantitative assessment of petroleum generation, migration and leakage. Marine Petroleum Geol., 45: 281-303. DOI: 10.1016/j.marpetgeo.2013.04.023

England, P. and P. Molnar, 1990. Surface uplift, uplift of rocks and exhumation of rocks. Geology, 18: 1173-1177. DOI: 10.1130/0091-7613(1990) 018<1173:SUUORA>2.3.CO;2

Faleide, J.I., F. Tsikalas, A.J. Breivik, R. Mjelde and O. Ritzmann *et al*., 2008. Structure and evolution of the continental margin off Norway and Barents Sea. Episodes, 31: 82-91.

Faleide, J.I., E. Vagnes and S.T. Gudlaugsson, 1993. Late Mesozoic-Cenozoic evolution of the South Western Barents Sea in a regional rift-shear tectonic setting. Marine Petroleum Geol., 10: 186-214. DOI: 10.1016/0264-8172(93)90104-Z

Gabrielsen, R.H., R.B. Færseth, L.N. Jensen, J.E. Kalheim and F. Riis, 1990. Structural elements of the continental shelf. Part I: The Barents Sea Region. Norwegian Petroleum Directoriate.

Gernigon, L., M. Bronner, D. Roberts, O. Olesen and A. Nasuti *et al*., 2014. Crustal and basin evolution of the southwestern Barents Sea: From Caledonian orogeny to continental breakup. Tectonics, 33: 347-373. DOI: 10.1002/2013tc003439

Glørstad-Clark, E., J.I. Faleide, B.A. Lundschien and J.P. Nystuen, 2010. Triassic seismic sequence stratigraphy and paleogeography of the western Barents Sea area. Marine Petroleum Geol., 27: 1448-1475. DOI: 10.1016/j.marpetgeo.2010.02.008

Green, P.F. and I.R. Duddy, 2010. Synchronous exhumation events around the Arctic including examples from Barents Sea and Alaska North Slope. Petroleum Geol. Conf. Series, 7: 633-644. DOI: 10.1144/0070633

Henriksen, E., H.M. Bjornseth, T.K. Hals, T. Heide and T. Kiryukhina *et al*., 2011a. Chapter 17 Uplift and erosion of the greater Barents Sea: Impact on prospectivity and petroleum systems. Geological Society, London, Memoirs, 35: 271-281. DOI: 10.1144/M35.17

Henriksen, E., A.E. Ryseth, G.B. Larssen, T. Heide and K. Ronning *et al*., 2011b. Chapter 10 Tectonostratigraphy of the greater Barents Sea: Implications for petroleum systems. Geological Society, London, Memoirs, 35: 163-195. DOI: 10.1144/M35.10

Jakobsson, M., R. Macnab, L. Mayer, R. Anderson and M. Edwards *et al*., 2008. An improved bathymetric portrayal of the Arctic Ocean: Implications for ocean modeling and geological, geophysical and oceanographic analyses. Geophysical Res. Lett., 35: L07602- L07602. DOI: 10.1029/2008GL033520

Japsen, P., P.F. Green, J.M. Bonow, E.S. Rasmussen and J.A. Chalmers *et al*., 2010. Episodic uplift and exhumation along North Atlantic passive margins: Implications for hydrocarbon prospectivity. Petroleum Geol. Conf. Series, 7: 979-1004. DOI: 10.1144/0070979

Knies, J., J. Matthiessen, C. Vogt, J.S. Laberg and B.O. Hjelstuen *et al*., 2009. The Plio-Pleistocene glaciation of the Barents Sea-Svalbard region: A new model based on revised chronostratigraphy. Quaternary Sci. Rev., 28: 812-829. DOI: 10.1016/j.quascirev.2008.12.002

Knies, J., R. Mattingsdal, K. Fabian, K. Grøsfjeld and S. Baranwal *et al*., 2014. Effect of early Pliocene uplift on late Pliocene cooling in the Arctic-Atlantic gateway. Earth Planetary Sci. Lett., 387: 132-144. DOI: 10.1016/j.epsl.2013.11.007

Laberg, J.S., K. Andreassen and T.O. Vorren, 2012. Late Cenozoic erosion of the high-latitude southwestern Barents Sea shelf revisited. Geological Society Am. Bull., 124: 77-88. DOI: 10.1130/B30340.1

Linjordet, A. and R. Grung-Olsen, 1992. The Jurassic Snøhvit Gas Field Hammerfest Basin, Offshore Northern Norway. In: Giant Oil and Gas Fields of the Decade, 1978-1988, Halbouty, M.T. (Ed.), American Association of Petroleum Geologists, Tulsa, Okla, ISBN-10: 0891813330, pp: 526.

Liu, G.J., S. Lippard, S. Fanavoll, O. Sylta and S. Vassmyr *et al*., 1992. Quantitative geodynamic modelling of Barents Sea Cenozoic uplift and erosion. Norsk Geologisk Tidsskrift, 72: 313-316.

Lothe, A., 2004. Simulations of hydraulic fracturing and leakage in sedimentary basins. University of Bergen.

Lothe, A., Ø. Sylta, O. Lauvrak and S. Sperrevik, 2006. Influence of fault map resolution on pore pressure distribution and secondary hydrocarbon migration; Tune area, North Sea. Geofluids, 6: 122-136. DOI: 10.1111/j.1468-8123.2006.00136.x

Ohm, S.E., D.A. Karlsen and T.J.F. Austin, 2008. Geochemically driven exploration models in uplifted areas: Examples from the Norwegian Barents Sea. AAPG Bulletin, 92: 1191-1223. DOI: 10.1306/06180808028

Ostanin, I., Z. Anka, R. di Primio and A. Bernal, 2012. Identification of a large Upper Cretaceous polygonal fault network in the Hammerfest basin: Implications on the reactivation of regional faulting and gas leakage dynamics, SW Barents Sea. Marine Geol., 332-334: 109-125. DOI: 10.1016/j.margeo.2012.03.005

Rasmussen, E. and W. Fjeldskaar, 1996. Quantification of the Pliocene-Pleistocene erosion of the Barents sea from present-day bathymetry. Global Planetary Change, 12: 119-133. DOI: 10.1016/0921-8181(95)00015-1

Richardsen, G., T.O. Vorren and B.O. Torudbakken, 1993. Post-early cretaceous uplift and erosion in the southern Barents Sea A discussion based on analysis of seismic interval velocities. Norsk Geologisk Tidsskrift, 73: 3-20.

Riis, F. and W. Fjeldskaar, 1992. On the magnitude of the Late Tertiary and Quaternary Erosion and its Significance for the Uplift of Scandinavia and the Barents Sea. In: Structural and Tectonic Modeling and its Application to Petroleum Geology, Larsen, R.M., H. Brekke, B.T. Larsen and E. Talleraas (Eds.), NPF Special Publication, pp: 163-185.

Sclater, G.J. and P.A.F. Christie, 1980. Continental stretching: An explanation of the post-mid-cretaceous subsidence of the Central North Sea Basin. J. Geophysical Res., 85: 3711-3739. DOI: 10.1029/JB085iB07p03711

Seton, M., R.D. Müller, S. Zahirovic, C. Gaina and T. Torsvik *et al*., 2012. Global continental and ocean basin reconstructions since 200 Ma. Earth-Sci. Rev., 113: 212-270. DOI: 10.1016/j.earscirev.2012.03.002

Sylta, O., 2004. A probabilistic approach to improved geological knowledge and reduced exploration risks using hydrocarbon migration modelling. Petroleum Geosci., 10: 187-198. DOI: 10.1144/1354-079303-607

Sylta, O. and W. Krokstad, 2003. Estimation of oil and gas column heights in prospects using probabilistic basin modelling methods. Petroleum Geosci., 9: 243-254. DOI: 10.1144/1354-079302-563

Tsikalas, F., 1992. A study of seismic velocity, density and porosity in Barents Sea wells, Northern Norway. MSc Thesis, University of Oslo, Oslo, Norway.

Vorren, T.O., G. Richardsen and S.M. Knutsen, 1991. Cenozoic erosion and sedimentationn in the western Barents Sea. Marine Petroleum Geol., 8: 317-340. DOI: 10.1016/0264-8172(91)90086-G

Walderhaug, O., 1992. Magnitude of uplift of the Stø and Nordmela Formations in the Hammerfest Basin-a diagenetic approach. Norsk Geologisk Tidskrift, 72: 321-323.

Walderhaug, O., 1996. Kinetic modeling of quartz cementation and porosity loss in deeply buried sandstone reservoirs. AAPG Bull., 80: 731-745. DOI: 10.1306/64ED88A4-1724-11D7-8645000102C1865D

Watts, A.B. and W.B.F. Ryan, 1976. Flexure of the lithosphere and continental margin basins. Tectonophysics, 36: 25-44.

Worsley, D., 2008. The post-Caledonian development of Svalbard and the Western Barents Sea. Polar Res., 27: 298-317. DOI: 10.1111/j.1751-8369.2008.00085.x

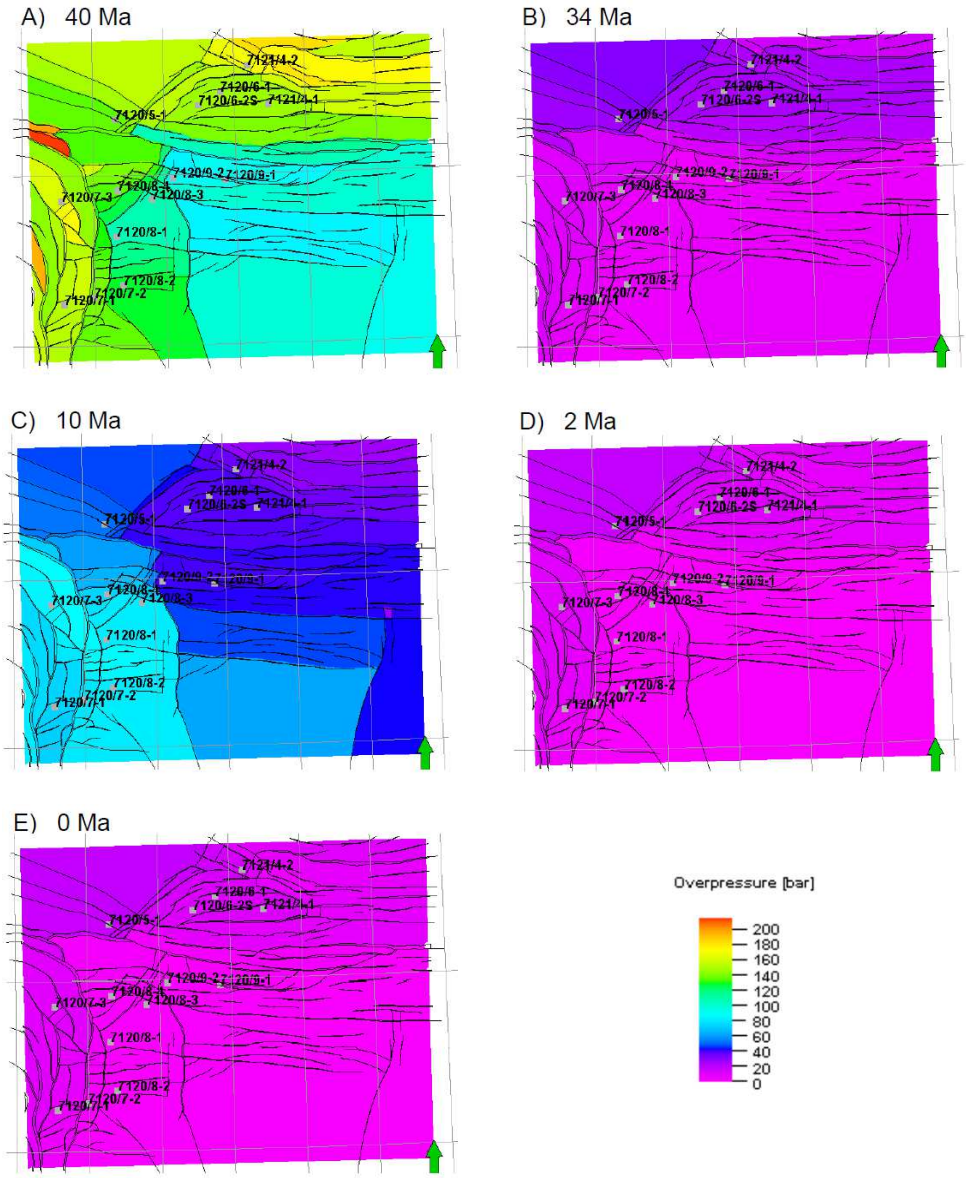

Appendix 1. Overpressure maps used as input for the basin model. These were used only in modeling scenario B (for details see section 3.4). No overpressure for the time steps before 40 Ma was detected

8.3 Conference abstracts

Emmel, B., **Zieba, K.J.** (2015). Thermochronology based revised Cenozoic uplift and erosion estimates for the western Barents Sea. Geo Berlin conference; 2015-10-04 - 2015-10-07.

From a hydrocarbon exploration perspective, the Norwegian Barents Sea is an immature area and until now the discoveries of gas and oil fields are below expectations. One main reason for this might be the complex Cenozoic thermo-tectonic and climate history of the region. During the Cenozoic the Barents Sea was affected by several episodes of vertical tectonic movements including build-up and retreat of ice sheets. These episodes were associated with sediment mass re-distribution influencing the rock and fluid properties of the underlying sedimentary units. Dry hydrocarbon traps with residual oil indicate trap filling during the geological past. Trap drainage most probably occurred during the Cenozoic.

We reviewed published and in-house apatite fission track data of ca. 120 surface samples to identify locations and quantify amount and timing of major erosion events. Youngest apatite fission track ages (< ca. 70 Ma) were found along the westernmost margin of the Barents Sea and along the northwestern continental margin of Norway. Joint inversion of apatite fission track and vitrinite reflectance data of some samples suggest major Cenozoic rock cooling. However, timing and magnitude are uncertain and vary significantly for different fault bounded structural elements. We speculate that the differential rock cooling is related to the Cenozoic development of positive and negative structures during transtension and transpression along the western Barents Sea transform margin. In contrast, youngest rock cooling of along near coastal regions (NW Norway) might be related to sea-level drop and subsequent exposure to erosion. In future, we will use apatite (U-Th)/He dating to further constrain the cooling history of critical areas.

Zieba, K.J., Felix, M. (2015). Impact of the Pleistocene Glaciations on Net Erosion Development in the Western Barents Sea. American Geophysical Union Fall Meeting; 2015-12-14 - 2015-12-18.

The Barents Sea shelf was subjected to both tectonic- and glacially-driven erosion during the Cenozoic. It is however unclear which of the erosion mechanisms had the most important role in generating net erosion that indicates a total effect of all erosion events. The literature estimates of glacial to tectonic erosion ratio vary significantly and often do not account for regional variations. The tectonic erosion is often attributed to plate reorganization in the Norwegian-Greenland Sea during the Cenozoic. The literature shows wide diversity of opinions regarding timing and thickness of the tectonic erosion. In contrast, glacial erosion thickness estimates are well constrained and show lower discrepancy in results. The glacial erosion thickness estimates are therefore key information that can be used for constraining the ratio between tectonic and glacial erosion. The glacial contribution to the net erosion is however also controlled by on-shelf deposition that counteracts the process of glacial erosion. However the on-shelf deposition rates have never been calculated. In result, the Pleistocene sediment budget and glacial contribution to the net erosion has never been assessed yet.

The Pleistocene contribution to the net erosion was approached by a new Monte-Carlo-type method where the Pleistocene-Holocene sediment budget is calculated and the net erosion thickness is determined as a balance between total deposition and erosion thicknesses. The proposed method requires definite ages of glacial and interglacial periods what is not available in the literature. The timeframe was established by using a new approach based on the regional ice-sheet volume curve. Also, the new glacial/interglacial timeframe enables calculating the erosion rates for glacial duration ($10^3 – 10^4$ yr) timescale what have not been performed before.

The results show that the western Barents Sea was glaciated during 4 marine isotope stages for a total duration of 29 kyr. The glacial erosion rates range between 25 and 40 mm/yr. On-shelf deposition rates vary from 0 to 35 mm/yr. In the western Barents Sea the net erosion was found to be mainly the effect of tectonic uplift and subsequent erosion prior to the glacial ages. The results show that the Pleistocene glaciations did not or slightly contributed to development of the net erosion.

Zieba, K.J., Felix, M. (2015). How to assess glacial sedimentary conditions in the light of missing local data? 7th International Conference on Arctic Margins ICAM 2015; 2015-06-02 - 2015-06-05

Pleistocene glaciations are assumed to have played a major role in the development of the Barents Sea basin. Glacial loading-unloading series as well as glacial erosion and deposition resulted in multiple uplift and subsidence events as a result of isostasy. A history of the Pleistocene basin development can be reconstructed by using modelling software. However no quantitative input data are available for the number of glaciations, or for erosion and deposition rates. Estimates for such values are only available for either the whole Barents Sea, of for very large timescales. This misses out a lot of detail both for temporal and spatial variations.

We approach this problem by using a new methodology based on Monte Carlo simulations where the Pliocene-Holocene sedimentary cover thickness is calculated as a function of glacial erosion and deposition as well as interglacial deposition. A glacial-interglacial timeframe used in the simulations is based on new results which were determined by using published historic ice-sheet volume estimations. We applied the methodology in the outer Bjørnøyrenna area (western Barents Sea) and compared the results with available data.

The results suggest that the study area was occupied by the ice sheets during four marine isotope stages: MIS 2, MIS 6, MIS 12 and MIS 16 for approximately 30 ka in total. By using the time-frame based on glacial volumes, the results show typical glacial erosion rates (between 25 and 38 mm/a) for short-timescale measurements. Glacial deposition rates were calculated to vary between 0 and 37 mm/a, fitting the rates estimated for the Last Glacial Maximum in the western Barents Sea. Although these results are still averages for longer time periods, the method does give more detail than regional estimates.

Zieba, K.J., Felix, M. (2015). The Pleistocene - Holocene sediment budget in the Barents Sea glacial-interglacial setting. Geological Winter Meeting, Abstracts and Proceedings of the Geological Society of Norway, v 1.

Glacial history in the southern Barents Sea region is assumed to have begun about 1.0 Ma ago, resulting in repeated glacial advances reaching the western shelf break (Knies et al., 2009). However, the number of glaciations is still disputed. Except for the Last Glacial Maximum (LGM), the Barents Sea ice sheet extent and ages of each advance are however very uncertain. Although average estimates exist, it is unknown how much sediment was eroded and how much was deposited on the Barents Sea shelf during each of the individual advances. Another problem is how much glacial erosion affected the sedimentary bedrock and how much affected soft glacial-interglacial sediments. These unknowns hamper detailed reconstruction of the burial history including contribution of the glacial-interglacial activity to the total net erosion amount.

In this study, these problems were tackled by using an approach consisting of two parts. In the first part, the ages of glacial events were determined based on a new method using published historic ice-sheet volume estimations (de Boer et al., 2014). In the second part, the problem of the sedimentary budget is investigated by using a new Monte Carlo modelling approach where the Pliocene-Holocene sedimentary cover is calculated as a function of glacial erosion and deposition as well as interglacial deposition. The study focuses on the outer Bjørnøyrenna area (western Barents Sea).

The results show that the study area was occupied by the ice sheet only during four marine isotope stages: MIS 2, MIS 6, MIS 12 and MIS 16. To validate the methodology, the same calculations were performed for the eastern Barents Sea, which showed that this area was glaciated during 8 marine isotope stages; this agrees with suggestions of Laberg and Vorren (1996). During these glaciations high rates of erosion (in the range of 25-38 mm/a) and deposition (up to 111 mm/a) prevailed. High deposition rates favoured erosion of soft glacial-interglacial sediments more than erosion of the sedimentary bedrock. The sedimentary bedrock is believed to contribute less than 50% of the total sediment eroded during the Pleistocene glaciations.

Zieba, K.J., Grøver, A. (2015). Glacial erosion, deposition and ice loading: Impact on structural development of the western Barents Sea sedimentary basins. Geo Berlin conference; 2015-10-04 - 2015-10-07.

Lack of major hydrocarbon discoveries in the western Barents Sea shelf is often attributed to the consequences of the Pleistocene rapid glacial erosion, subsidence and ice loading. In the relatively small area contrasting sedimentation patterns and uneven ice thickness distribution occurred leading to considerable structural changes. The structural changes include reactivation of faults, differential uplift, subsidence and tilting; potentially resulting in hydrocarbon remigration and leakage. Although new Pleistocene erosion and deposition estimates exist, resulting uplift, subsidence and tilting has not been quantified yet. Similarly, modern and detailed ice topography models are available but their impact on structural changes has not been calculated yet. For these reasons it remains unclear whether the Pleistocene tectonic events could contribute in the hydrocarbon leakage. If so, which of the Pleistocene tectonic event had dominant effect on depletion of hydrocarbon traps?

These questions can be answered by using modelling of isostatic effects of deposition/erosion and ice loading by using newly published data. Two different isostatic models are considered: Airy and flexural models. We will present effects of inhomogeneous erosion/deposition and ice loading on structural changes of underlying rocks with focus on reservoir units and hydrocarbon traps. In addition, reconstructed geometry of the trap structures prior to the glaciations will be shown. Also, we will demonstrate differences of the results between the used isostatic models in context of the Pleistocene tectonic events.

Zieba, K.J., Daszinnies, M., Lippard, S.J., Lothe, A.E. (2014). How to Benefit from Monte Carlo Simulations in Petroleum Systems Modelling to Estimate the Amount of Erosion? EAGE 6th Saint Petersburg International Conference & Exhibition; 2014-04-07 - 2014-04-10.

Is not included due to copyright

Zieba, K.J., Daszinnies, M., Lippard, S.J., Lothe, A.E. (2014). Estimation of Erosion Amount Through the Probabilistic Basin Modelling Approach. The Arctic Days Conference, Abstracts and Proceedings of the Geological Society of Norway, v 2.

In the Barents Sea, dry traps with residual oil shows may indicate a history of filling and subsequent emptying. This process is commonly attributed to hydrocarbon redistribution and leakage due to the Cenozoic uplift and erosion. Uplift and closely associated erosion may cause severe alterations for a petroleum system. The magnitude of these changes is related to the amount of erosion, therefore its estimation is a key parameter for the Barents Sea basin models. Many different methods (e.g. VR, mass balance, geochemical methods) have been used for quantifying the amounts of erosion in the south-western Barents Sea since the late 1980s. Published data display, however, differences in the amount and timing. Deterministic basin models show only single model solutions and do not consider uncertainties related to input data.

This problem was approached by using the Monte Carlo - secondary migration basin modelling method (Sylta and Krokstad 2003) where some of the basin model's input parameters are defined as *a priori* probabilistic distributions (constructed based on general geological knowledge). The probabilistic input parameter values are sampled randomly for each petroleum-system modelling run from defined distributions. Each modelling run produces one, individual hydrocarbon accumulation map. These of the runs which show the lowest misfit between modelled and measured (from wells) hydrocarbon column heights are further used for constructing *a posteriori* variable distributions. These distributions are considered to represent the most probable values.

In this project, the Middle Jurassic petroleum play was modelled where the Stø Formation is a carrier unit which is charged with hydrocarbons from the source rocks of the Kobbe and Hekkingen formations. This setting enables model calibration against hydrocarbon column heights which were measured in several wells drilled in the Stø Formation. Two erosion events were considered: the early and the late Cenozoic. The amount of erosion in these events was described as the product of deterministic maps and probabilistically distributed add-on modifiers. The palaeo-thermal gradient was also tested and defined as a set of base maps (individual for each time-step) and add-on modifier. Two pressure/leakage scenarios were modelled: simplified scenario A, and scenario B which takes into account additional overpressure build-up through chemical compaction and hydraulic leakage. Three thousand simulations were run for each scenario.

Results from stochastic basin modelling simulation show the early Cenozoic erosion event had generally higher magnitude than the late Cenozoic one. *A posteriori* distribution mean values were much lower than *a priori* mean values (representing initial beliefs) suggesting lower amount of erosion than expected. By using this approach, the additional overpressure build-up mechanism and hydraulic leakage modelling do not affect the minimum and the maximum erosion amount estimates to a high degree.

Sylta, O. and Krokstad, W. [2003] Estimation of oil and gas column heights in prospects using probabilistic basin modelling methods. Petroleum Geoscience, 9(3), 243–254.

Zieba, K.J., Daszinnies, M., Grøver, A., Lothe, A.E., Lippard, S.J. What are the consequences of the Cenozoic glaciation events on the petroleum systems in the Norwegian Barents Sea? 3P Arctic Conference; 2013-10-15 - 2013-10-18.

Widespread glaciations during the late Pliocene-Pleistocene resulted in extensive erosion from the continental shelf areas of the Norwegian Barents Sea. It also led to synchronous deposition of thick sedimentary wedges on the continental slopes (Laberg et al. 2010, 2012). This large-mass redistribution resulted in uplift and tilting of underlying traps, and most likely affected the entire hydrocarbon systems. Some of the potential consequences are: changes in hydrocarbon generation, secondary migration, fluid composition and location of pools (Doré et al. 2000, 2002). In the Norwegian Barents Sea many of the uplift consequences have not been fully understood yet. The most important questions are:

- Have the Cenozoic uplift and erosion events of the western Barents Sea caused gas expansion and leakage?
- What is a magnitude of gas expansion and leakage caused by these events?
- How much petroleum has leaked and how much is left?

In order to address these questions SINTEF Petroleum Research introduced the project 'Impact of Cenozoic structural development and glacial erosion on gas expansion, hydraulic fracturing and leakage' using basin modelling approaches. A key part of this project is my Ph.D. work.

I am going to present the Ph.D. work setup which includes building a complete basin model of a selected area in the Norwegian Barents Sea. The basin model input I am going to use includes a new source-rock model, new pressure and secondary migration model. Physical parameters of sedimentary rocks dependent on uplift will be refined by lab tests. Cenozoic burial history will be reconstructed, considering new erosion and glaciation concepts (Knies et al. 2012, Laberg et al. 2012). An impact of various ice-load scenarios on the pressure and migration modelling will be evaluated by using probabilistic Monte-Carlo modelling techniques.

References

Allen, P.A., Allen, J.R., 2004. Basin Analysis: Principles and Applications, 2nd Edition, 2nd ed. Wiley-Blackwell.

Andreassen, K., Laberg, J.S., Vorren, T.O., 2008. Seafloor geomorphology of the SW Barents Sea and its glaci-dynamic implications. Geomorphology 97, 157-177.

Andreassen, K., Nilssen, L.C., Rafaelsen, B., Kuilman, L., 2004. Three-dimensional seismic data from the Barents Sea margin reveal evidence of past ice streams and their dynamics. Geology 32, 729.

Anell, I., Thybo, H., Artemieva, I.M., 2009. Cenozoic uplift and subsidence in the North Atlantic region: Geological evidence revisited. Tectonophysics 474, 78-105.

Baig, I., Faleide, J.I., Jahren, J., Mondol, N.H., 2016. Cenozoic exhumation on the southwestern Barents Shelf: Estimates and uncertainties constrained from compaction and thermal maturity analyses. Marine and Petroleum Geology 73, 105-130.

Berglund, L.T., Augustson, J., Faerseth, R., Gjelberg, J., Ramberg- Moe, H., 1986. The evolution of the Hammerfest Basin. Habitat of hydrocarbons on the Norwegian continental shelf. Proc. conference, Stavanger, 1985, 319-338.

Bjarnadóttir, L.R., Winsborrow, M.C.M., Andreassen, K., 2014. Deglaciation of the central Barents Sea. Quaternary Science Reviews 92, 208-226.

Bjørlykke, K., Ramm, M., Saigal, G.C., 1989. Sandstone diagenesis and porosity modification during basin evolution. Geologische Rundschau 78, 243-268.

Breivik, A.J., Faleide, J.I., Gudlaugsson, S.T., 1998. Southwestern Barents Sea margin: late Mesozoic sedimentary basins and crustal extension. Tectonophysics 293, 21-44.

Butt, F.A., Drange, H., Elverhoi, A., Ottera, O.H., Solheim, A., 2002. Modelling Late Cenozoic isostatic elevation changes in the Barents Sea and their implications for oceanic and climatic regimes: preliminary results. Quaternary Science Reviews 21, 1643-1660.

Cardozo, N., 2009. 3D flexural modeling. Continuous plate of variable elastic thickness (finite difference solution). Matlab script, http://www.ux.uis.no/~nestor/work/matlabScripts.html. (accessed 04.10.2016).

Cavanagh, A.J., Di Primio, R., Scheck-Wenderoth, M., Horsfield, B., 2006. Severity and timing of Cenozoic exhumation in the southwestern Barents Sea. Journal of the Geological Society 163, 761-774.

Clark, S.A., Glorstad-Clark, E., Faleide, J.I., Schmid, D., Hartz, E.H., Fjeldskaar, W., 2014. Southwest Barents Sea rift basin evolution: Comparing results from backstripping and time-forward modelling. Basin Research 26, 550-566.

Close, D., 2010. Isostasy and Gravity Modelling: Integrating Potential Field Data in Interpretation Workflows. CSEG RECORDER 35, 34-39.

Corcoran, D.V., Doré, A.G., 2005. A review of techniques for the estimation of magnitude and timing of exhumation in offshore basins. Earth-Science Reviews 72, 129-168.

Dalland, A., Worsley, D., Ofstad, K., 1988. A lithostratigraphic scheme for the Mesozoic and Cenozoic succession offshore mid- and northern Norway. Norwegian Petroleum Directoriate.

de Boer, B., Lourens, L.J., van de Wal, R.S.W., 2014. Persistent 400,000-year variability of Antarctic ice volume and the carbon cycle is revealed throughout the Plio-Pleistocene. Nature Communications 5.

Dimakis, P., Braathen, B.I., Faleide, J.I., Elverhøi, A., Gudlaugsson, S.T., 1998. Cenozoic erosion and the preglacial uplift of the Svalbard–Barents Sea region. Tectonophysics 300, 311-327.

Doré, A., Corcoran, D.V., Scotchman, I.C., 2002. Prediction of the hydrocarbon system in exhumed basins, and application to the NW European margin, in: Doré, A.G., Cartwright, J.A., Stoker, M.S., Turner, J.P., White, N. (Eds.), Exhumation of the North Atlantic Margin: Timing, Mechanisms and Implications for Petroleum Exploration. The Geological Society of London, London, pp. 401-429.

Doré, A.G., 1995. Barents Sea Geology, Petroleum Resources and Commercial Potential. Arctic 48, 207-221.

Doré, A.G., Jensen, L.N., 1996. The impact of late Cenozoic uplift and erosion on hydrocarbon exploration: offshore Norway and some other uplifted basins. Global and Planetary Change 12, 415-436.

Doré, A.G., Lundin, E.R., Jensen, L.N., Birkeland, O., Eliassen, P.E., Fichler, C., 1999. Principal tectonic events in the evolution of the northwest European Atlantic margin, Petroleum Geology Conference Proceedings, pp. 41-61.

Duran, E.R., di Primio, R., Anka, Z., Stoddart, D., Horsfield, B., 2013. 3D-basin modelling of the Hammerfest Basin (southwestern Barents Sea): A quantitative assessment of petroleum generation, migration and leakage. Marine and Petroleum Geology 45, 281-303.

Ebbing, J., Braitenberg, C., Wienecke, S., 2007. Insights into the lithospheric structure and tectonic setting of the Barents Sea region from isostatic considerations. Geophysical Journal International 171, 1390-1403.

Eidvin, T., Jansen, E., Riis, F., 1993. Chronology of Tertiary fan deposits off the western Barents Sea: Implications for the uplift and erosion history of the Barents Shelf. Marine Geology 112, 109-131.

Elverhøi, A., Hooke, R.L., Solheim, A., 1998. Late Cenozoic erosion and sediment yield from the Svalbard–Barents Sea region: implications for understanding erosion of glacierized basins. Quaternary Science Reviews 17, 209-241.

England, P., Molnar, P., 1990. Surface Uplift, Uplift of Rocks, and Exhumation of Rocks. Geology 18, 1173-1177.

Faleide, J.I., Solheim, A., Fiedler, A., Hjelstuen, B.O., Andersen, E., Vanneste, K., 1996. Late Cenozoic evolution of the western Barents Sea-Svalbard continental margin. Global and Planetary Change 12, 53-74.

Faleide, J.I., Tsikalas, F., Breivik, A.J., Mjelde, R., Ritzmann, O., Engen, O., Wilson, J., Eldholm, O., 2008. Structure and evolution of the continental margin off Norway and Barents Sea. Episodes 31, 82-91.

Faleide, J.I., Vagnes, E., Gudlaugsson, S.T., 1993. Late Mesozoic-Cenozoic Evolution of the South-Western Barents Sea in a Regional Rift Shear Tectonic Setting. Marine and Petroleum Geology 10, 186-214.

Fanavoll, S., Ellingsrud, S., Gabrielsen, P.T., Tharimela, R., Ridyard, D., 2012. Exploration with the use of EM data in the Barents Sea: The potential and the challenges. First Break 30, 89-96.

Fiedler, A., Faleide, J.I., 1996. Cenozoic sedimentation along the southwestern Barents Sea margin in relation to uplift and erosion of the shelf. Global and Planetary Change 12, 75-93.

Fjeldskaar, W., 1997. Flexural rigidity of Fennoscandia inferred from the postglacial uplift. Tectonics 16, 596-608.

Fjeldskaar, W., Lindholm, C., Dehls, J., Fjeldskaar, I., 2000. Postglacial uplift, neotectonics and seismicity in Fennoscandia. Quaternary Science Reviews 19, 1413-1422.

Gabrielsen, R.H., Færseth, R.B., Jensen, L.N., Kalheim, J.E., Riis, F., 1990. Structural elements of the continental shelf. Part I: The Barents Sea Region. Norwegian Petroleum Directoriate bulletin 6, p. 33.

Gac, S., Huismans, R.S., Podladchikov, Y.Y., Faleide, J.I., 2012. On the origin of the ultradeep East Barents Sea basin. Journal of Geophysical Research: Solid Earth 117.

Gac, S., Klitzke, P., Minakov, A., Faleide, J.I., Scheck-Wenderoth, M., in press. Lithospheric strength and elastic thickness of the Barents Sea and Kara Sea region. Tectonophysics.

Gee, D.G., Fossen, H., Henriksen, N., Higgins, A.K., 2008. From the early Paleozoic platforms of Baltica and Laurentia to the Caledonide Orogen of Scandinavia and Greenland. Episodes 31, 44-51.

Gernigon, L., Bronner, M., Roberts, D., Olesen, O., Nasuti, A., Yamasaki, T., 2014. Crustal and basin evolution of the southwestern Barents Sea: From Caledonian orogeny to continental breakup. Tectonics 33, 347-373.

Glørstad-Clark, E., Birkeland, E.P., Nystuen, J.P., Faleide, J.I., Midtkandal, I., 2011. Triassic platform-margin deltas in the western Barents Sea. Marine and Petroleum Geology 28, 1294-1314.

Gowan, E.J., Tregoning, P., Purcell, A., Lea, J., Fransner, O.J., Noormets, R., Dowdeswell, J.A., 2016. ICESHEET 1.0: a program to produce paleo-ice sheet reconstructions with minimal assumptions. Geoscientific Model Development 9, 1673-1682.

Green, P.F., Duddy, I.R., 2010. Synchronous exhumation events around the Arctic including examples from Barents Sea and Alaska Slope. Petroleum Geology Conference series 7, 633-644.

Green, P.F., Duddy, I.R., Gleadow, A.J.W., Tingate, P.R., Laslett, G.M., 1986. Thermal annealing of fission tracks in apatite 1. A qualitative description. Chemical Geology 59, 237-253.

Gudlaugsson, S.T., Faleide, J.I., Johansen, S.E., Breivik, A.J., 1998. Late Palaeozoic structural development of the south-western Barents Sea. Marine and Petroleum Geology 15, 73-102.

Henriksen, E., Bjornseth, H.M., Hals, T.K., Heide, T., Kiryukhina, T., Klovjan, O.S., Larssen, G.B., Ryseth, A.E., Ronning, K., Sollid, K., Stoupakova, A., 2011a. Chapter 17 Uplift and erosion of the greater Barents Sea: impact on prospectivity and petroleum systems. Geological Society, London, Memoirs 35, 271-281.

Henriksen, E., Ryseth, A.E., Larssen, G.B., Heide, T., Ronning, K., Sollid, K., Stoupakova, A.V., 2011b. Chapter 10 Tectonostratigraphy of the greater Barents Sea: implications for petroleum systems. Geological Society, London, Memoirs 35, 163-195.

Hermanrud, C., Halkjelsvik, M.E., Kristiansen, K., Bernal, A., Stromback, A.C., 2014. Petroleum column-height controls in the western Hammerfest Basin, Barents Sea. Petroleum Geoscience 20, 227-240.

Hjelstuen, B., Elverhøi, A., Faleide, J.I., 1996. Cenozoic erosion and sediment yield in the drainage area of the Storfjorden Fan. Global and Planetary Change 12, 95-117.

Hurdle, B.G., 1986. The Nordic Seas. Springer Verlag.

Ingólfsson, Ó., Landvik, J.Y., 2013. The Svalbard–Barents Sea ice-sheet – Historical, current and future perspectives. Quaternary Science Reviews 64, 33-60.

Japsen, P., Green, P.F., Bonow, J.M., Nielsen, T.F.D., Chalmers, J.A., 2014. From volcanic plains to glaciated peaks: Burial, uplift and exhumation history of southern East Greenland after opening of the NE Atlantic. Global and Planetary Change 116, 91-114.

Johansen, S.E., Ostisty, B.K., Birkeland, Ø., Fedorovsky, Y.F., Martirosjan, V.N., Christensen, O.B., Cheredeev, S.I., Ignatenko, E.A., Margulis, L.S., 1992. Hydrocarbon potential in the Barents Sea region: play distribution and potential. Arctic Geology and Petroleum Potential, Norwegian Petroleum Society (NPF), Special Publication 2, 273-320.

Kjemperud, A., Fjeldskaar, W., 1992. Pleistocene glacial isostasy - implications for petroleum geology, in: Larsen, R.M., Brekke, H., Larsen, B.T., Talleraas, E. (Eds.), Structural and Tectonic Modelling and its Application to Petroleum Geology. NPF Special Publication, Amsterdam, pp. 187-195.

Klitzke, P., Faleide, J.I., Scheck-Wenderoth, M., Sippel, J., 2015. A lithosphere-scale structural model of the Barents Sea and Kara Sea region. Solid Earth 6, 153-172.

Knies, J., Matthiessen, J., Vogt, C., Laberg, J.S., Hjelstuen, B.O., Smelror, M., Larsen, E., Andreassen, K., Eidvin, T., Vorren, T.O., 2009. The Plio-Pleistocene glaciation of the Barents Sea–Svalbard region: a new model based on revised chronostratigraphy. Quaternary Science Reviews 28, 812-829.

Laberg, J.S., Andreassen, K., Knies, J., Vorren, T.O., Winsborrow, M., 2010. Late Pliocene-Pleistocene development of the Barents Sea Ice Sheet. Geology 38, 107-110.

Laberg, J.S., Andreassen, K., Vorren, T.O., 2012. Late Cenozoic erosion of the high-latitude southwestern Barents Sea shelf revisited. Geological Society of America Bulletin 124, 77-88.

Laberg, J.S., Vorren, T.O., 1996. The Middle and Late Pleistocene evolution of the Bear Island Trough Mouth Fan. Global and Planetary Change 12, 309-330.

Lambeck, K., Purcell, A., Funder, S., Kjær, K., Larsen, E., Möller, P., 2006. Constraints on the Late Saalian to early Middle Weichselian ice sheet of Eurasia from field data and rebound modelling. Boreas 35, 539-575.

Lambeck, K., Purcell, A., Zhao, J., Svensson, N.O., 2010. The scandinavian ice sheet: From MIS 4 to the end of the last glacial maximum. Boreas 39, 410-435.

Landvik, J.Y., Bondevik, S., Elverhøi, A., Fjeldskaar, W., Mangerud, J., Salvigsen, O., Siegert, M.J., Svendsen, J.I., Vorren, T.O., 1998. The last glacial maximum of Svalbard and the Barents sea area: Ice sheet extent and configuration. Quaternary Science Reviews 17, 43-75.

Larsen, E., Kjær, K., Demidov, I., Funder, S., Grøsfjeld, K., Houmark-Nielsen, M., Jensen, M., Linge, H., Lysså, A., 2006. Late Pleistocene glacial and lake history of northwestern Russia. Boreas 35, 394-424.

Larssen, G.B., Elvebakk, G., Henriksen, L.B., Kristensen, S.E.-, Nilsson, I., Samuelsberg, T.J., Svånå, T.A., Stemmerik, L., Worsley, D., 2002. Upper Paleozoic lithostratigraphy of the Southern Norwegian Barents Sea. Norwegian Petroleum Directoriate.

Lerche, I., Yu, Z., Tørudbakken, B., Thomsen, R.O., 1997. Ice loading effects in sedimentary basins with reference to the Barents Sea. Marine and Petroleum Geology 14, 277-338.

Linjordet, A., Grung-Olsen, R., 1992. The Jurassic Snøhvit Gas Field Hammerfest Basin, Offshore Northern Norway, in: Halbouty, M.T. (Ed.), Giant Oil and Gas Fields of the Decade 1978–1988. American Association of Petroleum Geologists, Memoirs.

Liu, G.J., Lippard, S., Fanavoll, S., Sylta, O., Vassmyr, S., Doré, A., 1992. Quantitative Geodynamic Modeling of Barents Sea Cenozoic Uplift and Erosion. Norsk Geol Tidsskr 72, 313-316.

Lowrie, W., 2007. Fundamentals of Geophysics. Cambridge University Press, Cambridge.

Løseth, H., Lippard, S.J., Sættem, J., Fanavoll, S., Fjerdingstad, V., Leith, T.L., Ritter, U., Smelror, M., Sylta, Ø., 1992. Cenozoic uplift and erosion of the Barents Sea—evidence from the Svalis Dome area, Arctic Geology and Petroleum Potential. Elsevier Amsterdam, pp. 643-6564.

Løseth, L.O., Wiik, T., Olsen, P.A., Hansen, J.O., 2014. Detecting Skrugard by CSEM — Prewell prediction and postwell evaluation. Interpretation 2, SH67-SH78.

Mangerud, J., Dokken, T., Hebbeln, D., Heggen, B., Ingólfsson, Ó., Landvik, J.Y., Mejdahl, V., Svendsen, J., Vorren, T.O., 1998. Fluctuations of the Svalbard–Barents Sea Ice Sheet during the last 150 000 years. Quaternary Science Reviews 17, 11-42.

McKenzie, D., 1978. Some remarks on the development of sedimentary basins. Earth and Planetary science letters 40, 25-32.

Nyland, B., Jensen, L.N., Skagen, J., Skarpnes, O., Vorren, T., 1992. Tertiary uplift and erosion in the Barents Sea: magnitude, timing and consequences. Structural and tectonic modelling and its application to petroleum geology, 153-162.

Ohm, S.E., Karlsen, D.A., Austin, T.J.F., 2008. Geochemically driven exploration models in uplifted areas: Examples from the Norwegian Barents Sea. AAPG Bulletin 92, 1191-1223.

Ostanin, I., Anka, Z., di Primio, R., Bernal, A., 2012. Identification of a large Upper Cretaceous polygonal fault network in the Hammerfest basin: Implications on the reactivation of regional faulting and gas leakage dynamics, SW Barents Sea. Marine Geology 332-334, 109-125.

Patton, H., Andreassen, K., Bjarnadóttir, L.R., Dowdeswell, J.A., Winsborrow, M.C.M., Noormets, R., Polyak, L., Auriac, A., Hubbard, A., 2015. Geophysical constraints on the dynamics and retreat of the Barents Sea ice sheet as a paleobenchmark for models of marine ice sheet deglaciation. Reviews of Geophysics 53, 1051-1098.

Peltier, W.R., Argus, D.F., Drummond, R., 2015. Space geodesy constrains ice age terminal deglaciation: The global ICE-6G_C (VM5a) model. Journal of Geophysical Research: Solid Earth 120, 450-487.

Rasmussen, E., Fjeldskaar, W., 1996. Quantification of the Pliocene-Pleistocene erosion of the Barents Sea from present-day bathymetry. Global and Planetary Change 12, 119-133.

Rebesco, M., Laberg, J.S., Pedrosa, M.T., Camerlenghi, A., Lucchi, R.G., Zgur, F., Wardell, N., 2014. Onset and growth of Trough-Mouth Fans on the North-Western Barents Sea margin – implications for the evolution of the Barents Sea/Svalbard Ice Sheet. Quaternary Science Reviews 92, 227-234.

Reemst, P., Cloetingh, S., Fanavoll, S., 1994. Tectonostratigraphic modelling of Cenozoic uplift and erosion in the south-western Barents Sea. Marine and Petroleum Geology 11, 478-490.

Richardsen, G., Vorren, T.O., Torudbakken, B.O., 1993. Post-early Cretaceous uplift and erosion in the southern Barents Sea: a discussion based on analysis of seismic interval velocities. Norsk Geologisk Tidsskrift 73, 3-20.

Riis, F., 1996. Quantification of Cenozoic vertical movements of Scandinavia by correlation of morphological surfaces with offshore data. Global and Planetary Change 12, 331-357.

Riis, F., Fjeldskaar, W., 1992. On the magnitude of the Late Tertiary and Quaternary erosion and its significance for the uplift of Scandinavia and the Barents Sea, in: Larsen, R.M., Brekke, H., Larsen, B.T., Talleraas, E. (Eds.), Structural and Tectonic Modelling and its Application to Petroleum Geology. NPF Special Publication, pp. 163-185.

Riis, F., Jensen, L.N., 1992. Measuring uplift and erosion - proposal for a terminology. Norsk Geologisk Tidsskrift 72, 223-228.

Roberts, D., 2003. The Scandinavian Caledonides: event chronology, palaeogeographic settings and likely modern analogues. Tectonophysics 365, 283-299.

Rydningen, T., Arne, 2014. Sedimentary processes, late Cenozoic evolution and sediment yield on the continental margin offshore Troms, northern Norway, Faculty of Science and Technology, Department of Geology. University of Tromsø, Tromsø.

Ryseth, A., Augustson, J.H., Charnock, M., Haugerud, O., Knutsen, S.-M., Midbøe, P.S., Opsal, J.G., Sundsbø, G., 2003. Cenozoic stratigraphy and evolution of the Sørvestsnaget Basin, southwestern Barents Sea. Norsk Geologisk Tidskrift, 107-130.

Rüther, D.C., Mattingsdal, R., Andreassen, K., Forwick, M., Husum, K., 2011. Seismic architecture and sedimentology of a major grounding zone system deposited by the Bjørnøyrenna Ice Stream during Late Weichselian deglaciation. Quaternary Science Reviews 30, 2776-2792.

Sclater, J.G., Christie, P.A.F., 1980. Continental Stretching: An Explanation of the post-mid-Cretaceous Subsidence of the Central North Sea Basin. Journal of Geophysical Research 85, 3711-3739.

Setoyama, E., Kaminski, M.A., Tyszka, J., 2011. The Late Cretaceous–Early Paleocene palaeobathymetric trends in the southwestern Barents Sea — Palaeoenvironmental implications of benthic foraminiferal assemblage analysis. Palaeogeography, Palaeoclimatology, Palaeoecology 307, 44-58.

Siegert, M., Dowdeswell, J.A., Hald, M., Svendsen, J., 2001. Modelling the Eurasian Ice Sheet through a full Weichselian glacial cycle. Global and Planetary Change 31, 367-385.

Siegert, M.J., Dowdeswell, J.A., 2002. Late Weichselian iceberg, surface-melt and sediment production from the Eurasian Ice Sheet: results from numerical ice-sheet modelling. Marine Geology 188, 109-127.

Siegert, M.J., Dowdeswell, J.A., 2004. Numerical reconstructions of the Eurasian Ice Sheet and climate during the Late Weichselian. Quaternary Science Reviews 23, 1273-1283.

Solheim, A., Kristoffersen, Y., 1984. Distribution of sediments above bedrock and glacial history in the western Barents Sea. Norsk Polarinstitutt Skifter 179B.

Svendsen, J.I., Alexanderson, H., Astakhov, V.I., Demidov, I., Dowdeswell, J.A., Funder, S., Gataullin, V., Henriksen, M., Hjort, C., Houmark-Nielsen, M., Hubberten, H.W., Ingólfsson, Ó., Jakobsson, M., Kjær, K.H., Larsen, E., Lokrantz, H., Lunkka, J.P., Lysså, A., Mangerud, J., Matiouchkov, A., Murray, A., Möller, P., Niessen, F., Nikolskaya, O., Polyak, L., Saarnisto, M., Siegert, C., Siegert, M.J., Spielhagen, R.F., Stein, R., 2004. Late Quaternary ice sheet history of northern Eurasia. Quaternary Science Reviews 23, 1229-1271.

Sweeney, J.J., Burnham, A.K., 1990. Evaluation of a simple model of vitrinite reflectance based on chemical kinetics. American Association of Petroleum Geologists Bulletin 74, 1559-1570.

Sættem, J., Bugge, T., Fanavoll, S., Goll, R.M., Mørk, A., Mørk, M.B.E., Smelror, M., Verdenius, J.G., 1994. Cenozoic margin development and erosion of the Barents Sea: Core evidence from southwest of Bjørnøya. Marine Geology 118, 257-281.

Sættem, J., Poole, D.A.R., Ellingsen, L., Sejrup, H.P., 1992. Glacial geology of outer Bjørnøyrenna, southhwestern Barents Sea. Marine Geology 103, 15-51.

Tsikalas, F., 1992. A study of seismic velocity, density and porosity in Barents Sea wells, Northern Norway, University of Oslo. University of Oslo, Oslo, Norway.

Turcotte, D.L., Schubert, G., 2002. Geodynamics second edition. Cambridge University Press.

van den Berg, J., van de Wal, R.S.W., Milne, G.A., Oerlemans, J., 2008. Effect of isostasy on dynamical ice sheet modeling: A case study for Eurasia. Journal of Geophysical Research: Solid Earth 113.

Vening-Meinesz, F.A., 1941. Gravity over Hawaiian archipelago and over Madeira area. Proc.K.Ned.Akad.Wet. 44, 1-12.

Vorren, T.O., Laberg, J.S., 1997. Trough mouth fans - palaeoclimate and ice-sheet monitors. Quaternary Science Reviews 16, 865-881.

Vorren, T.O., Lebesbye, E., Andreassen, K., Larsen, K.B., 1989. Glacigenic sediments on a passive continental margin as exemplified by the Barents Sea. Marine Geology 85, 251-272.

Vorren, T.O., Lebesbye, E., Larsen, K.B., 1990. Geometry and genesis of the glacigenic sediments in the southern Barents Sea. Geological Society, London, Special Publications 53, 269-288.

Vorren, T.O., Richardsen, G., Knutsen, S.M., 1991. Cenozoic erosion and sedimentation in the western Barents Sea. Marine and Petroleum Geology 8, 317-340.

Walderhaug, O., 1992. Magnitude of uplift of the Stø and Nordmela Formations in the Hammerfest Basin - a diagenetic approach. Norsk Geologisk Tidskrift 72, 321-323.

Watts, A.B., 2001. Isostasy and Flexure of the Lithosphere. Cambridge University Press, Cambridge.

Winsborrow, M.C.M., Andreassen, K., Corner, G.D., Laberg, J.S., 2010. Deglaciation of a marine-based ice sheet: Late Weichselian palaeo-ice dynamics and retreat in the

southern Barents Sea reconstructed from onshore and offshore glacial geomorphology. Quaternary Science Reviews 29, 424-442.

Winsborrow, M.C.M., Stokes, C.R., Andreassen, K., 2012. Ice-stream flow switching during deglaciation of the southwestern Barents Sea. Geological Society of America, Bulletin 124, 275-290.

Wood, R.J., Edrich, S.P., Hutchinson, I., 1989. Influence of North Atlantic tectonics on the large-scale uplift of the Stappen High and Loppa High, western Barents Shelf. Extensional tectonics and stratigraphy of the North Atlantic margins, 559-566.

Worsley, D., 2008. The post-Caledonian development of Svalbard and the western Barents Sea. Polar Research 27, 298-317.

Zattin, M., Andreucci, B., de Toffoli, B., Grigo, D., Tsikalas, F., 2016. Thermochronological constraints to late Cenozoic exhumation of the Barents Sea Shelf. Marine and Petroleum Geology 73, 97-104.

Zieba, K.J., Daszinnies, M., Emmel, B., Lothe, A., Grøver, A., Lippard, S., 2015. Assessment of the Cenozoic Erosion Amount Using Monte Carlo Type-Petroleum Systems Modeling of the Hammerfest Basin, Western Barents Sea. American Journal of Geoscience 4, 40-53.